HIPER

8TH INTERNATIONAL CONFERENCE

ON HIGH-PERFORMANCE MARINE VEHICLES

DUISBURG / GERMANY

27 – 28 SEPTEMBER 2012

UNIVERSITÄT DUISBURG ESSEN

Open-Minded

8TH INTERNATIONAL CONFERENCE

ON HIGH-PERFORMANCE MARINE VEHICLES

DUISBURG / GERMANY

27 – 28 SEPTEMBER 2012

UNIVERSITY OF DUISBURG-ESSEN

INSTITUTE OF SHIP TECHNOLOGY, OCEAN ENGINEERING

AND TRANSPORT SYSTEMS (ISMT)

Published by:	University of Duisburg-Essen Institute of Ship Technology, Ocean Engineering and Transport Systems (ISMT)
Publication:	September 2012
Editorial Processing:	Claudia O’Donoghue

Sponsored by

ABEKING & RASMUSSEN

ABEKING & RASMUSSEN Schiffs- und Yachtwerft Aktiengesellschaft

www.abeking.com

TABLE OF CONTENTS

Advanced Composites in Marine Applications

Hasso Hoffmeister, Germanischer Lloyd, Hamburg/Germany,
hasso.hoffmeister@GL-group.com

Abstract

From open spray moulding to autoclaved carbon structures; from chopped strand mat to Thin Ply Technology (TPT®); an overview of the variety of materials used for the construction in composites is given. Typical production methods and resulting specific material properties and failure modes are described. Implications of mechanical properties into engineering analyses are discussed. Recent examples from industry practice serve as illustrations.

1. Introduction

While experimental research on composite materials reaches back to the 1920´s and a first patent on fibreglass was given in 1936, the practical use of composite materials in marine application started in the 1940´s with the desire to have boats that were strong, lightweight, watertight and easy to maintain. Fibre Reinforced Plastics (FRP) evolved in all branches of the marine industry as accepted alternative construction material. The technology was firmly established through the 1970´s and 1980´s and today has become a serious competitor to steel and aluminium. Structural design, production processes and analysis methodologies continue to advance. It is expected that composites will continue to propagate into fields where the use of steel and aluminium today is still dominant. The speed and scope of this development will depend a lot on cost effectiveness of production methods.

FRP applications in neighbouring fields (such as automotive and aeronautical engineering) started later, but evolved then much faster. The marine industry has caught up meanwhile and nowadays provides customers with deep knowledge of material behaviour, damage modes, numerical methods and production technology. FRP materials have very attractive features, such as high specific strength and stiffness properties, but require a high level of expertise due to their anisotropic nature and their complex failure modes. Naval architects today share knowledge in technology clusters or networks like SAMPE (Society for the Advancement of Material Processing and Engineering) and the SNAME (Society of Naval Architects and Marine Engineers).

2. Typical applications

The recreational segment of the marine industry was the forerunner in composite applications in the early 1960´s. Back then builders could afford optimising their products by trial and error before, sometimes decades later, the technology was sound enough to move into mass production. Today the focus is more on design for production, reducing the building costs. On the other end of technology, racing boats were always designed with big budgets. Here still much innovation can be expected. Mainstream yachting benefits from these developments eventually with some time delay.

Fig. 1: Mass-produced yachts (left) and custom racer (right)
[Source: Bavaria Yachtbau, Green Marine]

The general industry structure is unchanged today, with different levels of sophistication in the use of composite materials. There are mass producers with output rates in excess of 500 boats per year, and pure one-offs performance optimised to the last gram.

Composite material technology is attractive for commercial boats as it saves time and money, as moulds can be used for serial production of smaller boats. In addition, composites lead to low maintenance cost. Composites are used for a wide variety of boats, Fig.2 to Fig.5: patrol boats, mine-counter measure boats, research vessels, fire fighting boats, supply vessels, utility vessels, ferries, passenger vessel, rescue boats and fishing boats.

Fig.2: Patrol boat [source: Lomocean]

Fig.3: Fire & rescue boat

Fig.4: Water taxi [source: Lomocean]

Fig.5: Fishing vessel

Composite material technology is very attractive due to the great strength/weight ratio. Therefore, composites are extensively employed in extremely weight-sensitive craft, such as air-cushioned vehicles (ACVs) and Wing-in-Ground (WIG) craft. Also the solar-powered catamaran “Tûranor PlanetSolar”, *Bertram et al. (2010),* Fig.6, and the bio-fuelled trimaran “Earthrace”, Fig.7, used extensively composite materials for weight reasons.

Fig.6: “Tûranor PlanetSolar”
[Source: Knierim Yachtbau]

Fig.7: Record breaking trimaran “Earthrace”
[Source: Earthrace]

Virtually all lifeboats today are made from composite materials. Manufactures hold a limited variety of hull moulds, so that series production or semi-custom series production leads to cost effective products. Lightweight canopy roofs and low maintenance cost for boats tied to a cradle for most of their life-time are arguments which have replaced metal construction for this purpose.

On manned submarines, the application of composite materials is restricted to non-pressurized areas and lower-priority components. However, on most unmanned underwater vehicles the hull is made of composites.

Besides hull, many components are made from composites. Many components in the marine industry now use composites rather than metal: hatches, doors, bulwarks, propeller shafts, etc. For some of these components, not only light weight (albeit at high cost) is a decisive argument, but the delivery times including construction and shipment, particularly for re-placement parts is favourable. Spars for sailing yachts have been built from carbon fibre composites for two decades. However, standard aluminium extrusion masts still dominate, for reasons of robustness, ease of design and construction and also cost. The disadvantages of carbon reinforced plastics (CRPs) are accepted when weight comes at a premium, namely in high-performance and competitive sailing, as well as for superyachts. Recent develop-ments include the substitution of steel standing rigging by polymer matrix composites, provid-ing a similar weight advantage as in replacing an aluminium mast by a CRP mast.

3. Materials used

Composite materials consist of a combination of structural fibres bedded in a stabilising ma-trix to develop their full potential, called “laminate”. Laminates can be solid, laid up in multiple layers, or combined to form a “sandwich” (with lightweight core material placed in between laminate facings). Unlike with metals, the builder of composite components creates the struc-tural material from constituents, making it essential to be aware of how these combine and how they work together.

The use of fluid resin before cure allows the creation of virtually any geometry. In the early days of composites, polyester resins were used as matrix to stabilise the yet dry fibres. Only a few decades ago, vinyl-ester and epoxy resins were formulated to compete against polyester providing higher quality laminates, in terms of strength, robustness and longevity. While stabilising the reinforcement fibres, the resin takes a certain role as a structural part. The type of resin, the amount of resin and the production method depend on each other and are vital for the performance of the composite.

Sandwich construction involving light weight cores is a unique technology very common in the marine industry. Taking the through-thickness shear forces and bringing the laminate skins apart yields very light-weight structures with high stiffness, making fewer supporting structures necessary. Sandwich cores are most often made of closed cell synthetic foams; more rarely, balsa end grain wood or honeycomb structures are employed.

3.1. Fibres

Today's composite technology involves the use of E-glass and Carbon fibres almost throughout. Certain applications include the use of Aramid fibres. Where cost-effectiveness is required, E-glass is the choice. Carbon fibres will be used where a high structural performance/weight ratio is required. Often this is accompanied by a much higher degree of engineering efforts to exploit the full potential of the sophisticated material.

Glass fibres are the most ancient fibre. Melting glass and drawing fibres from the melt is known to be done in the ancient world. The big step, after which glass fibres were used as reinforcement material and not simply in discontinuous wool applications, was made in the 1930´s, where industry started to draw continuous glass filaments used as textile reinforcement. The product was marketed as "Fibreglass" by one of the first industrial manufacturers. Glass fibres are primarily made from melted Silica (SiO_2). In order to avoid crystallisation and becoming quartz again when cooling off, temperatures and cooling rates are adjusted in order to support the alteration to amorphous chemical structure to become glass. From the melt, glass fibres are extruded through bushings, generating continuous filaments of between 4 and 34 mm in endless form. Fibres are coated with lubricants, binders or coupling agents, depending on the application. In the marine industry, two particular chemistries of glass fibres are most commonly used, E-glass and S-glass. S-glass is stronger, but more expensive.

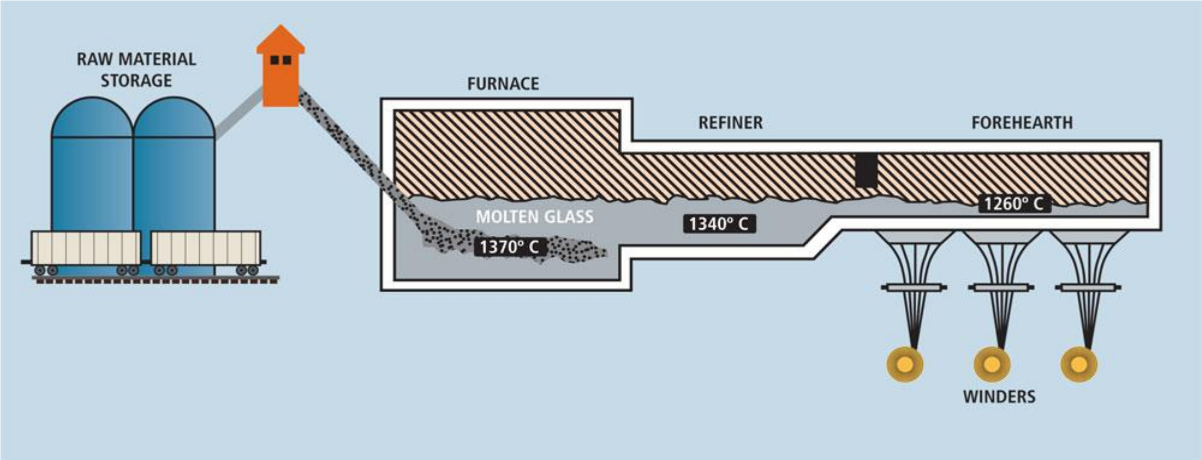

Fig.8: Glass fibre production [Source: www.compositesworld.com]

Carbon fibres offer the highest strength and stiffness to weight ratio of all commercially available fibres. Carbon fibres do not suffer from creep and their fatigue resistance is superior to Aramid or Glass fibres. A big downside is the cost, due to the complex manufacturing process. Unlike glass fibres, carbon fibres differ in production, with resulting different properties to suit intended purpose. There are high-strength grades and high-stiffness grades. The raw material of making roughly 10% of the world market's carbon fibres is either rayon- or pitch-based. The majority of carbon fibres today are based on a PAN (polyacrylonitrile) chemistry, which is made from propylene and ammonia, www.compositesworld.com. Here, only the two most important production steps shall be described. The carbon fibre, after a complicated chemical process (polymerisation) is spun off a fluid bath ("wet spinning"). After that, the fibres run through a post treatment, called oxidation and carbonization. Like glass fibres, the final treatment is a surface treatment, enhancing the fibre for adhesion. Carbon fibres are between 5 and 10 mm in diameter and are collected in tows.

Aramid fibre, an aromatic polyamide, is gained by spinning the solved polymer to a solid fibre from a liquid chemical blend. Known today under the different trade names "Kevlar", "Twaron" and "Technora", aramid fibres offer high impact resistance and tensile strength. In fibre form they are called Para-aramids. Para-aramids in the marine industry are used when impact protection and abrasion resistance is required.

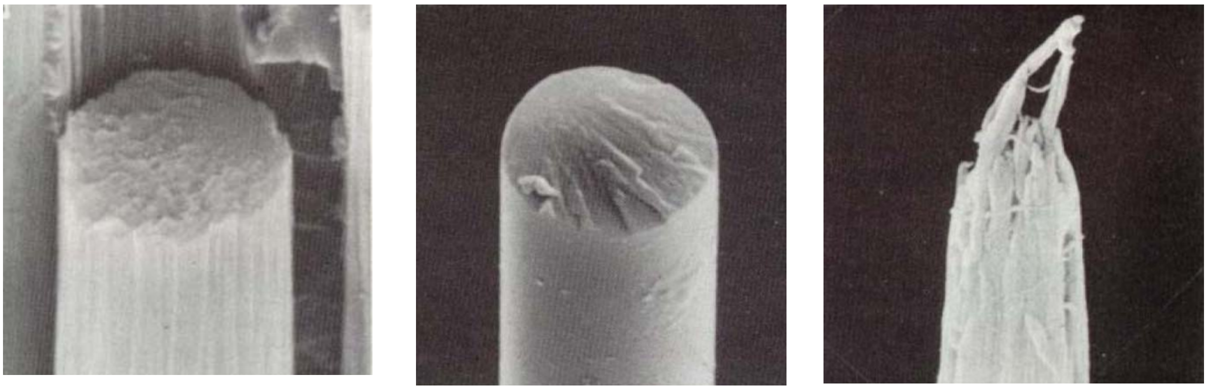

Fig.9: Microscopic views of carbon (left), E-glass (centre) and Aramid (right) fibres
[Source: Hamburg University of Applied Sciences]

3.2. Resins

Polyester resin is by far the most economical matrix system for reinforcement fibres. The thermosetting (irreversible in cure) resin is an unsaturated resin formed by the reaction of dibasic organic acids and polyhydric alcohols, being dissolved in a solvent, such as styrene. Two types of polyester resins are commonly used in the marine industry, orthophtalic and isophtalic resins. The orthophtalic system shows more sensitivity to chemical influences; the isophtalic resin has better mechanical properties, less absorption of water and thus is often used in the outer layers of hull laminates. Polyester resin is cured by cross-linking chemical chains. The cure is a chain reaction and occurs exothermically. Too great thickness of resin to cure or the use of too much catalyst will cause charring or even ignition. The surface of polyester resins will not cure when exposed to air; often paraffin is dissolved in the resin to form an air barrier, so that a total cure is assured. Thus, the cured surface has a wax film, making secondary bonding impossible without further surface preparation. Polyester resin is most often used together with glass fibre reinforcements as an economical, balanced laminate.

Epoxy resin systems are commonly used in advanced applications such as in combination with carbon fibre. Epoxy is a thermosetting co-polymer, consisting of two different chemicals, the epoxide “resin” and the polyamide “hardener”. The two agents each consist of monomers which make up a covalent bond when curing. Unlike polyesters curing under a chain reaction, each resin molecule matches a hardener molecule. Mixing ratios are very important. The cure of exact quantities can be influenced only by employing elevated temperatures. Resins made of epoxy are more robust than polyester, have a lower rate of water absorption and a higher strain to failure. Epoxy resins are also often used for adhesives in the marine industry.

Solid additives in form of powder are often added to resins to adjust their properties. In order to reduce the viscosity in adhesives, light-weight microscopic glass bubbles or rubber particles are stirred into the resin. Recently, solid additives have been developed to provide the resin system with more strength and toughness, without affecting the viscosity: this is by adding carbon nanotubes in small quantities to the resin, giving the resin more multidirectional linkage, thus strength and toughness. These nanotubes, Fig.10, have diameters of 1 nm = 10^{-6} m and are many million times longer.

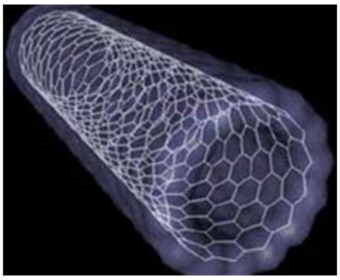

Fig.10: Schematic of nanotubes [Source: www.compositesworld.com]

3.3. Cores

Balsa lumber is a low density wood (density 90 to 220 kg/m^3), which is used in end grain plates to be glued between laminate faces. Having a high strength/weight ratio and high stiffness, the kiln dried balsa sheets exhibit good adhesive properties. Disadvantages include the low ability to absorb impact and the deterioration after prolonged water contact (fungi). The low elasticity makes it necessary to use cross-cut balsa sheets if curved sandwich panels are required.

Thermoset foams (e.g. polystyrene and polyurethane) have very low densities and are not susceptible to degradation from fungi or water absorption, but also have very low mechanical properties. These foams are most often used as buoyancy material.

PVC (polyvinylchloride) foams are the most common sandwich core material in the marine industry. They are available in densities of 30 to 300 kg/m^3. Sheets can be purchased typically between 5 and 50 mm. All PVC foams are closed celled and have a good resistance against water absorption. Operating temperatures and thus thermal stability is limited and reaches up to 80°C to 120°C. PVC foams are resistant to styrene and can be used with both epoxy and polyester resin systems. Some foam can be thermoformed. There are two main types of PVC foams, the cross-linked and the “linear” foams. Linear foams have slightly lower specific strength properties, but absorb more energy under impact and are heat-formable.

The arrangement of vertical hollow cells is a very effective way to fulfil the mechanical requirements of a sandwich core. Different styles of hexagonal honeycomb are available, in different densities and different cell arrangements, to cope with different requirements. Materials range from thin aluminium foils to aramid paper. Honeycomb core is extremely light. It is used often only in high-tech applications, as it is difficult to bond to the facing laminates.

4. Fibre reinforcement configurations

Fibre filaments as initially drawn or extruded during the manufacturing process are usually bundled to combine to a “tow”, most often consisting of between 1000 and 24000 filaments, wound on spools. This continuous tow is the constituent for all configuration textile arrangements of fibres. The most common arrangement is a cloth fabric, made from woven tows. Alternatively, tows can also be arranged in multi-axial direction, unwoven. In order to avoid falling apart, these fabrics are usually stitched together with lightweight yarn. In unidirectional plies, all fibre tows are aligned in one direction. Some applications promote random orientation of chopped short fibres. There is a great variety of tow arrangements:

- Tow bundle thickness to influence ply weight/thickness
- Different weaving/stitching patterns and methods provide different drapability.
- Fibre orientations can be prioritised provided on load transfer requirements, unidirectional, bi-directional, triaxial, quadraxial, and random orientation.
- Different fibre types can be combined for different structural requirements.

Random orientation fabrics are used only in low-strength applications. For high-tech applications, recent developments attempt to optimise fabric style for better structural performance. The ultra-thin fabrics are constructed using the “spread tow” method, Fig.13, where tows of fibres are “spread flat” to provide optimised fibre alignment and higher stiffness.

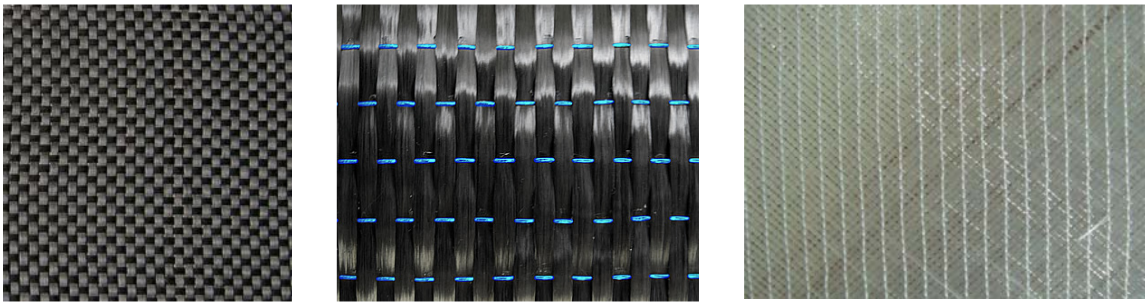

Fig.11: Carbon woven cloth (left), Carbon unidirectional (centre), E-glass multi-axial (right)

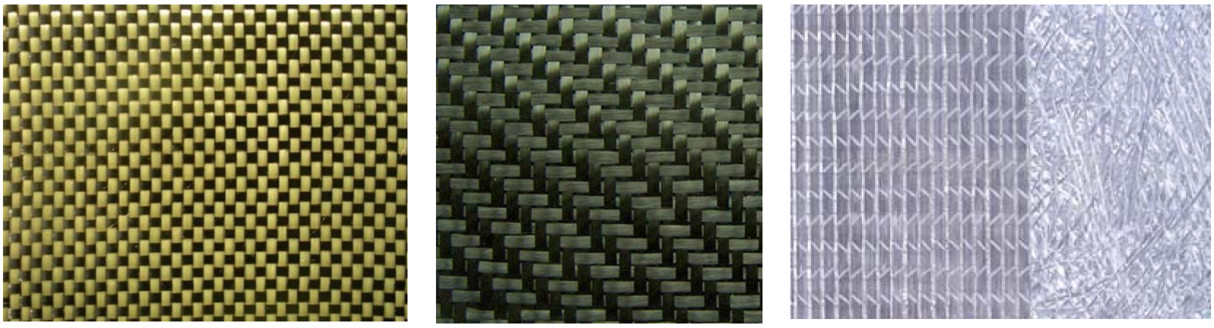

Fig.12: Hybrid plain weave cloth (left), Carbon twill weave cloth (centre), E-glass UD_CSM (right)

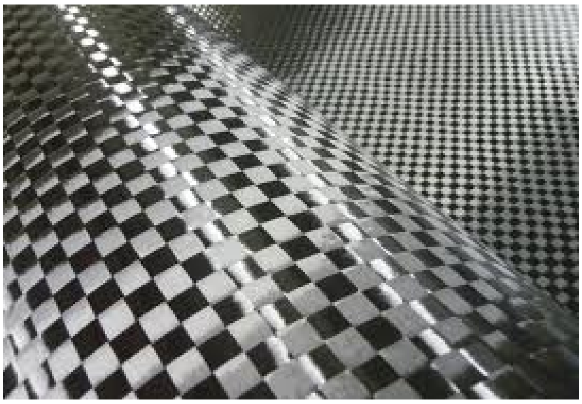

Fig.13: Spread tow [Source: www.HP-Textiles.com]

All fabrics are supplied as “dry fibre” fabrics. In order to further optimise structural behaviour, fabrics are also available as “pre-preg”; fabrics pre-impregnated with uncured resin at a precise resin content. These pre-pregs do not require mechanical fixation such as stitching yarns as they are held together by the yet un-cured resin. In order to avoid premature cure, these pre-pregs need to be stored at very low temperatures and the resin has a very low viscosity when laying out into a mould, in order to avoid resin bleed. This is where one of the latest developments steps in. The thin ply technology (TPT), a pre-preg technology combined with the “spread tow” method, provides very thin layers of pre-impregnated unidirectional fibre layers. This integrated solution provides possibilities to make high performance composite parts in a more industrial way. Possibilities include using an automated tape lay-down system for plies between 30 and 300 g/m^2, ply thickness between 0.03 and 0.3 mm.

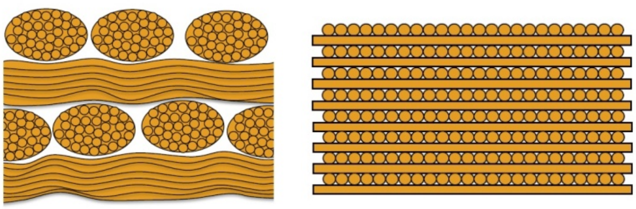

Fig.14: Regular tow laminates (left) and TPT (right) [source: North Thin Ply Technology]

Fig.15: TPT laying machine

5. Production methods

Almost all composite production methods involve moulds, in or over which a laminate is laid out wet and cures to obtain the intended geometry which is given by the mould. There are negative moulds, Fig.16, often used for series production where no finish work needs to be made on a part as the surface will have the same quality as the mould surface. Identical parts with high quality of exterior finish will be the result. Positive moulds are often used for single builds. Moulds need to be designed and built to provide similarity of series products; they need to be robust for repeated use and temperature and pressure applications during the curing process.

The constituent materials that can be combined to result in a cured composite which fulfils the defined demands are manifold. The options of how to combine fibre reinforcements with their supporting matrix depend on the available production methods and design purpose. A proper balance between economical and technical aspects must be found. The following production methods present typical applications in the marine industry:

Fig.16: Negative mould: Construction (left) and supporting structure (right), [Source: McMullen & Wing]

Spray Layup: The most economical method in building a laminate up fast is the spray layup, Fig.17. In a pressurized gun, resin and chopped glass fibre is combined and sprayed onto an open mould. The laminate cures under atmospheric conditions. This method involves polyester resin and has become less popular because of national restrictions on styrene emissions. The finished part is rather imprecise and has low strength. Laminates built this way usually have high resin ratios.

- Wet Layup: A very popular method involves laying down dry reinforcements into an open (typically negative) mould, Fig.18. Resin is then applied to the reinforcement fabrics, and rolled out to achieve uniformly penetrated reinforcements. Air inclusion is reduced with a sheet roller compressing the laminate. Laminate is often curing under atmospheric conditions. Medium resin ratios can be achieved this way. This method is often used for medium demand on structural performance and is fairly economical. Sandwich constructions can be built this way, too.

Fig.17: Spray layup
[Source: www.hennecke.com]

Fig.18: Wet layup

- Vacuum Bagging: This process is a possible follow-up and thus a variance of a wet layup. Before the laminate is allowed to cure, the laminate is covered with a vacuum bag and connected to a vacuum pump, Fig.19. While evacuating air from the area below the bag, atmospheric pressure helps removing air inclusions and excessive resin, by consolidating the laminate. Pressure applied can obviously not exceed 1 bar. Since this method involves more process steps, more accessories and more time, it is used for medium to high demand on structural performance and combined with using epoxy resins.

- Infusion: A more recent method of building high-quality composites is a derivate of hand lay-up assisted by vacuum. The pre-cut fibre fabrics are laid out dry in a mould, even including a sandwich core. Complete hull or deck shells or parts with complicated geometries can be prepared this way. After placing of the full stack of dry fabrics, the assembly is subjected to a vacuum, Fig.20. The vacuum pump attachment is placed on one side of the vacuum arrangement and on the other side a valve is opened to allow resin to be sucked into this vacuum. Constant pressure needs to be applied to the arrangement until all fabrics are impregnated by the resin front. A challenge in this process is that there is only one resin front on each suction side; otherwise the entrapped air could not be evacuated. Depending on the size and configuration of assembly, resins for injection need to have lower viscosity for enhanced flow. This method yields very high quality, low void content and a consistent resin ratio. There is no time constraint on the fibre placement, but the process of infusing the resin faultless is difficult. An extra advantage is the low emission of volatiles.

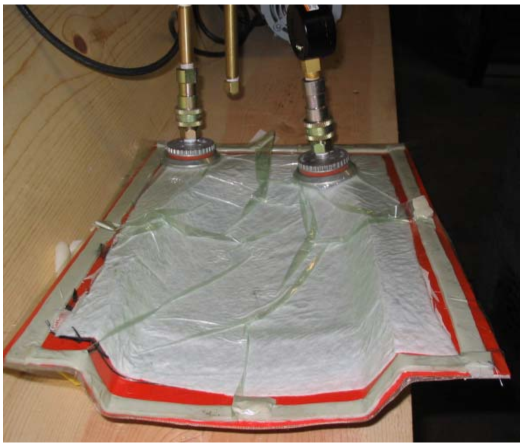

Fig.19: Vacuum bagging
[source: jumbocreations.com]

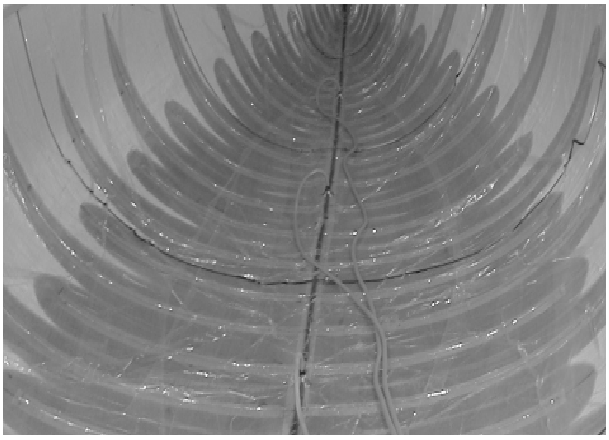

Fig.20: Resin infusion in a hull

- Post-Curing: The mechanical properties of a cured resin and thus the whole product depend on the degree of cure and the integrity of cross-linking of thermoset resin systems. A post-cure at elevated temperatures can lead to considerable increase in strength and elongation properties.

- Pre-pregs / Autoclave: Probably the most expensive method of consolidating and curing laminates is that of using an autoclave. Unlike a regular vacuum, where the atmospheric pressure of 1 bar cannot be exceeded, an autoclave allows higher pressures. Often pressures of 4-6 bar are obtained consolidating the laminate. Fibre alignment is straighter, void inclusions are reduced and resin ratio by volume can be as low as 35%, providing the best overall mechanical properties, before getting too dry. The pressurization is combined with a temperature assisted curing cycle, which is often tailored to the used resin and computer-controlled. This method is reserved for pre-pregs and limited size components. The use of cores is restricted to cores not containing air. Typical components to be cured in autoclaves are masts for sailing yachts. There are autoclaves of more than 40 m length available at many mast manufacturers.

6. Composite properties compared with steel and aluminium

If (mechanical) properties of composites are compared to those of steel and aluminium, there is the risk not being objective. These materials are so different and the base of a comparison must be clearly defined. For example, one should compare typical structural functional elements rather than the materials themselves. However, even that is difficult, because the structural set-up and the way of how a structural element works are different; and the physical nature of metals and composites requires different safety margins in design. Where with some technical applications weight is not critical and it might be alright to look at absolute values of stiffness or strength, often optimising strength and stiffness includes a look at the structural weight; a view at the specific properties might be more revealing. If weight of structures is critical, the benefits of composite materials arise, simply because structures can be much lighter for same strength and also stiffness, however at greater labour and material cost. Besides strength and stiffness, metals and composites differ widely when aspects such as degradation modes, robustness or maintenance are looked into.

Mechanical properties of composites can be tailored for given load paths by aligning fibres in force directions. For pure tensile elements (e.g. sailboat rigging), all fibres can be aligned in one direction, providing maximum tensile strength and stiffness. For most other marine components, it is common to find a compromise, where fibres are laid in multiple directions, with or without prioritizing one main direction. Often off-main axis properties must fulfil particular structural functions also. Different fibre types and fabric types can be utilized to suit particular needs. If no particular directional properties shall be obtained, fibres can be aligned such that the in-plane properties are constant in all directions ("quasi-isotropic"). To achieve this, the same numbers of fibres need to be arranged in three different directions ("triaxial", 33.3% 0°, 33.3% 60°, and 33.3% 120°). Most often however, marine structure laminates are arranged such that four different basic fibre directions are allocated, 0°, ±45° and 90°. For example, typically, a carbon mast has the following fibre fractions in those directions: 60% 0°, 30% ±45°, 10% 90°.

In the following, base the comparison of strength and stiffness on a small coupon or sheet. Fig.21 shows the significant density/weight differences between various materials. Fig.23 and 24 compare the tensile strength in different ways. The absolute strength values are related to material densities to pinpoint how effective the materials are when weight matters. Further, more related to design purposes, the allowable values (derived from GL Rules for typical structural hull components) are compared. While most other relevant strength properties (such as bending strength or compressive strength) are similar, big gains in strength and stiffness are obtained in sandwich laminates, Fig.22.

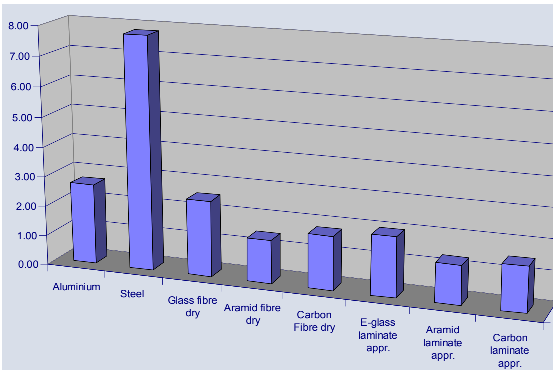

Fig.21: Density of various materials [kg/m^3]

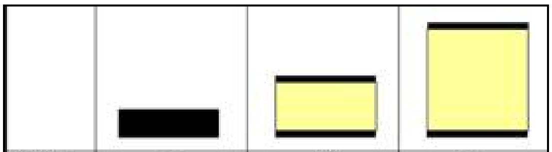

overall	t	2t	4t
Relative Stiffness	10	70	370
Relative Strength	10	33	850
Relative Weight	10	10.4	11.4

Fig.22: Bending stiffness and strength; sandwich effect

	Absolute ultimate tensile strength	Specific ultimate tensile strength
	[Mpa]	[Mpa*m3/to]
Aluminium 6061 T5 unwelded	260	100
Aluminium 6061 T5 welded	155	60
Mild Steel	450	58
Nitronic 50, high strength Stainless steel	1350	173
E-Glass Chopped Strand mat	123	62
E-Glass quasi-isotropic	232.5	116
E-Glass Laminate 60/30/10	339	170
T300 Carbon Laminate Quasi-isotropic	520	347
T300 Carbon laminate 60/30/10	860	573
M40J Carbon laminate 60/30/10	1050	700

Fig.23: Absolute tensile strength / specific absolute tensile strength (related to density)

	Allowable tensile strength per GL Rules	Specific allowable tensile strength per GL Rules
	[Mpa]	[Mpa*m3/to]
Aluminium 6061 T5 unwelded	118	45
Aluminium 6061 T5 welded	63	24
Mild Steel	150	19
Nitronic 50, high strength Stainless steel	483	62
E-Glass Chopped Strand mat	28.7	14
E-Glass quasi-isotropic	54.25	27
E-Glass Laminate 60/30/10	79.1	40
T300 Carbon Laminate Quasi-isotropic	130	87
T300 carbon laminate 60/30/10	215	143
M40J carbon laminate 60/30/10	262.5	175

Fig.24: Allowable tensile stress / specific allowable tensile stress (related to density

The off-axis stiffness and strength properties for non-quasi-isotropic composites vary from the given values. This variance increases the more emphasis is given on single fibre directions. Fig.25 illustrates the distribution of the in-plane tensile stiffness of carbon laminates for different orientation fractions. The through-thickness properties of composites add another dimension to the matrix of complex behaviours. Where metallic materials in general can be assessed as completely isotropic in all directions, through-thickness stiffness and particularly through-thickness strength of composites need to be considered when designing composites.

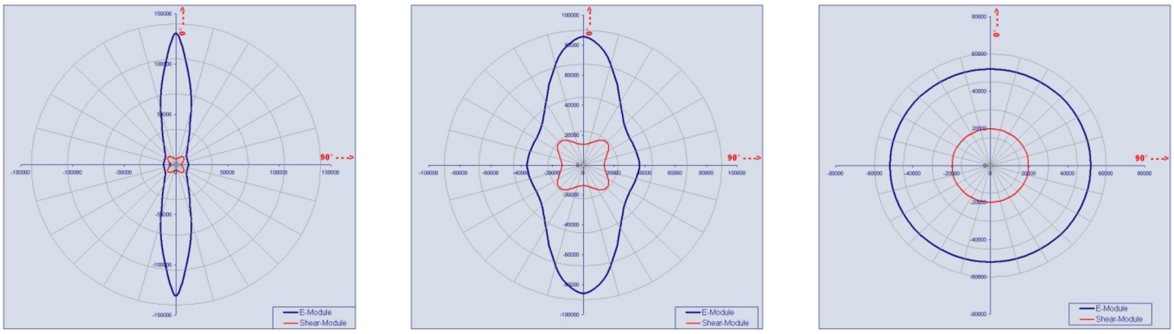

CRP 100/0/0 (%0°/±45°/90°) CRP 60/30/10 CRP 25/50/25 (quasi-isotropic)

Fig.25: In-plane tensile and shear stiffness of different carbon laminates (at different scale)

7. Failure and damage modes

7.1. Local failure modes

The main local failure modes are:

- Micro-cracking: “Ultimate strength” denotes the loading at which a structure or material completely fails. Before this final failure, mainly by the rupture or a collapse of the reinforcement fibres, composites suffer a premature partial damage: pre-stress in cured resin (i.e. microscopic stress concentration due to different fibre alignments) results in microscopical cracks which spread out through the resin matrix. As long as the load level is kept at certain magnitudes, this micro-cracking does not lead to premature ultimate failure, but can be considered as “aging” or fatigue. The susceptibility to this phenomenon depends on the resins; epoxy resin is much tougher than polyester resin and less prone to micro-cracking, thus aging.

- Fatigue: Fatigue in composites is mainly initiated in the composite matrix. Fatigue in composites occurs at different microscopic and macroscopic levels, including resin micro-cracking, delamination, fibre breakage and interfacial debonding, *Scott (1973)*. The failure mechanisms are very complex due to the highly anisotropic characteristics of composites. In fact, the complexity of composite fatigue has led some industries to be somewhat reluctant to use composites, *NN (2010)*. Fatigue prediction in design is common nowadays in the windmill industry, but done hardly at all in the marine industry. Thus, conservative design is required to avoid fatigue problems. Still, fibre reinforced polymer composites in general perform superior to metals in fatigue, if well designed. A fatigue threshold for a commonly used carbon/epoxy composite can be as high as 70% of the static strength under constant amplitude cyclic loading, *NN (2002)*.

- Water absorption: The polymer matrix of marine composites is prone to moisture absorption in typical humid or wet marine atmosphere. The absorption occurs on a molecular level, i.e. individual water molecules enter the polymer matrix network. When a composite is placed in water or in a humid environment, water molecules will diffuse into the plastic because they are small enough to pass through the spaces between the relatively large polymer molecules. The rate and the amount of absorption depend on the resin system, temperature and ambient humidity. Epoxy is less prone to absorption of moisture than polyester and vinyl-ester resins. Associated with the take up of moisture is the drop in strength. Where epoxy suffers only little degradation, polyester, due to its chemical constituency, degrades more. Water absorption can reach up to over 4% and interlaminar shear strength can reduce up to 60% of the original value.

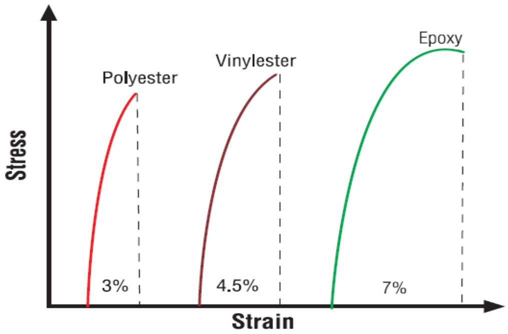

Fig.26: Typical Resin stress/strain curves, [source: www.gurit.com]

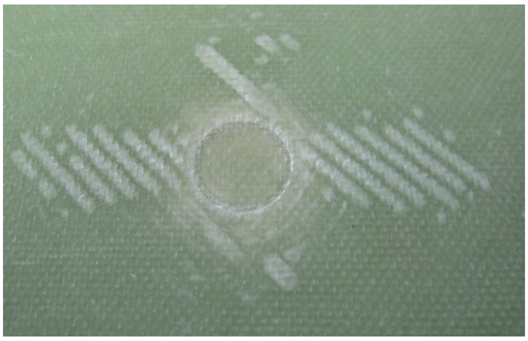

Fig.27: Surface impact with subsurface damage

- Impact: The ability of composite structures to resist or tolerate local impact damage depends strongly on the constituent resin, fibre material and the material form. The properties of the resin matrix are most significant and include its ability to elongate and to deform plastically. The area under a resin's stress-strain curve indicates the material's energy absorption capabilities, Fig. 26, *NN (2002)*. Local impact damage appears as a mixture of resin crushing, interlaminar shear failure, followed by delamination, Fig. 27. The extent of the damage imposed to a laminate depends on the laminate thickness; impact damage to very thin laminates may be more critical than to thick laminates. The macroscopic occurrence and consequences of damage are totally different to local damage in metals in form of dents and/or cracks.

- Corrosion: Galvanic corrosion may occur with carbon composites. Carbon fibres, consisting of graphite molecules, have very good electrical conductivity. Since graphite is rather "noble" on the electrode potential table, most metals corrode quickly, should the conductive circuit be closed between them. Also the carbon laminate itself suffers under galvanic current, as matrix materials are diffused by water molecules, making a through laminate thickness conductivity possible. The rate is lower by magnitudes lower than that of carbon fibres themselves. The result is a blistering of the matrix system, *Tucker and Brown (1999)*. Thus, metallic fittings must be insulated from carbon fibres. This is often done by installing fittings using a bedding compound or a separating layer of E-glass laminate. E-Glass has no electrical conductivity.

- Temperature: Temperature affects composites due to different thermal expansion of resin and fibre and because a resin is always associated with an upper temperature limit, above which a cured resin abruptly softens. This softening impacts several properties of the resin. There are significant drops in mechanical stiffness and strength. The “glass transition” is a reversible change-over from a hard and relatively brittle state into a molten or rubber-like state or vice-versa. This change in viscosity is not accompanied by a change in the material structure, though. It typically occurs in a temperature range of 10 to 30 degrees. For polyester resins the glass transition temperature (T_g) typically is between 65°C to 90°C, for epoxies above 50°C (depending on the type of resin system and the required temperature cure cycle), for high-performance pre-preg resin systems up to 200°C. There are different expressions associated with the effect of glass transition, depending on the underlying motivation. The “heat deflection temperature” (HDT) is determined following the ISO 75 standard, allowing comparison of materials. This HDT occurs at the start of the softening and thus is of high practical relevance, especially if the service temperatures are known. Service temperatures in marine applications can easily reach 80°C due to sun radiation on dark surfaces, such as on black painted laminates or un-painted carbon.

- Lightning strike: Polymer Matrix composites have either almost no (E-Glass composites) or much less electrical conductivity (carbon composites) than metals. This leaves them with a great electrical resistance too low to conduct a lightning strike. Consequences of an unprotected laminate include possibility of vaporization of laminate resin in the proximity of a strike, including a possible burn-through of the laminate, Fig. 28. Structural laminates shall be completely protected against the event of a lightning strike by providing higher electrical conductivity paths lightning conductors.

Fig.28: Lightning burn-through on carbon mast Fitting

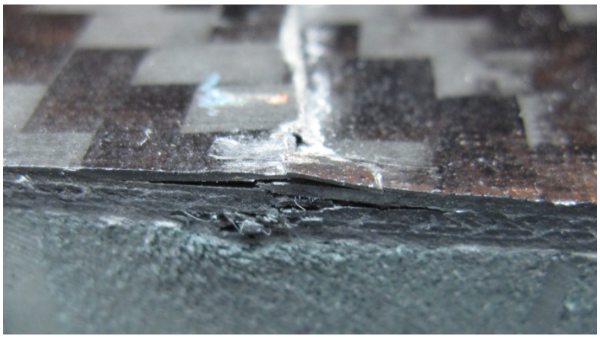

Fig.28: Face sheet failure in compression on a sandwich beam

7.2. Macroscopic failure and damage modes

Designing composite structures requires knowledge and insight to the pertinent failure modes of the material. Generally made from two different materials, fibre and resin, combined in a multiple ply arrangement, it is of utmost importance to be aware how this arrangement interacts and where its weaknesses are. This section concentrates on macroscopic strength and stiffness driven failure and damage modes.

Stiffness driven failures can be buckling of structural components, very similar to buckling in steel structures, but more complex in the analysis. Sandwich skins, lacking sufficient lateral support from the core material, can fail under compressive loads by buckling. This is called “face-wrinkling”. Buckling on a more microscopic level can occur when the lateral support of the stabilising resin is not sufficient and single fibres buckle.

Strength driven failures occur when ultimate strength is exceeded. This category encompasses different strengths of a laminate and has to be subdivided into fibre-related and matrix-related strength properties.

Typical failures, due to poor design or poor construction, are:

- Tensile failures: The tensile capacity of a laminate is best characterised by the strain-to-failure of the load carrying fibres, i.e. fibres/fibre plies running parallel to the applied tensile load. The tensile capacity is not very sensitive to laminate quality. Ultimate tensile stress/strain can be predicted fairly easily.

- Compressive failures: Often the compressive strength of a laminate is lower than the tensile strength, particularly with carbon laminates. Compressive failure involves the toughness of the resin supporting the fibres in a straight column. Sandwich laminates in bending are often designed against one face sheet in compression, Fig. 29.

- Bending failures: Special consideration to individual composite characteristics shall be paid when designing sandwich subjected to bending caused by out-of-plane loads. Not only the sandwich skins are loaded in compression and tension, but also the sandwich core fulfils a function of transferring shear forces across, causing shear stresses in the core. Being made of relatively light materials, a typical damage mode of sandwich laminates is shear failure of the core, Fig. 30. This makes the sandwich structure ineffective and bending on the face skins might become excessive without the shear connection provided by the core.

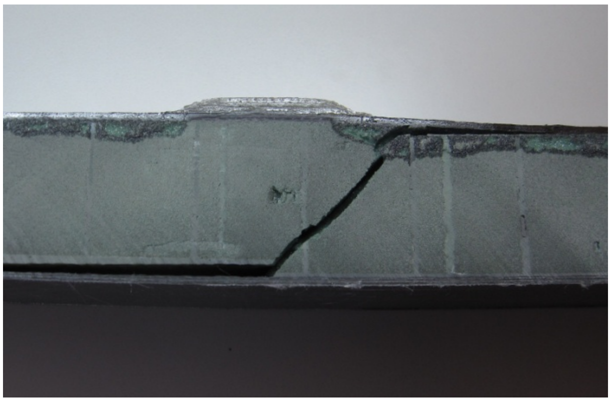

Fig.30: Typical sandwich core shear failure

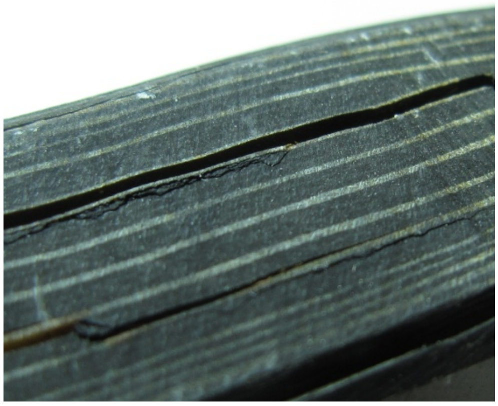

Fig.31: Interfacial delamination

- Shear failures: Apart from core shear, shear failure may occur at layer interfaces. For shear loads, the matrix plays a major rule, as it keeps the layers from sliding over each other. The resin shall not only be strong enough but also needs to have good adhesive properties. Interlaminar shear cannot always be totally avoided and leads to disintegration of laminates.

- Skin Wrinkling: The buckling phenomenon of skin wrinkling is not necessarily non-recoverable, but is associated with loss of stiffness and thus may cause unacceptable deflections, an increase in structural loading. This may be followed by a resin- or fibre-dominated failure. Skin wrinkling occurs with rigid foam cored sandwich laminates, if the support of the core for the skins loaded in compression is not sufficient and the core shear modulus too low so that a buckling of the skin occurs into the foam. For honeycomb sandwiches with very thin skin faces, this buckling can occur between honeycomb cell walls.

- Delamination: Delamination (loss in contact between layers of a laminate) can be initiated by excessive interlaminar shear stresses or poor adhesion between layers, Fig. 31. Delamination can also occur due to concentrated in-plane shear stresses and/or high through-thickness stresses, e.g. on free laminate edges, tapered laminates (ply drops), bonded joints or drilled holes. “Peel stresses” in excess of the through thickness strength of a laminate cause these failures and are one of the important basic aspects to consider when designing in composites.

8. Analytical engineering with composites

We illustrate the procedure for a specific example: Structural analysis of hull shell plating made of sandwich composites under lateral design pressure. The analysis procedure involves three main steps:

1. “Rule of mixture” and laminate theory yield the stiffness properties of the panel.
2. Plate theory provides stresses and strains in the sandwich panel und lateral design pressure.
3. Assessment of the safety margins required for various stress/strain states.

This approach is featured by relevant Germanischer Lloyd Rules and will be discussed in the following.

8.1. Rule of mixture and classical laminate theory

Starting on the fibre/resin level to make a ply analysis, the properties of a multiply layer followed by the panel properties will be derived. Representative and realistic panel stiffness is crucial since this determines how loads are carried by the structure.

It is straight-forward to compute the elastic moduli of a laminate ply containing unidirectional fibres. The Rule of Mixture is used, in which the individual elastic moduli of resin and fibre are combined using the fibre/resin volume ratio:

Longitudinal Young’s modulus: $$E_{11} = \phi \cdot E_{fL} + (1-\phi) \cdot E_m$$

Transverse Young’s modulus: $$E_{22} = \frac{E_m}{1-\nu_m^2} \cdot \frac{1+0.85 \cdot \phi^2}{(1-\phi)^{1,25} + \phi \cdot \frac{E_m}{E_{fT} \cdot (1-\nu_m^2)}}$$

Poisson’s ratios: $$\nu_{12} = \phi \cdot \nu_{f12} + (1-\phi) \cdot \nu_m ; \quad \nu_{21} = \nu_{12} \cdot \frac{E_{22}}{E_{11}}$$

Shear modulus: $$G_{12} = G_m \cdot \frac{1+0.8 \cdot \phi^{0.8}}{(1-\phi)^{1.25} + \frac{G_m}{G_{f12}} \cdot \phi}$$

ψ = mass content of reinforcing material in laminate

φ $= \dfrac{\psi}{\psi + (1-\psi)\cdot(\rho_f / \rho_m)} =$ volume content of reinforcement material in laminate

ρ_f = specific gravity of fibre material

ρ_m = specific gravity of matrix material

E_{fL} = Young's modulus of fibre in fibre direction

E_{fT} = Young's modulus of fibre transverse to fibre direction

E_m = Young's modulus of matrix

ν_{f12} = Poisson's ratio of fibre

ν_m = Poisson's ratio of matrix

G_m $= \dfrac{E_m}{2\cdot(1+\nu_m)}$ = shear modulus of the matrix

G_f = shear modulus of the fibre

To obtain compute the stiffness properties in all directions of a multiply laminate containing layers with fibers oriented in various directions, the classical laminate theory (CLT) is employed. Because the interaction of plies within a laminate, oriented in different directions and stacked in individual ways, is manifold, the relation between applied load and the response of the structure can only be handled with setting up a so-called ABD matrix, a 6x6 matrix containing individual stiffness values. This matrix contains stiffness properties and relations and provides the missing link between sectional loadings and the response of a structure. If a laminate layup for example is not symmetrical about its mid-plane, a pure tensile load on a flat sheet not only causes tensile deflection, but could also result in bending or twist. For relatively thin skins of a sandwich laminate, those coupling effects can be neglected. Thus, only those coefficients from this "ABD" matrix ("A" for extension terms, "B" for coupling terms and "D" for bending terms) are utilized, which contain relations to cover extension and bending terms, the coupling coefficients "B" are set to 0. The matrix is inverted yielding:

$$\begin{bmatrix} a11_L & a12_L & a13_L & 0 & 0 & 0 \\ a21_L & a22_L & a23_L & 0 & 0 & 0 \\ a31_L & a32_L & a33_L & 0 & 0 & 0 \\ 0 & 0 & 0 & d11_L & d12_L & d13_L \\ 0 & 0 & 0 & d21_L & d22_L & d23_L \\ 0 & 0 & 0 & d31_L & d32_L & d33_L \end{bmatrix} = \begin{bmatrix} a & b \\ b & d \end{bmatrix}_L = \begin{bmatrix} A & B \\ B & D \end{bmatrix}_L^{-1}$$

This ABD_L is used to compute the individual engineering constants of a laminate which will be used for the analytical sandwich panel analysis:

$$E_x = \frac{1}{t\cdot a11_L} \qquad E_y = \frac{1}{t\cdot a22_L} \qquad G_{xy} = \frac{1}{t\cdot a33_L} \qquad \nu_{xy} = -\frac{a12_L}{a11_L}$$

In the following, the structural design requirements for laterally loaded shells and plates are given. Lateral loading is usually caused by static or dynamic sea or water pressure (slamming) of hull shells, decks, superstructure, watertight bulkheads, tank walls, etc. The methodology presented here covers flat or slightly curved panels of generally square or rectangular geometry with different boundary conditions, Fig.32. Other geometries (e.g. triangular or trapezoid styled) require an equivalent approach.

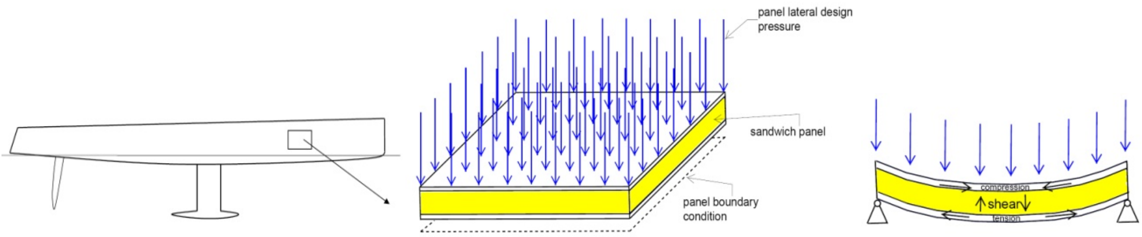

Fig.32: Flat or slightly curved panel considered

8.2. Plate theory

Elasto-mechanical properties of inner and outer sandwich skin should not differ significantly, in order to avoid secondary effects, such as superimposed twist or bending of plates. The following gives the ideas and the background of the "plate theory", established from *Young and Budynos (2001)*. The objective is to determine plate stresses and strains from plate bending moments and plate shear forces converted from a lateral pressure force. Within plate theory, the two-dimensional all-side supported panel is reduced effectively to a one-dimensional unit beam strip with appropriate coefficients. The evaluation of stresses/strains focuses on the spot where the maximum bending stress/strain occurs and a spot where the maximum through-thickness shear stress/strain occurs. A correction allows the use of orthotropic material and plate properties and the application to sandwich construction. Required parameters to perform such analysis include:

- Structural parameters
  EI_x = panel bending stiffness about panels global y-direction
  EI_y = panel bending stiffness about panels global x-direction
  t_c = thickness of sandwich core
  z_i = vertical distance from the neutral axis in bending

- Geometrical parameters
  s_x = unsupported span in global x-direction
  s_y = unsupported span in global y-direction

- Boundary conditions: All edges fixed or all edges simply supported.

- Load details and design pressures
  Lateral design pressures (for example according to GL Rules and Guidelines).

- Geometric aspect ratio $ar_g = \frac{s_x}{s_y}$

Effective aspect ratio

For orthotropic panel properties with $EI_x \neq EI_y$, the aspect ratio ar_g is corrected to fit simple plate theory:

$$ar_{corr} = ar_g \cdot \sqrt[4]{\frac{EI_y}{EI_x}}$$

The corrected aspect ratio ar_{corr} has to be related to the span of the panel that is considered to be effective to take up the major bending and shear loads, the "effective span" s_{eff}. The effective span (direction of main load take-up) runs in *y*-direction. For $ar_{corr} < 1$, $ar_{eff} = 1 / ar_{corr}$, i.e. the panel effective span runs in *x*-direction.

- Plate curvature
  Membrane effects occurring due to curved shells are treated with a linear reduction coefficient. Further contributions due to membrane effects, e.g. calculated by finite element analyses (FEA) or other methods, will generally not be accepted. Curvature will only be considered if the plate is curved in the direction of the effective span s_{eff}. The plate curvature correction coefficient is then:

$r_c = 1.15 - \left(5 \cdot \frac{h}{s_{eff}}\right)$ with $0.03 < \frac{h}{s_{eff}} < 0.1$ and $r_{c,min}$ = 0.65

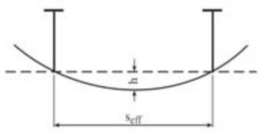

- Maximum bending moment, shear force and lateral deflection of panel
  The calculation is reduced to the assessment of a panel strip of unit width. Tables II and III give the coefficients required for the calculation. Maximum bending moment M_{b-max}, the maximum shear force F_{q-max}, and the maximum lateral deflection z_{max} are computed as follows:

$$M_{b-\max} = \frac{\beta \cdot p_d \cdot s_{eff}^2}{6} \cdot r_c$$

$$F_{q-\max} = \gamma \cdot p_d \cdot s_{eff}$$

$$z_{\max} = \frac{\alpha \cdot p_d \cdot s_{eff}^4}{12 \cdot EI_{eff}}$$

α	= see Tables II and III
β	= see Tables II and III
γ	= see Tables II and III
EI_{eff}	= plate bending stiffness relevant for the direction of the effective panel span
p_d	= lateral design pressure on associated plating.
s_{eff}	= effective panel span
r_c	= curvature correction coefficient

The maximum shear force reaction, occurring as a line force, emerges at the centre of the panel edges which are adjacent to the effective panel span. Should a sandwich panel be constructed using a core with different shear strength properties in different directions (honeycomb), the “secondary” maximum shear reaction line force $F_{q\text{-}sec}$ has to be determined. This force occurs at the panel edges spanning alongside the effective span.

$$F_{q-\mathrm{sec}} = \gamma_t \cdot p_d \cdot s_{eff}$$

γ_t = see Tables II and III

Table II: Plate coefficients for panel with all sides simply supported

ar_{eff}	1	1.2	1.4	1.6	1.8	2	3	4	5	∞
B	0.2874	0.3762	0.4530	0.5172	0.5688	0.6102	0.7134	0.7410	0.7410	0.7476
A	0.0444	0.0616	0.0770	0.0906	0.1017	0.1110	0.1335	0.1400	0.1417	0.1421
G	0.4200	0.4550	0.4780	0.4910	0.4990	0.5030	0.5050	0.5020	0.5010	0.5000
g_t	0.4200	0.3850	0.3620	0.3490	0.3410	0.3370	0.3350	0.3380	0.3390	0.3400

Table III: Plate coefficients for panel with all sides clamped

ar_{eff}	1	1.2	1.4	1.6	1.8	2	∞
b	0.3078	0.3834	0.4356	0.4680	0.4872	0.4974	0.5000
a	0.0138	0.0188	0.0226	0.0251	0.0267	0.0277	0.0284
g	0.4200	0.4550	0.4780	0.4910	0.4990	0.5030	0.5000
g_t	0.4200	0.3850	0.3620	0.3490	0.3410	0.3370	0.3400

- Determination of laminate strains and stresses
  The structural performance of a laterally loaded plate is characterized by the strains in the laminate. Strains at a distance of z_i from the plate’s neutral axis follow from:

$$\varepsilon_i = \frac{M_{b-\max} \cdot z_i}{EI_{eff}}$$

  The maximum strains through bending moments usually emerge at the outer surfaces of a composite. Hence, for evaluating the maximum strains, use the maximum distances from the neutral axis at each side of the plate. The calculated strains may not exceed the allowable strains as per Rules definition. Apart from the pure bending strains, stability issues such as skin wrinkling need to be considered.

The through-thickness interlaminar stress is design critical for lower density/strength cores in sandwich structures. The core has to transmit the through-thickness shear forces. A certain contribution by the skins is assumed. Core shear stress is calculated as being:

$$\tau_c = \frac{F_q}{t_c + \frac{t_{s1}}{2} + \frac{t_{s2}}{2}}$$

F_q = shear force

= $F_{q\text{-}max}$ for core evaluation along effective panel span

= $F_{q\text{-}sec}$ for core evaluation across effective panel span

t_c = core thickness

t_{s1}, t_{s2} = thickness of skins

8.3. Evaluation of safety margins

The above obtained results need safety margins. Safety margins cover uncertainties in load assumptions and variability of material properties (initially and after curing due to various production methods). Safety margins within GL Rules for boats made of composites categorize as follows:

- Safety margin for laminates is defined as a maximum allowable strain.
- Safety margin for sandwich cores is defined as a safety factor against ultimate shear strength.
- Safety margin for maximum deflection is to guarantee the validity of first principles in engineering analyses.

9. Numerical engineering with composites

The most important differences in finite element analyses (FEAs) between composites and isotropic materials (like steel) concern the more complex input and output. Main additional input parameters include:

- Number of layers
- Thickness of layers
- Orientation of layers
- Elasto-mechanical properties of layers

This input needs to be defined for each laminate used. For some applications, more material characteristics are required, e.g. strength properties. In modern FEA pre-processors, the required conversion to a complete stiffness matrix is automatically generated from the above input. The FEA itself is fairly similar, offering the usual options, but FEAs for composites require more memory space.

The output is similarly complex as the input. The design engineer must then focus on the important issues. Employing suitable failure criteria, such as those of Puck or Tsai Wu, *Robert M. Jones (1999),* the data deluge created by FEA can be condensed.

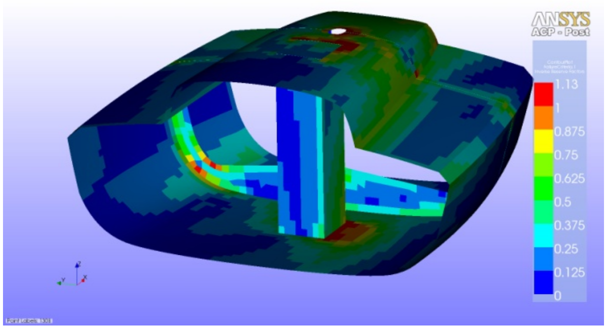

Fig.33: FEA for composite structure
Yacht
[Source: EVEN AG]

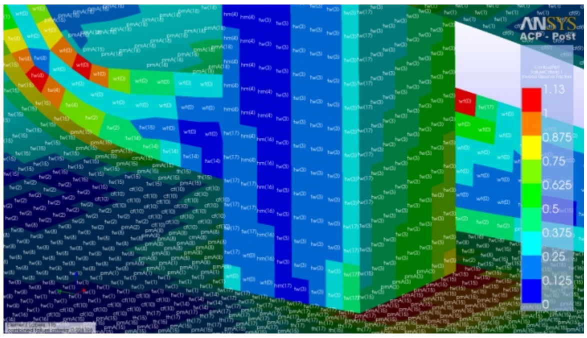

Fig.34: Failure mode evaluation of racing

Exemplarily presenting the complexity of numerical evaluation of composites is the relatively simple structural design of a 40 ft sailing yacht, Fig.33. The output presented in Fig. 34 is a summary of results presenting the inverse reserve factors for the most probable failure mode for each finite element. The variety of criteria typically referred to during numerical analysis [source: ANSYS Composite Prep-Post] include:

- Maximum Strain. Failure modes: *e1t, e1c, e2t, e2c, e12*
- Maximum Stress: *s1t, s1c, s2t, s2c, s3t, s3c, s12, s23, s13*
- Tsai-Wu 2D and 3D: *tw*
- Tsai-Hill 2D and 3D: *th*
- Hashin: *hf* (fiber failure), *hm* (matrix failure), *hd* (delamination failure)
- Puck (simplified, 2D and 3D Puck implementations are available): *pf* (fiber failure), *pmA* (matrix tension failure), *pmB* (matrix compression failure), *pmC* (matrix shear failure), *pd* (delamination)
- LaRC (2D): *lf* (fiber failure), *lmt* (matrix failure: tension), *lmc* (matrix failure: compression)
- Cuntze 2D and 3D: *cft* (fiber tension failure), *cfc* (fiber compression failure), *cmA* (matrix tension failure), *cmB* (matrix compression failure), *cmC* (matrix wedge shape failure)
- Sandwich failure criteria
  - Wrinkling: *wb* (wrinkling bottom face), *wt* (wrinkling top face)
  - Core Failure: *cf*
- Isotropic failure criteria - Von Mises: *vMe* (strain) and *vMs* (stress)

Terms:

- *e* = strain, *s* = stress
- *1* = material 1 direction, *2* = material 2 direction, *3* = out-of-plane normal direction, *12* = in-plane shear, 13 and *23* = out-of-plane shear terms
- *I* = principal I direction, *II* = principal II direction, *III* = principal III direction
- *t* = tension, *c* = compression

Structural evaluations using numerical methods require a thorough understanding not only of the behavior of composites but also a highly educated overall view in engineering in order to be able to do the interpretation of results correctly and appropriately.

References

BERTRAM, V.; HOFFMEISTER, H.; MÜLLER, S.; MOLTSCHANIWSKYJ, A. (2010), *Technological challenges for construction and classification "Tûranor PlanetSolar"*, 7th Int. Conf. on High-Performance Marine Vehicles (HIPER), Melbourne, pp. 76-85.

JONES, R.M. (1999), *Mechanics of Composite Materials*, Taylor & Francis

NN (2010), *Fatigue Life Prediction in Composite Materials*, Firehole Composites

NN (2002), *Polymer Matrix Composites Vol. 3*, Dept. of Defence Handbook; MIL-HDBK-17-3E

SCOTT, R.J. (1973), *Fibreglass Boat design and Construction*, 2nd Ed., SNAME

TUCKER, W.; BROWN, R. (1999), *Galvanic Blisters in Carbon Fibre Laminates,* Professional Boatbuilder 57:30

YOUNG, W.C.; BUDYNAS, R.G. (2001), *Roark´s Formulas for Stress and Strain*, McGraw-Hill

Design Improvement for a Fast Rigid-Inflatable Boat using CFD

Jan Kaufmann, Ould El Moctar, Volker Bertram, FutureShip GmbH, Hamburg/Germany
{{jan.kaufmann;ould.el-moctar;volker.bertram}@GL-group.com

Abstract

Modern computational fluid dynamics simulations were applied to a rigid-inflatable boat to predict the thrust requirements as function of longitudinal centre of gravity (LCG). After analyzing the results for the original hull, the design was modified reducing the required thrust by typically 40% for a large range of LCG values.

1. Introduction

Hard chine planing hulls represent the majority of pleasure craft, but are also widely used for military and civilian applications, e.g. as fast rescue boats. Despite their importance for the small craft market, there are few design tools for naval architects guiding hull design and power prediction. The classical design tools are all flawed:

- Analytical methods
  Analytical methods normally used to predict the boat's resistance and trim are based on variations of the Savitsky method. The Savitsky method is strictly speaking only applicable for monohedric hull shapes, i.e. variations of beam and deadrise angle cannot be taken properly into account.

- Systematic series
  There are several systematic series for planing hulls, but again the shape of real planing hulls has evolved and differs from those used in the series, making their application questionable.

- Model tests
  Model tests are too time consuming and costly for extensive parameter variations in design. Therefore most shipyards do not perform model testing in the design stage.

This makes detailed flow analyses using computational fluid dynamics (CFD) desirable for designers. However, the flow problem for planing hulls is particularly complex, due to spray, detaching flow at chines and transom sterns, breaking waves and strongly nonlinear interaction of resistance and dynamic trim and sinkage (or lift). Convincing free-surface CFD applications for planing hulls were first presented by the Italian CFD expert and boat designer Mario Caponnetto ten years ago, *Caponnetto (2000,2001),* both for planing hulls in steady motion and for planing hulls in waves, *Caponnetto (2002), Azcueta et al. (2003), Bertram et al. (2003).* The following decade brought assorted refinements in the computational techniques. Wider application in the boat industry is expected for the next decade. A typical design application is described in the following.

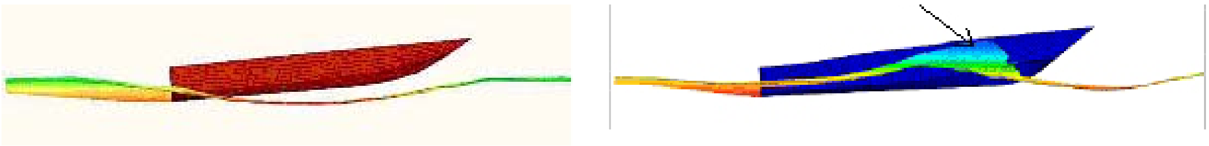

Fig.1: First CFD applications to planing hulls by Caponnetto, *Bertram et al. (2003)*

2. Work scope

A British client was tasked to design a paramilitary craft as rigid inflatable boat (RIB) driven by a waterjet. The first step was to evaluate the original design, predicting power (or thrust) requirements for a given speed and varying positions of the longitudinal centre of gravity (LCG). The LCG is a key parameter influencing trim, which in turn influences resistance and propulsive efficiency. Modern CFD simulations do not only predict the global values “trim” and “required thrust”, they also reveal detailed insight in the flow details, such as wave and spray formation and pressure distributions below the hull. These details are frequently the key to a better hull forms, combining design expertise and sophisticated flow analyses.

In a second step, the hull was modified to reduce the required thrust and re-analysed. The power requirements for given speed were typically reduced by 30% over a wide range of LCG values. The new design was thus substantially improved.

The analyses involved the following major steps:

- 3d CAD description of the hull as starting point for hull variations and grid generation
- Volumetric grid generation for the CFD analysis (for all hull variants)
- Time-domain CFD simulation for full-scale conditions computing dynamic trim and sinkage as part of the solution. The waterjet was modelled in a simplified way.
- Expert assessment of flow details for the original hull and re-design following the assessment.

Details of the analyses and the re-design are presented in the following.

3. Hydrodynamic analyses

3.1. Computational procedure

Reynolds-averaged Navier-Stokes equation (RANSE) solvers with interface-capturing techniques of the volume-of-fluid (VOF) type are suitable for handling two-phase flows with strong nonlinearities. Today, this kind of code is the obvious choice for computing complex free-surface shapes with breaking waves, sprays and air trapping, but also for flows involving cavitation.

The conservation equations for mass and momentum in their integral form serve as the starting point. The solution domain is subdivided into a finite number of control volumes that may be of arbitrary shape. The integrals are numerically approximated using the midpoint rule. The mass flux through the cell face is taken from the previous iteration, following a simple Picard iteration approach. The unknown variables at the centre of the cell face are determined by combining a central differencing scheme (CDS) with an upwind differencing scheme (UDS). The CDS employs a correction to ensure second-order accuracy for an arbitrary cell. A second-order central difference scheme (CDS) can lead to unrealistic oscillations if the Peclet number exceeds two and large gradients are involved. On the other hand, an upstream difference scheme (UDS) is unconditionally stable, but leads to higher numerical diffusion. To obtain a good compromise between accuracy and stability, the schemes are blended. Near the wall, the blending factor is chosen between 0.8 and 0.9. Pressure and velocity are coupled by a variant of the SIMPLE algorithm, *Ferziger and Peric (1996).* All equations except the pressure correction equations are under-relaxed using a relaxation factor 0.8. The pressure correction equations are under-relaxed using a relaxation factor between 0.2 and 0.4 for unsteady simulations, finding in each case a suitable compromise between stability and convergence speed.

The two-fluid system is modeled by a two-phase formulation of the governing equations. No explicit free surface is defined during the computations, and overturning (breaking) waves as well as buoyancy effects of trapped air are accounted for. The spatial distribution of each of the two fluids is obtained by solving an additional transport equation for the volume fraction of one of the fluids. To accurately simulate the convective transport of the two immiscible fluids, the discretization must be nearly free of numerical diffusion and must not violate the boundedness criteria. For this purpose, the high resolution interface capturing (HRIC) scheme is used, *Muzaferija and Peric (1998).* This scheme is a nonlinear blend of upwind and downwind discretization, and the blending is a function of the distribution of the volume fraction and the local Courant number. The free surface is smeared over two to three control volumes. Fluid structure interaction effects are presently not accounted for, i.e., the body is assumed to be rigid, and the fluid is assumed to be viscous and incompressible.

The nonlinear equations of the rigid body motions in two degrees of freedom (trim and sinkage) were solved in the time domain, taking into account all forces acting on the body. The position of the ship due to dynamic trim and sinkage is then successively updated, again computing the fluid flow for the new position until an equilibrium of all forces is reached.

3.2. Computational model

As a first step, a 3d CAD (computer aided design) model of the hull and waterjet was created, Fig.2 and Fig.3. The coordinate system was located at the lowest point, on the centre plane and the transom of the boat. The x-axis pointed forward, y-axis to port, and z-axis upwards. The CAD model served as starting point for the CFD grid generation. The grid was generated using the semi-automatic meshing software proam. The grid consisted of approximately 600000 volume cells, with local grid refinements in areas where high flow gradients were expected, near the bow and the waterjet, Fig.4.

The boundary conditions were as follows:

- Constant velocity (negative boat speed) at the upstream inlet of the computational domain
- Hydrostatic pressure at the downstream outlet of the computational domain
- No-slip boundary condition on the boat’s hull

A moving grid option allowed the boat to sink and trim freely, adjusting its position to achieve equilibrium of forces.

An internal velocity inlet was used as simplified model of the waterjet. The jet velocity was adjusted such that thrust and hull resistance were in equilibrium.

The load conditions were varied for 3 to 15 people on board, changing displacement and (vertical and longitudinal) centre of gravity. The longitudinal centre of gravity (LCG) was varied between 20% L_{oa} und 50% L_{oa}. The gyradius of the mass distribution was estimated based on experience for similar boats.

Fig.2: 3d CAD model of hull

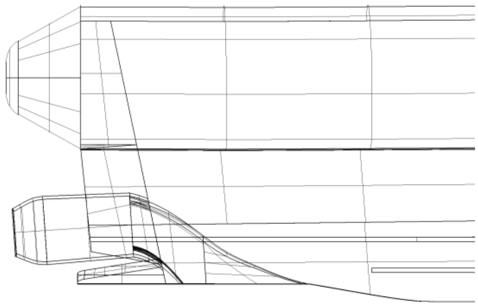

Fig.3: Waterjet geometry

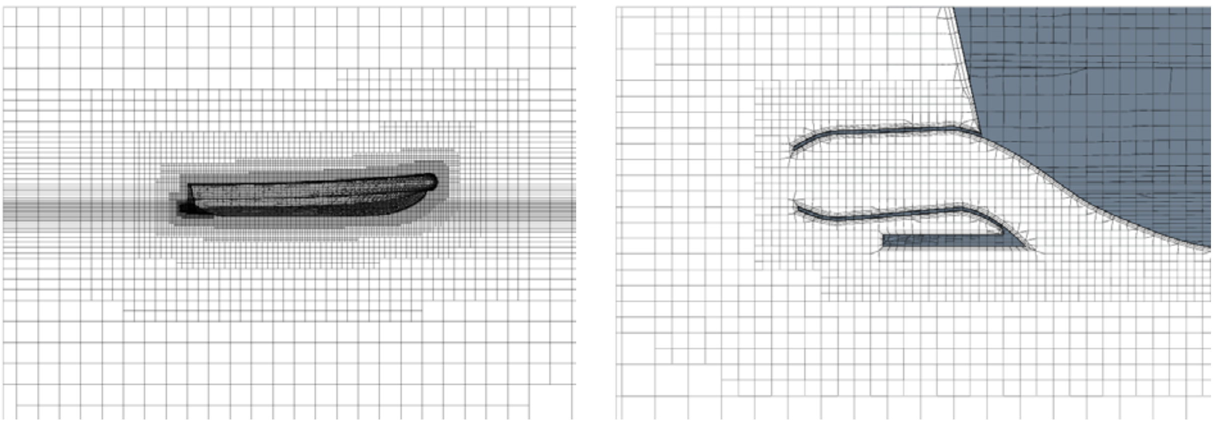

Fig.4: Grid for RANSE computation with detail zoom on waterjet region

4. Results

The hull was modified to reduce the required thrust for given speed for a wide range of LCG values. The following design measures were applied:

- Steeper deadrise in the bow region
- Flatter deadrise in the aft region
- Addition of spray rails
- Smoother transition of waterjet inlets

These modifications decreased the required thrust significantly for a wide range of LCG values, i.e. operational conditions, Fig.5.

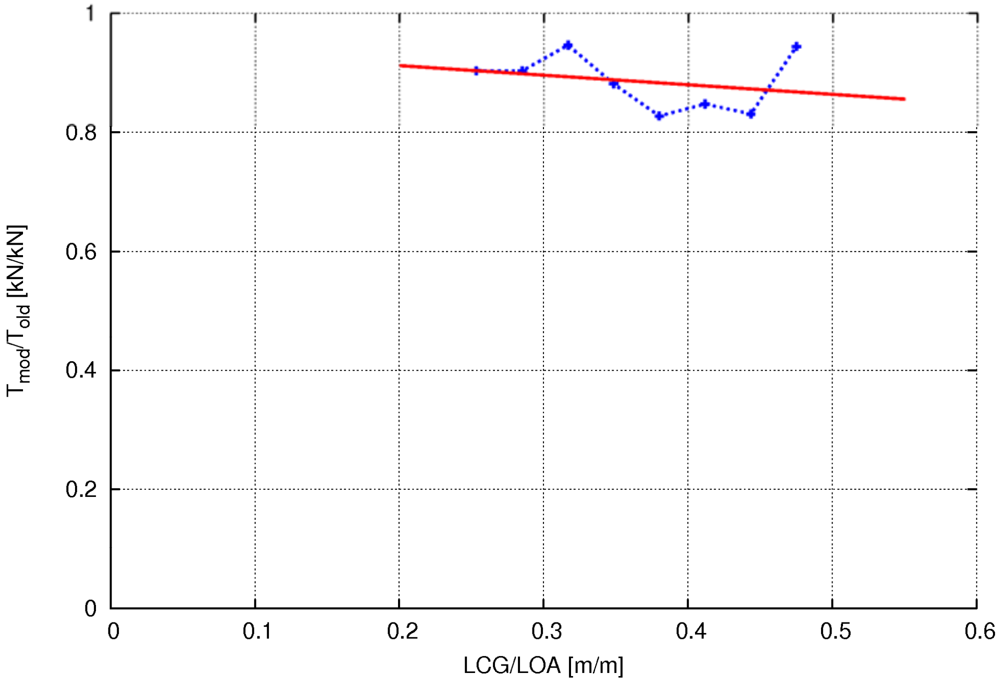

Fig.5: Required thrust ratio (new/old)

Typically, improvements of 10-12% were achieved in this case. The main underlying physical explanation is a higher dynamic lift and better trim angle, Fig.6, in the modified new hull shape. The smoother transition of the waterjet inlets reduced the pressure gradients, thus reducing the energy losses in the inflow to the waterjet, Fig.7.

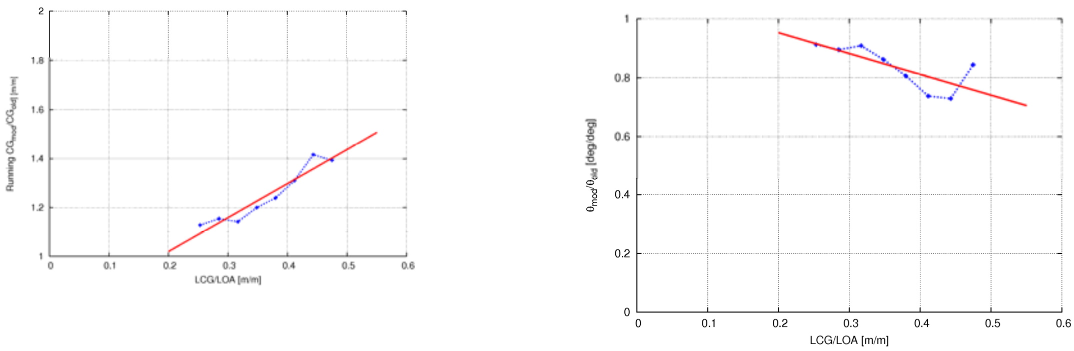

Fig.6: Ratios (new/old) for vertical translation of origin due to hydrodynamic lift (left) and running trim angle ratio (right)

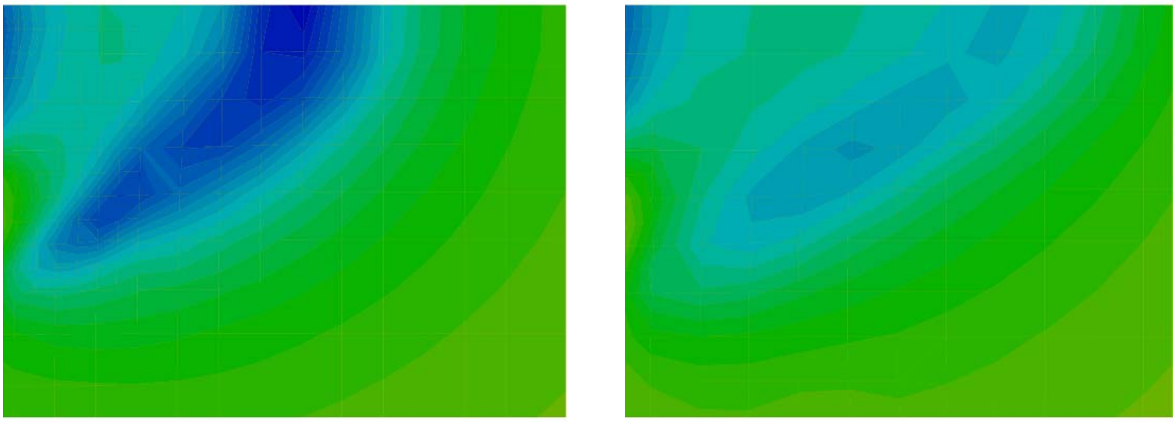

Fig.7: Pressure distribution at waterjet tunnel entry; original (left) and modified (right) design

5. Conclusion

Numerical flow simulations have matured to become a useful design tool also for planing boat designers. The simulations allow power prediction, but yield also detailed insight into the flow, thus guiding intelligent design decisions to improve the hydrodynamics. The application shown here were restricted to calm-water conditions, but similar time-domain simulations can assess also the nonlinear seakeeping behaviour of planing boats.

References

AZCUETA, R.; CAPONNETTO, M.; SÖDING, H. (2003), *Motion simulations for planing boats in waves,* Ship Technology Research 50/4, pp.182-198

CAPONNETTO, M. (2000), *Numerical simulation of planing hulls*, 3rd Numerical Towing Tank Symposium (NuTTS), Tjärnö
http://www.uni-due.de/imperia/md/content/ist/nutts_03_2000_tjaernoe.pdf

CAPONNETTO, M. (2001), *Practical CFD simulations for planing hulls*, 2nd Conf. High-Performance Marine Vehicles (HIPER), Hamburg, pp.128-138
http://www.caponnetto-hueber.com/Papers/Practical_CFD_simulations_for_planing_hulls_HIPER_2001.pdf

CAPONNETTO, M. (2002), *Sea keeping simulation of fast hard chine vessels using RANSE*, 5th Numerical Towing Tank Symposium (NuTTS), Pornichet
http://www.uni-due.de/imperia/md/content/ist/nutts_05_2002_pornichet.pdf

FERZIGER, J.; PERIC, M. (1996), *Computational Methods for Fluid Dynamics*, Springer

MUZAFERIJA, S.; PERIC, M. (1998), *Computation of free-surface flows using interface-tracking and interface-capturing methods*, Nonlinear Water Wave Interaction, Computational Mechanics Publ., pp. 59-100

Advanced Simulations for High-Performance Megayachts

Axel Köhlmoos, Volker Bertram, FutureShip, Hamburg/Germany,
{axel.koehlmoos;volker.bertram}@GL-Group.com

Abstract

An overview of simulations for assorted advanced analyses for megayachts is given, focussing on the benefit for the customer, i.e. how simulations support the business process of ship yard and ship owner. The analysis looks at the main operational problems such as ensuring comfort (noise, seakeeping, HVAC, smoke dispersion), increasing design freedom especially for unconventional designs, achieving better designs in shorter time, and ensuring fast and efficient trouble-shooting in case of need. The role of assorted advanced simulations (structure, noise & vibration, fluid dynamics, aerodynamics, etc) in this context is illustrated by case studies taken from industry experience. The importance of including appropriate simulations in the building specifications for optimal benefits for owner, yard and supplier are stressed.

1. Introduction

The word "simulation" is derived from the Latin word "simulare" which can be translated as "to reproduce" or "to mimic". According to VDI (Society of German Engineers), "simulation is the reproduction of a system with its dynamic processes in a running model to achieve cognition which can be referred to reality". The Oxford dictionary defines "to simulate" as "to imitate conditions of a situation or process", specifically "to produce a computer model of a process". In this sense virtually all computer models used in the design, construction or operation of ships would qualify as simulations.

The scope and depth of simulations guiding our decisions in design and operation of ships have developed very dynamically over the past decade. In previous publications, we have described in detail the scope and underlying techniques of simulations, e.g. *Fach (2006), Fach and Bertram (2006, 2009)*. These publications focussed on the technical aspects of simulation. In the present paper, we want to focus instead on the benefit of simulations from the customer's point of view. The "customer" may be the shipyard or the ship owner, buying services based on the special competence of simulation experts.

In such a customer-centric approach, simulations serve to support business processes through

- Ensuring comfort
- Increasing design freedom
- Achieving better designs in shorter time
- Ensuring fast and efficient trouble-shooting.

These items are discussed in the following sections in the context of large and unconventional yachts.

2. Ensuring comfort

Comfort is a key expectation for megayachts. Therefore, ensuring comfort (by suitable and reliable prediction methods) is an important issue in megayacht design. Simulations play a particular role in this aspect, as innovative and unusual designs appeal to customers, but pose risks as design cannot be based on experience as for conventional cargo ships. “Comfort” encompasses many aspects. The most important of which, from an engineering point of view, are discussed below.

Seakeeping is closely related to passenger comfort and, as such, is always an important topic for megayachts. For many seakeeping issues, linear analyses (assuming small wave height) are appropriate and frequently applied due to their efficiency. The advantage of this approach is that it is very fast and thus allows the investigation of many parameters (frequency, wave direction, ship speed, etc.). Non-linear CFD simulations are usually necessary for the treatment of extreme motions, particularly those involving slamming or green water on deck. These simulations require significant computer resources and allow only the simulation of relatively short periods (seconds to minutes). Combining intelligently linear frequency-domain methods with nonlinear time-domain simulations enables the respective strengths of each approach to be exploited, *Bertram and Gualeni (2011).* The approach starts with a linear analysis to identify the most critical parameter combination for a ship response. Then non-linear CFD analyses determine the design values of interest (motions, loads, speed loss in waves, etc.) for these critical cases. Such detailed analyses can lead to designs with considerably improved seakeeping behaviour and resulting benefits for passenger comfort, Fig.1.

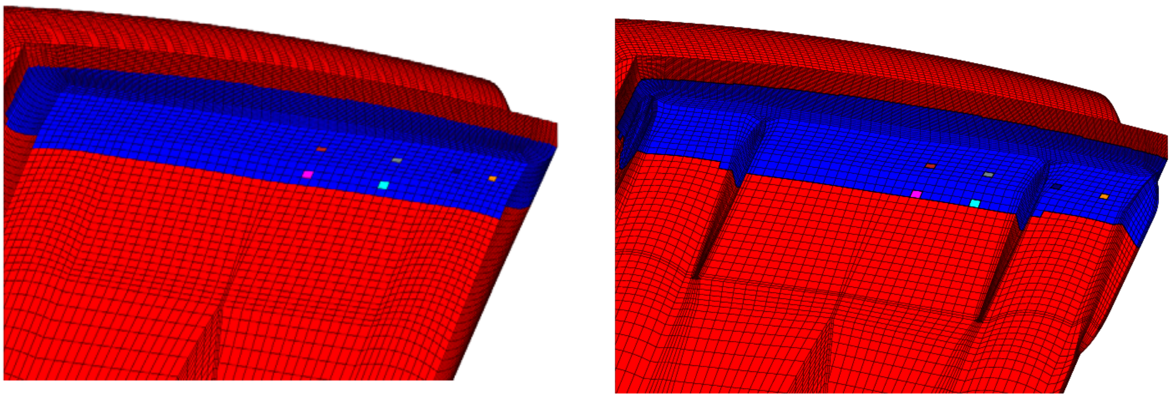

Fig.1: Megayacht stern with original design (left) and modified design for reduced slamming impact (right); slamming pressures were reduced by almost 30%

Fig.2: CFD simulation of smoke dispersion on megayacht

Aerodynamics play a role for megayachts, not so much for resistance, but for noise, smoke propagation, Fig.2, and local flow conditions on helicopter decks, sunbathing decks and similar locations, *Bertram et al. (2011)*. Although wind tunnel tests are still popular and widely used, CFD offers the advantage of overcoming scale effects which can be significant if thermodynamic processes are involved, *El Moctar and Bertram (2002)*. CFD can be coupled with formal optimisation for ship or funnel designs to minimize smoke dispersion on decks, Fig.3, *Harries and Vesting (2010)*.

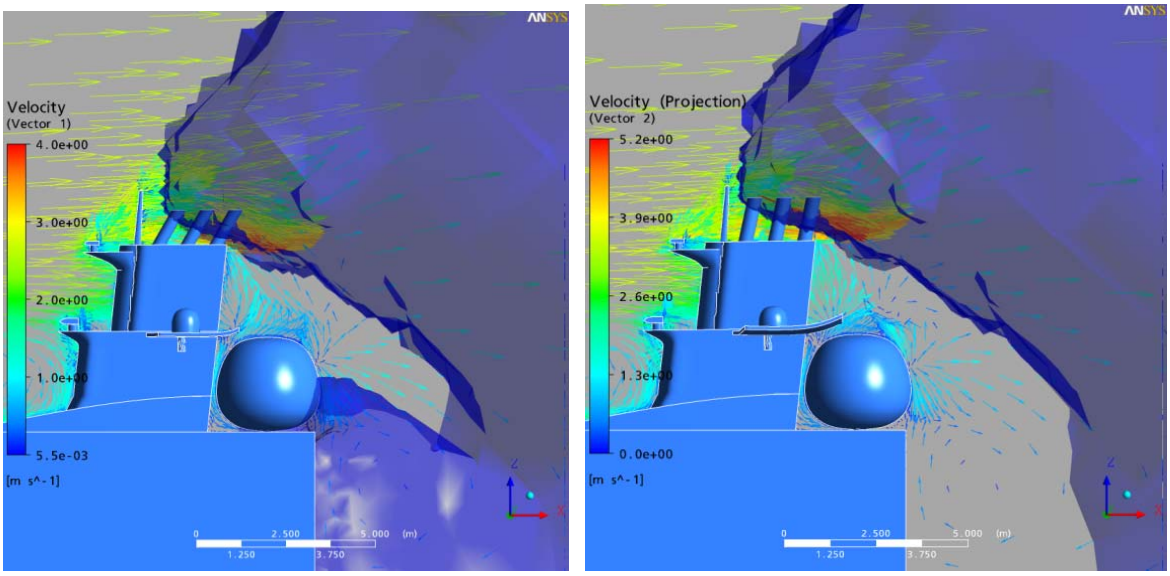

Fig.3: Funnel optimization for minimum smoke dispersion on megayacht

Ventilation systems are still largely designed based on simple estimates, often resulting in over-dimensioned and energy inefficient systems, sometimes in insufficient performance. CFD can guide more intelligent layout, based on reliable detailed insight.

Noise and vibration limits are standard parts of building specifications for megayachts. High comfort expectations are common and must be implemented at the earliest design stage of the project. With our software GL.NoiseFEM, we are able to trace and evaluate major structure-borne noise transmission paths, Fig.4, which helps to locate and economize areas for noise abatement measures. In the hands of experts, simulations yield reliable predictions as validated in detailed measurements, e.g. *Wilken et al. (2004)*. Most recently, underwater noise has also become an issue for megayachts. Our procedures to predict underwater noise were extensively validated in 2010, Fig.5. Underwater noise is expected to become a design issue for megayachts operating in environmentally sensitive regions, e.g. the Glacier Bay. The simulation tools to support design for low noise are already in place. In fact, simulations have become a standard tool to support designers in predicting vibration and noise levels.

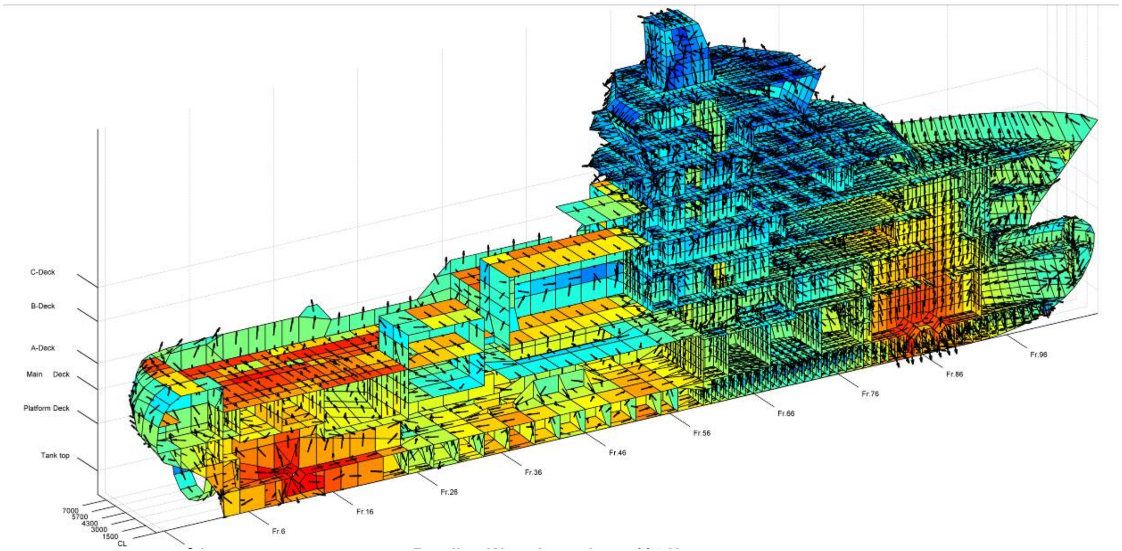

Fig.4: Noise simulation on offshore supply vessel

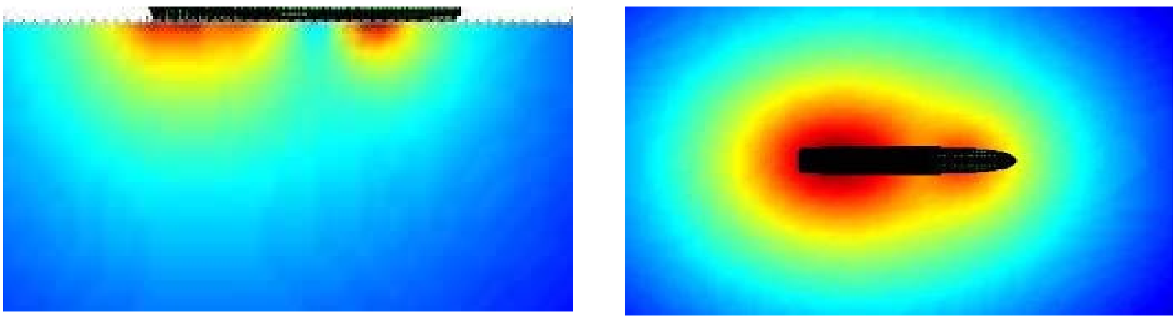

Fig.5: Underwater noise radiation prediction due to structure-borne noise excitation of the vessel, side view (left) and top view (right)

3. Increasing design freedom

Traditionally, ship design is based on experience. This is still true to some extent, but increasingly we rely on "virtual experience" from appropriate simulations. The rapid development of fast and unconventional ships after the 1980s was only feasible with advanced simulations. Megayachts have grown to beyond 200m in length, but this is just one example of how designers push the limits for megayachts. Whenever we leave our "comfort zone" of experience moving to new designs, simulations ensure that these designs are efficient and not only feasible, but safe.

Several projects illustrate how modern simulation-based design increases the design freedom for shipyards and owners. The lightweight design of the record-breaking trimaran "Earthrace" was only made possible using sophisticated CFD simulations for the loads, Fig.6, and subsequent finite-element analyses for the composite hull structure, *Ziegler et al. (2006)*. For the "Turanor PlanetSolar", the focus was the obtainable speed in waves which was predicted at the conceptual design stage for this record-breaking solar catamaran, Fig.7, *Köhlmoos et al. (2012)*. Yet another example concerns the largest megayacht at that time, which, due to size and speed, set new standards. In all these cases, the very innovative designs were made feasible by high-performance simulations, both for hydrodynamic and structural aspects.

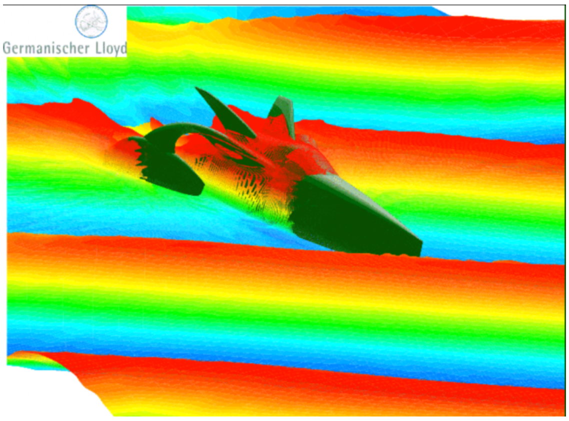

Fig.6: Seakeeping simulation for "Earthrace" Trimaran

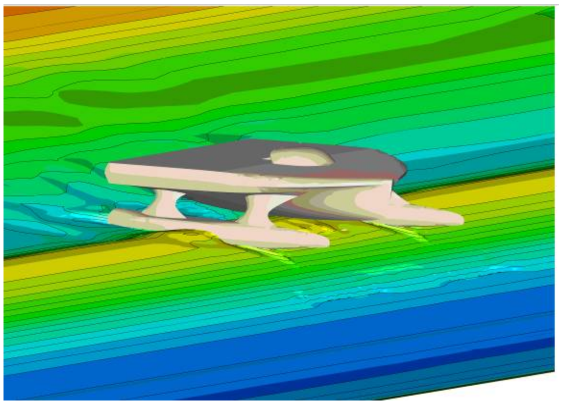

Fig.7: Simulation of obtainable speed in Waves for unconventional catamaran "Turanor PlanetSolar"

Integrated design environments, such as the FRIENDSHIP Framework, e.g. *Abt and Harries (2007), Abt et al. (2010), Mizine et al. (2011),* have made simulation-based design much more accessible to designers. The FRIENDSHIP Framework, Fig.8, combines ship hull description using parametric modelling, interfaces to many CFD solvers, several optimization algorithms, and software to handle process management and user interface. The design engineer can then work on simulation driven designs (e.g. of hulls, appendages or propellers), with one integrated user interface from model generation to post-processing.

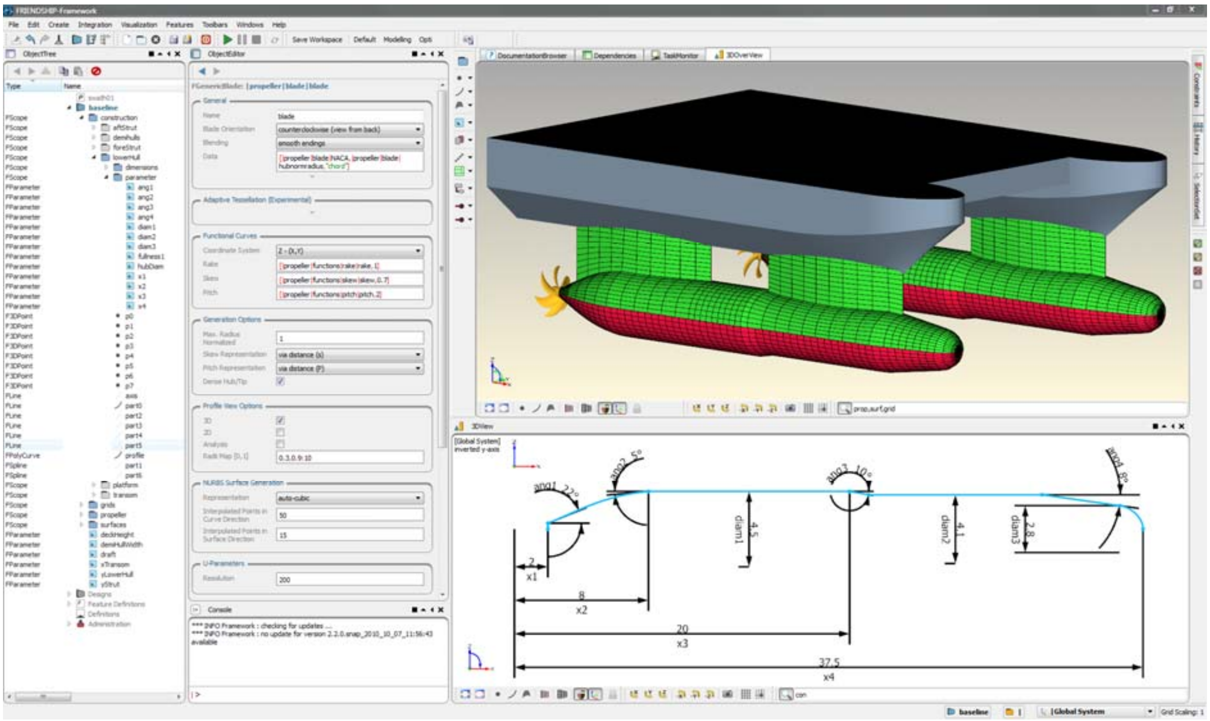

Fig.8: Integrated design environment FRIENDHSIP Framework to support simulation-based design

Composite materials are increasingly used in high-performance vessels, including megayachts. The combination of light weight, high strength and mouldability make these materials highly attractive for designers. The variety of possibilities to design a particular component to suit its purpose is manifold and is often only bound to development budgets or creativity. However, classical "cook-book" approaches in structural design do not work for high-performance light-weight designs, *Bertram et al. (2010)*. Prescriptive rules are often too inflexible; especially for advanced composite designs. The "Earthrace", "Turanor PlanetSolar" and "LAMU III", Fig.9, are just three high-profile examples of many advanced yacht projects that have proven that characteristic tailored solutions for composite structures require particular attention and understanding. Besides strength and hydrodynamic aspects, environmental aspects should also be considered, namely the different recycling properties of composite materials, *Gramann et al. (2008)*.

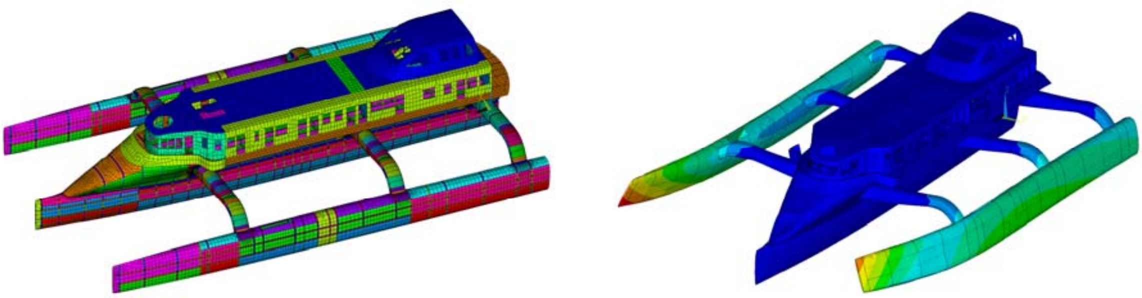

Fig.9: Finite-element model (left) and results (right) for composite material trimaran "LAMU III"

4. Achieving better designs in shorter time

The design of hull lines for high-performance yachts has been based to some extent on CFD simulations for many years now. However, formal optimization for industry projects have been reported only relatively recently, e.g. *Oossanen et al. (2009)*. Such formal optimizations may offer significant improvement in required power (and associated weight) for moderate to fast yachts, Fig.10. Alternatively, the optimization may be used to increase the speed of the boat for given installed power. Optimization requires considerable computer resources due to the complex flow and the thousands of design alternatives investigated. However, in our experience the effort is justified by the good results obtained and formal optimization of hull lines is quickly becoming a standard option in high-performance yacht design. Such optimization can also be applied to planing hulls if appropriate CFD tools are used, e.g. *Kaufmann et al. (2010)*.

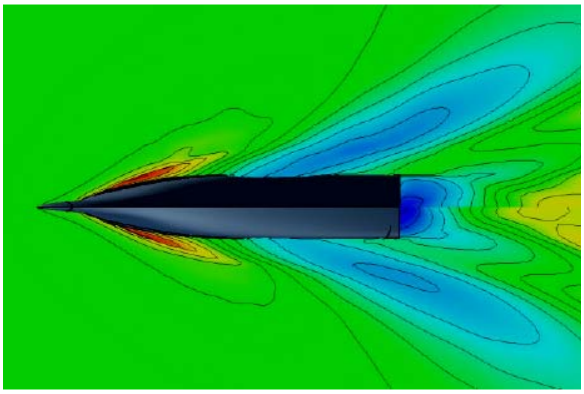

Fig.10: Hull line optimization of fast hull, *Oossanen et al. (2009)*

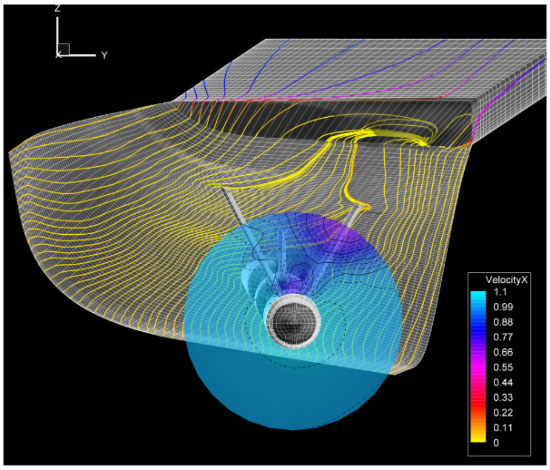

Fig.11: CFD for appendages of fast ferry, source: www.friendship-system.de

Simulations can be used similarly for the design of propulsors, rudders and other appendages, Fig.11, see also *Peric and Bertram (2012), Hochkirch and Bertram (2012a,b)*. For fast ships, these are in principle susceptible to cavitation problems. Unfortunately, problems are often detected late, in sea trials or after some time in operation. Simulations can then guide efficient trouble-shooting and re-design, but it is preferable to avoid cavitation related problems by appropriate checks during the design stage. Computational fluid dynamics (CFD) coupled with cavitation models (describing the formation and collapse of cavitation bubbles) can guide the design of waterjets, propellers and rudders in terms of low cavitation, Fig.12, *El Moctar (2007), Brehm et al. (2011)*.

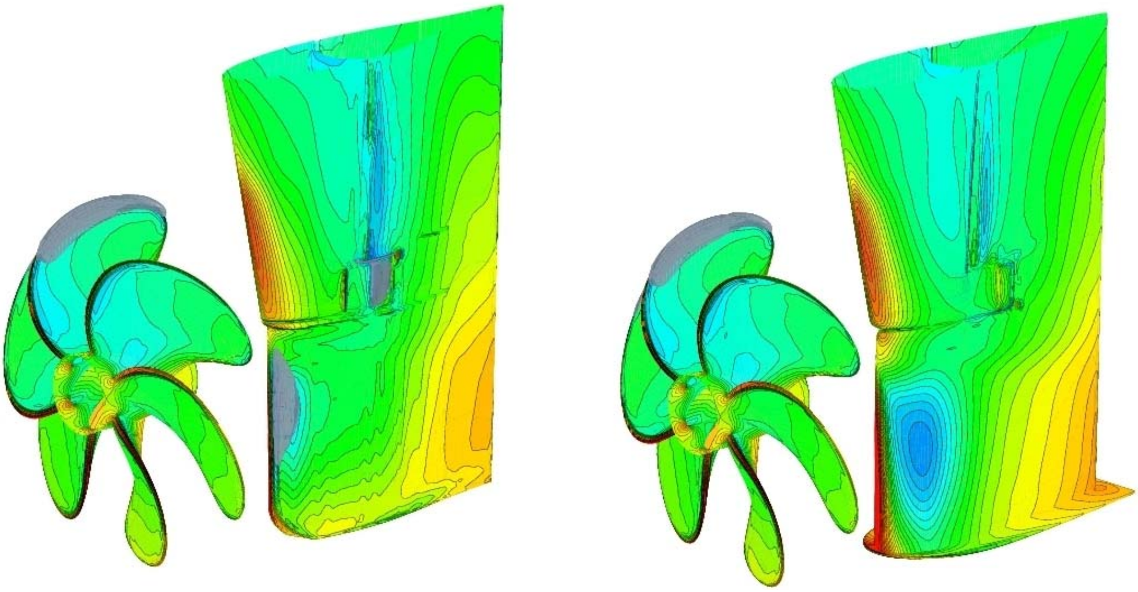

Fig.12: Cavitation check for rudder based on CFD; conventional (left) and advanced (right) Design. Grey areas indicate regions of cavitation

Traditionally, naval architects have resorted to similar baseline designs, statistical regression models, and systematic series data in initial design. Most of such series, however, are hopelessly outdated. Today, tailored series can be created using numerical simulations. For a parametric design, Fig.13, a family of designs can be created by systematic variation of the parameters describing the design. The key benefit of the proposed method is that it allows the designers to build up a knowledge base ahead of an anticipated project. Once this has been done, they can quickly extract data from the numerical model series to substantiate their design during the bidding and tendering process (which normally takes place under considerable time pressure). The approach is described in more detail in *Harries (2010), Couser et al. (2011)*.

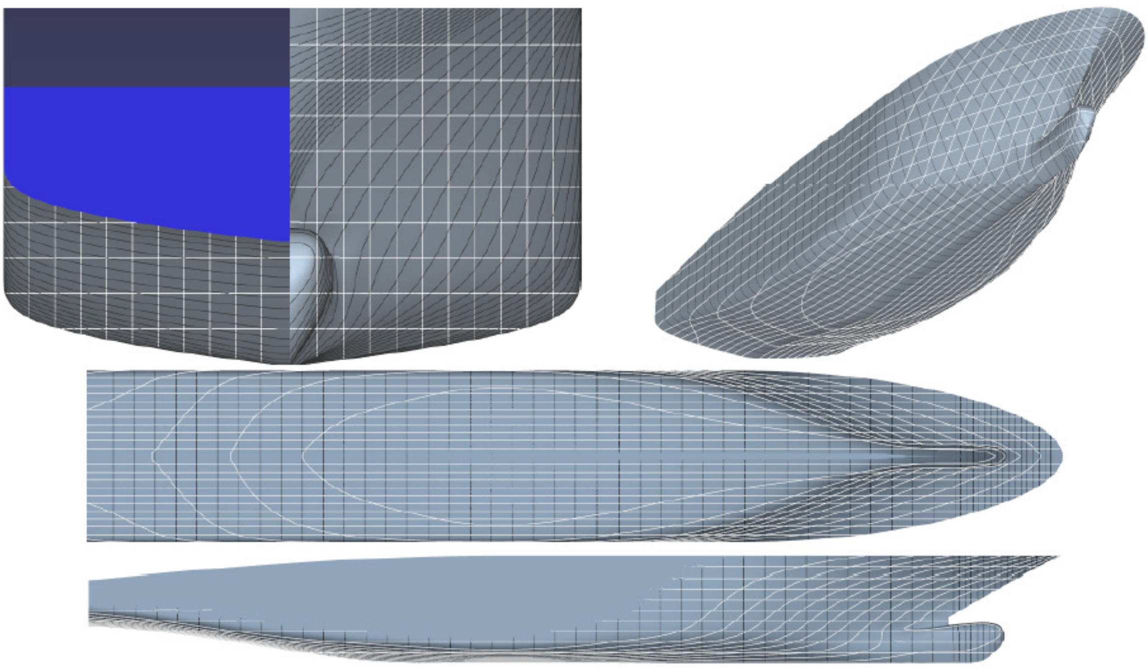

Fig.13: Example of typical bare hull with bulbous bow generated from the fully parametric model, *Couser et al. (2011)*

5. Ensuring fast and efficient trouble-shooting

Sea trials often give the first indication of design problems, for example in terms of noise and vibrations. But in some cases, problems occur only after months or years of operation (as in fatigue cracks or cavitation erosion on rudders) or in rare off-design conditions. Defining the cause of the problem is the first step towards solving it. Frequently, dedicated measurements give a detailed diagnosis to characterize the problem, for example severity of noise and vibration levels and associated frequency.

In some cases, the diagnosis of the problem is straight-forward, in other cases a more extensive analysis is required to determine unequivocally the root cause of a problem. Once the cause of the problem is defined, the re-design of structure or operational procedures is straightforward. Simulations are employed both in the diagnosis phase and in assessing the effectiveness of potential re-design options.

Megayachts may encounter problems with vortex induced vibrations (VIV). Ships have many degrees of freedom for local vibrations and these may be excited by vortex shedding at many local structures, typically at appendages or hull openings (e.g. sea chest). The traditional trial-and-error approach to localise the source of vortex-induced vibrations may today be replaced by a much more time and cost efficient search guided by CFD and vibration analyses, Fig.14, *Menzel et al. (2008), Köhlmoos and Bertram (2009).*

In time, vibrations (induced by vortices, engine or propeller) may lead to fatigue cracks despite relatively small amplitude. Fatigue cracks may become an issue of discussion between owners and yards sometimes after years of operation. They occur in the hull structure or in equipment, for example gears or shaft bearings. Light-weight designs and high engine power contribute to their increased occurrence in mega yachts. While appropriate care in the design stage is preferable, practice shows that fatigue problems appear in operation and then require efficient trouble-shooting. Here finite-element analyses are the appropriate tool. The approach may differ depending on the source of excitation causing the fatigue and the affected part of the ship (structure or equipment), Fig.15.

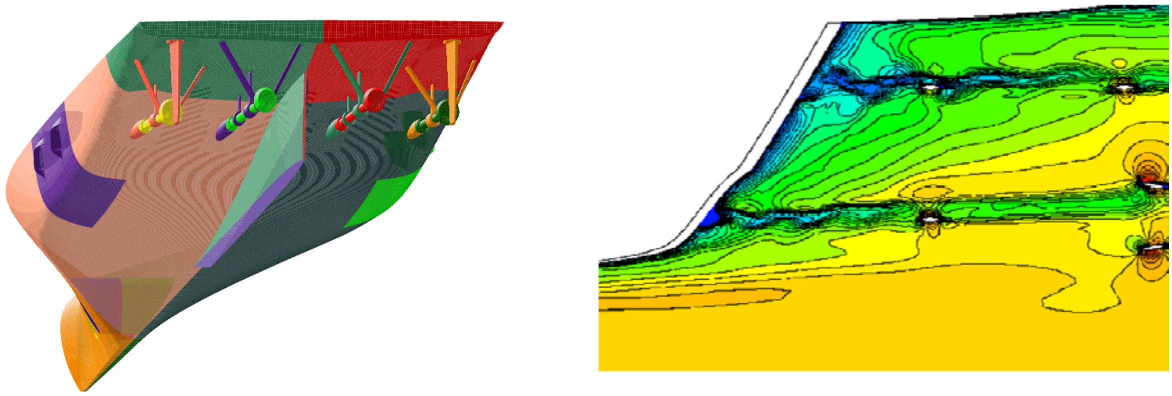

Fig.14: Megayacht with appendages and CFD results on port half showing vortices generated at both port shafts. The frequency of the outer shaft vortex street matched problematic vibrations in the owner's cabin

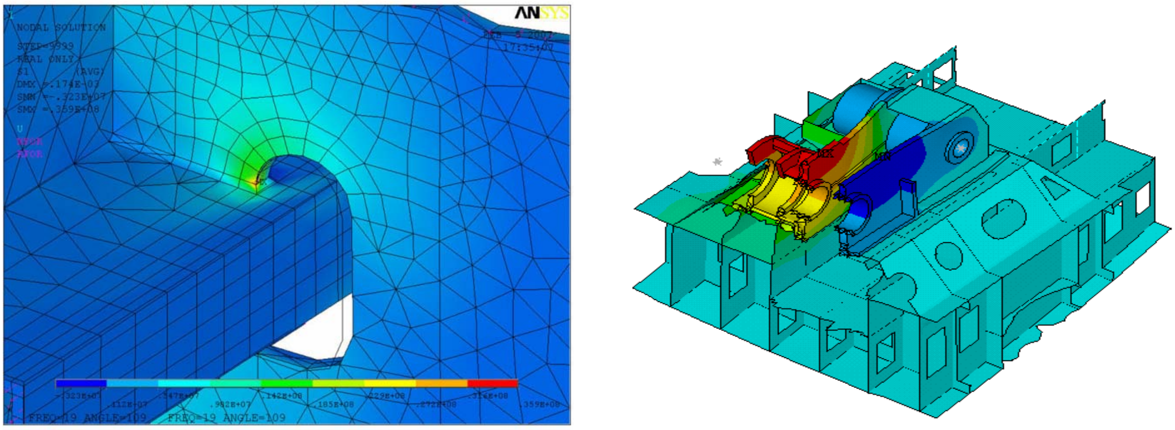

Fig.15: FEA for stiffener (left) and gearbox (right) to investigate fatigue

6. Requirements

So far, we have shown the manifold benefits of using simulations for megayacht shipyards and owners, contributing to better designs (supporting the architect's vision) and decreased costs (risk cost, repair cost).

Having discussed rather extensively the benefits of advanced simulations, let us have a brief look at the requirements for such simulations:

- Software
  It is generally preferable to use commercial software from large, well established vendors. This software is extensively validated and widely used, with known scope and limits of applications. This adds transparency for both sides, supplier and buyer of engineering services. The commercial software still needs to be adapted for fast and specific model generation, in our case to ships. Assorted macros, pre- and processing software has been developed and maintained. The model generation is often crucial for time, costs and quality of results in simulation projects. See e.g. *Bertram and Couser (2010)* for a more extensive discussion.

- Hardware
  State-of-the-art computations frequently employ parallel computers. The costs for hardware within a simulation project are still relatively small, but care has to be taken to exploit the parallel computing hardware efficiently.

- Trained experts
  In short, "the pilot is more important than the plane". Experience is needed in modelling and modelling determines response time, cost and quality of result. The combination of research and extensive industry experience with feedback from large full-scale measurements, model tests and several codes ensures best value.

7. Concluding remarks

Simulation is a powerful tool that can support better business processes within the maritime industry. Simulations for numerous applications now often aid decisions, sometimes 'just' for qualitative ranking of solutions, sometimes for quantitative 'optimization' of advanced engineering solutions. Continued validation feedback serves to further improve the simulation tools as well as build confidence in their results. Our many projects have proven time and time again that the appropriate use of simulations saves time and money for advanced designs. Ideally, for all parties involved, the scope and procedure for simulations are agreed upon at an early stage. Unless the ship owner (as main benefactor) includes simulations for design optimization in the specifications, time and budget constraints will often prevent them from being utilised.

Finally, the use of advanced simulation software alone is not enough. Engineering is more than ever the art of modelling, finding the right balance between level of detail and resources (time, man-power). This modelling often requires intelligence and considerable (collective) experience. The true value offered by advanced engineering service providers thus lies not in software licenses or hardware, but in the combination of highly skilled staff putting these resources to best use.

8. Acknowledgements

Many colleagues at GL Group have supported this paper with their special expertise, namely (in alphabetical order) Stefan Harries, Karsten Hochkirch, Jan Kaufmann, Bettar El Moctar, Wolfgang Menzel, Holger Mumm, Vladimir Shigunov, Stefan Semrau, Gundula Stadie-Frobös, and Tobias Zorn.

References

ABT, C.; HARRIES, S. (2007), A *new approach to integration of cad and CFD for naval architects*, 6th Conf. on Computer Applications and Information Technology in the Maritime Industries (COMPIT), Cortona, pp.467-479
http://www.ssi.tu-harburg.de/doc/webseiten_dokumente/compit/dokumente/compit2007_cortona.pdf

ABT, C.; HARRIES, S.; WENZEK, A. (2010), *Simulated prototyping. FRIENDSHIP-Framework: A holistic approach to optimization in ship design*, Nonstop 01/2010, Hamburg
http://www.gl-group.com/assets/downloads/nonstop_2010-01_E.pdf

BERTRAM, V.; BREHM, A.; KÖHLMOOS, A. (2011), *Smoke assessment for megayachts*, Via Mare XI/1, pp.49-51.

BERTRAM, V.; COUSER, P. (2010), *Aspects of selecting the appropriate CAD and CFD software,* 9th Int. Conf. Computer and IT Applications in the Maritime Industries (COMPIT), Gubbio, pp.20-29.
www.ssi.tu-harburg.de/doc/webseiten_dokumente/compit/dokumente/compit2010_gubbio.pdf

BERTRAM, V.; GUALENI, P. (2011), *An overview of seakeeping tools for maritime applications,* IMAM 2011 Conf., Genoa

BERTRAM, V.; HOFFMEISTER, H.; MÜLLER, S.; MOLTSCHANIWSKYJ, A. (2010), *Technological challenges for construction and classification "Tûranor PlanetSolar",* 7th Int. Conf. on High-Performance Marine Vehicles (HIPER), Melbourne, pp.76-85.

BERTRAM, V.; PERIC, M. (2012), *Trends in CFD applications for high-performance marine vehicles*, 8th Int. Conf. on High-Performance Marine Vehicles (HIPER), Duisburg

BREHM, A.; BERTRAM, V.; EL MOCTAR, O. (2011), *CFD guided improvement of a cavitation-prone rudder*, 14th Numerical Towing Tank Symp. (NuTTS), Poole
http://www.uni-due.de/imperia/md/content/ist/nutts_14_2011_southampton.pdf

COUSER, P.; HARRIES, S.; TILLIG, F. (2011), *Numerical hull series for calm water and sea-keeping,* 10th Int. Conf. Computer and IT Applications in the Maritime Industries (COMPIT), Berlin, pp.206-220.
www.ssi.tu-harburg.de/doc/webseiten_dokumente/compit/dokumente/compit2011_berlin.pdf

EL MOCTAR, O. (2007), *How to avoid or minimize rudder cavitation*, 10th Numerical Towing Tank Symp. (NuTTS), Hamburg
http://www.uni-due.de/imperia/md/content/ist/nutts_10_2007_hamburg.pdf

EL MOCTAR, O.; BERTRAM, V. (2002), *Computation of viscous flow around fast ship superstructures*, 24th Symp. Naval Hydrodyn., Fukuoka

FACH, K. (2006), *Advanced simulation in the work of a modern classification society*, 5th Int. Conf. Computer and IT Applications in the Maritime Industries (COMPIT), Oegstgeest, pp.34-44.
www.ssi.tu-harburg.de/doc/webseiten_dokumente/compit/dokumente/compit2006_oegstgeest.pdf

FACH, K.; BERTRAM, V. (2006), *High-performance simulations for high-performance ships*, 5th Int. Conf. High-Performance Marine Vehicles (HIPER), Launceston, pp.455-465.

FACH, K.; BERTRAM, V. (2009), *Advanced simulations as design decision support*, 10th Int. Marine Design Conf., Trondheim

GRAMANN, H.; KRAPP, R.; BERTRAM, V. (2008), *Disposal and recycling of HSC materials,* 6th Int. Conf. High-Performance Marine Vehicles (HIPER), Naples, pp.271-280.

HARRIES, S. (2010), *Investigating multi-dimensional design spaces using first principle methods*, 7th Int. Conf. on High-Performance Marine Vehicles (HIPER), Melbourne, pp.179-194.

HARRIES, S.; VESTING, F. (2010), *Aerodynamic optimization of superstructures and components,* 9th Int. Conf. Computer and IT Applications in the Maritime Industries (COMPIT), Gubbio, pp.335-347.
www.ssi.tu-harburg.de/doc/webseiten_dokumente/compit/dokumente/compit2010_gubbio.pdf

HOCHKIRCH, K.; BERTRAM, V. (2012a), *Hull optimization for fuel efficiency – Past, present, future,* 11th Int. Conf. Computer and IT Applications in the Maritime Industries (COMPIT), Liège, pp.39-49,
http://www.ssi.tu-harburg.de/doc/webseiten_dokumente/compit/dokumente/compit2012_liege.pdf

HOCHKIRCH, K.; BERTRAM, V. (2012b), *Ship hull optimization – Past, present, future,* Hansa 149/6, June

KAUFMANN, J.; KÖHLMOOS, A.; BERTRAM, V. (2010), *CFD guided hydrodynamic design of a rigid-inflatable boat*, Via Mare X, August

KÖHLMOOS, A.; BERTRAM, V. (2009), *Vibration analysis for a mega yacht*, RINA Conf. Design, Construction & Operation of Super & Mega Yachts, Genoa.

KÖHLMOOS, A., BERTRAM, V., HOFFMEISTER, H., HANSEN, H., MOLTSCHANIWSKYJ, A. (2012), *Design by best engineering principles for the solar catamaran Tûranor Planetsolar*, 4th High Performance Yacht Design Conf., Auckland

MENZEL, W.; EL MOCTAR, O.; MUMM, H. (2008), *Advanced thinking on tricky excitations*, The Naval Architect, March, pp.64-69.

MIZINE, I.; BRENNER, M.; CHITRAPU, M.; DANILCZYK, W.; HAGESTEIJN, G.; HARRIES, S. (2011), *Trimaran hull form development for America's marine highways EXPRESS SERVICE trailership*, 11th Int. Conf. Fast Sea Transportation (FAST), Honolulu

OOSSANEN, P.VAN; HEIMANN, J.; HENRICHS, J.; HOCHKIRCH, K. (2009), *Motor yacht hull form design for the displacement to semi-displacement speed range*, 10th Int. Conf. Fast Sea Transportation (FAST), Athens
http://www.futureship.net/download/vanOossanen_etal_FAST2009_Paper143_090630.pdf

ZIEGLER, W.; FACH, K.; HOFFMEISTER, H.; EL MOCTAR, O.; BETHANE, P. (2006), *Advanced analyses for the EARTHRACE project*, 5th Conf. High-Performance Marine Vehicles (HIPER), Launceston, pp.101-108.

Trends in CFD Applications for High-Performance Marine Vehicles

Volker Bertram, FutureShip, Hamburg/Germany, volker.bertram@GL-group.com
Milovan Peric, CD-adapco, Nuremberg/Germany, milovan.peric@de.cd-adapco.com

Abstract

The paper surveys developments in CFD applications for high-performance marine vehicles with particular focus on the past decade. Progress is significant in integrating the process chain, particularly more automated model generation. Increased hardware power and progress in various aspects of the flow solvers allow more sophisticated applications and wider scope of applications. These concern particularly two-phase flows (involving complex wave breaking and cavitation). Selected examples taken from industry and research applications demonstrate scope and maturity of CFD applications for high-performance marine vehicles.

1. Introduction

Computational fluid dynamics (CFD) denotes collectively techniques solving equations describing the physics of flows. We interpret "CFD" here as techniques solving Euler, RANSE (Reynolds Averaged Navier-Stokes Equations) or Navier-Stokes equations, using field methods, *Ferziger and Peric (2010), Bertram (2012)*.

CFD became a research field in the late 1960s. First commercial CFD software appeared in the 1980s including codes like PHOENICS, FLUENT, STAR-CD, CFX, TASCFLOW, and FLOW3D. By today's standard, these codes were very limited in terms of complexity of geometry and physics. Applications were severely limited by the available computer power in those days. An example may illustrate how CFD progressed over the decades. In 1988, an advanced CFD application in the automotive industry investigated the coolant flow in an engine block using some 10000s of cells. Two decades later, the progress in CFD allows the simulation of fluid and heat flows in engine compartments with some 700 parts and typically around 30 million control volumes, even 100 millions for detailed studies. However, the increase in grid size and associated capturing of geometry and flow details is only one aspect of the CFD developments of the past decades. It is a perhaps surprising fact that computational times have increased over the years. The demand for ever more ambitious simulations (in terms of cell count and flow complexity) thus outpaced the exponential growth in computational power.

Despite the increase in average computational time, CFD projects today are often noticeably shorter than they were two decades ago. This is due to less frequent re-modelling and re-analyses, and also generally significantly reduced time in pre-processing. The reason is that CFD tools have become more user-friendly, Fig.1. This is perhaps best illustrated in the case of integrated design environments, e.g. the Friendship Framework, *Abt and Harries (2007)*. The integrated design environment combines freeform hull description using parametric modelling, interfaces to most modern CFD solvers including STAR-CCM+, several optimization algorithms, and software to handle process management and user interface. The design engineer can then work on simulation driven designs (e.g. of hulls, appendages or propellers) with one integrated user interface from model generation to post-processing. The user-friendliness of this approach has certainly lowered thresholds in using CFD for designers.

There are many more aspects that have in sum advanced the wide acceptance of simulation first as a design and more recently as an optimisation tool in industry. The most important among these aspects are:

- The ability to handle complex geometry with all relevant details, including moving parts
- Efficient simulation process (from geometry to solution, parametric studies, optimization studies, user interface...)
- Adequate modelling of turbulence, free-surface effects and cavitation
- Coupled simulation of flow and flow-induced motion (and in some cases deformation) of bodies.

These will be discussed in more detail in the following.

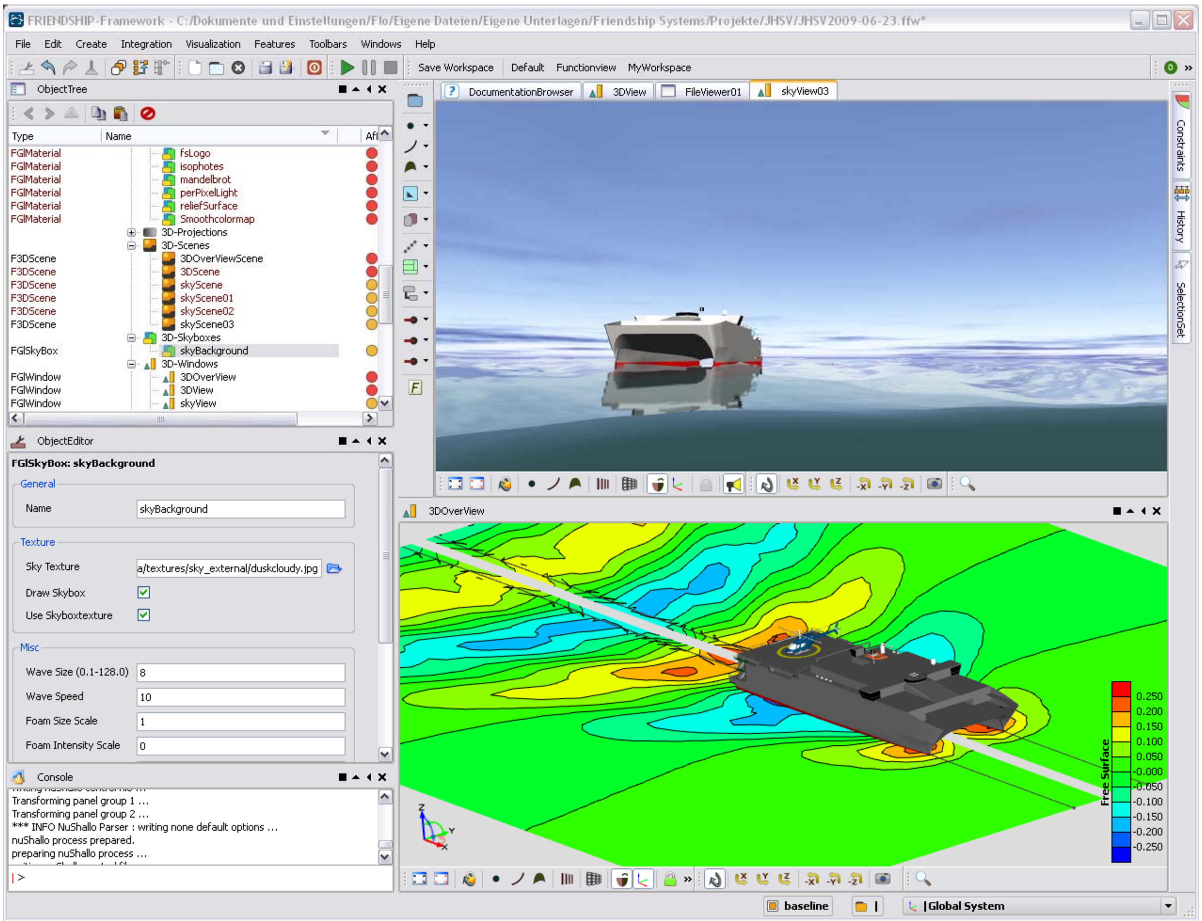

Fig.1: Integrated design environments allow simulation driven designs

2. Key aspects of progress in CFD for maritime flows

2.1. Handling of complex geometry

During the past decade, the ability to handle complex geometry with all relevant details has been greatly improved. Components that have contributed to this trend include:

- Tools for automatic and user-friendly manual repair of CAD models (which are often imperfect) have been developed; IGES files coming from designers frequently feature overlaps and gaps. These are not problematic for design purposes (e.g. volume computations are required for ship stability and capacity), but frequently lead to fatal errors for CFD grid generation.

- Surface-wrapping tools have been introduced, which create a closed surface around assemblies of solid parts;
- Tools for automatic generation of polyhedral, trimmed hexahedral or extruded meshes have been developed;
- Automatic and manual definition of local mesh refinement requirements have been created, based on:

  – local curvature, proximity of other walls etc.
  – pre-defined regions, interfaces, wakes etc.
  – indication or estimate of numerical error...

Grid generation has improved, making it easier to generate high-quality grids for accurate CFD simulations. A key aspect for complex geometries consisting of many components (such as offshore platforms in the maritime context) is geometry recognition. The software then recognizes automatically cylinders (with extrusion along centreline, using prismatic cells) and thin solids or gaps, with projection from one side to another, using prismatic cells).

More sophisticated analyses for ships and offshore platforms employ a variety of techniques that have become widely available (through commercial and open-source software):

- The ability to handle moving parts using morphing, sliding interfaces or overlapping grids (e.g. propellers, rudders etc.), *Brehm et al. (2011)*
- The ability to model complete systems rather than single parts (e.g. ship with all appendages), Fig.2
- The ability to easily replace geometry and perform a new simulation; automation of simulation process, with parametric description of ship including appendages and fully automatic grid generation and CFD simulation, *Abt and Harries (2012)*. Parametric studies may then serve to optimize also appendages such as interceptors or trim wedges, Fig.3.

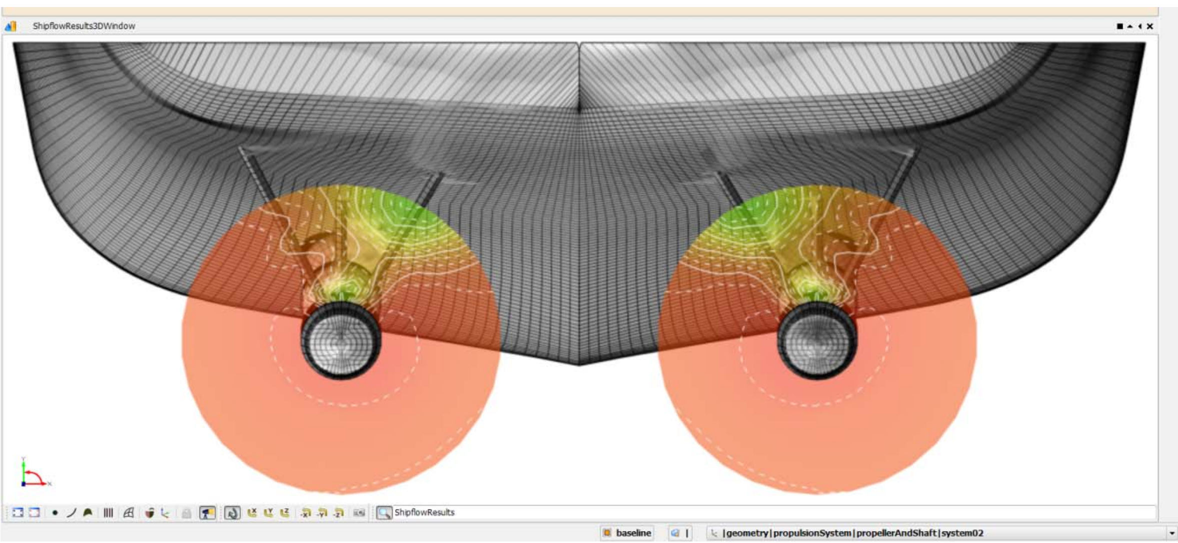

Fig.2: Fast twin-screw ship with appendages and propellers, illustrating the trend towards modeling complete systems, Source: Friendship Systems

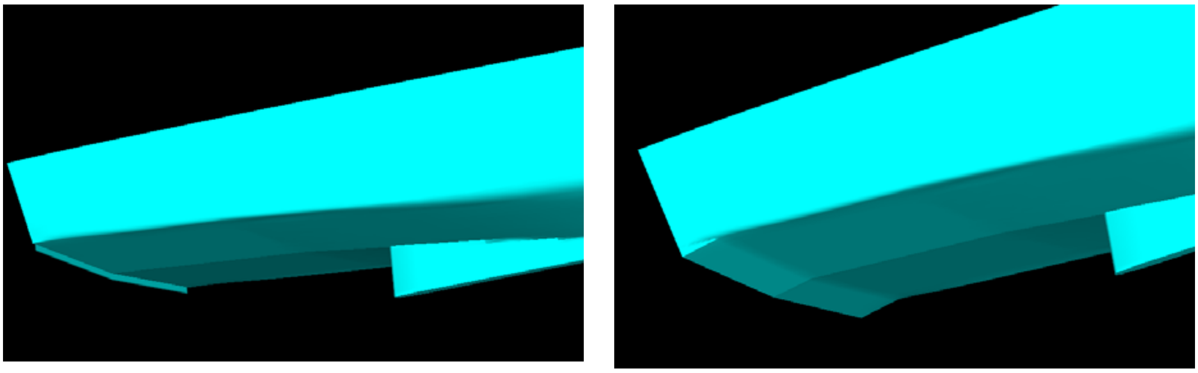

Fig.3: Analyses of ship with interceptor (left) and trim wedge (right), Source: Voith Turbo

2.2. Turbulence modelling

Turbulence modelling was in the “villain” of the 1980s and 1990s. Unsatisfactory results were often blamed on turbulence modelling. Several dedicated validation workshops have shed more light on adequacy and inadequacy of turbulence modelling for marine flows. For most applications in industry practice, the importance of turbulence modelling is over-rated. Turbulence models play a significant role on the flow structures and resulting resistance of bare hulls, as investigated in most validation studies. However, the propeller behind the ship dominates flows and reduces the effect and importance of the turbulence model. Since only the propulsion case is relevant for industry, turbulence modelling is thus of lesser importance for classical resistance & propulsion applications. For seakeeping, the free-surface effects dominate anyway. This leaves manoeuvring and propeller flow investigations as areas of application where turbulence modelling remains an important issue.

For most applications in industry, the standard k-ε or k-ω turbulence models are adequate. In order to predict secondary flows better, more sophisticated models are needed. The Reynolds-stress model (RSM) is then frequently a popular and appropriate option. A special turbulence model is needed to predict transition from laminar to turbulent flow, e.g. when predicting resistance of a competitive sailing yacht. Such models are also available. For predicting noise sources, wall vibration etc., large-eddy-simulation (LES) or detached eddy simulation (DES) type of analyses with special subgrid-scale turbulence models are used. These are rather subject to research than state of the art in industry. The CFD expert needs to select the most appropriate model for any given analysis task (and may decide not to use any turbulence modelling…).

2.3. Modelling of free-surface effects

Ships operate at the interface of water and air. Correspondingly, free-surface flows are of prime interest for naval architects. The wave resistance of a ship is one example, as this component of the total resistance offers the largest improvement potential for small to moderate changes in the hull shape. Other applications of free-surface flows are seakeeping (interaction with waves), slamming (external impact due to waves) and sloshing (internal impact in partially filled tanks). Interface-capturing methods (volume of fluid, two-phase flow, level set, etc) allow the simulation of highly nonlinear free-surface flows. Where the two fluids (typically water and air) are not expected to mix, a sharp interface (within one control volume) can be obtained. This minimizes numerical mixing. Arbitrary free-surface deformation, even trapped air bubbles or detaching droplets are adequately accounted for, as gravity and surface tension effects are included. Applications concern hull and propellers alike, Fig.4 and Fig.5. Phase change models (cavitation) may be integrated into this method to allow more complex phenomena to be modelled. Resulting quantities of engineering interest, e.g. slamming forces or added resistance in waves, *Köhlmoos et al. (2012),* are also well predicted.

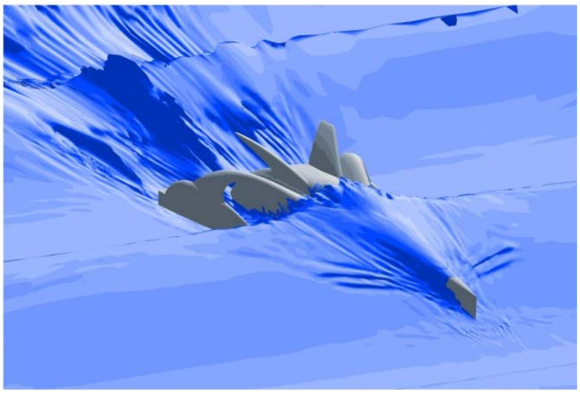

Fig.4: Free-surface flow with breaking waves around wave-piercing trimaran

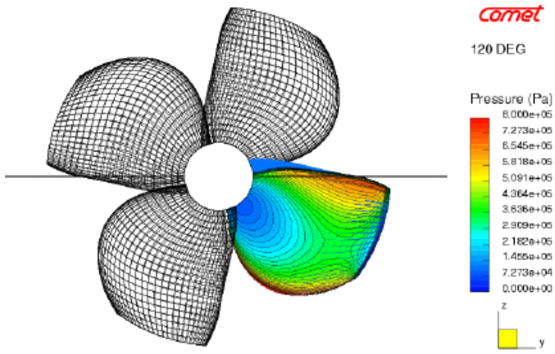

Fig.5: Surface-piercing propeller, *Caponnetto (2003)*

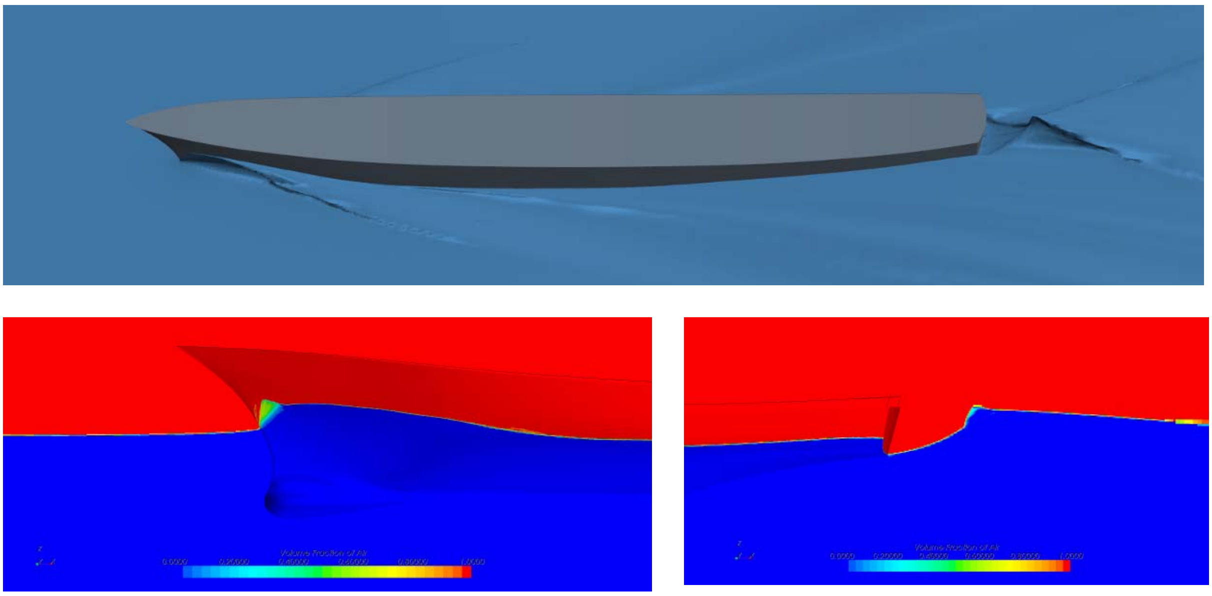

Fig.6: Computed wave field around DTMB 5415 (destroyer geometry); smeared surface at bow and stern where waves break, sharp surface elsewhere

Despite the significant progress in free-surface modelling, research continues in this field, as the modelling of breaking waves can still be improved in terms of air mixing and turbulence interaction with the free surface. In regions, where in reality white foam appears (mix of air and water), current CFD simulations show smeared surfaces, Fig.6, and predict the propagation of these waves less accurately.

2.4. Cavitation modelling

Cavitation modelling may seen as an extension of free-surface modelling, as it involves the interface between water and gas (or vapour in this case), which is a priori unknown and part of the solution. Albeit, in this case, also the growth and collapse of cavitation bubbles need to be described adding a further complexity.

If the aim is to avoid cavitation, one only needs to predict its onset (usually expressed by a pressure below saturation level). However, in most propellers and several rudders, cavitation is unavoidable. If cavitation cannot be avoided, its effect on performance needs to be assessed, hence the need for cavitation modelling. Despite their theoretical shortcomings, models based on bubble dynamics (Rayleigh-Plesset equation) have proven robust and sufficiently accurate for most industrial applications, Fig.7. One additional equation for volume fraction of vapour is then solved, with two parameters: (1) seed density in liquid (number of seeds per m^3 of liquid) and on solid walls (surface-roughness effects); (2) initial (representative) radius of seed bubble. These parameters are related to the "liquid quality" and depend on region (for sea water) or treatment (like de-gassing or filtering in a cavitation tunnels).

RANSE simulations with cavitation modelling have become part of modern design procedures for advanced propulsors, such as Voith Schneider Propellers (VSPs). For illustration, Fig.8 shows a snapshot with the extent of vapour regions on each blade of a VSP in off-design condition. The associated diagram shows propulsor performance (torque) full-scale measurements and CFD results. The cavitation model significantly improves the quality of the prediction. Fig.9 shows another application taken from industry practice. Rudders behind highly loaded propellers are susceptible to cavitation and associated erosion which endangers the ship. CFD is by now regularly employed to predict location and extent of cavitation on rudders in these cases. The concerned regions are then often built in more enduring steel, unless local redesign avoids the formation of cavitation erosion.

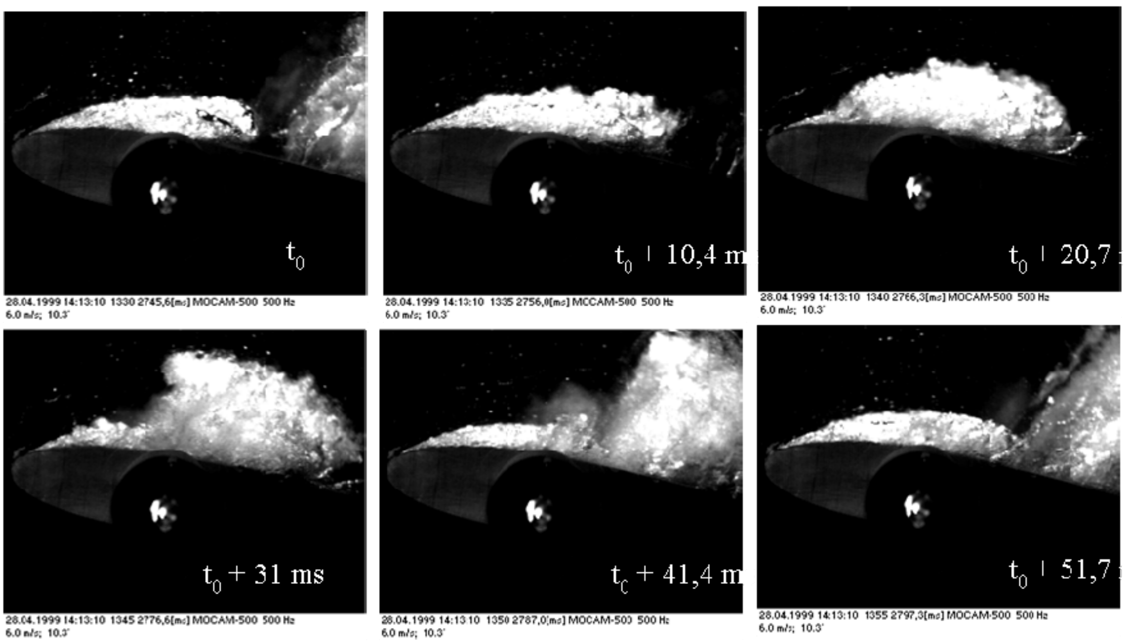

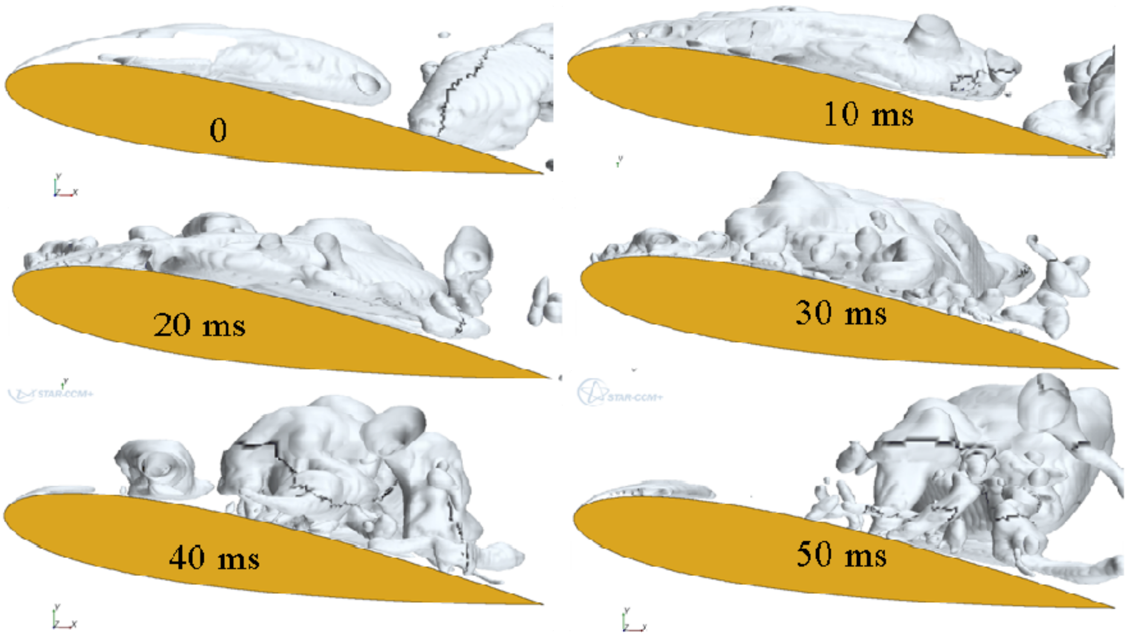

Fig.7: Cavitation around NACA0015 foil at 10.3° angle of attack; experiment of HSVA (top) and CFD simulation (bottom)

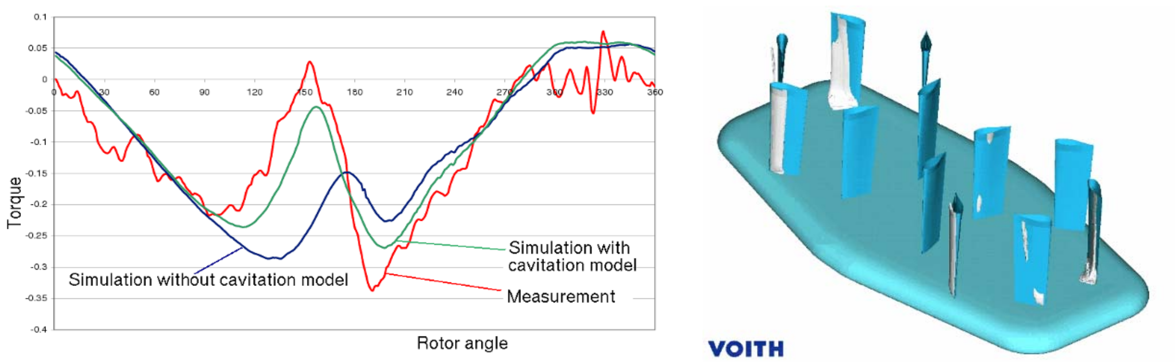

Fig.8: VSP in off-design condition; performance in full-scale measurements and simulations (left) and simulated cavitation extent at all blades (right); source: Voith

Fig.9: CFD prediction of rudder cavitation (left) and observed erosion at actual ship (right)

2.5. Motion of floating bodies

For a variety of seakeeping problems, implicitly coupled simulations of flows and flow-induced motions of floating bodies (ships or offshore structures) are desired. These simulations should be implicit, as implicit simulations pose no restrictions on the time-step size for stability reasons. The time step can be chosen then according to accuracy requirements. Highly nonlinear motions (e.g. launching of free-fall lifeboats with subsequent water entry and resurfacing) are better handled in implicit simulations. Such rigid-body motions of freely moving ships have been presented for a variety of applications including many industry projects, e.g. for slamming investigations, Fig.10. The simulations can handle in principle all complexity required in offshore and naval architectural applications, including multi-body configurations moving relative to each other, possible coupling between bodies (via elastic moorings, rigid connections, or flexible links with constraints), inclusion of external forces (e.g. thrusters, mooring, towing), or relative motion of system components (e.g. propellers).

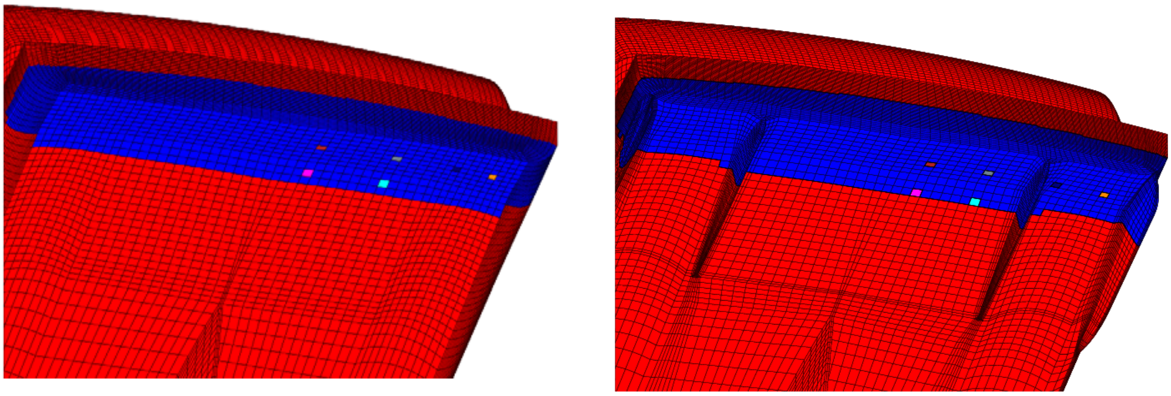

Fig.10: Megayacht stern with original design (left) and modified design for reduced slamming impact (right); slamming pressures were reduced by almost 30%

2.6. Fluid-Structure-Interaction (FSI)

Coupled simulation of flow and flow-induced deformation of solid structures have evolved more recently for marine applications. FSI is important for relatively soft structures, for very large ships (e.g. whipping and springing, i.e. hydro-elastic vibrations of the ship hull), inflatable boats, and for better prediction of impact loads (slamming and sloshing). So far, coupling of RANSE CFD codes and finite-element codes (for the structural analyses) is usually explicit, making the computations inefficient to the point where they are not applicable to most practical problems. Implicit coupling (as already in place for rigid-body motions in waves) is required for robustness and computational efficiency. On the other hand, the structural model can be simplified (e.g. treating the ship as a beam subject to bending and torsion). Such simplified structural models with implicit coupling have already been implemented, e.g. *Oberhagemann et al. (2008)*, Fig.11.

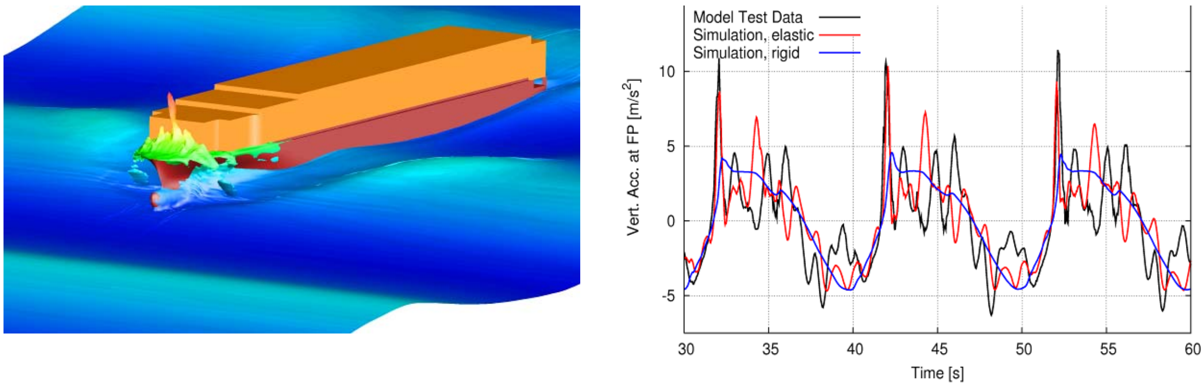

Fig.11: Green water on deck after one slamming event (left); measured and computed accelerations in bow region for a rigid and an elastic ship structure (right)

3. Trends

Computer hardware continues to become more and more powerful. Highly parallel computing environments have become affordable even for small and medium enterprises. The appetite grows at least as fast as the more powerful capabilities become available. Higher demands from simulations come in various forms:

- More complete system analysis, with all geometrical details
- More transient simulations (URANS (= unsteady RANS), DES and LES)
- Prediction of pressure fluctuation and noise sources (turbulence, cavitation)
- More fluid-structure-interaction (slamming, sloshing) and other multi-physics (wind, fire, pollution etc.) applications
- Simulation of full manoeuvring tests (circle, zigzag, etc.) already in conceptual design
- Simulation of interaction (ship + ice, ship + platform, ship + ship etc.).
- More automatic optimization studies...

Of the many developments on the horizon, we select two for illustrative purposes, namely coupling CFD with formal optimization in ship design and coupling CFD in simulators for training and assessment purposes.

3.1. Design optimization

Optimization strives to maximize desired features (objectives) subject to constraints. The difficulty in practice lies in the expressing all objectives and constraints in mathematical functions of sufficient accuracy and numerical efficiency, *Bertram (2003).* This task is often more difficult than it sounds. It requires

- a smart engineer, who is able to model the problem at hand with just the right level of detail and sets up a design search space that is large enough to find significant improvements, yet small enough to allow efficient exploration
- a tool to help the engineer to convert his model into an efficient optimization process.

The mathematical algorithm for the actual optimization is secondary. Simulations play a pivotal role as they are used to assess a design, e.g. in terms of required power in fuel efficiency optimizations. Care is needed when changes in candidate designs are small, as then the required accuracy in turn is high. Fortunately, often the task is to find the design that is optimum, rather than an accurate determination of the object function (e.g. required power) for this design. Thus if the relative ranking is right independent of (similar or constant) errors in objective function the task can be solved even with usual discretisation or model errors.

Optimization software, e.g. the Friendship Framework, *Abt and Harries (2007*), is available to guide an automated simulation process towards a (near) optimum design, combining automatic generation of parameterized geometry, automatic mesh generation, automatic CFD simulation and analysis, and subsequent automatic determination of new parameters. Examples of marine applications include funnel optimization for minimum smoke dispersion on the deck of a yacht, Fig.12, *Harries and Vesting (2010),* the optimization of the nozzle geometry for a Voith radial propeller, *Palm et al. (2010),* and the optimization with respect to seakeeping performance, *Harries et al. (2012).*

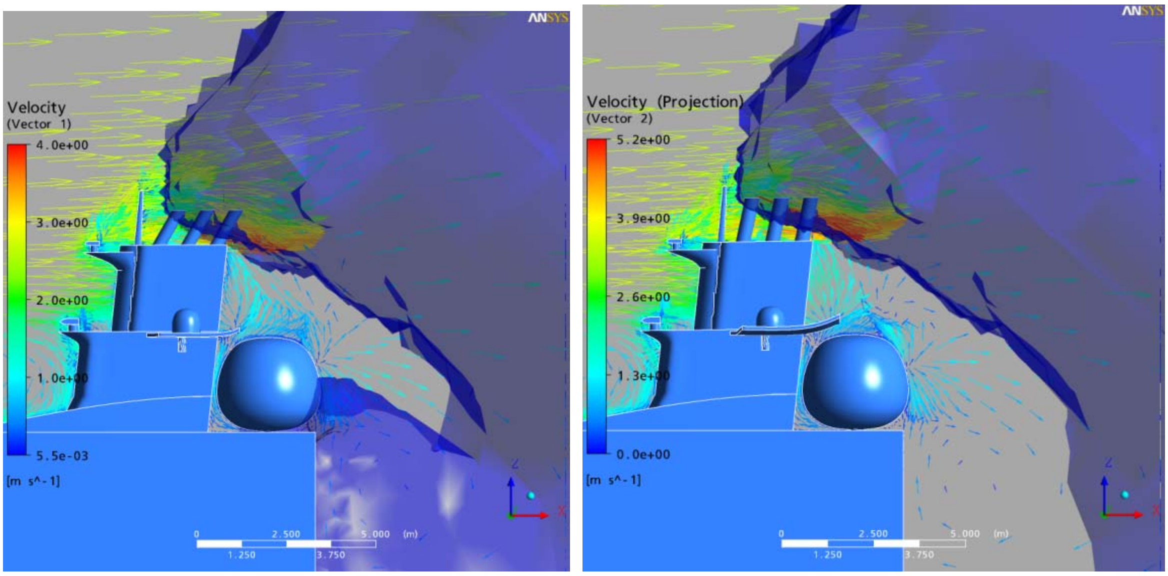

Fig.12: Funnel optimization for minimum smoke dispersion on megayacht

3.2. Simulation of experiments

CFD can be used to generate data sets for subsequent fast evaluation in design and operation. *Harries (2010), Couser et al. (2011)* present such an application to megayachts, using response surfaces based on a Kriging approach. *Calcagni et al. (2012)* presents metamodels for propeller design, combining CFD and artificial neural networks.

4. Final remarks

No matter what the software can do, it remains just a tool. How quickly and well problems get solved depends on the craftsman using the tool – the engineer remains indispensable. With this in mind, proper training for CFD analyst is vital. Engineers need to be educated how to best use the tools at hand, be it theoretical or qualitative analysis, numerical simulation (based on different tools involving different limitations and required effort) or experiments (in model or full scale). Never fall in love with your model; be aware of different approaches and choose intelligently. In the end, the engineer is paid for his modelling skills, choosing the model that offers reliable and sufficiently accurate answers obtained with minimum cost (in terms of time and money).

References

ABT, C.; HARRIES, S. (2007), A *new approach to integration of cad and CFD for naval architects*, 6th Conf. on Computer Applications and Information Technology in the Maritime Industries (COMPIT), Cortona, pp.467-479

ABT, C.; BERGMANN, E.; HARRIES, S. (2012), Domain preparation for RANSE simulations about assemblies of functional surfaces, 11th Conf. on Computer Applications and Information Technology in the Maritime Industries (COMPIT), Liege, pp.408-421

BERTRAM, V. (2003)*, Optimization in ship design,* OPTIMISTIC (Eds. Birk and Harries), Mensch+Buch Verlag, ISBN 3-89820-514-2

BERTRAM, V. (2012), *Practical Ship Hydrodynamics*, 2nd Ed., Butterworth & Heinemann

BREHM, A.; BERTRAM, V.; EL MOCTAR, O. (2011), *CFD guided improvement of a cavitation-prone rudder,* 14th Numerical Towing Tank Symposium (NuTTS), Poole

CALCAGNI, D. (2012), *Automated marine propeller optimal design combining hydrodynamics models and neural networks*, 11th Conf. on Computer Applications and Information Technology in the Maritime Industries (COMPIT), Liege

CAPONNETTO, M. (2003), *RANSE simulations of surface piercing propellers*, 6th Numerical Towing Tank Symposium (NuTTS), Rome

COUSER, P.; HARRIES, S.; TILLIG, F. (2011), *Numerical hull series for calm water and seakeeping,* 10th Conf. on Computer Applications and Information Technology in the Maritime Industries (COMPIT), Berlin, pp.206-220

FERZIGER, J.; PERIC, M. (2010), *Computational Methods for Fluid Dynamics*, 3rd Ed., Springer

HARRIES, S.; VESTING, F. (2010), *Aerodynamic optimization of superstructures and components,* 9th Conf. on Computer Applications and Information Technology in the Maritime Industries (COMPIT), Gubbio, pp.335-347

HARRIES, S.; LAND, J.; WEICKGENANNT, S.; QIU, W. (2012), *From analysis towards design in seakeeping,* 11th Conf. Computer and IT Applications in the Maritime Industries (COMPIT), Liege, pp.27-38

KAUFMANN, J.; KÖHLMOOS, A.; BERTRAM, V. (2010), *CFD guided hydrodynamic design of a rigid-inflatable boat,* Via Mare X, August

KÖHLMOOS, A.; BERTRAM, V.; HOFFMEISTER, H.; HANSEN, H., MOLTSCHANIWSKYJ, A. (2012), *Design by best engineering principles for the solar catamaran Tûranor Planetsolar*, 4th High Performance Yacht Design Conf., Auckland

OBERHAGEMANN, J.; EL MOCTAR, O.; HOLTMANN, M.; SCHELLIN, T.; BERTRAM, V.; KIM, D.W. (2008), *Numerical simulation of stern slamming and whipping*, 11th Numerical Towing Tank Symposium (NuTTS), Aberwrach

PALM, M.; JÜRGENS, D.; BENDL, D. (2010), *CFD study on the propeller-hull-interaction of steerable thrusters,* 13th Numerical Towing Tank Symposium (NuTTS), Duisburg

BB GREEN – Development of the World's First Zero Emission Air Supported Battery Electric Fast Commuter Ferry, Concept and First Project Results

Ulf Stephen Tudem, **Tor Kolbjorn Livgard**, SES Europe AS / Effect Ships International AS, Sandefjord/Norway, ulf.tudem@effectships.com
Hans Liljenberg, SSPA Sweden AS, Gothenburg/Sweden, hans.liljenberg@sspa.se

Abstract

Based upon Effect Ships International AS Air Supported Vessel (ASV) technology, a new high efficiency, Zero emission waterborne transport solution, supported by EU under the 7th Framework, is under development. The 6 partner strong BB GREEN team started with an assessment of owners/route requirements (partner Aqualiner) and critical factors, then followed up with analyses and development of a suitable ASV hull form. Tank testing of two candidates, one ASV Cat and one ASV Mono variant was carried out at SSPA Sweden. In parallel work on the single most critical factor, testing and evaluation of most suitable battery cell technology was carried out by Amberjac Projects. To minimize overall weight with excellent strength, carbon sandwich engineering will be used. Partner Diab AS has been responsible for the lightweight hull engineering. In phase 2 of the project a full scale BB GREEN test vessel, of approx 20 m x 6 m will be built, outfitted and tested "on route" in the Netherlands. Design speed is 30 knot. As a commercial vessel some 60 – 80 passenger and a few bicycles may be transported fast, efficient and environmental friendly on waterways throughout Europe and beyond. The paper will concentrate on presenting the overall concept, tank testing of the ASV hulls and key achievements during the first year of the 3 year project.

1. Introduction

Development of the BB GREEN concept was initiated by SES Europe AS a subsidiary of Effect Ships International AS (ESI). Their patented low resistance Air Supported Vessel (ASV) technology is a key component to realise the vision of a fast and emission free commuter ferry. Across Europe and beyond numerous existing and planned operations can benefit from a new breed of Green ferries. However there are also a few sceptics to the proposed concept. Their main arguments and resistance are related to overall feasibility. Will the proposed concept work? And will the ASV deliver according to expectation? Is it possible to go 30 knots with a battery electric passenger ferry?

EU agreed the vision was innovative and promising so they said – let's find out!

In the Euro 3.2 mill project funded under the 7th Framework, the 6 partner strong team is now carrying out the development process of concept and subsystems. Following a tender process planned to be advertised this autumn the intention is to build a full scale prototype/test vessel to be tested under realistic conditions and to be used for concept verification, documentation and demonstrations.

ESI have during the last decade conducted a considerable amount of research on air assisted hull forms leading to the latest technical ASV solutions. The targeted BB GREEN type of vessels has been designed for and will be operated in sheltered / relatively calm waters. Vessel size will be approx 20 x 6 m for the start up craft.

This paper will give an introduction to the concept, the hull form development; discuss some of the main systems and design/engineering of the hull. In the project two candidate ASV hulls, one ASV Catamaran and one ASV Mono have been prepared. Both were tank tested at SSPA Sweden during this winter and benchmarked against State of the Art (SOA) conventional monohulls with a design speed of 30 – 35 knots. Results related to hull resistance, lift fan powering, motions in waves, wake wash and more will be presented.

2. The BB GREEN concept

The idea behind BB GREEN was to apply a holistic approach, taking advantage of inventions, technologies and solutions each representing SOA in their respective fields, to create a Zero emission fast and efficient new waterborne transport concept.

Slow battery electric ferries crossing rivers and the like are nothing new, electric ferries with speed capability in excess of 30 knots and a range of 10 + NM is another matter.

During the last few years, electric cars, busses and trucks are become increasingly more accepted in the market place. Most car manufacturers have electric solutions either in their portfolio or soon to be launched. In the pleasure boat industry there has also been a few electric attempts lately, mainly hybrid solutions, diesel and electric combined.

One should remember that there are vital differences between the operational profile of a car and a commercial fast ferry. While a car is going uphill as well as downhill/breaking electric power can be regained and feed back into the battery bank. A commercial fast ferry can be compared with a heavily loaded truck going steep uphill – all the time. The average energy consumption pr time unit/distance and consumption pr day for a vessel going fast is high. There is no regeneration of electric power as for the car. In other words developing a fast battery electric ferry seems to be a tough challenge.

Range on battery power (before recharging is required) is a direct function of total energy consumption (kWh) of the vessel pr distance at operated speed, related to energy availability in the battery / acceptable drain of the battery. The feasibility of the vessel or service offered by the vessel is also closely linked to the time required for recharging the battery, and further how many cycles the battery will last with a typical charge/recharge- and use profile. Price of the battery pack is another important factor; same is sourcing- and cost of electric energy (in absolute terms and related to alternative fossil fuel).

Based upon existing ASV hull and fan powering test data, scaled to the targeted vessel's size, assuming operational weight, design speed, expected propulsion efficiency etc, a first assessment indicated a power consumption of approx 25 kWh / NM. In the BB GREEN set up a 400 kWh battery was suggested. 70 – 80% max drain of battery capacity will give approx 300 kWh of power available, enough to secure a 10 NM + effective range.

As for any high speed vessel concept the optimization is a design spiral exercise. Improving each component individually and in relation with other components is paramount.

For BB GREEN reducing the hull resistance at design speed/conditions is a first concern. Compared with current conventional hulls any reductions from use of unconventional ASV technology will reduce the number of kWh/NM and improve the performance and range. Based upon available ASV results the project aimed at a reduction in hull resistance of 40 % for BB GREEN.

As ESI today has a similar size ASV Mono test-vessel in the water delivering efficiency improvements compared with conventional monohulls of 40 – 50 % at design speeds, the project had a good level of confidence in the technology. Below picture is showing the ASV test vessel at 33 knots during testing in Turkey. The ASV concept won the European Power Boat of the Year Innovation Award in 2011.

As weight and hull resistance go hand in hand, reducing the weight of the hull, superstructure, outfitting and systems is given high priority. Whereas aluminum or conventional GRP is generally used for this type of vessels, BB GREEN will be constructed from vacuum infused carbon sandwich. A weight saving of 30-40% for the structural weight should be possible.

With regards to selecting battery cell technology for the demanding commercial use profile of a BB GREEN type of ferry an acceptable combination of below requirements will have priority:

- Battery life / number of recharging cycles at a given rate of charge/recharge and % drain
- Battery recharging time (the faster the better)
- Battery price and expected price developments
- Acceptable weight for battery pack (kg/ kWh of capacity).

It is important still to agree a lower battery weight cannot compensate for lack of the three first mentioned criteria.

Selecting the correct drive line and propulsion system is important for several reasons: Propulsion efficiency and operational / maneuvering ability. The project initially planned to use a pair of large diameter surface piercing propellers, expected to offer 70% + operational efficiency at design speed, but decided to change to contra rotating pod propulsion although the latter was slightly less efficient, due to the superior handling and close up steering capability. In this evaluation a combination of improved safety and ability to manage frequent stops fast and efficient were deciding factors.

Final decisions on the electric propulsion motor to be used have not yet been made, but it will be compact and light offering a very high torque from first RPM. This characteristic enables with ASV technology a fast and efficient transit from start up to design speed. The lift fan system, also electric, will be located in the bow and will support 70–80+ % of the vessel's loaded displacement when underway. Approaching and at the pontoon the vessel will be operated with the fan system disengaged in "off cushion" mode.

Power supply will ideally come from renewable energy sources – thus claimed zero emission. Recharging the battery will be at one or more pontoons, depending on among other the route length / profile and timetable / length of time at recharging pontoon. Availability and electric power supply to the pontoon is considered to be outside the scoop of the project. According to the project and as specified by the battery cell technology provider, recharging the battery (up to 70 % of full capacity) should be possible in less than 30 minutes. At an average speed while underway of 25 knots, and a roundtrip distance between each recharging of 10 NM, an hourly timetable will be possible. Assuming recharging the battery 10 times each day, with 300 days of operation in a year, 3.000 cycles of the battery life will be used pr year. With the proposed Lithium Ione Titianate battery a total life securing at least 4 years or more operation with mentioned use profile is expected. During the last year the project has successfully tested this technology on cell level. Unlike in a car where the battery volume is a critical factor and the battery cells needs to be packed in a very confined space, the BB GREEN has plenty of volume available for the 400 kWh and close to 6 tons heavy battery pack. This is a great advantage for keeping temperature and stain on the battery down.

3. Requirements and critical factors

During the initial phase of the project operational requirements and critical factors related to among other hull concept, main systems /technology /installations, route requirements (here wake wash is one example), practical arrangement of the recharging and more were discussed. Issues related to passengers and crew safety in conjunction with day to day operation of the vessel were given high priority, and was a major contributor to shift from the initially proposed large surface piercing propellers to contra rotating pod propulsion, already successfully in use on another similar size ASV.

According to the project it is more important to reduce risk and improving probability of a successful concept feasibility documentation/demonstration than to gamble on a marginal efficiency improvement (with potentially also other negative side-effects).

4. Hull form design development

The project aim has been to create a waterborne transportation concept for commuter service in comparatively sheltered waters, carrying up to 100 pax + 30 bicycles. The transport should be "fast" and in this respect a time saving alternative to available land transportation easing traffic congestion ashore is presented. The primarily intended operation area is the Rotterdam surroundings, but it should suit other areas of similar conditions as well. To minimize air pollution from combustion engines electric motor propulsion has been selected.

The vessel should consume a minimum of energy per unit of transportation work - preferably the same amount or less than available transportation alternatives on shore do. It should have a minimum of impact on the environment in terms of air pollution, noise, wave erosion estuaries and other nuisance to surrounding activities within its area of operation. The tentatively anticipated concept is an Air Supported Vessel (ASV) of $(L \times B)_{design} \approx 20 \times 6$ m, weighing about 25 tons, with a speed of maximum 35 knots. The hull could either be of catamaran or mono-hull ASV design. Such ASV concepts have proven to be considerably more efficient re powering than corresponding displacement and planing solutions.

Another factor influencing the hull form design process was the original selection of propulsion, twin large diameter (1100 mm) surface piercing propellers. Later in the project it was decided to replace this propulsion with duo prop contra rotating pod propulsion (i.e. Volvo Penta IPS). For the ASV Mono these new props could be easily fitted. If the ASV Cat design had been chosen the fit would have required further changes to the hull design.

4.1. ASV Catamaran design

A total of 3 designs with 8 revisions were produced and modeled. The final design (without the air cushion enclosure flap arrangement) is showing here.

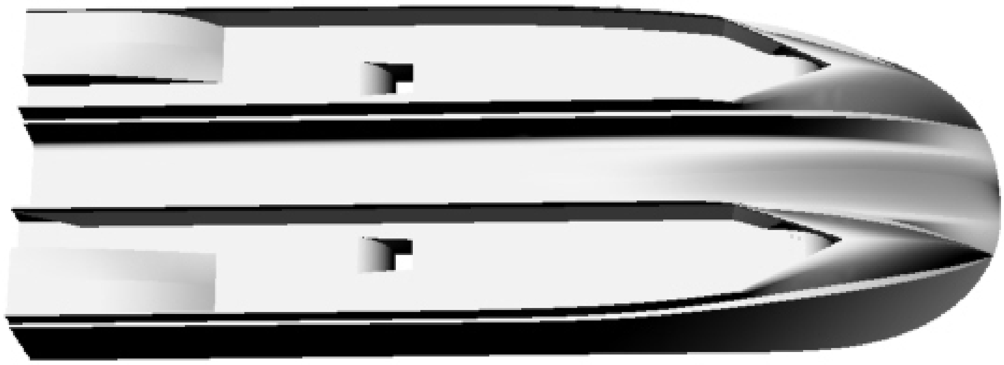

4.2. ASV Mono design

For the ASV Mono, 4 designs and 6 revisions were produced prior to the testing, and another 2 revisions after the testing. Below is showing the last version prior to tank testing (showing without the air cushion enclosure flap arrangement).

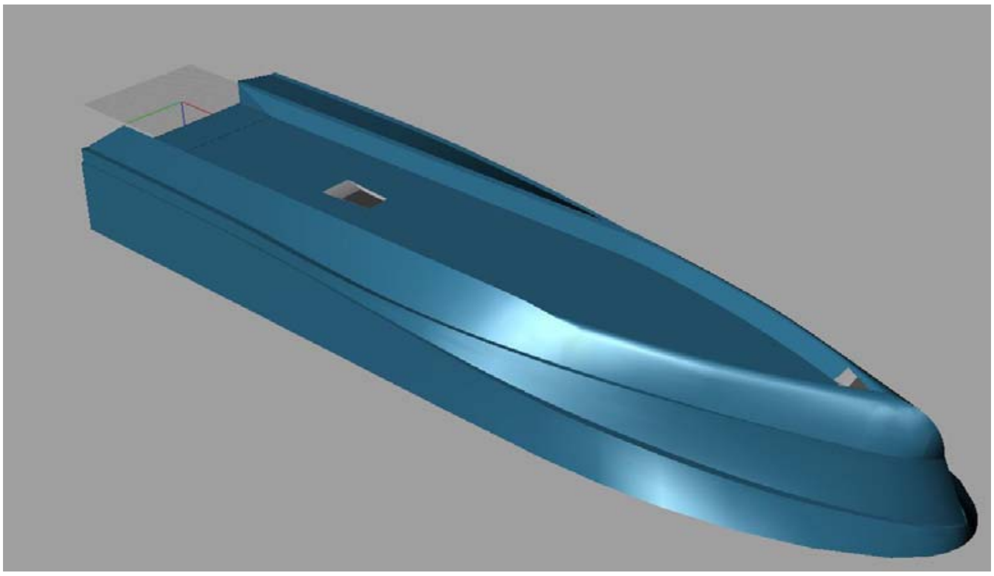

5. Tank testing

To determine the overall most competitive of the ASV Catamaran or the ASV Mono candidates, it was agreed to tank-test both designs. The models had the same overall measurements and displacements, scale 1/8 of the full size length / beam of 20 / 6 m and 22 – 28 tons respectively. (25 tons design). The tests started out with calm water testing, and the most efficient model was then tested in waves. The tank testing took place at the SSPA Sweden facilities in Gothenburg.

In the following only a few of the most relevant results and achievements will be presented.

5.1. Test results in calm water

- Tests were carried out at 3 different displacements (Full scale) 22, 25 and 28 m3.
- Model speed was varied between 10 and 35 knots with a couple of runs at 50 knots.
- Lift fan PRM and flow were varied too (giving a change in cushion pressure /air support rate).
- The ASV Cat was run with 2 fans and 4 fans, the ASV Mono with 1 and 2 fan.
- The LCG was also varied.
- Same with the air cushion enclosure flap tension.

All changes were carried out in order to minimize the hull resistance vs. speed, and to find the optimum combination of other parameters in this respect, such as LCG, air chamber pressure and air flow rate; also to observe the dynamic behavior of the hull regarding, trim, stability etc while underway.

5.1.1. ASV Catamaran

The optimum resistance seems not very sensitive to the LCG position though one might expect an optimum around 44%. It is sooner a high cushion pressure that is important for a low hull resistance. Incorporating the air flow/pressure and propulsion efficiency the total power prediction is shown below for different loadings and cushion pressures. (At 30 knots speed).

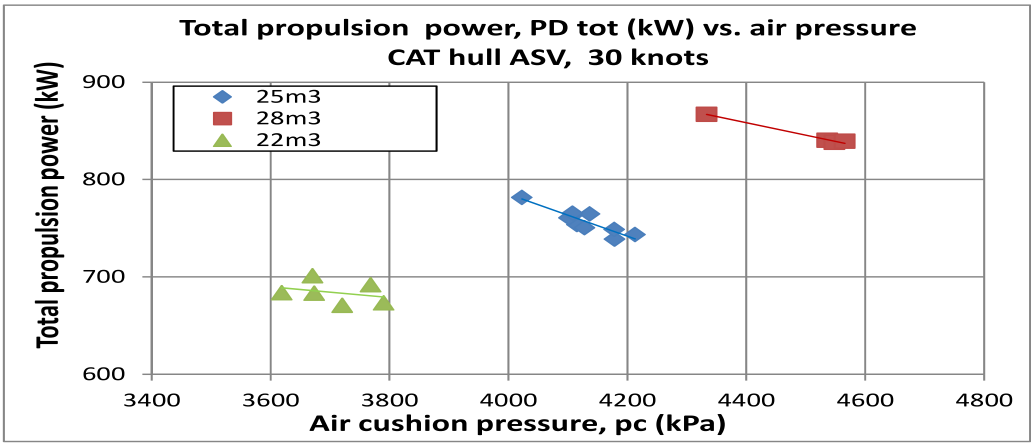

The dynamic trim angle was for the tested ASV Cat model somewhat higher than expected, approx 1,5° at 30-35 knots. The dynamic wetted surface was also a bit larger than expected. One contributing factor was the design restriction on beam, and deeper inner side keels. Within the design restrictions the cat tunnel was quite narrow, resulting in increased water level inside the tunnel and correspondingly more wetted surface. Due to the intended propulsion system (large diameter surface piercing propellers with Ø approx 1100 mm) the aft section of the demihulls were enclosing the air cushions with a combination of propulsion gondolas and air cushion enclosure flaps. The set up functioned well but was in the opinion of the test team not ideal.

5.1.2. ASV Mono

Also for the ASV Mono the optimum resistance seems not very sensitive to the LCG position, though one might expect an optimum around 43.5 %. As for the cat a high level of cushion pressure is important for a low hull resistance. The cushion pressure of the ASV Mono was throughout lower than for the ASV Cat, contributed to a larger air cushion surface of the mono.

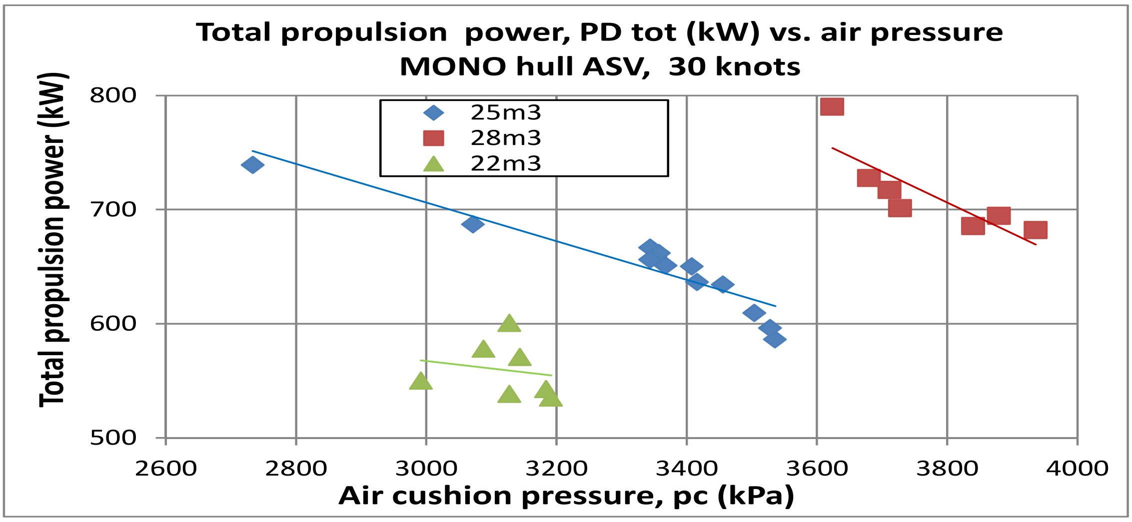

It was easier to find out where the optimum LCG vs. propulsion power should be for the ASV Mono than for the ASV Cat. Here the tendency was is that with increased weight the optimum LCG moves somewhat aft.

The dynamic wetted surface areas as determined from the under-water photos was in general somewhat smaller than expected. The dynamic trim was between 0,5 and 1 deg at 30 knots and above.

On the ASV Mono one movable air cushion flap is used.

5.1.3. Comparison of calm water results

For evaluating the calm water resistance the ASVs were compared with that of a leading conventional planing monohull (with design speed 30-35 knots). For the initial comparisons the propulsion efficiency of anticipated optimum SPP was used. As it was decided to go for another system (Volvo Penta IPS type) the powering data has used the efficiency curve for this system. For the ASVs the fan power (assuming a fan efficiency of 0,82 has also been added).

Below is a comparison of full scale resistance vs. speed for standard design displacement (25 m3) when choosing the optimum results.

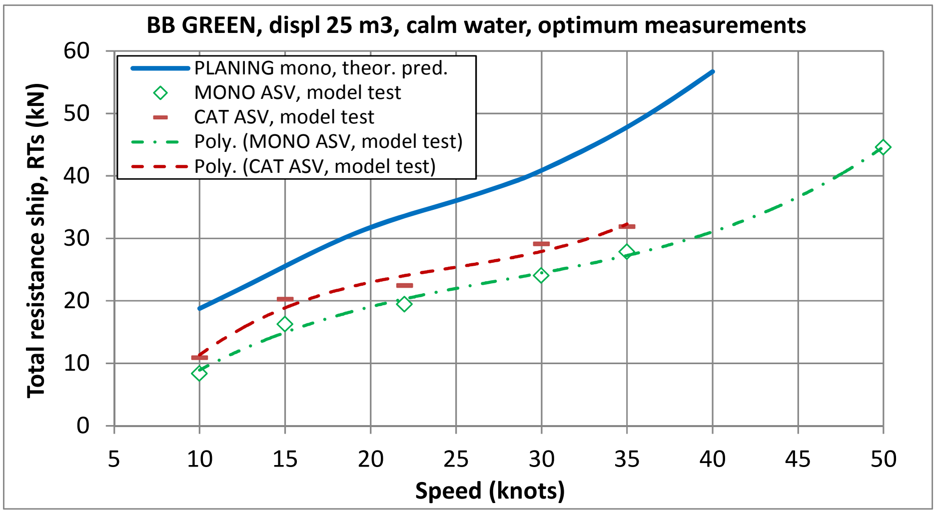

The corresponding total power for the ASV's, showing below with pod propulsion Volvo Penta IPS and with fan power included at 22, 25 and 28 m^3. In the same graph is also showing fan power requirements for the 3 displacements in calm sea and in rough sea. Compared with SOA conventional hulls the hull resistance of both the ASV Cat and even more so the ASV Mono is extremely good (low). The ASV benefits are not only valid for a limited design speed range, but for almost any speeds, from slow to design and far beyond. With more than 5.000 models of different concepts tested at SSPA, the ASVs are the most efficient tested to this data. For the ASV Mono a 40% improvement is evident over a wide range of speeds. The hull resistance gradient for both designs is remarkably flat. Still the ASV Mono stands out as a clear winner.

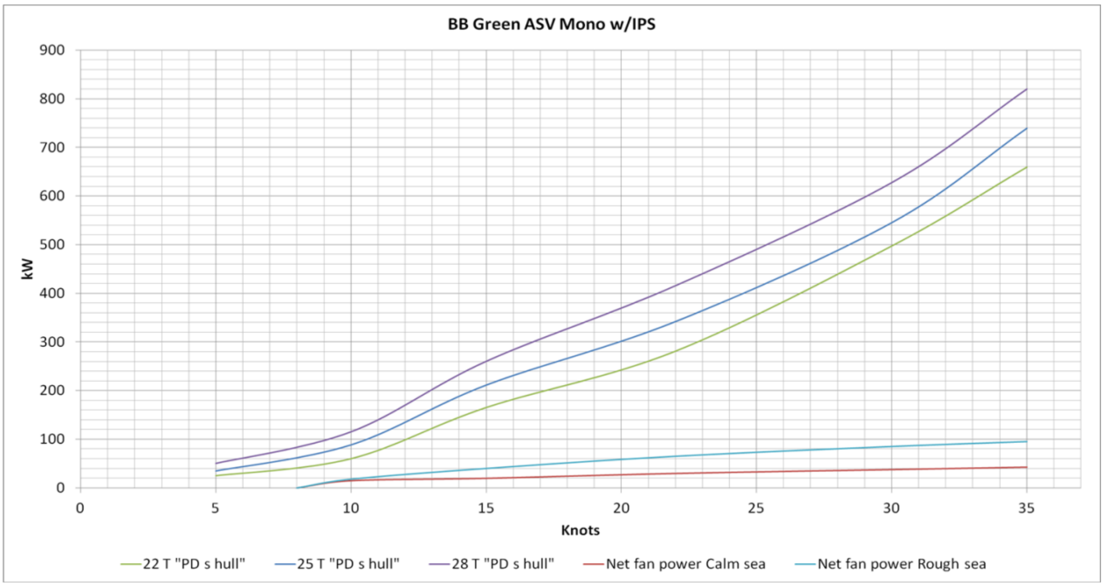

Adding the simplicity of the ASV Mono design, the great interior volumes and how "construction friendly" the design is; ASV Mono's can be built with less use of material and man hours in a mould tool, at a very competitive price.

5.1.4. Results from wash wave measurement

For BB GREEN applications and on routes close to shore and with heavy traffic, low wave wash is a firm requirement from the authorities. During the calm water testing, wave wash measurements were carried out for all runs using a wave recording device of a radar type. Distance between vessel centre line and measuring point wave cut was 24 m. The wave double amplitudes – and corresponding periods- that have been used in the comparison below are the largest one within the first three recorded periods.

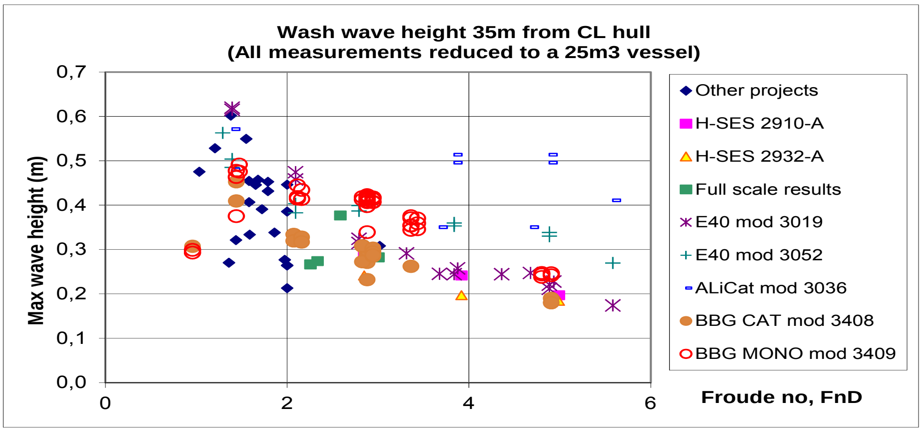

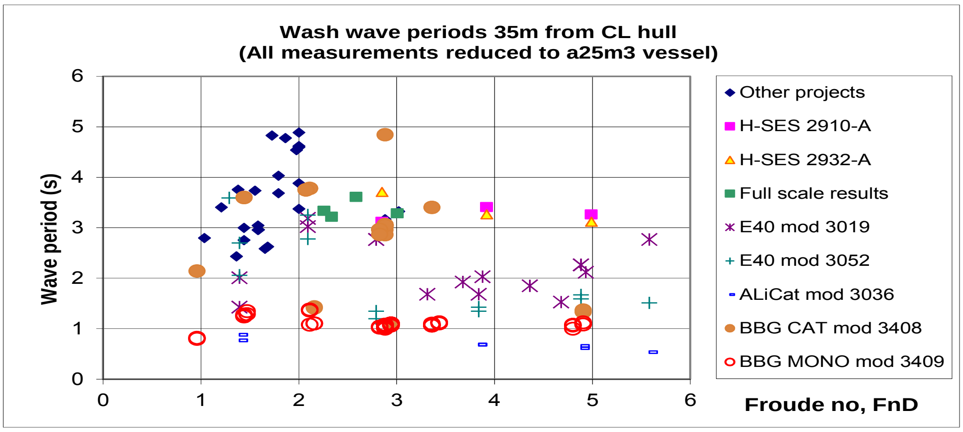

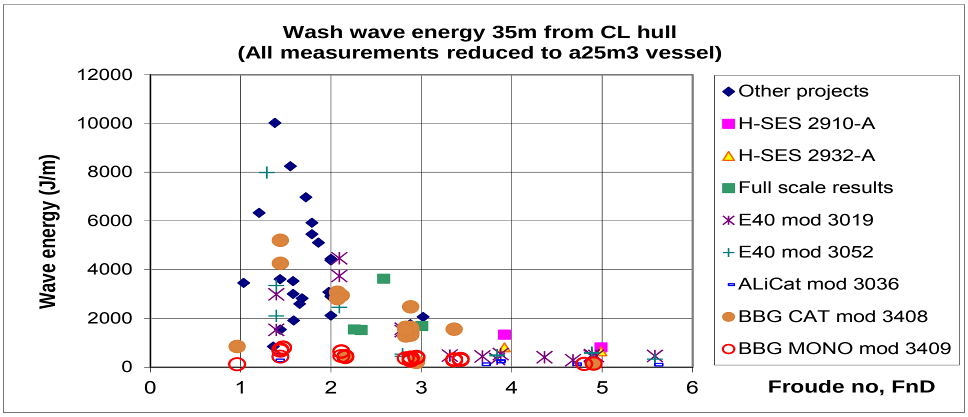

The test results are presented above vs. the displacement Froude number, together with statistics from other wash wave measurements on mono and twin hull vessels, full scale registrations as well as model test results. As an example, related to these graphs; the ASV Mono at 22 knots shows a wave height of 0.3 m, with a wash wave period of 0.9 s. As seen from the wave energy graph, the resulting wash wave energy is remarkably low. The energy for other FnD is also showing very low values indeed. These results are very encouraging for the viability of the hull form.

5.2. Test results in waves with ASV Mono

The tests in a seaway were carried out to determine the added resistance in waves, vertical accelerations and motions, and for observing and identifying any tendency to unexpected dynamic behavior. The tests in irregular head- and following seas were made mainly in order to judge the passenger comfort and added resistance. The tests in regular waves were thought to represent occasional larger wash waves created by passing larger vessels. The tests in regular following waves were also made to find any tendency to bow diving.

5.2.1. Irregular head seas

The testing was focused on 3 speeds 22, 30 and 35 knots. Wave height Hs = 0.5 m and 0.88 m, the latter was agreed to be higher than what could be expected for the targeted operations. Wave frequency Tz= 3.0 and 3.9 s. Fan flow/RPM of the fan system was also varied with higher flow rate with the higher waves. Vertical motions, vertical acceleration, pitch angle, heave motion and added resistance of the model were measured.

For the BB GREEN type of ferries the duration of the travel is very short, never exceeding 30 minutes, in most cases only lasting a few minutes. The maximum length of the journey is set by the battery capacity. As to passenger comfort with regards to motion sickness incidence the r.m.s. acceleration response at LCG has been plotted again in ISO 2631/3-1985 (E), graphs, where the limit for 10% motion sickness incidence with respect to exposure time are included.

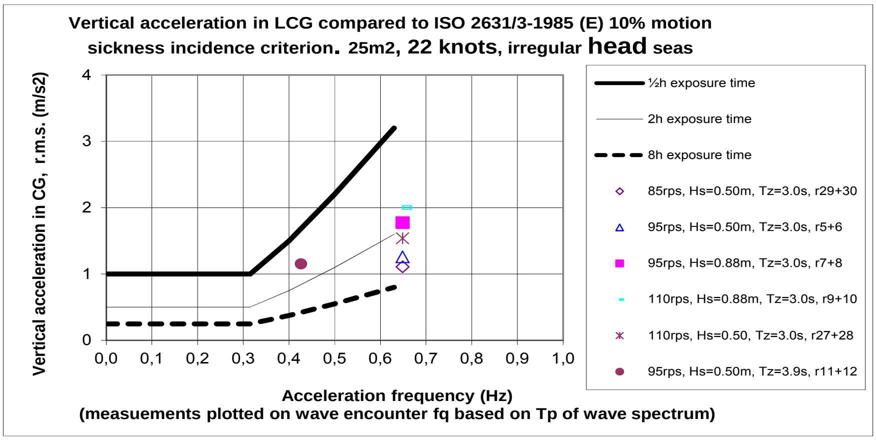

At the example presented above for 22 knots speed one will see that the vertical accelerations for most runs with 0.5 m significant wave height, approx 2 h of travel will be acceptable. Such duration is far exceeding the max travel time for the targeted type of operation. Even with 0.88 m sign wave height the vertical accelerations will be acceptable. When looking at higher speeds (30 and 35 knots) the vertical accelerations are equally acceptable.

5.2.2. Irregular following seas

Tests were made at 22 and 30 knots and waves of $H_{1/3}$ = 0.5 m and T_z= 3.0 s. The encounter period is much longer and as the encountering period is further away from the hull natural pitch period the response become smaller than in head waves. Even if the vertical motions could be of the same magnitude as in head seas the accelerations are generally lower in following seas since the encounter period is longer.

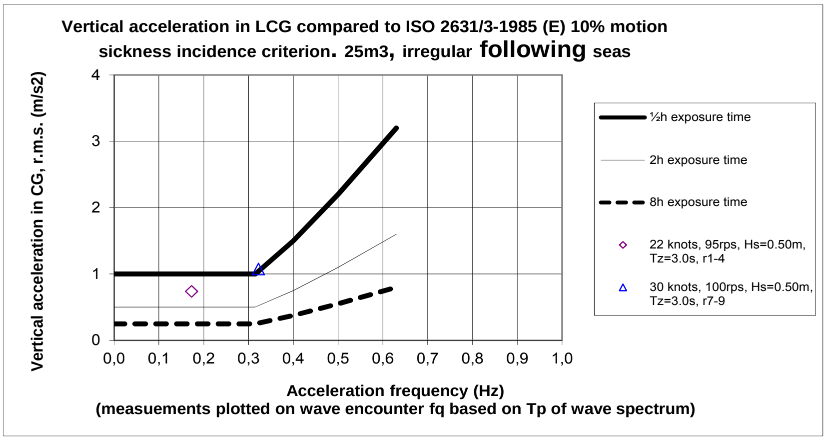

Both motions and accelerations are smaller in following seas but also the encounter frequency is smaller. Therefore the acceleration response moves into a frequency range where the human body is more sensitive to motion sickness. Anyhow, it seems that some ½ to 1 hour exposure time will be acceptable with regards to 10 % MSI.

5.2.3. Regular head seas

Tests were done to simulate occasional wash waves from other vessels. Such waves are typically only occurring as trains consisting of a few waves. Like in irregular head seas the minimum motion is located around the aft ¼ length, same as with the acceleration. With increasing speed the location moves a little backwards. The exposure will be too short to initiate any motion sickness.

5.2.4. Irregular following seas

Motions are of the same order but accelerations are smaller than in regular head waves; this is similar to the behavior in irregular following vs. head seas. In relation to the speed of travel of the regular wave with period T=5.86 s the vessel sails some 25 % faster at 22 knots, 46 % at 26 and 69 % faster at 30 knots. In these range of speed ratio vessel/wave one might expect to find any tendencies to bow diving if there is any; however nothing of that was seen.

Below is summarized pitch, heave, added resistance and added total propulsion power for the three regular wave conditions:

Test condition	Sign. Pitch angle, single amplitude (°)	Sign. Heave, single amplitude (m)	Resistance in waves vs. calm water (-)	Resistance in Waves & wind vs. calm water (-)	Total propulsion power in a seaway vs. calm water (-)
30 knots, 95 rps, H=0.50m, T=5.86s, run 10	1.60	0.15	1.19	1.15	1.21
30 knots, 100 rps, H=0.50m, T=3.29s, run 11	0.77	0.07	1.29	1.25	1.28
26 knots, 100 rps, H=0.50m, T=5.86s, run 12	1.51	0.15	1.15	1.11	1.18

5.3. Fan flow calibration and assessment of fan powering

After completion of the calm water and sea keeping tests, the air flow through the fans were calibrated. During the testing in calm water the ASV Mono was tested out with both 1 and 2 fans, in sea tests with 2. Below are presented a couple of pictures of the rigging of the model.

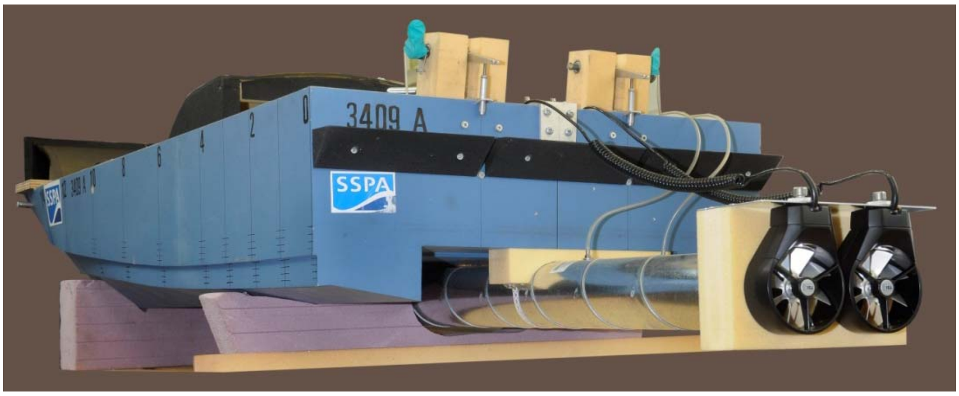

6. Development of systems

During second phase of the project the following systems will be developed:

- Battery pack: For the test vessel a (½ size) battery with a 200 kWh capacity will be developed. The battery will have a nominal voltage of approx 750 - 800 V DC.
- Electric drive lines for propulsion and lift fan system: The propulsion driveline will be configured to match the shafts speed (RPM in) for the selected prop propulsion system. The electric motors will be set up for up to 400 kW (peak power).
- Power management system: To handle all onboard electric consumers (propulsion, lift fan and onboard domestic systems) as well as power in (from the onshore recharging system; and from an onboard recharging system (diesel generator)). Pending.
- Lift fan system: To handle with high efficiency the air cushion requirements in terms of pressure (up to approx 5 kPa) and flow (up to approx 10 m3/s). The fan, ducting and bell mouths will be made from lightweight composite materials.
- Propulsion and steering: Pod proulsion will be supplied in a ready to install package. A main challenge is converting/adapting the handling of the system to electric operation.

Finally installing and integrating the systems in the vessel is another main task when the hull has been built.

7. Battery technology and accelerated testing on cell level

Lithium Ion batteries with Atairnano's patented Nano Technology has not yet been developed for heavy duty marine propulsion power application. In BB GREEN, partner Amber is developing a "marine" battery pack to propel the BB GREEN vessel and ASV lift fan system. The planned unit will have capabilities beyond current state of the art, which are conventional Lithium Ion batteries, on level (kW) of power charge/discharge, short time for recharging and expected number of cycles (battery life).

Consideration should be given to designing hull and drive line with optimum efficiency. This is a key factor to the battery design as any additional loading will increase the cost, size and weight of the battery. Acceptable recharging profile, full capacity may not be used at once and the battery may require a "warm up" time that reduces the actual average recharging capacity. Care must be taken, however, to avoid over heating the battery is important. Temperature increases beyond acceptable levels will reduce battery life and be a safety risk.

The battery could take recharge from two or more sources at the same time, i.e. shore power in combination with an on-board generator / range extender.

Although not part of the project securing enough grid capacity where the battery charging will be taking place will be important when addressing commercial BB GREEN routes.

One of the biggest issues associated with large scale integration of battery cells in transport applications is to understand the actual duty cycle that the battery assembly will undergo. This is important as the control system needs to regularly monitor certain parameters in known conditions to optimize the battery functionality and maximize its lifetime. To this end, the BB Green application has an ideal duty cycle that has both predefined and consistent discharge and charge cycles that make software configuration and calibration relatively straight forward.

Environmental standards will need to be careful chosen and tuned to battery technology. The existing industry standards are not currently appropriate for this type of energy storage.

Testing on cell level. Below illustration shows BB GREEN duty test profile for 5 cycles.

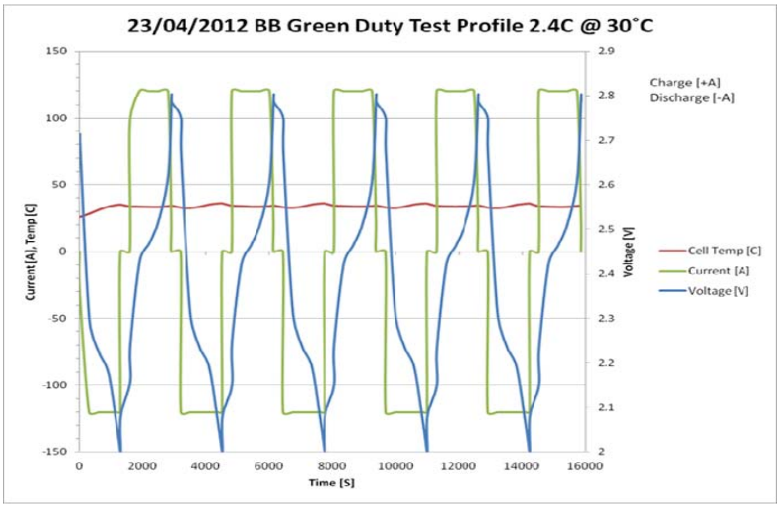

The graph below shows the test results when 1900 cycles accelerated testing cycles had been completed. The capacity of the battery cell was still above nominal capacity level of 50 Ah.

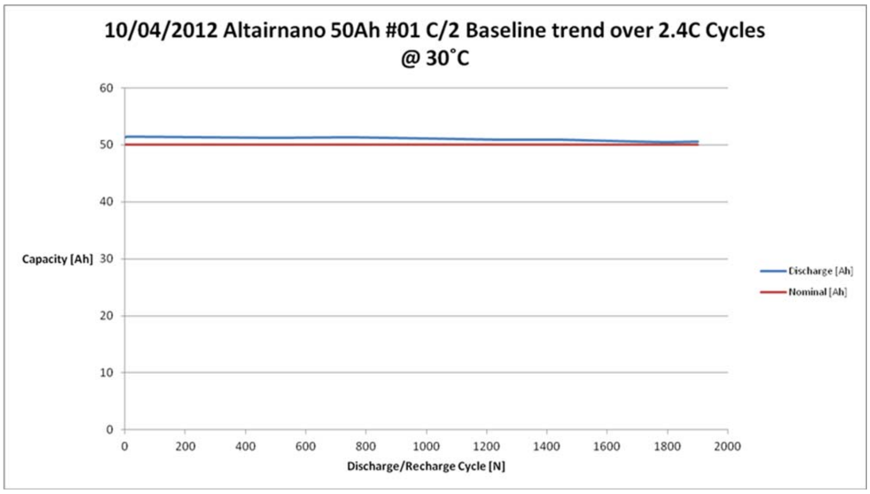

The second graph demonstrates very good resemblance between the test-data and data sheet from the cell provider.

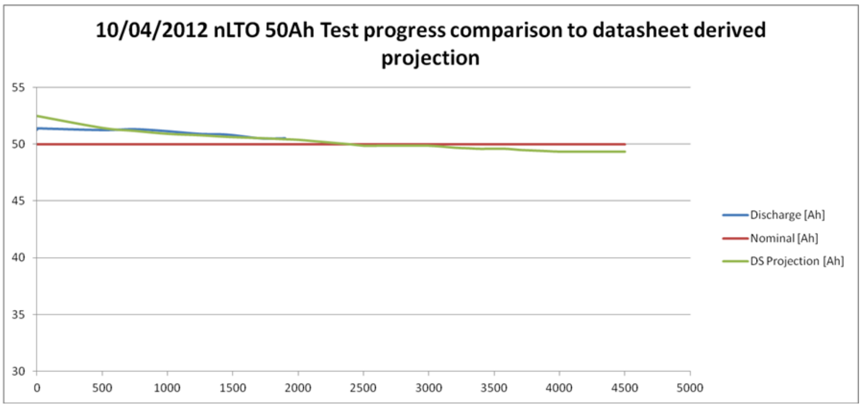

Evaluating the data arrived from tank testing, etc., the following conclusions can be drawn:

- Traction power @ 25T and 30 knots = 545 kW
- Fan power @ rough sea = 80 kW
- Domestic consumption overhead @ 5% = 6 kW

- Total load = 631 kW (equates to approximately 800A continuous current)
- Journey Time of 15 minutes (7.5 NM), capacity = 616kW * 0.25h = 158 kWh
- Giving approximate consumption in kW/NM = 21.07

This value is more than 15% better than the original prediction (24 kW/NM) and verifies the suggested battery configuration and cell test to date.

8. Construction of test vessel, outfitting and planned testing

Assuming construction of the vessel gets its final go ahead from the Commission, a construction and outfitting period of approx 1 year is foreseen. Where it will be built is subject to the outcome of the tender process. The vessel will be fully instrumented on concept as well as system level. Testing and data collection will be done primarily on a number of selected appropriate routes. Following debugging and completion of optimization the vessel will be made available for demonstrations. The academia, press, operators and ship owners will be invited onboard for demonstrations. These activities will be handled primarily by the end user partner (Aqualiner) and the project coordinator (SES Europe). Additional information and results will be disseminated at conferences and in the press when available.

9. Design

In general the selected ASV Mono hull is quite unique with regards to great interior volumes in the hull. The sides are almost vertical and the air water foot print is quite large. For a commuter vessel like BB GREEN the main deck of the vessel can be set quite low. The propulsion / drivelines are quite small and the battery can be packed in almost any shape to maintain a low main deck level. In other words the owner / operator and designer have a great degree of freedom in designing the superstructure and arrangement onboard. Preparing a specific design has not been the main focus for BB GREEN, the important task is to prove, given a defined total displacement, that the vessel will perform and function as planned. To visualize one possible design students in collaboration with SES Europe have prepared a possible design. With this design the vessel will carry approx 80 Pax and 30 bicycles (another request from the Dutch partner) on main deck. In addition there is a full fly deck, which can come handy when/if the vessel will have a second duty as a charter/ excursion vessel.

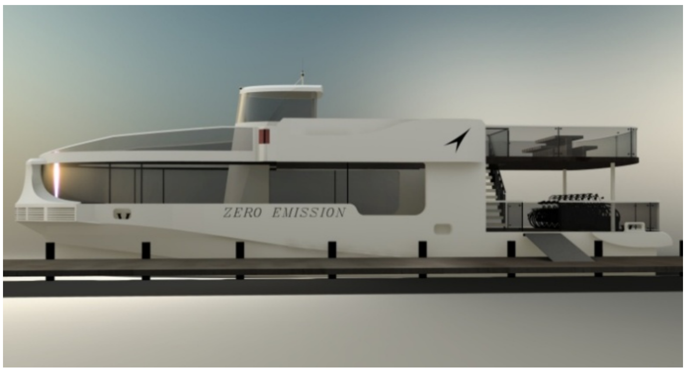

10. Conclusions

The BB GREEN project is making good progress. The concept- and hull form development have been completed to the full satisfaction of the project team. From evaluation of alternative battery cell technologies in the opinion of the project only the selected Lithium Ion Nano technology seems capable of handling the though use profile, many cycles and fast recharging required for a tough BB GREEN use. However, constructing and testing a full scale BB GREEN vessel under realistic operational conditions is the only way to finally prove feasibility of the concept and to boost concept dissemination and secure exploitation.

11. Acknowledgements
The research leading to these results has received funding from the European Union 7th Framework Program under grant agreement no. 234124.

References

ALLENSTROEM, B.; LILJENBERG, H.; TUDEM, U. (2003), *Concept development and model testing - new generation Air Assisted Vessels (AAV) with Water Jet propulsion,* FAST 03, Ischia

EILERTSEN, A.; TUDEM, U. (2003), *Design development – 23 m Air Supported Vessel (ASV) with WJ,* Int. Air Cushion Technology and Exhibition, Southampton

EILERTSEN, A.; GRIEG EIDE, J.; TUDEM, U. (2004), *Design development of advanced air supported Vessel (ASV) designs,* RINA WARSHIP, London

LIVGARD, T.K.; TUDEM, U. (2009), *High performance with improved onboard comfort: Introducing ASV "Soft Motion" mono with water jet propulsion,* RINA SURV 7, Poole

LIVGARD, T.K.; TUDEM, U. (2009), *Design development, prototype construction and test outfitting of the air supported monohull by Effect Ships International AS,* RINA, London

LIVGARD, T.K.; TUDEM, U. (2010), *Air supported vessel (ASV) monohull, design development of test vessel and proof of concept,* 31. Symp. Yachtentwurf und Yachtbau, Hamburg

LIVGARD, T.K.; TUDEM, U. (2011), *Air supported vessel (ASV) monohull demonstrator. Design development, testing at sea and results proving the concept,* HSMV, Naples

TUDEM, U. (2011), *Air supported vessel (ASV) – innovative fast vessel technology with great operational and environmental benefits,* TEKNA 2011 Copenhagen

On the Design and Resistance Prediction of Large Medium-Speed Catamarans

Max Haase, Giles Thomas, Jonathan Binns, Neil Bose, Australian Maritime College, Launceston/Australia, mhaase@amc.edu.au
Gary Davidson, Revolution Design Pty Ltd, Derwent Park/Australia

Abstract

Medium-speed catamarans are under development as a new class of vessels to meet requirements for highly efficient sea transportation with a low environmental impact. A reduction in service speed and an increase in deadweight will lead to high transport efficiency. Compared to current high-speed catamarans, these new vessels will operate at a transitional speed range between those of high-speed craft and conventional displacement ships. In this paper, design guidelines to choose appropriate hull form parameters for medium speed catamarans with minimum resistance were derived and a preliminary design made. Most important these vessels will operate at Froude numbers of Fr = 0.35 and have a relatively low prismatic coefficient of $C_P \approx 0.5$ in conjunction with a low transom immersion. To correctly predict the calm water resistance, different methods to predict the calm water resistance of such vessels are discussed, whereas viscous free-surface flow simulations are most promising. It is shown that they are capable of predicting the hydrodynamic behaviour of medium-speed catamarans, such as drag force, trim and sinkage within an acceptable range of accuracy.

1. Introduction

Large high-speed catamarans have evolved in the last two decades as an efficient vessel class for fast sea transportation. To promote sustainable sea transportation and to meet rising ecological requirements to reduce environmental impact, a new class of large fuel-efficient medium-speed catamaran ferries is under development. Rising fuel prices and society's increasing awareness in environmental sustainability raise the demand for highly fuel-efficient vessels. As shown in earlier work, an increase in vessel size and deadweight, combined with a reduction in velocity, can lead to a significant increase in transport efficiency compared to existing catamaran ferry designs, *Haase et al. (2012)*. This combination of length and speed transfers the design from the planing regime, where tangential stresses dominate, to a transitional speed between the displacement and planing regime where tangential and normal stresses cause drag at a similar magnitude or the latter one being dominant. A possible general arrangement of such a large medium-speed catamaran can be seen in Fig.1.

Fig.1: General arrangement of a large medium-speed design by *Davidson et al. (2011b).*

To efficiently develop hull forms with low drag for such craft the potential design space needs to be reduced. This includes defining zones for the vessel's length, prismatic coefficient, transom immersion and demihull separation. Once an initial set of appropriate hull form coefficients is identified, suitable methods are required to evaluate parameter variations towards minimum resistance.

Nowadays, different methods are utilised to determine the calm water resistance of ships each having their specific advantages and disadvantages for certain types of ship at particular speed ranges, as they vary in cost, effort and accuracy. The most important procedures are listed and discussed with respect to their suitability for medium-speed catamarans. Following this, results of inviscid free-surface simulation compared to experimental results are presented.

1.1. Initial design space

To derive preliminary design parameters for large medium-speed catamarans recommendations from the literature were surveyed. In Fig. 2, designs of high-speed catamarans of the early 1990's, recently built high-speed ferries, a recently proposed medium-speed design and fast monohull ferries are compared by their speed and length, *Trillo (1991), Incat (2011), Austal (2011), Davidson et al. (2011b)*. It can be observed that monohull ferries stay below a Froude number of 0.35 and that recent high-speed catamarans increased in length compared to earlier high-speed catamarans and established a service speed of around 40 knots. For high-speed ferry designs exceeding a length of 100 m a reduction in speed can be identified. It is expected, that the prospective design of a highly fuel efficient large catamaran ferry will be in the range of L = 100 - 160 m and at a speed of approximately 25 knots, which presumes a design space somewhere between fast monohull ferries and modern multi-hull high-speed ferries.

It was presumed that medium-speed catamaran designs will differ from modern high-speed catamarans in size and speed significantly and new design guidelines for such craft are required, *Davidson et al. (2011a)*. To determine hull form parameters for such vessels that feature a minimum resistance, recommendations based on statistics from existing monohull ships and model test series of single and twin-hull vessels will be analysed.

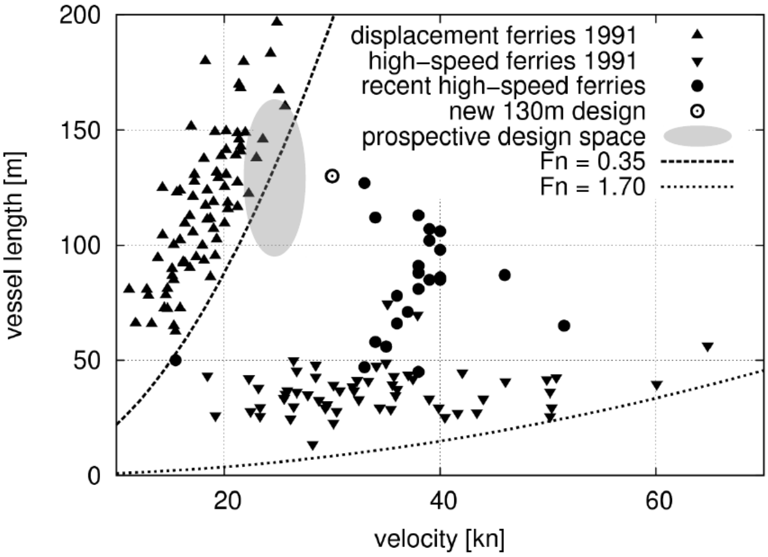

Fig.2: Comparison of fast ferries by length and speed *(Haase et al., 2012).*

1.2. Resistance components

The total drag of ships can be subdivided into viscous and potential flow components. Generally spoken, the first one is expressed by a friction line and multiplied by a form factor (C_F $(1 + k)$), the latter one can be obtained from the integration of normal pressure on the hull or ideally from wave cut methods and therefore be considered as wave pattern resistance (C_W). For catamarans the demihull interaction, influencing the viscous and potential flow components, needs to be considered, *Insel and Molland (1991)*. *Couser (1997)* mentions two additional significant resistance components, namely transom drag and wave-breaking drag which especially occur in the medium-speed range of catamarans. Neither are reflected in the viscous or wave pattern components and a discrepancy between the classically decomposed resistance ($C_T = (1 + k)C_F + C_W$) and model experiments can be observed, *Molland et al. (1994)*. This is why resistance prediction tools for craft operating in the medium-speed range need to be carefully chosen to consider all governing physical effects.

1.3. Methods of resistance prediction

a) Empirical Methods
   Empirical methods are robust and can deliver good estimates at low costs, if the characteristics of the proposed catamaran design fall into the validity range of the method under consideration, *Sahoo et al. (2007,2008)*. Unfortunately, most regression models for catamarans, such as that by *Sahoo et al. (2007)*, have been developed for high speeds and therefore they deliver good results in the high-speed range, but at low speeds, especially below hump speed the predictions are not sufficiently accurate.

b) Potential Flow Methods
   Neglecting viscous components, potential flow methods are suitable to predict flow effects that are related to normal pressure on the hull, such as the wave-making resistance. *Sahoo et al. (2004)* and *Salas et al. (2004)* presented potential flow simulations to predict the resistance of catamarans for a wide range of Froude numbers. Both show good agreement for Froude numbers exceeding 0.5, but deliver poor results for

medium-speed range. While the wave resistance by *Sahoo et al. (2004)* is under-predicted, the total resistance of *Salas et al. (2004)* is over-predicted. This discrepancy may be allocated to resistance components such as transom drag or wave-breaking which are not or not accurately resolved by these methods in the medium-speed range.

c) Model Tests
Even though model tests are time and cost consuming they are an essential part in the ship design process to determine the ship resistance and to validate numerical simulations, *Bertram (2000)*. Hydrodynamics of catamarans have been experimentally investigated by *Molland et al. (1994)* and *Molland and Lee (1995)*. These experiments significantly contributed towards the understanding of the hydrodynamic performance of such vessels in the low, medium, and high-speed range. Regardless, for nearly all experiments the total drag is measured only and thus model tests do not provide details on the physics of the flow around the vessel unless measured with a considerable effort. However, the uncertainty of experimentally measured values can be as high as 10% for the resistance coefficient, 42% for sinkage and 52% for trim, *Gorski et al. (2011)*.

d) RANSE Methods
The Reynolds-Averaged Navier-Stokes Equation (RANSE) is capable of describing a viscous free-surface flow mathematically. The equations are solved in a spatially discretized domain around the hull. They are still gaining popularity in marine applications and are mainly used for flow investigation around the vessel's aftbody where viscous effects are dominant, but they are also capable of modelling the free-surface and dynamically moving ships. Furthermore, RANSE simulations can deliver an insight to flow phenomena around the hull, and may be used in conjunction with model tests during the ship design process *(Bertram, 2000)*. Compared to other computational methods RANSE-based methods require a relatively high computational effort, but are able to resolve viscous effects such as friction and separation and phenomena caused by normal pressure such as wave-making. *Stern et al. (2006), Broglia et al. (2009)* and *Haase et al. (2011)* used RANSE methods to successfully predict hydrodynamic forces and dynamic floating positions of catamarans and demihull interaction effects in the medium speed range within 15% of accuracy. *Stern et al. (2006)* state it is less accurate for catamarans compared to monohulls due to an under estimated demihull interaction.

2. Hull form parameters

2.1. Speed-length relation

The length of the design has to be determined according to the vessel's speed. For advantageous wave-making properties, the interaction of length and vessel speed by the Froude number (*Fr*) has to be taken into account. Compared to monohull designs *Michel (1961)* states that catamarans can have a lower total resistance at Froude numbers around 0.35. At this certain speed, a hollow in the resistance curve has been observed in the majority of surveyed experimental data such as by *Vollheim (1968)*, *Insel and Molland (1991)*, *Molland et al. (1994)*, *Davidson et al. (2011a,b)*. For any speeds beyond, a significant change in trim is related with an increased resistance gradient. As suggested by *Davidson et al. (2011a)* or recently proposed by *Austal (2012)* a target Froude number of Fr = 0.35 is focused on in the design.

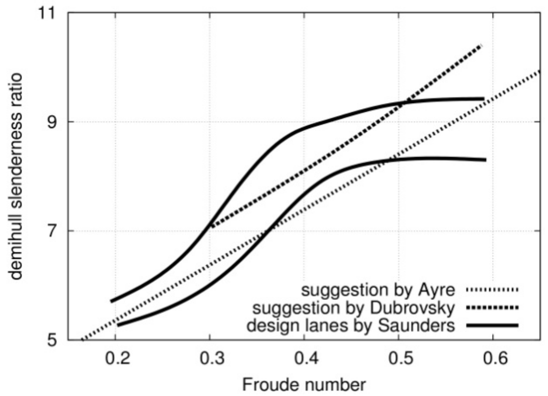

Fig.3: Recommendation for slenderness ratio as a function of Froude number.

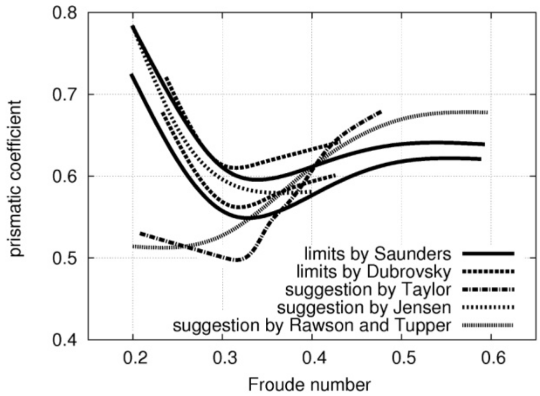

Fig.4: Recommendation for prismatic coefficient as a function of Froude number.

2.2. Slenderness ratio

The slenderness ratio is known to be the predominant hull parameter influencing the calm water resistance of high-speed displacement hulls *(Molland et al., 1994)*. While a slender hull is favourable for wave-making resistance, it is also related to a relatively large wetted surface area and therefore frictional resistance *(Sato et al., 1991)*. Recommendations for slenderness ratio have been made by different authors that expressed appropriate values with respect to Froude number. In Fig. 3 propositions from *Saunders (1957)*, *Dubrovsky and Lyakhovitsky (2001)* and *Ayre (Schneekluth and Bertram, 1998)* can be seen. The values of recommended slenderness increase with an increase in Froude number, apart from the recommendation from *Saunders (1957)*, who suggests the slenderness should not increase for Fr > 0.5.

Insel and Molland (1991) reported high-speed displacement hulls having a typical slenderness ratio between 6 and 9. *Sato et al. (1991)* investigated catamarans at Froude numbers below unity utilising a slenderness ratio of 10 - 13 for an optimum performance. *Davidson et al. (2011a,b)* experimentally studied the calm water resistance of medium-speed hull forms utilising slenderness ratios of 10 - 12 for Froude numbers of 0.3 < Fr < 0.6.

Table 1: Parameters of considered catamaran designs derived from the Molland series.

NPL	L [m]	B_{OA} [m]	∇[m3]	$L/\nabla^{1/3}$	s/L	A_{deck}[m^2]	S [m^2]	λ
4b	110	56	6,676	7.4	0.4	6,160	3,200	68.8
5b	130	51	6,260	8.5	0.3	6,630	3,649	81.3
6b	145	40	7,270	9.5	0.2	5,800	3,825	90.6

2.3. Prismatic coefficient

The prismatic coefficient (C_P) provides information on the ship's buoyancy distribution. The displacement can be concentrated at amidships (low C_P) or equally distributed over the ship length (high C_P). Values of C_P suitable for monohulls are not necessarily optimum for catamarans, appropriate values of C_P for twin-hull vessels may be smaller than suitable ones for monohulls (*Sato et al., 1991, Molland and Lee, 1995).* Moreover, *Molland and Lee (1995)* propose that the effect of prismatic coefficient on the resistance is more pronounced at slow speeds, whereas a smaller prismatic coefficient is to be preferred for single and twin-hull ships using fast displacement hulls at low Froude numbers. Fig. 4 shows recommendations from *Rawson and Tupper (2001)*, *Jensen (1994)*, *Taylor (1943)*, *Dubrovsky and Lyakhovitsky (2001)* and *Saunders (1957)* for optimum prismatic coeffcient with respect to varying Froude number. The majority of the recommendations suggest decreasing prismatic coefficients for smaller Froude numbers with a minimum of $C_P \approx 0.55$ up to $Fr \approx 0.33$ and further increasing values for increasing Froude number, but not exceeding a prismatic coefficient of $C_P = 0.7$.

2.4. Demihull separation

The separation of demihulls has a significant inuence on the resistance of catamarans. It can be estimated by considering by two basic flow phenomena: Firstly the wave systems of the two demihulls superimpose upon each other and secondly the demihulls induce velocity fields on each other *(Vollheim, 1968; Everest, 1968 and Miyazawa, 1979)*. *Eggers (1955)* and *Saunders (1957)* mention the interference effects depend on the separation-length ratio (s/L), rather than on separation-width ratio (b/B), because the bow wave of the one demihull interacts with the stern wave of the other. *Everest (1968)* mentions favourable combinations are $0.2 < s/L < 0.4$ and $Fr = 0.26$ or $0.30 < Fr < 0.38$, and Froude numbers above 0.38 should be avoided. *Eggers (1955)* found preferable powering performance experimentally at Fr = 0.24 - 0.28 and Fr = 0.34 - 0.38 for s/L = 0.19. Correlating with that, *Tasaki (1962)* mathematically derived areas of reduced wave-making of catamarans at around $Fr \approx 0.26$ and $Fr \approx 0.33$ for different separation ratios. With reference to his work, the most advantageous wave interaction occurs at s/L = 0.3 and Fr = 0.33. As discussed in *Turner and Taplin (1968)*, wave resistance reduction can only occur due to stern waves cancelling the bow waves and an optimum interference factor is inuenced not only by the separation ratio s/L and Froude number, but also by hull form or particular stern shape.

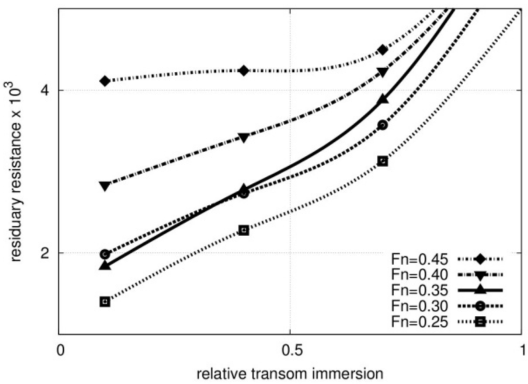

Fig.5: Residuary resistance for catamarans at certain speeds with varying transom immersion ratios as determined by *Hadler et al. (2009)*.

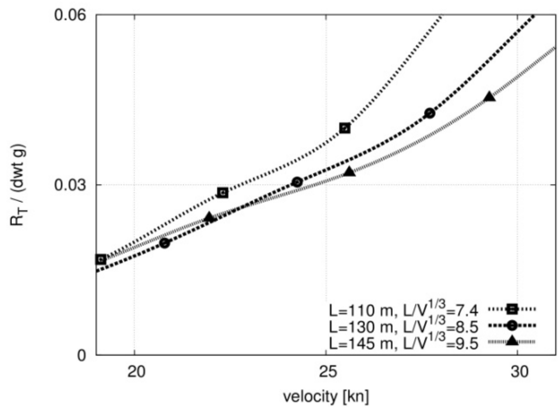

Fig.6: Normalised resistance for varying velocity of extrapolated models of the Molland series *(Molland et al., 1994)*.

2.5. Transom immersion

Hadler et al. (2007) studied different transom immersion ratios over a wide range of Froude numbers for single and twin-hull vessels *(Hadler et al., 2009)*. The transom immersion ratios A_T/A_X ranged from 1.0 to 0.1. Both investigations led to the conclusion that a reduction in immersion ratio decreases the residuary resistance of a vessel, especially for Froude numbers below 0.5 (Fig. 5), same was mentioned by *Fry and Graul (1972)*. A stern wedge at the hull with the lowest transom immersion increases the relative transom area, but results in a further decrease in residual resistance for $Fr > 0.3$. Trim and sinkage is more pronounced for decreasing transom immersion, but an applied stern wedge will outweigh this effect. It has to be mentioned that the prismatic coefficient of the hull forms of *Hadler et al. (2007, 2009)* decreases with decreasing transom immersion. Therefore, the decrease in resistance cannot be correlated with the transom immersion ratio only.

2.6. Overall slenderness

The study on hull form parameter concluded that slender hulls have favourable wave making properties, but unfavourable wave interference properties. Hulls with a low L/B_{OA} ratio have considerable wave-making characteristics but can have favourable interference behaviour. The question is, if the slenderness optimal for a single demihull in isolation appropriate for two demihulls in close proximity or do demihull interference effects changes the values of slenderness optimum? Therefore an optimum configuration is expected to exist, which provides the lowest total drag force at a certain speed. Model test data of *Molland et al. (1994)* with catamarans of varying slenderness and separation ratios have been examined. Considering a large medium-speed catamaran able to carry 4,500 dwt, specified by a deck area of A_{deck} = 6,000 m^2 and a service speed of 26 knots, several configurations of the model test series of *Molland et al. (1994)* differing in demihull slenderness and separation ratio can satisfy these specifications. In Table 1, the main particulars of the designs under consideration are summarised. The model test results were extrapolated to full scale using the formulation:

$$C_{TS} = C_{TM} - (1 + k)\,(C_{FS} - C_{FM})$$

where C_T is the total resistance, $(1+k)$ the form factor and C_F the ship-model correlation line. The subscripts S and M denoted the values for the full scale ship and for model scale, respectively. The above approach assumes that not only the wave pattern resistance, but also the residual components such as transom drag and wave-breaking as mentioned by *Couser (1997)* are scaled by the similarity law of Froude. In earlier work *(Haase et al., 2012),* the latter two have been scaled according to the ship-model correlation line which means they would be less pronounced at full scale which may lead to different results. The total resistance is normalised by gravity (g) and deadweight tonnes (dwt) and plotted with respect to velocity in Fig. 6. In the speed range of 20 - 30 knots, a design of 130 m in length having an overall slenderness of L/B_{OA} = 2.5 would be beneficial up to a speed of 23 knots and above that speed a design of 145 m with an overall slenderness ratio of L/B_{OA}= 3.6 would provide the preferable resistance characteristics.

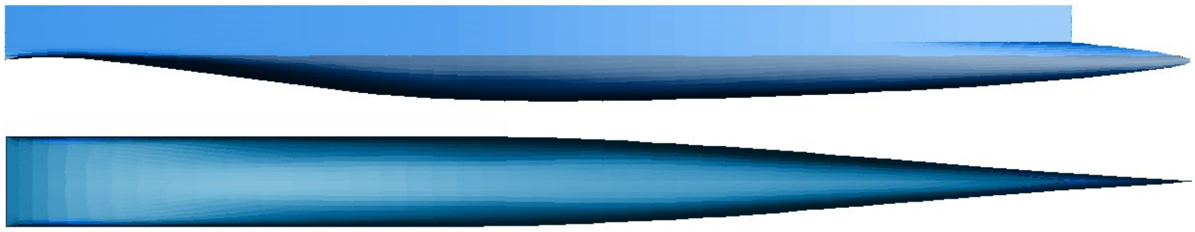

Fig.7: Profile (top) and plan view (bottom) of a possible design of a demihull for a medium-speed catamaran with hull form coefficients appropriate for minimum resistance.

2.7. Possible medium-speed design

Using the hull form parameters derived in the previous section, an initial hull design for a medium-speed catamaran demihull can be drawn. First of all the overall length and demihull slenderness for a certain speed can be found from Fig. 6. Specifying the required deck area, the related demihull separation ratio is de_ned accordingly. Appropriate hull form parameters such as prismatic coefficient can be determined depending on the Froude number, whereas zero transom immersion in conjunction with a stern wedge may be optimum regarding to the above section. For a vessel with a load of 4,500 dwt, a deck area of A_{deck} = 6,000 m^2 and a service speed of 26 knots, a Froude number of Fr = 0.35, a prismatic coefficient C_P = 0.5 and slenderness ratio of $L/\nabla^{1/3}$ = 9.5 will deliver initial optimum values for a hull with minimum resistance. Significant for this wave-piercer design is the wave-piercing bow from which the lines fair into a semi-circular cross section on to the rectangular transom featuring a stern wedge. Fig.7 shows the profile and plan view of such a design, the main particulars are summarised in Table 2.

Table 2: Approximate values of preferable hull form parameters for large medium-speed catamarans at a service speed of 26 knots.

L [m]	Fr	$L/\nabla^{1/3}$	C_P	s/L	L/B_{OA}
145	0.35	9.5	0.5	0.2	3.6

3. Resistance prediction ssing RANSE tools

The ability of viscid methods to resolve the major ow phenomena of viscous and potential origin make them a suitable tool to investigate the ow around medium-speed catamarans. During the course of this research, a viscous freesurface solver of the open-source RANSE code Open- FOAM has been utilised to determine the clam water performance of a medium-speed catamaran of the NPL series of *Molland et al. (1994)*. The computational grid consist of 1.3 M cells and has been generated using STAR-CCM+.

Fig.8 shows the sinkage and trim of such craft, numerically and experimentally predicted. The numerical values are generally in good correlation with the experimental values.

In Fig.9 the total resistance coefficient predicted using a RANSE solver and due to experiments is displayed for different Froude numbers. Throughout the speed range under consideration, the computational results agree with the reference values from the experiments.

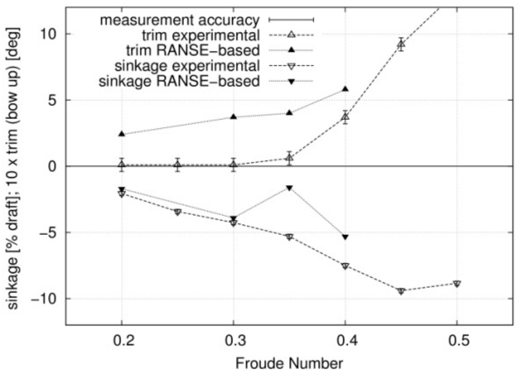

Fig.8: Sinkage (increasing draft) and trim (positive bow-up) of NPL 6b model with *s/L* = 0.2.

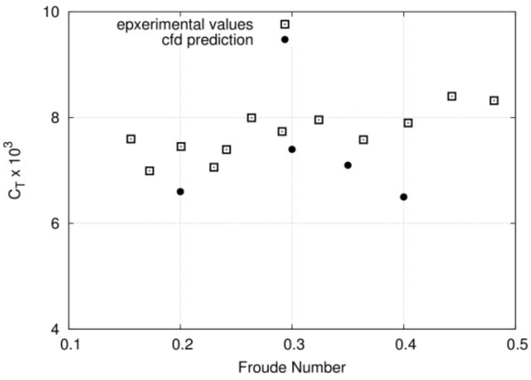

Fig.9: Total resistance coefficient of NPL 6b catamarans derived from experiments by *Molland et al. (1994)* and numerical simulations.

4. Conclusions

Recommendations for hull form coefficients based on data from built monohull ships and model test series of single and twin-hull models have been developed. An initial set of parameters were derived to reduce the design space for medium-speed catamarans with minimum resistance. This methodology can be considered as being valid as recommended hull form coeficients from different sources agree with each other. Most coefficients are presented as a function of Froude number. Furthermore, an approach has been derived to determine appropriate parameters for large catamarans specified by the required deadweight, deck area and service speed. An example has been introduced.

Resistance prediction methods have been introduced and their suitability to estimate the drag of medium-speed catamarans has been discussed. RANSE based methods have been found most appropriate to resolve govern hydrodynamic phenomena around medium-speed catamarans, which comprise wave-making, frictional effects, and transom drag.

Results of RANSE-based simulation to determine the total drag of a catamaran have been presented and good agreement of total drag, sinkage and trim has been found for the medium-speed range compared to experimental data. For resistance the accuracy is within 10 % for $Fr \leq 0.35$.

Future work will concentrate on further numerical simulations to investigate resistance properties of medium-speed catamarans with varying hull form parameters.

5. Acknowledgements

This research has been conducted as part of a collaborative research project between Incat Tasmania Pty Ltd, Revolution Design Pty Ltd, Wärtsilä Corporation, MARIN, and the Australian Maritime College at the University of Tasmania with support from the Australian Research Council's Linkage Project funding scheme, project ID: LP110100080.

References

AUSTAL. (2011), *Commercial products: Ferries – vehicle/passenger*. www.austal.com

AUSTAL. (2012), *Repeat austal customer orders efficient medium speed ferry.* www.austal.com/en/media.aspx

BERTRAM, V. (2000), *Practical Ship Hydrodynamics*. Butterworth-Heinemann

BROGLIA, R.; ZAGHI, S.; DI MASCIO, A. (2009), *Analysis of the Hydrodynamic Performances of High-speed Catamarans by Viscous Flow Solver*. In Proceedings of the 19th International Offshore and Polar Engineering Conference

COUSER, P.R. (1997), *Calm Water Powering Predictions for High-speed Catamarans.* In Proceedings of International Conference on Fast Sea Transportation

DAVIDSON, G.; ROBERTS, T. R.; FRIEZER, S.; DAVIS, M. R.; BOSE, N.; THOMAS, G.; BINNS, J.; VERBEEK, R. (2011), *Maximising Efficiency and Minimising Cost in High-speed Craft.* In International Conference on Fast Sea Transportation, volume 11

DAVIDSON, G.; ROBERTS, T.R.; FRIEZER, S.; THOMAS, G.; BOSE, N.; DAVIS, M.R.; VERBEEK, R. (2011), *130m Wave Piercer Catamaran: A New Energy Efficient Multihull Operating at Critical Speeds.* In Proceedings of International RINA Conference on High Speed Marine Vehicles, pages 61-72

DUBROVSKY, V.A.; LYAKHOVITSKY, A.G. (2001), *Multi Hull Ships*. Backbone Publishing Company

EGGERS, K. (1955), *Über die Widerstandsverhältnisse von Zweikörperschiffen*. In STG Jahrbuch, pages 516- 537. Julius Springer Verlag

EVEREST, J. T. (1968), *Some Research on the Hydrodynamics of Catamarans and Multi-hulled Vessels in Calm Water.* Transaction of NECI, 84

FRY, E. D.; GRAUL, T. (1972), *Design and Application of High-speed Catamarans.* Marine Technology

GORSKI, J.; TURNOCK, S.R.; ALESSANDRINI, B.; CHUN, H.; HOLLENBACH, U.; MIKKOLA, T.; TAHARA, Y.; VALLE, J.; YING, L. (2011), *The Resistance Committee - Final Report and Recommendations to the 26th ITTC*. In Proceedings of 26th International Towing Tank Conference

HAASE, M.; WINKLER, S.; KORNEV, N.; BRONSART, R. (2011), *Experimental Validation of Viscous Free Surface Flow Computation Around Fast NPL Catamarans at Large Drift Angles*. In Proceedings of 1st International Symposium of Naval Architecture and Maritime

HAASE, M.; DAVIDSON, G.; FRIEZER, S.; BINNS, J.; THOMAS, G.; BOSE, N. (2012), *On the Macro Hydrodynamic Design of Highly Efficient Medium-speed Catamarans with Minimum Resistance*. International Journal of Maritime Engineering, acepted

HADLER, J.B.; KLEIST, J.L.; UNGER, M.L. (2007), *On the Effect of Transom Area on the Resistance of Hi-speed Monohulls*. In Proceedings of International Conference on Fast Sea Transportation

HADLER, J. B.; CAIN, K.M.; SINGLETON, E.M. (2009), *On the Effect of Transom Area on the Resistance of Highspeed Catamaran Hulls*. In Proceedings of International Conference on Fast Sea Transportation

INCAT (2011), *Fleet*. www.incat.com.au

INSEL, M.; MOLLAND, A.F. (1991), *An Investigation into the Resistace Components of High-speed Displacement Catamarans*. RINA Transactions, 134

JENSEN, G. (1994), *Handbuch der Werften XXII, chapter Moderne Schiffslinien*. Hansa

MICHEL, W.H. (1961), *The Sea-going Catamaran Ship and its Features and its Feasibility*. International Shipbuilding Progress, 8

MIYAZAWA, M. (1979);. *A Study on the Flow Around a Catamaran*. Journal of the Society of Naval Architects of Japan, Vol. 145

MOLLAND, A.F.; LEE, A.R. (Feb. 1995), *Resistance Experiments on a Series of High-speed Displacement Catamarans Forms: Variation of Prismatic Coefficient*. Technical report, University of Southampton

MOLLAND, A.F.; WELLICOME, J.F.; Couser, P.R. (March 1994), Resistance *Experiments on a Series of High-speed Displacement Catamarans Forms: Variation of Length-Displacement Ratio and Breadth-Draught Ratio*. Technical report 71, University of Southampton

RAWSON, K.J.; TUPPER, E.C. (2001), *Basic Ship Theory*. Butterworth-Heinemann

SAHOO, P.K.; BROWNE N.; SALAS, M. (2004), *Experimental and CFD Study of Wave Resistance of High-speed Round Bilge Catamaran Hull Forms.* In Proceedings of International Conference on High-Performance Vehicles

SAHOO, P.K.; SALAS, M.; SCHWETZ, A. (2007), *Practical Evaluation of Resistance of High-speed Catamaran Hull Forms - Part I*. Ships and Offshore Structures, 2(4):307-324

SAHOO, P.K.; MASON, S.; TUITE, A. (2008), *Practical Evaluation of Resistance of High-speed Catamaran Hull Forms - Part II*. Ships and Offshore Structures, 3 (3):239-245

SALAS, M.; LUCO, R.; SAHOO, P.K.; BROWNE, N.; LOPEZ, M. (2004), *Experimental and CFD Resistance Calculation of a Small Fast Catamaran* . In Proceedings of International Conference on High-Performance Vehicles

SATO, R.; NOGAMI, H.; SHIROSE, Y.; ITO, A.; MIYATA, H.; MASAOKA, K.; KAMAL, E.; TSUCHIYA, Y. (1991), *Hydrodynamic design of fast ferries by the concept of superslender twin hull*. In Proceedings of International Conference on Fast Sea Transportation

SAUNDERS, H.E. (1957), *Hydrodynamics for Ship Design*. Society of Naval Architects and Marine Engineers

SCHNEEKLUTH, H.; BERTRAM, V. (1998), *Ship Design for Efficiency and Economy*. Butterworth-Heinemann

STERN, F.; CARRICA, P.; KANDASAMY, M.; GORSKI, J.; O'DEA, J.; HUGHES, M.; MILLER, R.; HENDRIX, D.; KRING, D.; MILEWSKI, W.; HOFFMANN, R.; CARY, C. (2006), *Computational Hydrodynamic Tools for High-speed Transports*. SNAME Transactions, 114:55-79

TASAKI, R. (1962), *A Note on Wavemaking resistance of Catamarans*. Technical report, University of Michigan, Ann Abour, MI

TAYLOR, W.D. (1943), *The Speed and Power of Ships*. United States Maritime Commision

TRILLO, R.L. (1991), *High Speed Over Water, Ideas From The Past, The Present And For The Future.* In Proceedings of International Conference on Fast Sea Transportation

TURNER, H.; TAPLIN, A. (1968), *The Resistance of Large Powered Catamarans*. SNAME Transactions, 76

VOLLHEIM, R. (1968), *Über Formgebung und Widerstand von Katamaranen*. Schiffbaufor-schung, 7

Design Development of Air Supported Vessel (ASV) Hull Forms for Passenger Ferries and Work Boat Applications

Ulf Stephen Tudem, SES Europe AS / Effect Ships International AS, Sandefjord, Norway, ulf.tudem@effectships.com
Tor Kolbjorn Livgard, SES Europe AS / Effect Ships International AS, Sandefjord, Norway, tor.livgard@effectships.com
Hans Liljenberg, SSPA Sweden AS, Gothenburg, Sweden, hans.liljenberg@sspa.se

Abstract

With more than 1300 tank test runs with ASV designs under their belt, Effect Ships International AS (ESI), skipped tank testing of the hull for their first ASV Mono full scale vessel. Based upon ASV knowhow developed over more than 10 years, the company went ahead and built a 20 m test vessel. This selected hull was primarily designed to deliver a large interior volume matched with market leading efficiency; a hull just perfect for among other pleasure boats. Further the hull was designed to be simple and easy to build using series production techniques. Following completion of the test vessel, a comprehensive testing- and documentation process was carried out. The results were quite extraordinary. The test vessel demonstrated a reduction in fuel consumption at medium speeds (14 – 30+ knots) of up to 50% compared with market leading conventional boats. With such performance the ASV concept was awarded the European Power Boat of the Year 2011 Innovation Award at the world leading Düsseldorf Boat Show.

Unfortunately, these days, the pleasure boat sector is facing tough times and many yards are struggling to obtain orders and make ends meet. Consequently the willingness to invest in new technology is therefore quite limited.

In other sectors, like fast crew-boats (serving offshore installations), windmill support vessels, commercial work boats, small fast ferries etc there are however more activities. Common for these vessels are a high number of operational hours per year, and increasingly more focus on achieving a higher utilization level at reduced operational cost. Increasing fuel cost is a global phenomenon and fast vessels with significantly reduced fuel consumption per NM have obvious advantages. For several of these types of applications passenger comfort and onboard motion related capabilities play a very important role. These realities triggered the ASV team to prepare new high efficiency designs with focus on motion suppression. Although the ASVs in general have a motion damping effect from their air cushion(s), the new range of ASV Mono hulls focus even more on passenger comfort and reduced onboard motions/accelerations in a sea state. Internally these new designs are referred to as "Soft Motion" ASV hulls.

In collaboration with a leading Indonesian yard, Orela Shipyard, the first ASV Mono Soft Motion fast crew boat with WJ propulsion is now under construction. This first vessel, with aluminum construction, will have a length of approx 22 m and design speed will be 40 knots +. Planned launch is during last weeks of 2012.

Another project, using a similar type of hull, this time for passenger and light cargo transport, is also in progress. In collaboration with a leading Norwegian fast ferry operator a range of ASV Mono ferries is under development. The hull will be configured for pod propulsion (Volvo Penta IPS or similar) and construction will be carbon sandwich. This combination of light construction weight, high efficiency propulsion and very low hull resistance is expected to

give market leading overall efficiency. Tank testing of the new design is scheduled for week 43 at the SSPA towing tank in Gothenburg.
The ASV technology is patented in 60 countries worldwide.

1. Introduction

Small and medium size ferries and work boats alike are often operated 2.000 – 3.000 hours a year. With a length of 15 – 40 + meters they come in almost any shape and configuration; and are serving a wide range of operations/duties/missions. Other applications for these vessels are duties for different kinds of authorities; from navy/paramilitary use (patrol vessels, coastguard crafts) to pilot shuttle crafts.

For these types of crafts the fuel cost is the single largest operational cost component. With high oil, and even more so refined diesel prices, the owners / operators are today seeking more efficient hull forms / vessel concepts in order to improve their operational economy and competitiveness in the market place.

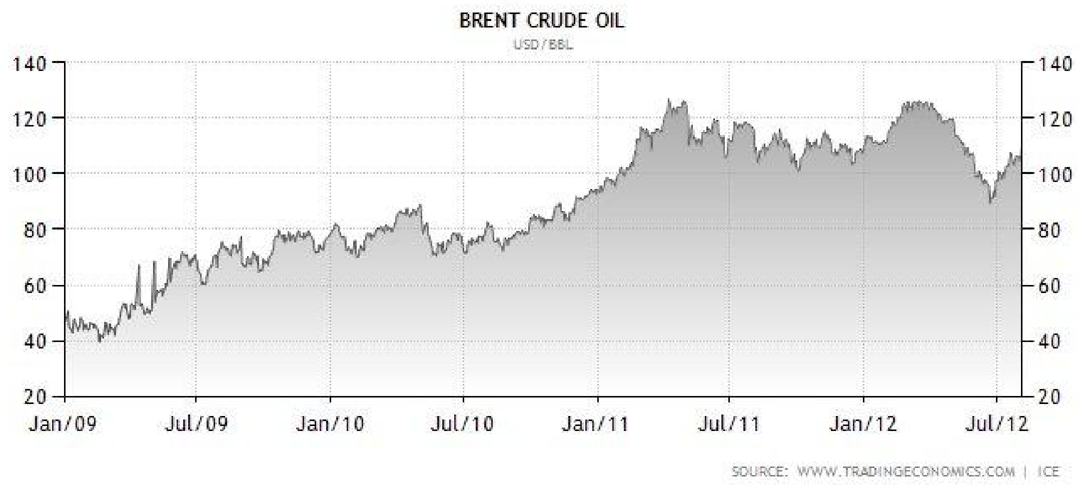

Fig1: Oil price developments in USD/barrel.

Lately environmental related arguments have been used quite frequently in all market segments. It is a fact that many conventional fast and medium speed vessels are quite ineffective, are consuming a considerable amount of fuel and are emitting a large amount of CO2/NOX and particles. The combined economical and environmental arguments open up market opportunities for a new generation of innovative vessels with enhanced capabilities.

2. The ASV Mono Soft Motion concept – twin propulsion

ESI has earlier and with support from EU successfully developed and tested ASV catamarans with Soft Motion (SM) characteristics. The idea to the ASV Mono SM was uncovered following demonstrations with US Navy on an earlier ASV cat demonstrator. Having told “horror stories” related to effects from life onboard high speed conventional patrol boats operated at high speeds in waves, and being impressed about the motion damping effects from the air cushion concept the US Navy experts challenged ESI to design a Soft Motion Mono variant.

Although the ASV mono from the outside looks very similar to a conventional mono hull, the vessel is in reality a mix between a catamaran and a monohull, where air support and reduced wetted surface areas are combined with displacing bodies and planing surfaces; contributing to extra “lift” at speed.

At rest and in “off cushion mode” the vessel will, in the same fashion as a catamaran, have self righting and roll suppressing properties. At speed the vessel has been designed to operate at close to neutral trim (0 – 1 deg bow up). If required the trim can be altered by means of interceptors (Humphree) mounted on each of the propulsion gondolas at the stern. Below illustration shows aft section of an ASV Mono hull, with air cushion enclosure flap, Volvo IPS propulsion and Humphree interceptors.

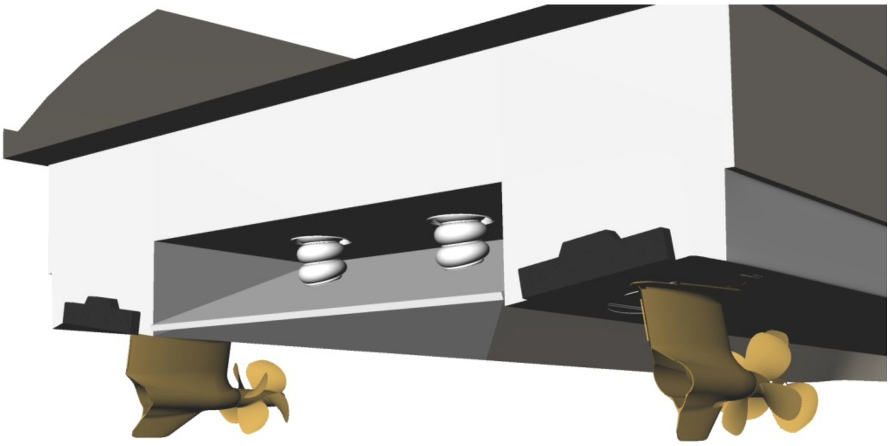

Fig.2: Aft section of ASV Mono set up with Pod Propulsion and Interceptor systems.

The ASV Mono can be configured for most known propulsion systems; water jets, pod propulsion, Servo Gear variable pitch propellers, stern drives or conventional shaft propellers. In this paper water jet and Volvo Penta IPS pod prop designs will be discussed.

The innovative ASV Mono Soft Motion hull is characterized by a sharp bow section, with a narrow bulbous bow, typically stretched out to the tip of the bow to take advantage of a longer water line length. Most of this bow will remain out of the water when the vessel is travelling at high speed in calm waters, and will be acting as a combined volume body / pitch damping unit when travelling at speed in waves.

Above this wave piercing bow, the lower part of the hull is quite narrow and sharp at first, widening out to meet a knuckle line – arranged quite high at the utmost bow and gradually dropping until it meets the wide spray rails where the hull widens out. The purpose is to reduce accelerations resulted from fast wave impacts.

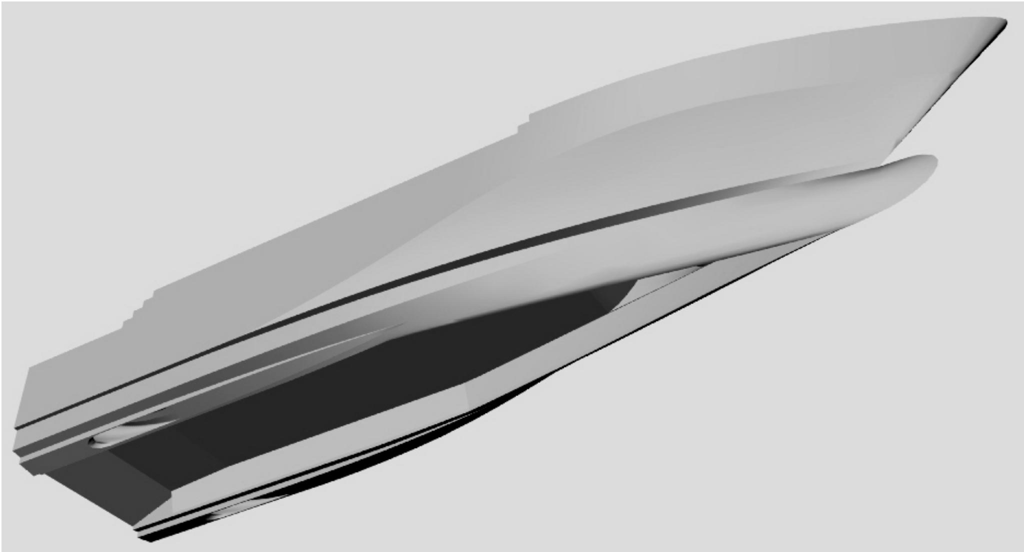

Fig.3: Illustration of ASV Mono SM showing in set up for water jets.

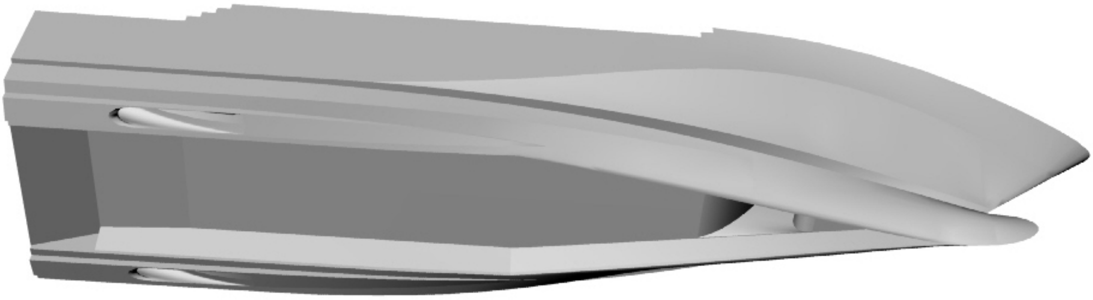

Fig.4: Side/below view of ASV mono SM hull for WJ propulsion.

The ASV's "water foot print area" is mainly taken up by a V-shaped air cushion / cavity, starting directly behind the bulbous bow and running the full length of the hull until meeting the air cushion enclosure flap. The main function of the hinged flap is to maintain the pressurized air inside the air cushion chamber. The system does not have a trim tab type of function. The flap is controlled by an atomized air cushion/flap management system with overriding options if the master has a different preference to the standard setting to among other flap damping level.

A lift fan system is located in the bow of the vessel, and is powered either by a hydraulic or an electric motor is securing sufficient pressurized air to the air cushion chamber, and to maintain a steady pressure inside the cavity even in quite serious sea states. The centrifugal fan has enough capacity (volume flow) to maintain a "full" air cushion without "cushion collapse" or green water slamming through the air cavity and hitting the cushion ceiling.

The propulsion bodies or propulsion gondolas, typically one on each side, have several functions. Housing the propulsion system is the obvious one, securing buoyancy (as pontoons) is another; acting as dynamic/planing surfaces at speed is a third. Due to the relative short length of these bodies and the angle of attack between the gondola and the water, the lift is considerable already at relatively low speed. For a 20 m vessel the planing part of the gondola can be approx 4 – 5 m, and will have planing effect at approx half the speed of the main vessel.

The forward part of the propulsion gondolas/side keels is quite narrow with a deep V shape. The main function is to enclose the air cushion well to avoid access ventilation from the air cavity; with a minimum of wetted surface areas. The sharpness of these hull elements is also positive from a motion point of view when operated at high speeds in waves. Heavy pitching of the bow will increase ventilation (and fan power) and contribute to higher overall / added resistance.

Moving aft wards the gondolas widens into planing surfaces. The location - around the LCG, - will contribute to a soft heave support, contradictory to a conventional planing boat where the planing surfaces more often are located far forward (and sometimes also aft) typically generating uncomfortable pitch motions.

The air support rate can be varied by a combination of air volume flow/pressure and air cushion flap control. For a 20 – 40 m vessel the support rate is typically between 70 and 85% depending on hull configuration/loading etc.

3. The ASV Mono Soft Motion – single propulsion

Due to the significantly reduced hull resistance characteristics of the ASV concept, ESI has also developed a SM variant set up for one propulsor. Launching of the new ZF Single Pod propulsion system with hybrid electric unit and integrated electric bow thruster opened very interesting design perspectives for ASV variants. It may be argued that there is some market reluctance against single motor/prop set ups, although in several markets use of single driveline is more the norm than the exception.

The hull form resembles the twin engine ASV SM, but the side mounted hull bodies are narrower, and a propulsion body has been fitted along the vessels centre line aft. The air cushion enclosure flap has been split in two elements.

Suitable size for this set up (with the available ZF units) are vessels between 14 and 17 m, with a beam between 4,5 and 5 m. The resulting air cushion is quite large, allowing for a lower cushion pressure to achieve the requested support rate of 70 – 85% at operational displacement.

Here the driveline installation is very compact, comprising of the pod unit, a hybrid electric unit and the engine. (See illustration fig 6). The hybrid electric unit will power the lift fan system as well as a bow thruster. The bow thruster fits in the bulbous bow, and is located above the water line during normal “on cushion” operation. When a thruster is required for close up maneuvering the vessel is operated “off cushion” and the thruster is well submerged.

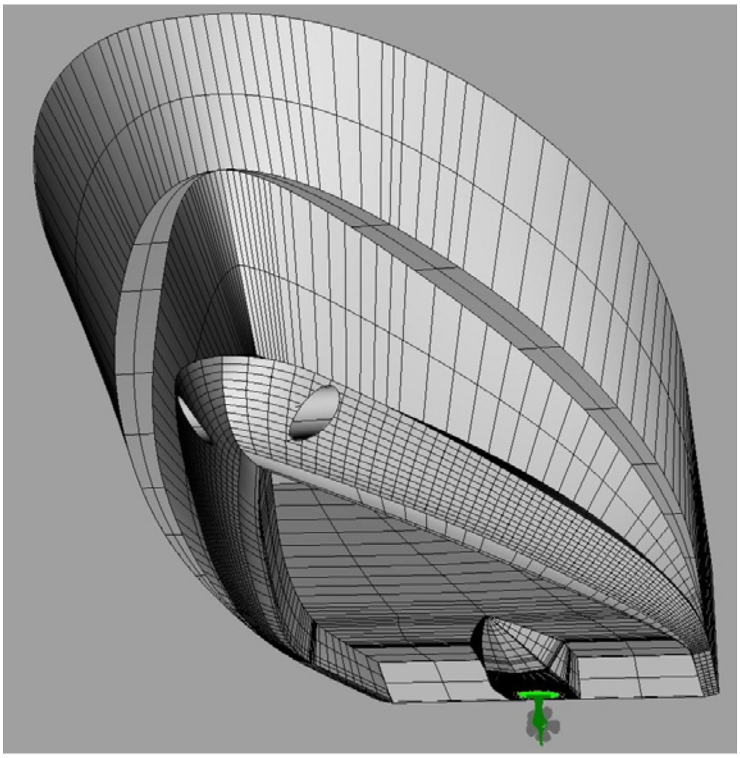

Fig.5: ASV Mono SM single pod prop set up.

To illustrate the drive line and fan system installation inside the hull figure 6 will give a good indication. In this rendering the actual pod drive / hybrid unit / engine and fan system / duct are showing. This hull is approx 15 m with a beam of 4,7 m. The small 5,9 liter CMD engine produces 350 kW (in light duty rating).

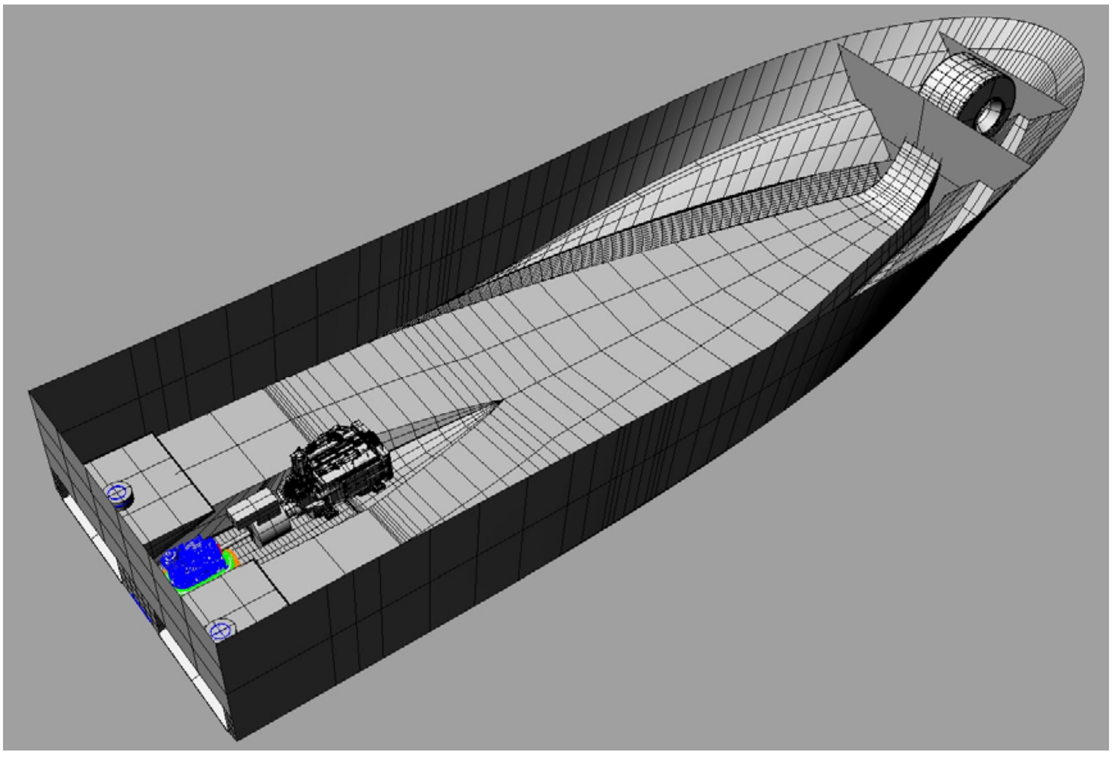

Fig.6: ASV Mono SM single pod prop set up showing driveline and fan set up.

Initial assessments of hull resistance and lift fan powering for a 15 x 4,7 m hull, 14 tons ASV Mono SM Single Pod vessel indicate a top speed of close to 30 knots with a fuel consumption of approx 3 – 3,3 liter /NM, equivalent to less than half that of what the market leading conventional hulls of same size will require.

4. ASV Mono SM 22 m fast Crew with water jet propulsion

In collaboration with Orela Shipyard, Indonesia the first commercial ASV Crew boat with the following dimensions is currently under construction.

L = 22m	B = 5,2m
Air cushion area = 45,5m2	Air cushion press approx 6,5-7,0 Kpa
Load full = 38 tons	Load half = 34 tons
Main engine = 2x880 kW MAN	Fan power = Up to 160 kW
Max speed = 40 knots +	Propulsion = WJ MJP 450 CPU

At full load the air cushion support ratio is approx 80%.

Propulsion for this vessel will consist of twin MJP 450 CPU (Compact Steering Units) water jets with specially designed water jet intake / water jet pick up geometry. With a propulsion power of 2 x 800 kW the vessel is estimated to achieve 40 knots + at full load.

The fist vessel will have seating capacity for 50 Pax on the main deck. Aft of the cabin area there will be a large deck area of almost 40 m2 to take different type of light cargo, container modules of different kinds or as showing on the general arrangement (GA), a second passenger cabin module with additional 40 seats. In addition space is allocated for crew accommodation, toilets, medical room, galley, baggage storage etc. Other general arrangements will naturally be on request depending on the end use.

As information on the new vessel type is starting to spread, Effect Ships and Orela Shipyards are already reporting considerable interest from potential ship owners and operators.

Other yards are also closely following the developments.

Based upon feedback from the market, Orela has already started the design of larger ASV's, among other 34-36 m vessels for various commercial and navy/paramilitary applications. Fast and efficient passenger ferries with ASV Mono technology seems yet another highly likely application.

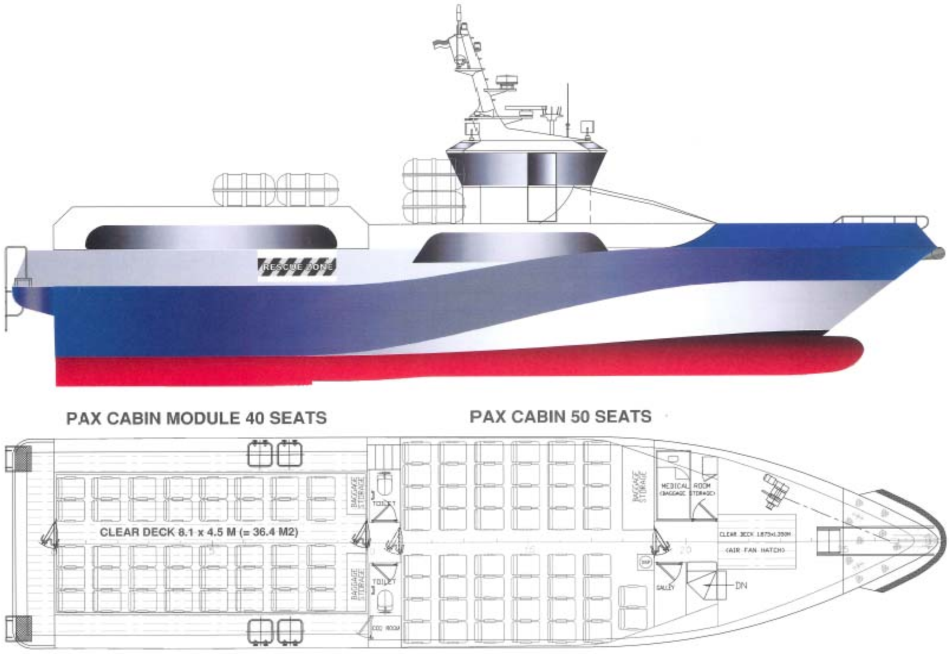

Fig.7: ASV Mono SM 40 knots + crew boat / concept demonstrator (Orela Shipyards, Indonesia).

Fig.8: ASV Mono Indonesian crew boat under construction at Orela Shipyard.

5. ASV Mono SM fast ferry range

ESI has another project going, a Norwegian Environmental project, supported by Innovation Norway, and with Torghatten Nord AS (main end user client). In short the project will develop a new range of air supported (medium/fast) ferries based upon a variant of the ASV Mono SM hull form. Although Norwegian coastal operations are the primary target, the project sees applications for these new ferries worldwide. The project consists of two phases; the first being the hull form, GA and design developments; followed by comprehensive tank testing at SSPA Sweden in calm waters and waves. Provided the project goal of improved efficiency (and reduced emissions) of 30 % at design speed compared with current leading ferries can be documented; Innovation Norway is positive to support development , construction , testing and documentation of a full scale test vessel to be benchmarked under real operational conditions on route in Norway.

Construction of the 20 – 24m vessel will be from carbon sandwich, where Diab AS will be responsible for the carbon engineering and world leading carbon ferry builder Br Aa AS for the construction. Propulsion will be pod propulsion (Volvo Penta IPS). Design will be by Italian Studio Sculli.

The new ASV Mono SM ferry range will start at 20m, with 3 – 4 designs up to 40 m +. Although main function will be coastal passenger transport, the vessels may also be configured to handle a combination of passengers and lighter cargo, for increased flexibility.

Provided the tank testing results are as expected the new ASV hulls will be adapted to several additional applications, including fast crew- and light cargo carrying duties as well as patrol / paramilitary and navy applications.

6. Conclusions

A high number of operational hours pr year will maximise the economical and environmental benefits from use of the ASV technology. Due to high fuel prices there is a strong market demand for more efficient and economical to use vessels. Effect Ships International will tailor make their ASV hull forms to meet the owner/operator's requirements for these kinds of vessels.

Results from tank testing of ASV cats and - mono hulls; tests with larger manned models and a 20 m operational ASV Mono hulled vessel, and comparison studies with market leading conventional hull hull forms, conclude the ASV Mono variants display the best overall capabilities and cost/efficiency/performance.

The ASV Mono is reducing the wetted surface area and corresponding hull/water resistance in several cases by approximately 50 %. The patented concept seals off the air cushion very well without the use of any "flexible skirts" or rubber arrangements as seen on conventional surface effect ships (SES), hovercrafts or hybrid SES solutions. The power to "stay on the cushion" for an ASV mono is low, in calm waters representing only 3-5% of installed power, in a sea state naturally more (up to 10%) due to more ventilation / air flow.

Well worth noticing is the fact that great efficiency improvement does not only occur at high speeds. The ASV Mono offers superior efficiency a very wide band of speeds; from below 10 knots all the way to 50 knots + (exemplified for a 20 m vessel), making the concept suited for a wider range of vessel sizes and speeds.

The air cushion system offers motion damping in waves. Wave impact, pitch and roll motions are reduced not only at speed but also at rest in waves. The ASV Mono SM will be particularly suited for operation in more demanding waves/sea states; conditions many work boats are frequently encountering.

From a construction point of view an ASV Mono hull is typically simpler and less expensive to build; demands less material with lower weight – compared with a similar size catamaran. As for any medium/high speed vessel lower weight gives less power requirement. Aluminium construction, GRP or even better carbon sandwich are recommended. The ASV mono hulls are very well suited for series production in moulds.

Unlike slender catamarans, the interior volume and space an ASV Mono can offer is excellent. Typically the engine/driveline size is smaller than for a conventional vessel, the sides of the hull are close to vertical and the fan system takes up little space. Most of the volumes above the air cushion ceiling can therefore be used for accommodation etc.

References

ALLENSTROEM, B.; LILJENBERG, H.; TUDEM, U. (Oct. 2003), *Concept development and model testing - new generation Air Assisted Vessels (AAV) with Water Jet propulsion,* FAST 03, Ischia

EILERTSEN, A.; TUDEM U. (Oct. 2003), *Design development – 23 m Air Supported Vessel (ASV) with WJ,* Int Air Cushion Technology and Exhibition, Southampton

EILERTSEN, A.; GRIEG EIDE, J.; TUDEM, U. (June 2004), *Design development of advanced air supported Vessel (ASV) designs* RINA WARSHIP, London

LIVGARD, T.K.; TUDEM, U. (May 2009), *High Performance with Improved Onboard Comfort: Introducing ASV Soft Motion Mono With Water Jet Propulsion,* RINA SURV 7, Pool, UK

LIVGARD, T.K.; TUDEM, U. (Nov. 2009), *Design Development, prototype construction and test outfitting of the Air Supported Monohull by Effect Ships International AS.* RINA, London

LIVGARD, T.K.; TUDEM, U. (Nov. 2010), *Air Supported Vessel (ASV) monohull, design development of test vessel and proof of concept.* 31. Symposium Yachtentwurfund Yachtbau, Hamburg

LIVGARD, T.K.; TUDEM, U. (May 2011), *Air Supported Vessel (ASV) monohull demonstrator. Design development, testing at sea and results proving the concept,* Naples

TUDEM, U. (Dec. 2011), *Air Supported Vessel (ASV) – innovative fast vessel technology with great operational- and environmental benefits.* TEKNA 2011 Copenhagen

Preliminary Design Study on Medium-speed Monohull Passenger Ferries

Wolter Roberth HETHARIA, Andre HAGE, Philippe RIGO

University of Liege - ANAST, Liege, Belgium, hethariawr@yahoo.com
University of Liege - ANAST, Liege, Belgium, ahage@ulg.ac.be
University of Liege - ANAST, Liege, Belgium, ph.rigo@ulg.ac.be

Abstract

The recent development of medium-speed monohull passenger ferries has shown their performance for short trips in some regions. The existence of those ships is to fulfill the transition region between conventional ferries and HSC crafts. In fact, they operate at the Froude number range of 0.55 to 0.80 which is beyond the hump speed. Therefore they need the high engine power to maintain their operation speeds. The present project is to find the minimum resistance due to the minimum length of the ship. A parent ship of 254 passengers is designed in this study. The variation of passenger distributions at main-upper decks, applied in this task, end-up with the variation of the ship lengths and center of weights. Furthermore, those lengths affect the performance of the resistance, stability (particularly at the large angle of inclination) and other ship design parameters. The results of computation are presented for two loading conditions (departure and arrival). The excel solver is used to find the minimum resistance with the constraints of stability and seakeeping of the ship. The results of study are presented and provided for future study of optimization, particularly to find the best design of hull form with the minimum power.

1. Introduction

Nowadays, the medium-speed passenger ferries play an important role to carry passengers in some regions of the world. Those ships operate at the short distance with the top speed of around 23 knots. Their existence is to fulfil a transition speed region between the conventional ferries (speeds < 15 knots) and HSC (speed ranges 25 to 40 knots). Since the emerging-time of those ships, they had been developed to be operated in many regions. Most of the ships are multi-hulls but due to their simplicity, the monohulls have also been developed and have a promising future markets. Most of those ships constructed recently use Aluminium as hull material. The application of this material to those ships gives the benefits of increasing the payload or reducing the engine power. In addition, in some Asian regions, there are a lot of monohull medium-speed passenger ferries in composite hull material (FRP). In fact, those medium-speed ships operate at the range of Froude number Fn from 0.55 to 0.80. This range is beyond the hump speed (Fn > 0.50). In fact, they need a great engine power to maintain their service speed. The efforts should be done in order to minimize the engine power of the ship.

Many works deal with ship optimization and different objectives. During the optimization process some constraints were added in order to get a feasible solution. For the case of the passenger ships the initial arrangement would be provided before the optimization process. In fact, the stability of these ships is the most important. Therefore this issue of stability should be evaluated first. The overall works of this study consist of global optimization of hull arrangement, hull form optimization and local hull refinement. This paper deals with optimization of hull dimension (length) due to the arrangement of passenger distribution on main deck and upper deck. While keeping the ship beam is constant then the distribution of passenger affects the dimension of ship length. This arrangement affects the ship parameters such as stability, resistance or power and seakeeping. Since there is not database available for this study then a parent ship of 254 passengers are designed first. The modification of the ship was based on the parameters of the parent ship.

2. Design of parent ship

2.1. Input design

Several important key factors were summarized from Knox (2003), Levander (2003), Calhoun (2003), Gale (2003) and Olson (1990) concerning the arrangement of the passenger ferries. They are:

- Spaces, volumes, service rooms, access and services are provided for the passengers.
- Accommodations are provided on board to ensure the comfort for the passenger.
- The arrangement of ship is fixed to fulfill the safety standard regulations.
- The facilities are provided to support the operation of the ship.
- The design parameters that should be considered during the operation such as safety, stability, sea keeping and maneuvering capability.

Input design parameters include:

- Type of ship: passenger ferry/class B — Number of passengers: 254 pax
- Passenger distribution, main deck: 70% — Upper deck:30%
- Number of crews: 5 — Service speed: 20 knots
- Navigation range: 200 n.m — Type of pax accommodation: seat
- Number of seats in row: 10 — Type of seat: West Mekan
- Type of pax room: passenger saloon

The input design parameters were computed and analyzed during the design process. The process is finished when the outputs meet the ship requirements. The layout of the ship was determined to fit the rules of International Code of Safety for HSC (2000), 2008 Edition. The structure components of the ship were determined based on the Rules for the Classification of High Speed Craft, Bureau Veritas (Edition February 2002). The hull material of the ship is Aluminum Alloy. The types of alloys used for the ship are 5083 H111 for plating and 6082 T6 for profile.

2.2. Ship dimensions

The dimensions of the parent ship, obtained from the design process are presented in Table 1. The hydrostatic parameters of the ship were computed by using Maxsurf Software. The results of hydrostatic parameters are presented in Table 1.

2.3. Ship layout

The layout of the ship was arranged due to the requirement to serve the passengers during the travel. The placement of passengers is in the passenger saloon. In addition, access and services were provided for the passengers. Other service rooms such as toilets and small kiosk are provided also in this layout. The equipments and ship systems of the ship are also provided and placed to their proper locations. The layout of the ship is shown in Fig.1.

Table 1: Dimensions of Parent Ship

Parameters	Unit	Value
Number of passenger on main deck–upper deck		177 - 77
Percentage of passenger on main deck	%	70
Length overall, L_{OA}	m	32.00
Length of waterline, L_{WL} (= L_{BP})	m	28.96
Ship beam (deck), B	m	7.00
Ship beam (waterline), B_{WL}	m	6.68
Draft, T	m	1.40
Deck height, D	m	2.600
Displacement, Δ	tone	105.3
Block coefficient, C_B		0.373
Midship coefficient, C_M		0.552
Prismatic coefficient, C_P		0.686
Water plane coefficient, C_{WP}		0.850
Longitudinal center of buoyancy, LCB (from AP)	% LWL	48.36
Vertical center of buoyancy, KB	m	0.971
Radius metacenter, BM_T	m	5.336
Vertical center of gravity, KG	m	3.057
Initial metacenter, GM_T	m	3.250

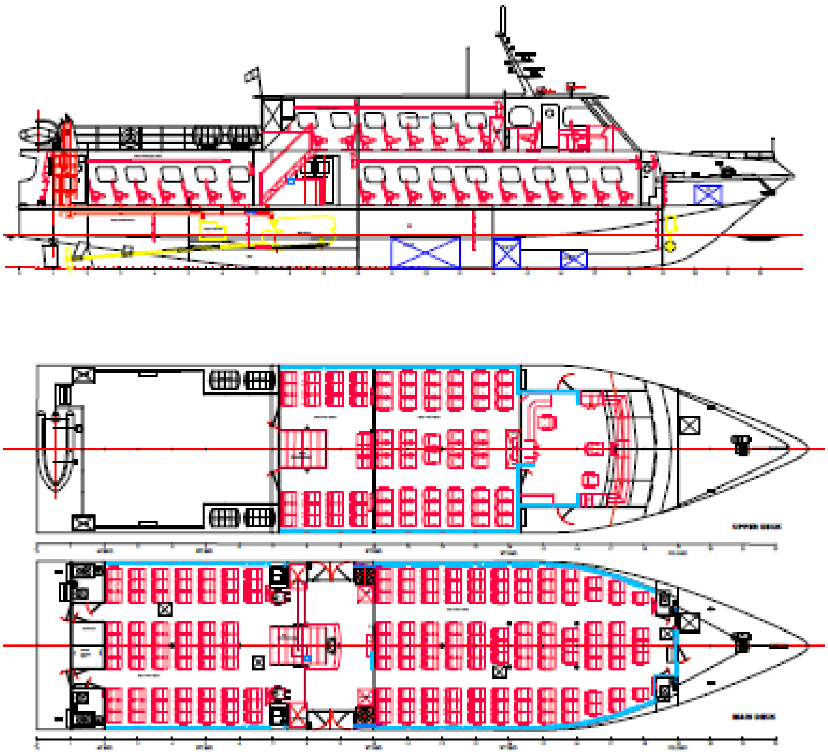

Fig.1: Layout of parent ship

3. Assessment of ship weight, engine power and ship stability

3.1. Assessment of ship weight

Since there is no database available for this kind of ship then the total weight of the ship is computed and estimated directly from the parent ship. The weights and their centers are presented in Table 2. A margin weight of 4% is added to the ship lightweight. In addition, a margin of VCG of 0.150 m was added for the VCG of the ship lightweight (Parson, 2003).

Table 2: Weight and centers of the parent ship

Item weight	Weight (tone)	LCG (m)	VCG (m)	TCG (m)
Structural weight	38.902	-0.628	2.882	0.000
Machinery and system	15.725	-2.900	1.418	0.000
Ship outfits	13.960	-0.381	3.773	0.000
Sum lightweight	68.587	-1.099	2.728	0.000
Margin weight	2.743	-1.099	2.728	0.000
Deadweight (pax & liquids)	33.922	0.764	3.355	0.000
Total weight	105.252	-0.498	2.930	0.000

3.2. Ship resistance

Three available statistical methods were applied for the computation of ship resistance, i.e. Holtrop (1978), Savistsky pre-planning (Lewis, 1988) and WUMTIA (Molland, 2011). The statistical resistance prediction method derived by Mercier and Savitsky is suitable for the semi-planning ships. The general form of the resistance equation adopted by Mercier and Savitsky is as follows:

$$R_T/W = A_1 + A_2X + A_4U + A_5W + A_6XZ + A_7XU + A_8XW + A_9ZU + A_{10}ZW + A_{15}W^2 + A_{18}XW^2 + A_{19}ZX^2 + A_{24}UW^2 + A_{27}WU^2 \quad (1)$$

where: $X = \nabla^{1/3}/L$; $Z = \nabla/B^3$; $U = \sqrt{2i_E}$,; $W = A_T/A_X$.

The values of the coefficients A_1 to A_{27} and correction factors are presented in Lewis (1988). This method and also the statistical method derived by Holtrop are provided in the Maxsurf software. Meanwhile the method derived by WUMTIA (Wolfson Unit for Marine Technology and Industrial Aerodynamics) presented the power prediction as follows:

$$P_E = 453.8 \times \Delta \times (V^2_K / \sqrt{L}) \times (1/C^2_{FAC}) \quad (2)$$

where: Δ = displacement; Vk = ship speed in knots; L = ship length

The constant values of C^2_{FAC} may be found in Molland (2011). The result of the resistance is shown in Fig. 2. From the figure, it was found that the method of Holtrop was out of range and the other two methods are in good pattern. For the next computation, the resistance is computed based on Savitsky pre-planning method.

The effective power of the ship is computed as:

$$P_E = R_T \times V \quad (3)$$

where: R_T = total resistance and V = speed of the ship

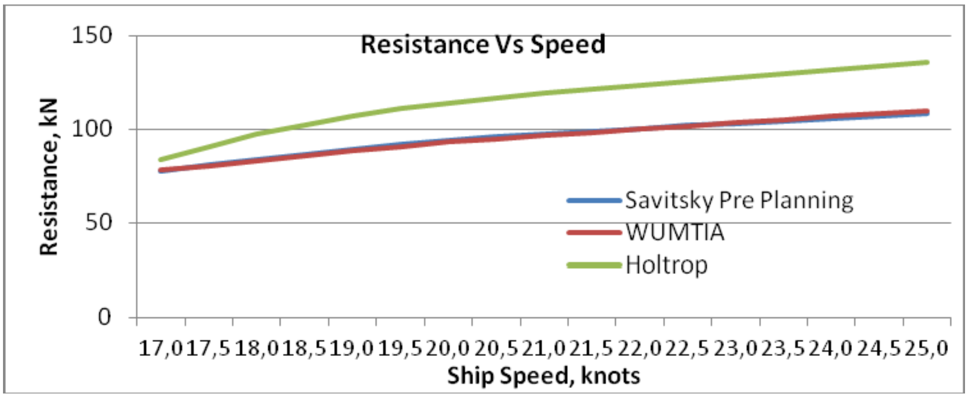

Fig.2: The resistance of parent ship for three methods.

3.3. Engine power

The engine power (brake power P_B) is computed in relation with the effective power P_E (Parsons, 2003).

$$P_B = P_E / (\eta_h \eta_o \eta_r \eta_s \eta_b \eta_t) \qquad (4)$$

where:

η_h = hull efficiency;

η_o = propeller efficiency;

η_r = relative rotative efficiency = 1.0

η_s = seal efficiency;

η_b = line shaft bearing efficiency;

η_t = transmission efficiency;

$\eta_s \eta_b$ = 0.97 for machinery amidships

η_t = 0.975 for medium speed diesel plant

Hull efficiency is computed as:

$$\eta_h = (1 - t)/(1 - w) \qquad (5)$$

where:

w = Taylor wake fraction = $0.5\ C_B - 0.05$ (6)

C_B = block coefficient

t = thrust deduction factor = 0.6 w (7)

The maximum continuous rating (MCR) of the main engine is determined by adding a power service margin as 10% to the brake power.

$$MCR \geq (1 + MS)\ P_B \qquad (8)$$

where: MS = power service margin

Two units for the main engines are selected for the propulsion system of the ship. It would be better to select the existing types of main engine to be used for the ship. However, as assumption for this preliminary study, the main engine and following characteristics were selected.

Type of main engine : MTU Marine Diesel Engine 10V 2000 M70
Rated power : 1205 bhp
Rated speed : 2250 rpm
Gearbox : ZF 3000, i = 2.0

3.4. Propeller selection

Two screw propeller units are used for the parent ship. The screw propellers are evaluated based on the propeller data from the Wageningen B-Screw Series (Lewis 1988). The propeller types of B 4-55, B 4-70, B 4-85 and B 4-100 are evaluated for a range of ship speed from 19 to 21 knots. In addition, an evaluation for the cavitations of the propeller is executed based on Burril Diagram of cavitations. The trend line of suggested upper limit for merchant ship propeller is used in this evaluation. In fact, this trend line is still subjected to back cavitations of propeller blade (less than 5%). The results of computation of the propeller parameters are shown in Fig.3.

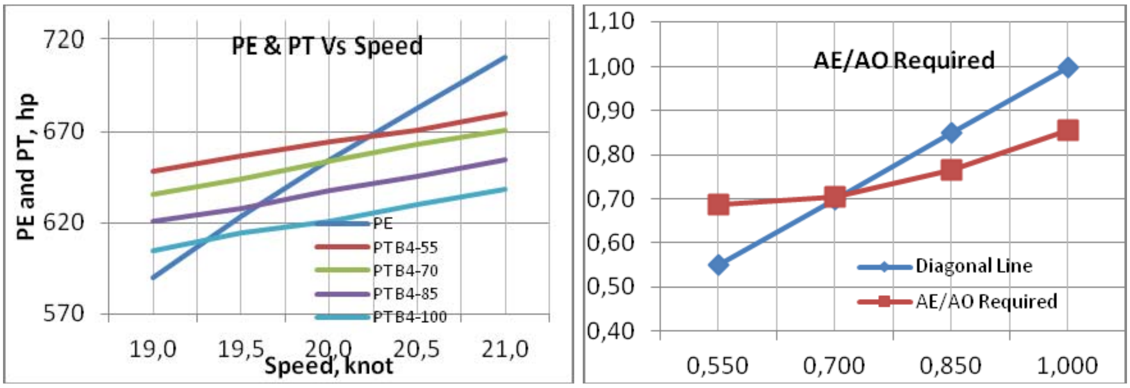

Fig.3: The screw propeller parameters of parent ship

The selected screw propeller:

Type	: B 4-70	BAR	: 0.70
Number of blade	: 4	P/D	: 0.799
Diameter	:1.078 m	Efficiency	: 0.584
Speed maximum for the ship		: 19.98 knots	

3.5. Assessment of ship stability

The parameters of ship resistance and stability were computed by using Maxsurf software. The criteria that have been used for the ship stability are based on HSC Code 2000 MSC 97(73)- Annex 8 Monohull Intact, HSC Code 2000 Chapter 2 Part B Passenger Craft Intact and IMO MSC 36(63) HSC Code Monohull Intact. In addition, the ship resistance was computed based on the statistical method of Savitsky pre-planning. The results of computations are shown in Table 4 and Fig.5.

3.6. Assessment of ship seakeeping

The sea keeping parameters were evaluated for rolling, pitching and heaving natural periods. Those are computed due to the following formulas (Parsons, 2004).

Roll natural period: $T_\phi = 2.007\, k_{11} / \sqrt{GM_T}$ (9)

where: $k_{11} = 0.40\, B$

Pitch natural period: $T_\Theta = 1.776\, C_{WP}^{-1} \sqrt{(T\, C_B\, (0.6 + 0.36\, B/T)}$ (10)

Heave natural period: $T_h = 2.007 \sqrt{(T\, C_B\, (B/3T + 1.2)/C_{WP})}$ (11)

The results of computations are shown in Table 4 and Fig.5.

4. Modification and optimization of ship length

4.1. Modification of ship length

The modification of parent ship was executed due to the distribution of passengers on main deck and upper deck. This modification affected the total length of ship. The distribution of passengers on board was based on the seat arrangement. The parent ship has a seat row of 10 passengers. The distribution of passenger was done by shifting each seat row of passengers from main deck to upper deck or vice versa. It was noticed that during the shifting of seats, the weight components of passengers and their belongings were not changing. The only effect of mevement of passengers was the changing of vertical and longitudinal centers of weights. However, this shifting of passengers affected the ship dimension (length) due to the required space. In addition, the weight of structural items and its centers were changed. As a result the total ship weight or displacement of the ship was changed.

During the modification, the main dimensions such as ship beam, deck and draft were kept constant. In addition, some parameters of hull form configuration were not changed. They were midship area A_M and coefficient of midship C_M, dead rise angle, top side flare, width and height of hard chine and transom area and draft. These parameters will be investigated later for the next studies. The main changing of the ship parameters were: length, displacement, block and prismatic coefficients, longintudinal center of buoyancy, and half angle of entrance. During the modification of ship length, the structural weight was changed. To add or reduce one meter length of ship, the longitudinal structural weight will increase or decrease as much as 0.818 tonne (2.10 % of total structural weight) for all structures below the main deck. With the addition of transverse structures this will increase to 1.033 tonne (2.65 % of total structural weight). In addition, for the structure components of the upper deck, weight increases by 0.235 tonne (0.6 %) for longitudinal structures and 0.262 ton (0.67 %) for longitudinal and transversal structures. The ship parameters due to the modification of length are presented in Table 3.

Table 3: Ship parameters due to the modification of the length

Parameters	Unit	Results							
No. of pax m. deck		137	147	157	167	177	187	197	207
No. of pax u. deck		117	107	97	87	77	67	57	47
Pax at main deck	%	54	58	62	66	70	74	78	82
Ship length (L_{OA})	m	28.12	29.09	30.06	31.03	32.00	32.97	33.94	34.91
Length $L_{WL} = L_{BP}$	m	26.14	26.76	27.60	28.14	28.96	29.79	30.45	31.41
Displacement Δ	ton	102.6	104.1	104.4	104.7	105.3	105.8	106.7	107.4
Block coefficient C_B		0.410	0.405	0.387	0.385	0.373	0.362	0.360	0.342
Prismatic coef. C_P		0.747	0.738	0.723	0.704	0.686	0.671	0.666	0.654
Waterplane coef. C_{WP}		0.857	0.856	0.857	0.855	0.850	0.845	0.846	0.846
VCB, KB	m	0.954	0.959	0.971	0.967	0.971	0.976	0.969	0.981
Rad. metacenter BM_T	m	5.069	5.186	5.261	5.298	5.336	5.381	5.243	5.539
V. cent of gravity KG	m	3.208	3.202	3.162	3.133	3.057	3.052	3.026	2.987
Init. metacenter GM_T	m	2.816	2.943	3.069	3.132	3.250	3.296	3.386	3.534
Side wind area	m^2	132.3	133.5	134.7	136.0	137.2	138.3	139.6	140.9
Center of wind force	m	4.032	3.980	3.928	3.876	3.826	3.777	3.727	3.679
H. lateral resistance	m	0.954	0.959	0.961	0.967	0.971	0.976	0.979	0.981

Some ship parameters were kept constant during modification procces i.e. beam deck = 7.00 m, beam waterline = 6.68 m, draft = 1.40 m, main deck height = 2.60 m, midship area = 5.16 m^2, midship coefficient = 0.551, dead rise angle at midship = 20.59 degree, top side flare = 5.22 degree, height of hard chine at midship = 1.25 m, width of hard chine at midship = 3.327 m.

The parameters of ship resistance and stability were computed by using Maxsurf software. The criteria that have been used for the ship stability are based on HSC Code 2000 MSC 97(73) - Annex 8 Monohull Intact, HSC Code 2000 Chapter 2 Part B Passenger Craft Intact and IMO MSC 36(63) HSC Code Monohull Intact. In addition, the ship resistance was computed based on the statistical method of Savitsky pre-planning. The results of the computations are shown in Table 4 and Fig.4.

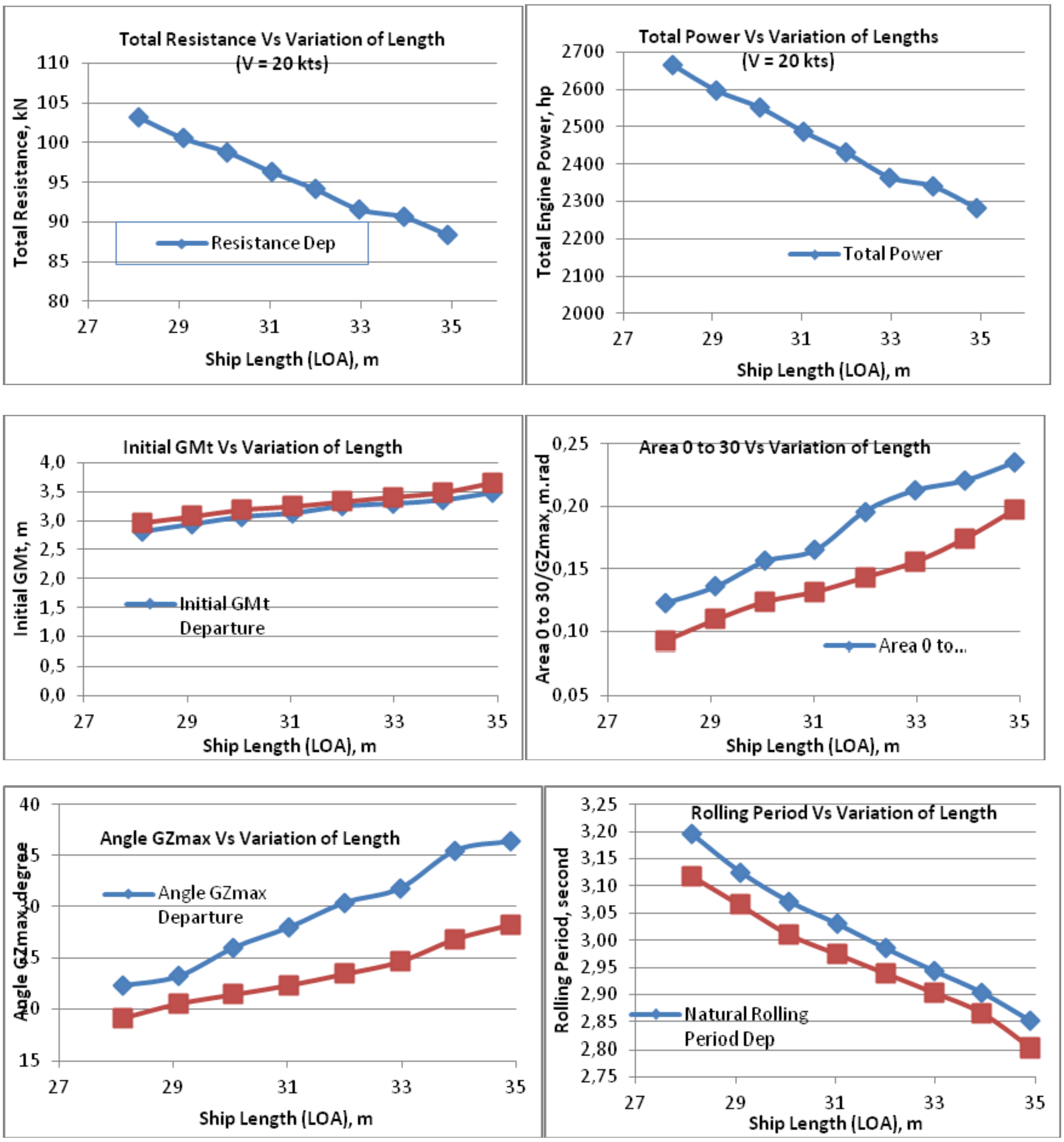

Fig.4: The results ship parameters due to the modification of ship length

Table 4: Impacts on resistance and stability parameters

Parameters (criteria)	Unit	Results							
Pax at main deck	%	54	58	62	66	70	74	78	82
Ship length, L_{OA}	m	28.12	29.09	30.06	31.03	32.00	32.97	33.94	34.91
Resistance, Vs at 20 kt	kN	103.2	100.6	98.84	96.36	94.17	91.62	90.68	88.44
Stability (departure):									
Angle steady hell (≤16)	deg.	4.50	4.20	3.90	3.80	3.60	3.50	3.40	3.20
Angle s.h/m.l im. (≤80)	%	13.93	13.06	12.16	11.92	11.18	10.84	10.71	9.68
Area1/Area2 (≥100)	%	94.86	112.74	133.00	145.50	168.70	178.43	188.09	211.88
Angle of GZ_{max}	deg.	22.3	23.2	24.5	25.5	31.4	31.8	35.5	36.4
Angle vanishing stab.	deg.	57.6	59.0	60.9	62.0	64.4	64.6	65.9	68.3
Area 0-GZ_{max} (≥0.055)	m.rad	0.123	0.136	0.156	0.165	0.196	0.213	0.220	0.235
Area 30 to 40 (≥ 0.03)	m.rad	0.070	0.075	0.083	0.085	0.092	0.093	0.097	0.105
Angle GZ_{max} (≥ 15)	deg.	22.30	23.20	26.00	28.00	30.40	31.80	35.50	36.40
Initial GMt (≥ 0.15)	m	2.820	2.943	3.069	3.132	3.250	3.296	3.360	3.480
Angle pax crowd (≤10)	deg.	8.84	8.20	7.70	7.40	7.00	6.80	6.65	6.10
Angle hs turning (≤10)	deg.	4.10	3.80	3.40	3.20	2.95	2.80	2.65	2.30
Angle wind heel (≤16)	deg.	4.50	4.20	4.00	3.80	3.60	3.50	3.40	3.10
Period of rolling	sec.	3.20	3.13	3.07	3.03	2.99	2.94	2.90	2.85
Period of pitching	sec.	2.39	2.36	2.32	2.31	2.30	2.28	2.31	2.21
Period of heaving	sec.	2.74	2.72	2.67	2.66	2.63	2.60	2.61	2.52
Stability (arrival):									
Angle steady hell (≤16)	deg.	4.75	4.50	4.30	4.12	4.02	3.93	3.85	3.65
Angle s.h/m.l im. (≤80)	%	14.61	13.62	12.84	12.37	11.76	11.24	10.00	10.14
Area1/Area2 (≥100)	%	54.96	75.14	95.82	106.84	120.93	133.92	146.12	167.41
Angle of GZ_{max}	deg.	19.1	20.5	21.4	22.3	23.2	23.6	26.8	22.2
Angle vanishing stab.	deg.	53.6	56.2	58.1	59.2	60.5	61.8	63.2	65.6
Area 0-GZ_{max} (≥0.055)	m.rad	0.093	0.110	0.124	0.132	0.143	0.156	0.174	0.197
Area 30 to 40 (≥ 0.03)	m.rad	0.057	0.064	0.070	0.074	0.078	0.082	0.087	0.096
Angle GZ_{max} (≥ 15)	deg.	19.10	20.50	21.40	22.30	23.4	24.60	26.80	28.20
Initial GMt (≥ 0.15)	m	2.97	3.08	3.19	3.25	3.33	3.41	3.48	3.65
Angle pax crowd (≤10)	deg.	19.20	9.50	8.90	8.40	8.00	7.60	7.40	6.70
Angle hs turning (≤10)	deg.	4.55	4.10	3.73	3.50	3.20	3.00	2.85	2.50
Angle wind heel (≤16)	deg.	4.89	4.60	4.38	4.10	4.00	3.80	3.67	3.44
Period of rolling	sec.	3.12	3.07	3.01	2.97	2.94	2.90	2.87	2.80
Period of pitching	sec.	2.32	2.30	2.56	2.26	2.24	2.22	2.40	2.17
Period of heaving	sec.	2.65	2.64	2.58	2.57	2.55	2.52	2.53	2.46

4.2. Optimization of ship resistance

Since the modification of the ship was done due to the ship length, then all parameters of resistance, stability and seakeeping are presented as the function of ship length. From Fig.5 it seems that the trend lines of the curves of ship parameters is almost linear. As assumption, the equations of the trend line are set to be linear. The equations of linear trend line of the resistance and stability parameters are presented at Table 5. The parameters seakeeping (periods of rolling, heaving and pitching) are not evaluated further here. Especially for rolling period, the values are smaller (≈ 3 seconds) than what is expected which is about

12 seconds for the passenger ferries. This phenomenom exists mostly for passenger ships where special treatment would be introduced later in this study.

Table 5: The equations of linear trend line for the resistance and stability parameters

Parameters	Equations of linear trend line	
Resistance (Vs: 20 kt)	f(x) = -2.1714x + 163.92	
Stability criterion:	**Departure**	**Arrival**
Angle steady hell ≤ 16	f(x) = -0.178x + 9.3708	f(x) = -0.1492x + 8.8433
Angle s.h/m.l im. ≤ 80	f(x) = -0.567x + 29.554	f(x) = -0.6118x + 31.477
Area1/Area2 ≥ 100	f(x) = 16.635x – 370.09	f(x) = 15.592x – 378.74
Area 0-GZ_{max} ≥ 0.055	f(x) = 0.0172x – 0.3626	f(x) = 0.0142x – 0.305
Area 30 to 40 ≥ 0.03	f(x) = 0.0048x – 0.0625	f(x) = 0.0052x – 0.0879
Angle GZ_{max} ≥ 15	f(x) = 2.2091x – 40.421	f(x) = 1.2997 x – 17.673
Initial GMt ≥ 0.15	f(x) = 0.0925x + 0.2545	f(x) = 0.0927 x – 0.3723
Angle pax crowd ≤ 10	f(x) = -0.3686x + 18.951	f(x) = -0.4823x + 23.538
Angle hs turning ≤ 10	f(x) = -0.2504x + 11.04	f(x) = -0.2834x + 12.36
Angle wind heel ≤ 16	f(x) = -0.1902x + 9.7576	f(x) = -0.2042 x + 10.546

The objective of the study is to find the minimum resistance of the modified ship. Here the length of ship (L_{OA}) becomes a single control variable (x). Set the length as control variable x and the resistance as objective function f(x) then the solution of the optimization problem is stated as:

Minimize: $f(x) = -2.1714x + 163.92$ (12)

In fact, another important objective beside minimizing the resistance is minimizing the ship length. In this study some hull parameters are kept constant (beam, draft, midship area) and other parameters are changed (length, displacement, block and prismatic coefficients, half angle of entrance) then the resistance decreases as the length increases as seen at the resistance curve in Fig. 4. Then, to find the the minimum resistance based on minimum length, the solution of the optimization problem is stated as:

Maximize: $f(x) = -2.1714x + 163.92$ (13)

Subject to the constraints:

(for departure condition)		(for arrival condition)	
-0.178x + 9.3708	≤ 16	-0.1492x + 8.8433	≤ 16
-0.567x + 29.554	≤ 80	-0.6118x + 31.477	≤ 80
16.635x – 370.09	≥ 100	15.592x – 378.74	≥ 100
0.0172x – 0.3626	≥ 0.055	0.0142x – 0.305	≥ 0.055
0.0048x – 0.0625	≥ 0.03	0.0052x – 0.0879	≥ 0.03
2.2091x – 40.421	≥ 15	1.2997 x – 17.673	≥ 15
0.0925x + 0.2545	≥ 0.15	0.0927 x – 0.3723	≥ 0.15
-0.3686x + 18.951	≤ 10	-0,4823x + 23,538	≤ 10
-0.2504x + 11.04	≤ 10	-0,2834x + 12,36	≤ 10
-0.1902x + 9.7576	≤ 16	-0,2042 x + 10,546	≤ 16
x	> 0	x	> 0

Using excel solver to solve the problem, it was found that for departure condition, the minimum length of ship (L_{OA}) is 28.26 m. Meanwhile the minimum length of the ship for arrival condition is 30.70 m. In fact, for the arrangement of the ship, the minimum length may fit the nearest length based on the arrangement. Therefore, based on the stability of the ship at arrival condition, the length of the ship was selected for L_{OA} = 31.03 m to fit the percentage of 66% passenger at the main deck.

Therefore for the selected ship length of 31.03 m, the total resistance is 96.54 kN and the total engine power (MCR) is 2487 hp for two units of main engines. Meanwhile, other stability criterion are fulfill the requirements. In fact, for the seakeeping problems particularly the natural period of rolling the results are too small. This problems will be investigated in the future study.

4.3. Discussion

1. During the process of modification of ship length, some parameters were kept constant such as ship beam, draft, deck height, midship coeficient, midship and transom sections. Meanwhile, the structural weight (total weight) increases with the increasing of the length. Therefore as the length increases then block and prismatic coefifients and half angle of entrance decreased. The decreasing of those parameters contributed to decrease of ship resistance though the wetted surface area increases due to the length.
2. The longer the ship the more stable it would be however, the rolling period become more lower or the rolling movement of ship become stiffer. This means that selecting the longer ship will be better for stability point of view. However selecting the minimum length would be better as long as it satisfy all the constraints. In addition, this is also due to the construction and other operation costs.
3. This small passenger ship has a difficulty with seakeeping, particularly the period of rolling. The rolling period depends on the metacenter height (GM_T). The higher the metacenter height the stiffer the ship movement. In fact, the higher metacenter is required to satisfy the stability of the ship. The application of anti-rolling devices should be used for this ship to improve the seakeeping qualities.
4. Two operational conditions of the ship were presented here i.e. departure and arrival. During these conditions, ship the parameters change particularly the ship stability. The results from these conditions may be used for the future works especially the possibility of application of the temporary ballast (at arrival conditions) to increase the ship stability or to decrease the ship length.

5. Conclusion and recommendations

5.1. Conclusion

- For the input design of 254 passengers with the constant beam of 7.00 m and other constant parameters (draft, deck height, midship and transom sections) then the minimum length of the ship is 30.70 m and a little increase to 31.03 m to fit the configuration of 66% passenger at the main deck.
- The longer the ship the less resistance or power of the ship, however the selection of lower length also benefits for construction and operational costs. Then the minimum resistance and other parameters were found due to the selected length.

- In fact, this study is conducted for only one configuration of ship beam which is 10 seats in a row. Other variation of ship beams (seat configurations) and draft variation will end-up with other results.
- Since there is no available database provided for such medium-speed passenger ferry, then the results of parent ship provides some relevant data for the ship during the modification process.

5.2. Recommendations

The future works would be recommended for:

- Variation of ship beams and drafts for the modification process
- Optimizing the hull forms and local refinement to reduce the resistance
- Optimizing the ship structure in order to reduce the structural weight of the ship
- Executing the model tests in order to achieve better results of ship resistance.
- Selecting the proper screw propeller to reduce the engine power

References

BUREAU VERITAS (2002), *The Rules for the Classification of High Speed Craft,* Bureau Veritas - February 2002, pp. 11-217

CALHOUN, S.R.; STEVEN, S.C. (2003), *Human Factor in Ship Design*, Ship Design and Construction, Writen by an International Group of Authorities, Thomas Lamb, Editor, SNAME Publication, Jersey City, New York, USA, Vol. 2, Chapter 15, pp. 15.1– 15.26

GALE, P.A. (2003), *The Ship Design Process*, Chapter 5 - Ship Design and Construction, Written by an International Group of Authorities, Thomas Lamb, Editor, SNAME Publication, Jersey City, New York, USA, Vol. 2, pp. 5.1–5.22

HOLTROP, J.; MENNEN, G.G.J. (1978), *A Statistical Power Prediction Method*, ISP, Vol. 25

KNOX, J. (2003), *Ferries*, Chapter 38 – Ship Design and Construction, Written by an International Group of Authorities, Thomas Lamb, Editor, SNAME Publication, Jersey City, New York, USA, Vol. 2, pp. 38.1–38.29

LARSSON, L.; HOYTE, C.R. (2010), *Ship Resistance and Flow*, The Principles of Naval Architecture Series, J. Randolph Paulling, Editor, 2010, Published by The SNAME, 601 Pavonia Avenue, Jersey City, New Jersey 07306, pp. 178-210

LEVANDER, K. (2003), *Passenger Ships,* Ship Design and Construction Vol. 2, Chapter 37, Writen by an International Group of Authorities, Thomas Lamb, Editor, SNAME Publication, Jersey City, New York, USA, pp. 37.1–37.38

LEWIS, E.V. (1988), *Resistance, Propulsion and Vibration*. Principles of Naval Architecture, The Society of Naval Architects and Marine Engineers, 601 Pavonia Avenue, Jersey City, NJ, Vol. 2, pp. 93–105

MOLLAND, A.F.; TURNOCK, S.R.; HUDSON, D.A. (2011), *Ship Resistance and Propulsion*, Cambridge University Press, 32 Avenue of the Americas, New York, N.Y, USA, pp. 208-216

OLSON, H.A. (1990), *Trends in Modern Ferry Boat Design*, Paper Presented at the February 8 1990 Meeting of The Northern California Section of The SNAME, pp. 6–37

PARSONS, M.G. (2003), *Parametric Design*, Chapter 11 - Ship Design and Construction, Written by an International Group of Authorities, Thomas Lamb, Editor, SNAME Publication, Jersey City, New York, USA, Vol. 2, pp. 11.1–11.34

WATSON, D.G.M. (1998), *Practical Ship Design*, Elsevier Ocean Engineering Book Series, Volume I, ELSEVIER, pp. 155–360.

Transient Wave Loads on Large High-Speed Catamarans

Walid Amin, Australian Maritime College, **Davis, M.R.**, School of Engineering University of Tasmania, waiamin@amc.edu.au, m.r.davis@utas.edu.au
Giles Thomas, Australian Maritime College, giles@amc.edu.au
Damien S. Holloway, School of Engineering, University of Tasmania, Australia, Damien.holloway@utas.edu.au

Abstract

The demand for large high-speed wave piercing catamarans has developed strongly over the past two decades for their superior performance in commercial and military applications. In severe sea conditions, wave piercing catamarans experience a unique transient loading, known as slamming, when incoming waves impact the centre bow and the wetdeck. Mathematical models up to date have failed to predict the impact loads accurately as most codes are based on two dimensional simulations which have predicted up to five times the actual loads. Three dimensional codes are still under verification which is difficult due to the lack of published trials data. Incat Tasmania monitored the performance of most of their vessels in terms of motion and structural behaviour. A 98m Incat platform, HSV2-SWIFT, that was configured for military operations underwent an extensive sea trials program by the US Navy to define the vessel's operational envelop. Data measured during sea trials of motion and structural response has been analysed using the wavelet transform. Also, experimental pressure mapping of slam loads on a towing tank model and finite element analysis of the full scale ship are used to predict slamming loads at full scale by both quasi-static and dynamic analyses. Normal modes were investigated using FEA simulations and the slam load time history was predicted by a direct transient dynamic analysis. The study shows that quasi-static analysis of slamming loads can be used to predict slamming loads to an acceptable accuracy with some caution in the prediction procedures. A characteristic slamming load time history is introduced and the investigation shows that the vessel experienced and withstood slamming loads in excess of two thousand tonnes.

1. Introduction

Fig.1: Damage of bow structure on HSS 1500 Stena due to severe slamming loads

High speed multi-hull ferries operating in rough seas may experience water impact loads due to excessive relative motion between the vessel and the wave surface. A shudder or vibration occurs following such impacts known as whipping. Severe slamming loads might also result in abrupt changes in vessel motion and generate high stress levels which may in turn cause structural damage. Such damage has a direct impact on short term repair cost and loss of service time; in addition, long term losses may occur due to bad publicity resulting from severe ship motions and damage where catamarans are used for passenger service.

Slamming on multihull ships is different from slamming on monohulls in terms of slam location and severity. Twin hull ships experience unique type of slamming called wetdeck slamming, when the underside of the cross deck structure comes in contact with the wave surface in the presence of sufficient relative motion between the vessel and the water surface. Serious damage occurred on the Stena HSS 1500 bow structure due to a severe slamming event in rough seas as shown in . Deformation of longitudinal stiffeners has been reported on an 86 m Austal vessel due to severe slamming loads Rothe et al. (2001). On wave piercing catamarans, INCAT Tasmania Hull 050 suffered side shell buckling and tripping of brackets in the centre bow area, Thomas et al. (2002). In general, severe slamming loads can result in (a) Localised dishing of plating between longitudinal stiffeners and side frames, (b) Distortion of centre bow longitudinal stiffeners, (c) Side shell buckling, (d) Distortion of frames and stiffeners aft of the centre bow, (e) Crack propagation due to the effect of whipping in the form of material fatigue. INCAT Tasmania Hull 061 (HSV2-Swift) has shown and demonstrated greatly improved structural integrity when the vessel underwent an extensive sea trials program by the US Navy to define its operational envelope. The vessel was tested significantly beyond the service criterion it was designed to withstand according to the DNV rules. Consequently high motion acceleration records were reported, (Brady, 2004). Based on the current study of these trials, the calculated loads during the design process were smaller than those imparted on the structure during trials. However, the ship withstood these high loads without any structural damage. This suggests that the ship structure may be further optimised to reduce the lightship displacement and consequently increase the payload. However, the calculation of slam loads on large catamarans fitted with a centre bow is a complex task and extreme loads to date have not been established through a proven theoretical approach.

Unfortunately the kinematics of slamming events is also not well understood on large high-speed catamarans. At this stage classification of slamming events and the factors affecting the slamming occurrences can only be easily evaluated by full scale measurement and/or model testing. In comparison with the extensive work that has been carried out for slamming on monohulls, such as that due to Aertssen (1979), Iaccarino et al. (2000), and Bigot et al. (2011), little work has been published on full scale measurement of loads and motions of large high speed catamarans. Roberts et al. (1997) extrapolated sea trials stresses for an 81 m and an 86 m INCAT Tasmania catamaran at a probability of 10^{-8} using Weibull and Gumbel extreme value plots. The analysis assumed that extrapolated full scale stresses could be directly compared with the FE model stresses at the same locations obtained by a quasi-static analysis. Steinmann et al. (1999) extrapolated sea trials extreme value stresses at a probability of 10^{-8} using the Ochi extrapolation procedure which assumes a linear relationship between stresses and wave height: this assumption may not be true for moderate to heavy seas for large high speed catamarans. Individual slamming events were identified during post processing of trials data. Slamming dynamic effects were also studied by Thomas et al.(2006) and the effect on fatigue damage to aluminium hulls was estimated. Sea Fighter FSF-1 was comprehensively tested in up to SS4 and 5, Fu et al. (2007). The study introduced the characteristics of four slamming events. It was found that for a slam to happen, the bow lifts in a trough and then that lift is followed by encounter with a wave that is at least 50% higher than the significant wave height. Lin et al. (2007) validated a 2-D numerical slamming model developed by Ge (2002), which was integrated into a 3-D time domain Large Amplitude Motion Program LAMP, originally developed by Lin and Yue (1990). Results were compared with experiments and full scale trials data. Calculations were based on hydrodynamic analysis for a rigid body and the resulting loads on the structure, structural vibrations and peak slamming pressures were determined. The study showed that a 2-D simulation is limited in the applicability to a fully 3-D slamming event. Further, a complicated wet deck configuration contributed to the uncertainty of the determination of the pressure coefficient. However, model tests showed good matching with acceleration and pressure transients, but with some discrepancy in magnitudes. It was also found that maximum slamming pressures do not necessarily occur at the most forward wetdeck location. Trials analysis showed that a model of long crested waves is needed instead of the reconstruction of the irregular wave profile using Fourier Transform.

Slamming dynamic effects were also studied by Thomas et al. (2006) and it was found in analysis of full scale trials of INCAT Tasmania Hull 042 that slamming significantly contributes to fatigue damage in aluminium hulls . Peak slam loads have also been compared to the quasi-static global response design loads as defined by DNV Rules, Thomas (2003). Extreme value analysis has also been implemented to compensate for the dynamics of slamming. Thomas et al. (2002) and Thomas et al. (2003) have explored the slam dynamics extensively to investigate loads during an extreme slamming event that caused buckling of the superstructure shell plates on an 96 m INCAT Tasmania catamaran during her regular service across Cook Strait in New Zealand. The investigation resulted in improved understanding of slamming dynamics showing that the asymmetric slamming load during this particular event was in excess of 1000 tonnes. In the present paper, we extend the investigation of slamming dynamics through the improvement of slamming identification techniques, by quasi-static and dynamic finite element analysis (FEA) and by conducting model experiments to measure dynamic pressures in regular waves on the centre bow and the bridging structure. The key novel objectives in the current work are: (a) Introduction of new trials interpretation technique (b) The introduction of the Continuous Wavelet Transform (CWT) as a new signal analysis method to investigate the ship structural performance during slamming sea trials; (c) Hydrodynamic pressure measurements on the centre bow and wet deck structure in regular waves; (d) Prediction of the linear and non-linear wave loads using the capabilities of finite element analysis in combination with sea trials data.

2. Identification of slamming loads

To predict slamming loads we seek to identify the loading pattern that will give the same response as measured during sea trials using Finite Element Analysis (FEA) as a modelling tool for the structure and imposed hydrodynamic loads. For a large complex structure such as a wave piercing catamaran the loading pattern needs to include the underlying regular wave loads, slamming loads and inertia loads resulting from the ship motions. The slamming load pattern is not easily identified and therefore we incorporate model testing in which pressure mapping on the centre bow and the wetdeck forms the basis for developing loading models in terms of their spatial and temporal distributions. The strategy in identifying slam loads is as follows:

1. Processing of trials data to extract the wave data, motion response data, structural response data as well as motion control system forces at any given instant.
2. Conduct of model test experiments to establish the spatial distribution of slam loads under similar conditions to trials (vessel Froude number and scaled sea state).
3. Extraction of slam loading patterns from model test data and application to the FE model in combination with the full scale motion data to calculate the structural response at the strain gauge locations.
4. Modification of slam loading model until the best match between predicted and measured strains is obtained.

3. Vessel under investigation

LOA	97.22 m
LWL	92.00 m
BOA	26.60 m
Demi-hull beam	4.50 m
Demi-hull separation	21.66 m
Full load draft	3.43 m
Full load displacement	1850 tonnes
Full pay load	744 tonnes
Fuel capacity	841 m^3
Service Speed	38 knots

Table 1: Hull 61 (HSV2-SWIFT) specifications

The vessel is an INCT 98m wave piercing catamaran with centre bow, configured for military applications and known as HSV2-Swift. The vessel is built and operated to the DNV Rules and HSC Code. The vessel is propelled by four LIPS LJ 120E waterjets, driven by four 9655 HP Caterpillar 3618 high speed marine diesel engines through ZF5300 NRH gearboxes. Motion control retractable T-foil is attached to the centre bow in addition to active trim tabs at the stern. To suit military applications, the vessel was equipped with a flight deck and rotating/swinging aft ramp for RO/RO of military vehicles. The ship particulars are listed in Table 1.

Structurally, the vessel is constructed using a longitudinal framing system which has the advantage of light construction weight. Cross bracing is introduced to provide longitudinal strength in both the longitudinal directions and in the superstructure raft (in addition to transverse beam) to withstand longitudinal and lateral deformations. The superstructure raft transverse beams are connected to the main hull girder through rubber mounts to reduce the vibration levels in the passenger lounges. INCAT Tasmania catamarans are characterised by a centre bow between the demi-hulls. The centre bow length was 28% of the waterline length. Its main purpose is to counteract bow diving in following seas as well as reducing the vessel pitching motion by offering extra buoyancy as the bow pitches into the wave. Consequently, the vessel has two archways between the centre bow and demi-hulls in the forward part of the vessel. Behind the centre bow, the wet-deck is flat.

4. Sea trials

The main objective of the HSV-2 SWIFT trials was to assess the vessel's seakeeping and structural performance for specific military operations and to define the safe operational envelop. The vessel was instrumented by structural response monitoring system of three groups of strain gauges denoted T1, T2 and T3 groups at the recommendation of R & D department at Revolution Design. T1 and T2 groups were sampled at 100 Hz to measure response due to global and local loads respectively. T3 group was sampled at 1000 HZ to capture the response to impact loads on the centre bow. Fig.2 shows two strain gauges of group T1 fitted on the keel plate near Fr46 and 61. The vessel was also equipped by motion monitoring system composed of three-axis accelerometers at the centre of gravity, the centre bow and the flight deck. The wave height record was obtained during the trials by means of a TSK wave height system at the bow.

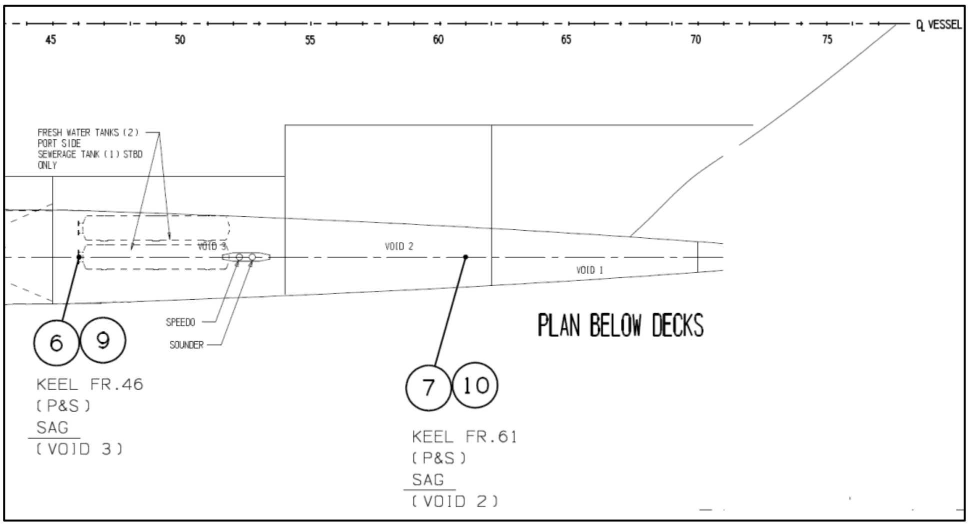

Fig.2: Forward keel T1 group strain gauges

During trials the vessel experienced extreme conditions beyond the design envelope and therefore peak responses beyond alarm levels occurred during trials. However, the vessel structure withstood these harsh conditions when high vertical bow accelerations up to 3g were experienced due to excessive slamming loads. This raises a question regarding the appropriateness of applying a classification society design code intended for civilian ferry operations subject to maximum operation wave height to a vessel in military service.

5. Model testing

A segmented model was designed to simulate hydro-elastic response effects due to transient wave loads, Lavroff et al. (2007). The model was designed so that it has a correctly scaled frequency of whipping response (14 Hz at model scale, 2.1 Hz at full scale). The design frequency of the vessel was determined from the FE model of the full scale vessel. Two transverse cuts run through the model allowing the longitudinal bending moment to be measured at two locations. The centre bow was isolated from the rest of the model and was joined to the demi-hulls by means of two transverse beams each having two elastic links so that the upward force on the model centre bow could be measured. In addition the centre bow segment of the model contained 84 pressure tappings between Frame 55 and Frame 82 for mounting pressure sensors over the starboard side of the arch and the centre bow. Frames are numbered from the transom and are set at 1.2m intervals.

Using 12 Endevco Piezoresistive pressure transducers, the pressure on the wet deck and the centre bow was mapped and used in the finite element model to represent the slam load spatial distribution in longitudinal and transverse directions. Fig.3 shows the simultaneous pressure distributions at 12 locations along the top of the arch line between the demi-hull and the centre bow. From the model test data, three individual slams,Table **1**, were selected and the pressure distributions were extracted and input into the finite element analysis.

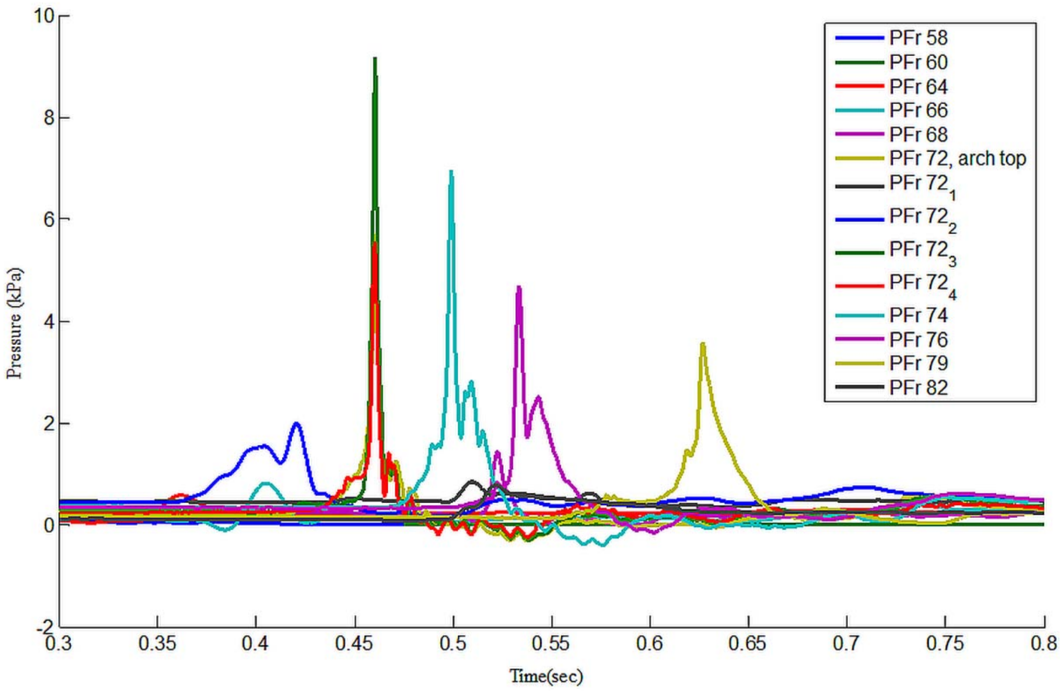

Fig.3: Typical pulse time history for 14 pressure transducers along the top arch line and at Fr 72 transversely at 5 locations, wave height 120 mm, wave freq. 0.625 Hz, model speed 1.53 m/s (ω_e* 3.1).

	(A) at 856.14 s	(B) at 710.89 s	(C) at 773.89 s
Max Bow vert. acc. (g)	3.03	2.24	1.72
Max. CG vert acc. (g)	0.76	0.39	0.36
Max. Relative bow vert vel. (m/s)	5.13	4.4	4.05
Wave height (m)	6.81	2.24	2.02

Table 1: Slamming events under investigation; head seas, vessel speed 20 knots.

6. Quasi-static analysis

Quasi static analysis is usually performed by placing the vessel on a static wave of a certain height and calculating the strains numerically by finite element methods. As the relation between loading (Bending moment in this case) and the local strain is linear, a matrix of calibration coefficients can be established between the BM and the resulting strains at different locations. Then the calibration factors can be used to derive the bending moments from sea trials strains, Hay and Bourne (1994), Sikora et al. (1991), Stredulinsky et al. (1999) and Sikora et al. (2004). The method can predict the bending moments, however, cannot predict the transient wave loads in terms of its temporal and spatial distribution which is the focus of the current study.

The current study uses an approach in which the slamming loads are modelled as additional loads to the hydrostatic wave loads according to the instantaneous ship immersion. Thus by using FE analysis and motion response during sea trials as input parameters, we obtain the maximum benefit of using FE in simulating reality. The vessel immersion was obtained from the measured wave motion at the bow by decomposing the trial time record using a Fourier Transform. The slam load was then added on the centre bow, the arch area and a part of the cross deck structure behind the centre bow. The slam load was then scaled and adjusted in location and distribution until the best match between the trials and the numerical simulation was achieved. Fig. 4 shows six iterations in adjusting the total slam load and location of the resultant slam force.

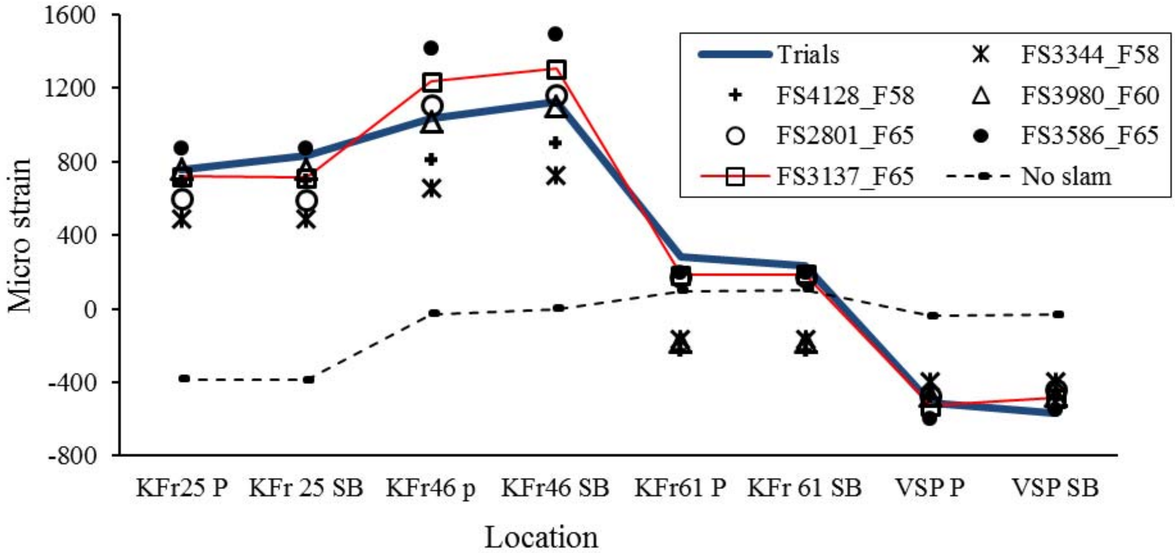

Fig.4: FE numerical response at strain gauge locations to various slam loads in comparison to trials.

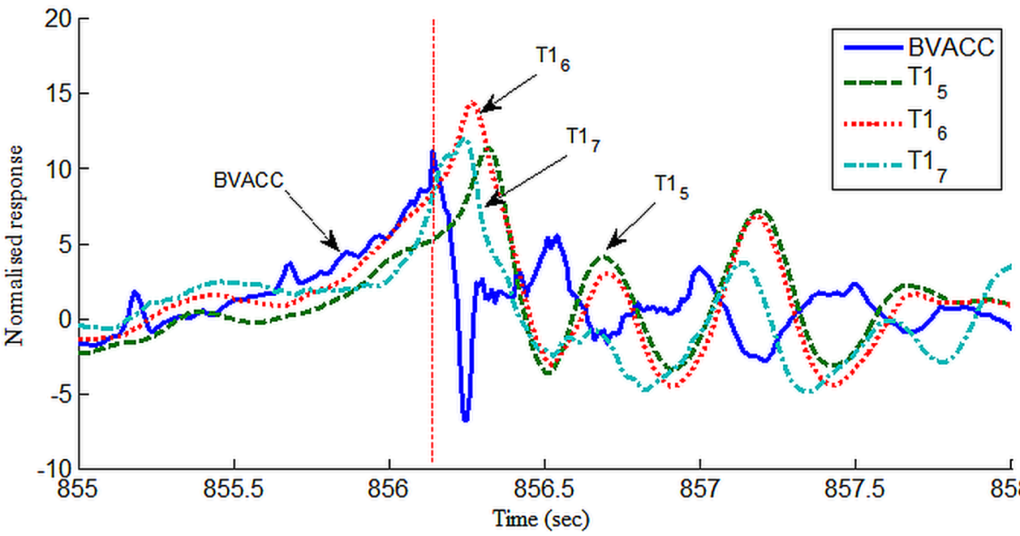

Fig 5: Trials records during a slamming event. Simultaneous approach considers trials responses at the instant of maximum bow vertical acceleration (marked by the dashed line). Peaks approach considers peak response values during the slamming event regardless of time differences of the peaks.

Quasi-static analysis was carried out for the three most severe slamming events observed in head seas of sea state 5 at a vessel speed 20 knots. The results showed that the time differences between the peaks of bow vertical acceleration and structural responses along the vessel keel can affect the predicted loads based on the comparative approach used here Amin et al. (2009). One approach is to consider the slam event as a whole and use the acceleration peak magnitude in the FEM to calculate the inertia loading and thus calculate the strains. The FE strains were then compared to the trials peak strains. The second approach also made reference to the peak acceleration in the same manner; however, the calculated strains were compared to the trial strains that are simultaneous with the acceleration peak instant. It was found that the difference in predicted slamming using these approaches was up to 48%.

Fig 5 shows the time difference between occurrence of the peaks of individual strain gauges and so reflects the propagation of the impulse wave through the hull. In the quasi-static analysis, these time differences cannot be incorporated in the solution. From a FEA modelling point of view, it is common in such large structures to model a stiffened panel as a laminate of three layers representing the plate, stiffener web and stiffener flange respectively. However, to obtain reliable results, the structure can be modelled in the area surrounding the strain gauge shell by plates stiffened by beam elements which results in very close results when all elements (shell plates and stiffeners) are modelled as plates.

Comparison approach	(a) Peak trials strain approach.			(b) Simultaneous trials strain approach.		
Slam	(A) 856.14 s	(B) 710.89 s	(C) 773.89 s	(A) 856.14 s	(B) 710.89 s	(C) 773.89 s
Load (tonne)	3317	1891	837	2241	1543	578
Loc. (%LWL)	83.1	75.3	79.2	83.1	74	81.8
Load/Disp	1.7	1.025	0.454	1.215	0.836	0.313
Correlation. %	97.2	96.4	93	97.1	94	82
NRMSE	6.8	11.7	14.7	8.9	11.2	23.5

Table 2: Comparison of FE and trials strain based on (a) peak trials strain and (b) simultaneous trials strain, NRMSE is the normalised root mean square error.

The uncertainty in the quasi-static analysis procedure and the dynamic nature of slamming event made the need for a complete dynamic analysis a priority.

7. Dynamic analysis

An important parameter in carrying out dynamic analysis is the global structural damping characteristics of the hull. The direct transient dynamic analysis algorithm does not permit imaginary (out of phase) magnitudes of structural damping. Therefore, the analysis is valid only at one frequency component at which the structural damping can be expressed as an equivalent viscous damping. This equivalence occurs at the dominant frequency of the vibrating structure, MSC Software (2008).

FE normal mode analysis was used to estimate the natural frequency of the ship structure for dry and wet conditions. Both dry and wet analysis resulted in a series of closely spaced frequencies for each dominant mode shape, there being minor variations within this set of closely spaced and generally quite similar modes. The dominant frequency was chosen on the basis of the largest participation factor as calculated by the FE solver according to:

$$M_R = \{\varepsilon\}^T [\phi]^T [M][\phi]\{\varepsilon\} = \{\varepsilon\}^T [m]\{\varepsilon\}. \tag{1}$$

Where M_R is the rigid body mass, ε is a vector of scaling factors of the eigenvectors, M is the generalised mass matrix, m is the diagonal matrix of generalized masses for the normal modes and ϕ is the eigenvector or mode shape, MSC Software (2008) and MSC Software (2007).

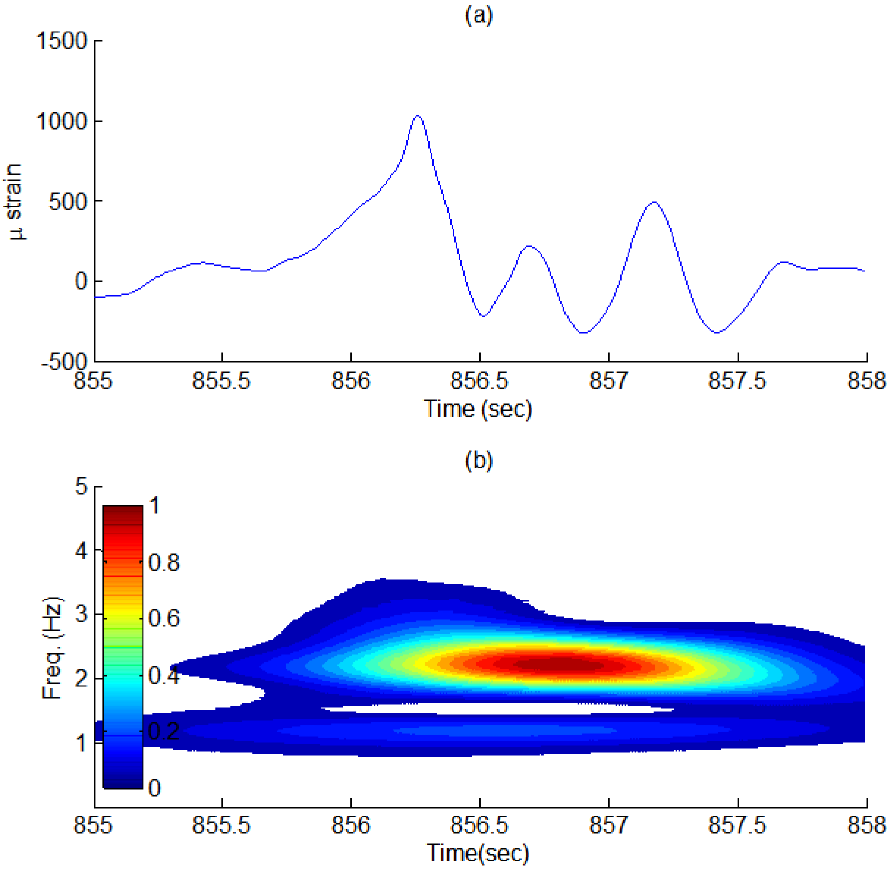

Fig.6: Wavelet transform analysis of a slamming event, (a) strain gauge signal amidships, (b) Wavelet Transform spectrum. Transform parameters set for optimum frequency resolution.

Dry normal modes analysis was found to overestimate modal frequencies by 28% for the first longitudinal mode, 58% for the first transverse bending mode and 41% for the lateral torsion mode when compared to wet modal analysis in which the water added mass is included.
Wavelet Transforms of sea trials motion and structural response records were used to investigate the natural frequencies at full scale. Fig.6 shows the wavelet transform of a strain gauge slam record in which the transform parameters are selected to give good frequency resolution. In this case the strain gauge is on the keel at Fame 46 (approximately amidships). The natural frequency of the hull during trials is clearly evident. The fluid structure interaction was accounted for in terms of the surrounding fluid added mass when calculating wet modal modes. It was found that the added mass is approximately 73% of the ship's mass at the

load waterline. The added mass was applied as lumped masses at a single node per frame. The dominant longitudinal bending mode was identified at a frequency of 2.48 Hz. The dominant transverse bending mode was identified on the basis of the largest participation factor to be the mode at 1.74 Hz. The vessel did not show as many lateral torsion modes and only two modes were identified at 1.101 and 1.135 Hz. The dominant mode was at 1.135 Hz on the basis of a higher participation factor.

It can be seen that the frequencies of the wet longitudinal bending, lateral torsion and transverse bending modes were respectively 78%, 71% and 64% of the dry modal frequencies. This is broadly in line with the increase of added mass which is expected to have an effect in inverse proportion to the square root of the ratio of ship plus added mass to ship mass, a reduction of 76%. The effect of added mass of course depends on the added mass distribution convolved with the mode shape, and so smaller effects are evident in the other two modes where there is relatively less motion at the extremities of the hulls. The wet mode natural frequencies were checked against sea trials and good correlation was found especially for the first longitudinal bending mode (only 4% overestimate). However, FEA procedure under-estimated the lateral torsion mode by 17%. The transverse bending mode was not observed in the trials and could not be checked.

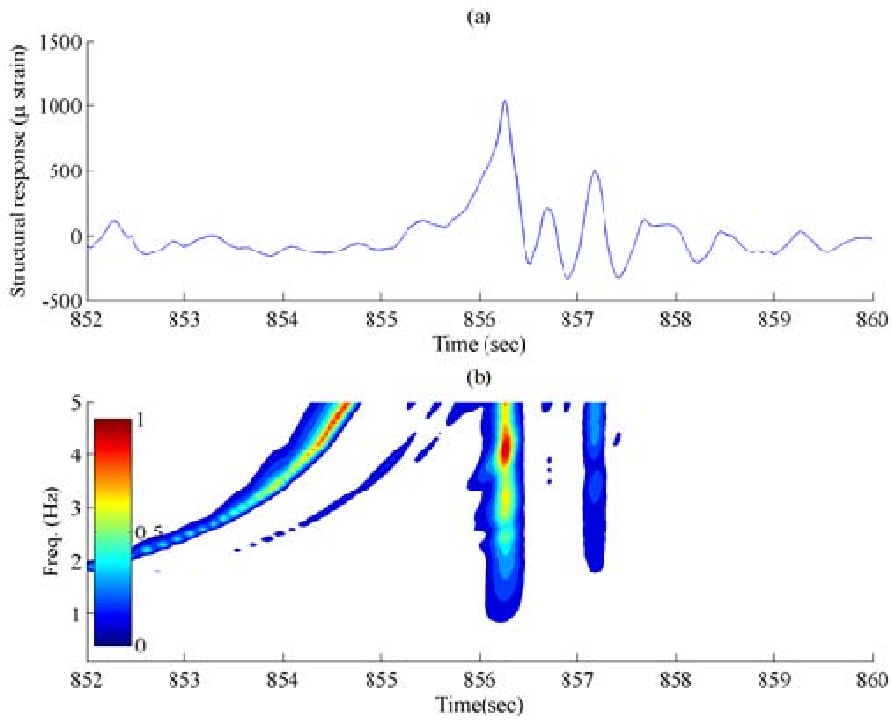

Fig.7: Most severe observed slam in head seas, (a) time history of strain gauge T1_6, keel,

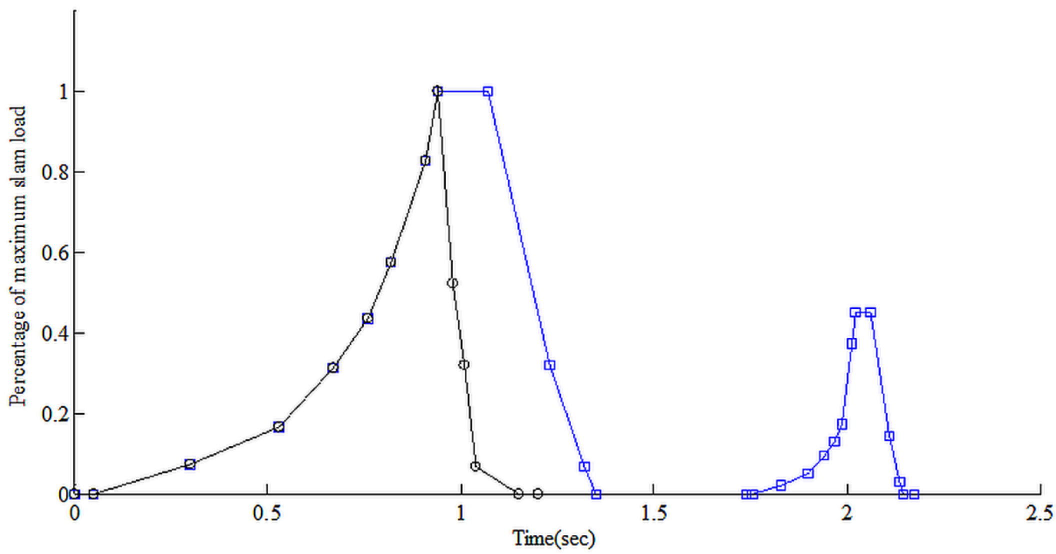

Fr 46 and (b) its wavelet transform. Transform parameters set for optimum time resolution.

Fig.8: Slam load time history input to the numerical model for the slam at 856.13 sec.

The importance of knowing the natural frequency of the system is in the formulation of the direct transient analysis in which complex coefficients of the structural damping are not allowed. However, structural damping can be included in the solution as an equivalent viscous damping. The equivalent structural damping has been obtained from the wavelet analysis of the trials signals, Amin (2009).

One of the challenges in the dynamic analysis is the description of dynamic loadings, in terms of their spatial and temporal behaviour which is a very lengthy process and is considered as inappropriate for practical design purposes. The underlying wave loads were assumed to be static during the transient solution period while all other loadings (inertia and slamming) were considered to change with time. The spatial distribution of slamming loads was assumed to be constant. Although the actual time history is different for each nodal load as observed during model testing, the same slamming load time history was assumed to apply for all nodal forces of the slamming load in order to simplify the loading input data re-

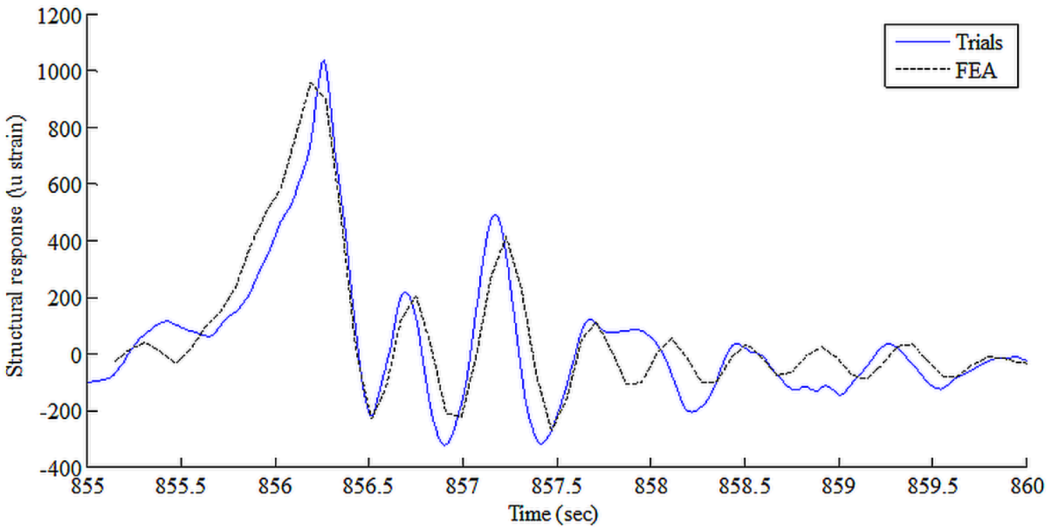

quired.

Fig.9: Full scale trials structural response and FE dynamic analysis response for strain gauge T1_6, keel centre girder, Fr 46

The temporal behaviour of the slam load was originally based on the time history of the bow vertical acceleration during the slamming event as seen on trials data, the slam being assumed to commence when the acceleration reached one standard deviation of the complete record to the peak point. Then the slam interval lasted until the record again returned to the one standard deviation level. This resulted in a good match with the first peak strain value. However, the subsequent oscillations were slightly out of phase and of slightly different magnitude. For this particular slam at the instant 856.13 sec, Fig.9 shows a third peak in the structural response, this being smaller than the first peak and higher than the second peak. This suggests that in this case the vessel might have been subjected to another impact within the same overall slamming event. This was confirmed by the high time resolution Wavelet Transform of this specific event shown in Fig.78. The wavelet spectrum shows two energy concentrations corresponding to the first and third peaks. This was resolved in the FE analysis by applying a scaled second loading impulse in proportion to the third peak in response records as shown in Fig.88. Also, the maximum force duration was increased to 0.13 s to represent a damped response by the action of the slam force itself to control the magnitude of the second response peak. For the gauges that represent the global behaviour of the vessel, the numerical modelling gave a relatively good match with trials as shown in Fig.9. However, the simulation was found very sensitive in areas affected by local structural response such as the forward regions of the hull. The slam load predicted by dynamic analysis was found to be 2272 tonnes which is 1.5% in excess of the result from quasi-static analysis using the optimum procedure in respect of simulating trials records as indicated in section 6.

8. Conclusion

The novel achievements of the current study are: (a) The introduction of new trials interpretation technique in place of the conventional calibration factor techniques (b) The introduction of the wavelet transform as a new signal analysis method for the investigation of the ship structural performance during sea trials involving slam events (c) Hydrodynamic pressure measurements on the centre bow and wet deck structure of towing tank models in regular waves and (d) The identification of the non-linear slam wave loads using the combined capabilities of finite element analysis, model testing and sea trials data. The study shows that quasi-static analysis can be used in place of the complicated and lengthy dynamic FE analysis to investigate the peak magnitude of the transient slamming load within a reliable margin of accuracy provided an appropriate procedure is applied to reconcile measured full scale trials responses and numerically predicted structural responses. Pressure measurements on the centre bow and the cross deck structure provided a reliable means of applying a realistic slam load spatial distribution in the finite element numerical analysis and thus increase confidence in the predicted loads which have been determined. However, it was found that a complete dynamic analysis gave a good definition of the modal frequency response of the structure both dry and wet. When the fluid structure interaction is modelled there was good agreement with measurements of modal frequencies at full scale. Comparison of dynamic simulations and trials showed that the structural response was well represented with regard to the form of transients, frequency of response modes and that the modal damping was identified accurately.

9. Acknowledgement

The authors would like to thank Revolution Design and Incat Tasmania for providing the support, FE model and sea trials data of the vessel under investigation. The research was supported by the Australian Research Council through a linkage grant with Incat Tasmania.

References

AERTSSEN, G. (1979), *An Estimate of Whipping Vibration Stress based on Slamming Data of Four Ships*. International Shipbuilding Progress 26 (294), 23-31.

AMIN, W. (2009), *Non-Linear unsteady wave loads on large high-speed wave piercing catamarans.* PhD at the University of Tasmania, Hobart.

AMIN, W.; THOMAS, G.A.; DAVIS, M.R.; HOLLOWAY, D.S. (2009), *SLAMMING QUASI-STATIC ANALYSIS OF AN INCAT 98-m HIGH-SPEED WAVE PIERCING CATAMARAN*, HSMV 2009, Fremantle, Australia.

BiIGOT, F.; DERBANNE, Q.; SIRETA, F.X.; MALENCIA, S.; TUITMAN, J.T. (2011), *Global Hydroelastic Ship Response Comparison of Numerical Model and WILS model Tests*, International Offshore and Polar Engineering Conference. International Society of Offshore and Polar Engineers (ISOPE), Maui, Hawaii, USA.

FU, T.C.; FULLERTON, A.M.; MINNICK, L.M. (2007), *Charachterization of Sea Fighter, FSF-1, Wave Slam Events*, 9th International Conference on Numerical Ship Hydrodynamics, Michigan.

GE, C. (2002), *Global hydroelastic response of catamarans due to wetdeck slamming*.PhD at the Department of Marine Technology, Norwegian University of Sience and Technology, Trondheim.

HAY, B.; BOURNE, J. (1994), *Characteristics of Hydrodynamic Loads Data for a Naval Combatant*, International Conference on Hydroelasticity in Marine Technology. A.A.Balkema, pp. 169-187.

IACCARINO, R.; MONTI, S.; SEBASTIANI, L. (2000), *Evaluation of Hull Loads and Motion of a Fast Vessel Based o Computations and Full Scale Experiments*, NAV 2000, Genova, Italy.

LAVROFF, J.; DAVIS, M.R.; HOLLOWAY, D.; THOMAS, G. (2007), *The Whipping Vibratory Response of a Hydroelastic Segmented Catamaran Model*, 9th International Conference on Fast Sea Transportation, Shanhai, China.

LIN, W.-M.; ZHANG, S.; WEEMS, K.; JONES, P.; MEINHOLD, M.; METCALF, B.; POWERS, A.M. (2007), *Numerical Simulation and Validation Study of Wetdeck Slamming on High Speed Catamarann*, 9th International Conference on Numerical Ship Hydrodynamics, Michigan.

LIN, W.M.; YUE, D. (1990), *Numerical Solutions for Large-Amplitude Ship Motions in the Time Domain*, 18th Symposium on Naval Hydrodynamics Michigan.

MSC Software (2007), *Dynamic Analysis Using MD NASTRAN and MD PATRAN R2*, NAS122 Course Notes.

MSC Software (2008), *MD NASTRAN R3 Documentation, Advanced Dynamics User Guide*.

ROBERTS, T.J.; WATSON, N.L.; DAVIS, M.R. (1997), *Evaluation of Sea Loads in High Speed Catamarans*, FAST '97, Sydney, Australia, pp. 311-316.

ROTHE, F.; SAMES, P.C.; SCHELLIN, T.E. (2001), *Catamaran Wetdeck Structural Response to Wave Impact*, FAST '01, Southampton, England.

SIKORA, J.; PAUL, H.; BRIAN, S. (1991), *DTRC Report*. DTRC.

SIKORA, J.P.; FORD, H.M.; RODD, J.L. (2004), *Seaway Induced Loads and Sructural Response of the HSV-2.* Naval Surface Warfare Center, Cardrock Division, pp. 1-11.

STEINMANN, P.; FACH, K.; MENON, B. (1999), *Global and Slamming Sea Loads Acting on an 86m High Speed Catamaran Ferry,* Fast'99, USA, pp. 709-718.

STREDULINSKY, D.C.; PEGG, N.G.; GILROY (1999), *Motion, Load and Structural Response Predictions and Measurements on CFAV* Quest. Trans. RINA Part B (141), 117-123.

THOMAS, G. (2003), *Wave Slam Response of Large High Speed Catamarans. at the Department of Mechanical and Civil Engineering,* University of Tasmania, Hobart.

THOMAS, G.; DAVIS, M.R.; HOLLOWAY, D.; Roberts, T. (2002), *Extreme Asymmetric Slam Loads on Large High Speed Catamarans*, High Speed Marine Vehicles, Naples, Italy.

THOMAS, G.; DAVIS, M.R.; HOLLOWAY, D.; ROBERTS, T. (2003), *Transient Dynamic Slam Response of Large High Speed Catamarans*, FAST'03, Italy.

THOMAS, G.; DAVIS, M.R.; HOLLOWAY, D.; ROBERTS, T. (2006) *The Effect of Slamming and Whipping on the Fatigue Life of a High-Speed Catamaran.* Australian Journal of Mechanical Engineering 3 (2), 165-174.

Model tests for the hydrodynamic behavior of a semi-planing hull form in calm and rough waters

Gregory J. Grigoropoulos, N.T.U.A, Athens/Greece, gregory@central.ntua.gr
Agapoula A. Gerogiannaki, N.T.U.A, Athens/Greece, agerogiannaki@yahoo.ca

Abstract

The paper presents the experimental results of the hydrodynamic performance of a hull form with L/B=3.25, extending NTUA series to lower L/B ratios. A model of the hull form was tested in the Towing Tank of the LSMH / NTUA in calm water and in regular and random head waves. The dynamic responses encompass heave, pitch, vertical accelerations along the hull form and added resistance in waves in terms of RAO curves and RMS values. In a previous paper, Gerogiannaki (2011) demonstrated the suitability of the investigated hull form for vessels with length 15-30 and its superiority over competitive commercial yachts of similar size.

1. Introduction

The evolution of technology during the last fifty years resulted in a significant reduction of the actual travelling time of transportation through air and sea. Fast craft proved to be advantageous over conventional vessels sailing at relatively low speeds, both for passenger and for cargo transportation. High speed craft, nevertheless, are the majority of hull designs of recreational boats. Additionally, optimizing design and trying to achieve higher speeds with boats, does not necessarily prevent designers from creating energy efficient vessels. The extra operational cost to sail at high speeds is passed to owners or to the passengers, in order to enjoy high level services.

The large demand of high speed crafts and new designing methods motivated *Grigoropoulos and Loukakis (2002)* to introduce a systematic series of double-chine, wide-transom hull forms with warped planning surface and an increasing deadrise angle from 10o at stern to 70o at bow. The series, inspired by a proposal of *Savitsky et al. (1972)*, provides a handy and suitable base for the design of medium and large modern monohull ships and pleasure craft, which operate at high, pre-planing and planing speeds.

The original NTUA series consists of five hull forms with L/B ratios equal to 4.00, 4.75, 5.50, 6.25 and 7.00. Since the systematic series was created having in mind ships with length from 30 meters up to 150 meters, the ratio L/B was selected in the 4.00 to 7.00 range. Two scaled models for each hull form have been constructed and tested at six displacements, including very light ones. The small-scale models that have been constructed had length from 2.0 m to 2.7 m while the large-scale models had length from 3.2 m to 4.3 m. Models have been tested at different displacements and at different speeds up to Froude number $Fn = V\big/\sqrt{gL_{WL}}$, where V is the ship speed, g is the gravity acceleration and L_{WL} is the waterline length of the craft. The above mentioned resistance characteristics of the series were presented by *Grigoropoulos and Loukakis (2002)*. A fast craft made using NTUA systematic series is in service in South Italy. Similar hulls with NTUA series are constructed fast ferries with length from 90 to 100 m operating in the Aegean Sea at cruising speeds corresponding to Fn up to 0.60.

The series is extended in this paper with a model having L/B=3.25, which is suitable for smaller vessels 15-30 m in length. The full set of the experimental results in calm and rough water are presented in the sequel.

NOMENCLATURE

a_i	Vertical acceleration at point i
A	Wave amplitude
B	Breadth molded
B_{WL}	Max breadth at waterline
B_{PX}	Maximum breadth over chines
C_B	Block coefficient
C_{DL}	Displacement-length ratio at rest $C_{DL} = \nabla / (0.1 L_{WL})^3$
Fn	Froude number, $Fn = V / \sqrt{g L_{WL}}$
FP	Fore perpendicular
g	Acceleration of gravity
$H_{1/3}$	Significant wave height
$H_{1/3MFD}$	$H_{1/3M}$ for fully developed seas (m)
k	Wave number, k=2π/λ
L, L_{OA}	Length overall
L_{BP}	Length between perpendiculars
LCG	Longitudinal centre of gravity
L_{WL}	Length at waterline at rest
M	Subscript to denote the model size
R_{AW}	Mean added resistance
S	Subscript to denote the ship size
T	draught
T_P	modal period of the spectrum
T_P'	non-dimensional modal period, $T_P^{'} = T_P / \sqrt{L/g}$
WS	Wetted surface
∇	Volume of displacement at rest
Δ	Displacement at rest
λ	Wave length
ξ_3	Heave response
ξ_5	Pitch response
ρ	Density of water
Sc	Model to Ship Scale

2. The models of the NTUA extended Systematic Series

The hull forms of the NTUA series have two successive chines running forward of the transom up to 70% of the hull length. Fine highly flared lines form the bow region. Among the five hull forms of the series with L/B ratios equal to 7.00, 6.25, 5.50, 4.75 and 4.00 the one with ratio L/B = 5.50 was the parent hull form of the series. Its lines plan is shown in Fig.1. The angle of entrance is very small for all waterlines tested. The series members with the higher L/B ratios were derived from the parent by keeping the same midship section and altering appropriately the station spacing, while those with the lower L/B ratios, as the one considered herein, were derived from the parent by keeping the profile and modifying the midship section accordingly.

Grigoropoulos and Loukakis (2002) presented the calm water resistance results for the initial series and *Grigoropoulos et al. (2010)* presented systematic results in regular waves, for the first time after 40 years, when *Fridsma (1969)* presented systematic results in regular waves for planing surfaces with constant deadrise angles of 10o, 20o and 30o and parabolic finishing in the bow region. Finally, *Grigoropoulos and Damala (2011)* presented a first set of experimental results in real sea states (random waves) for the parent and the two corner hull forms with L/B = 4.00 and 7.00.

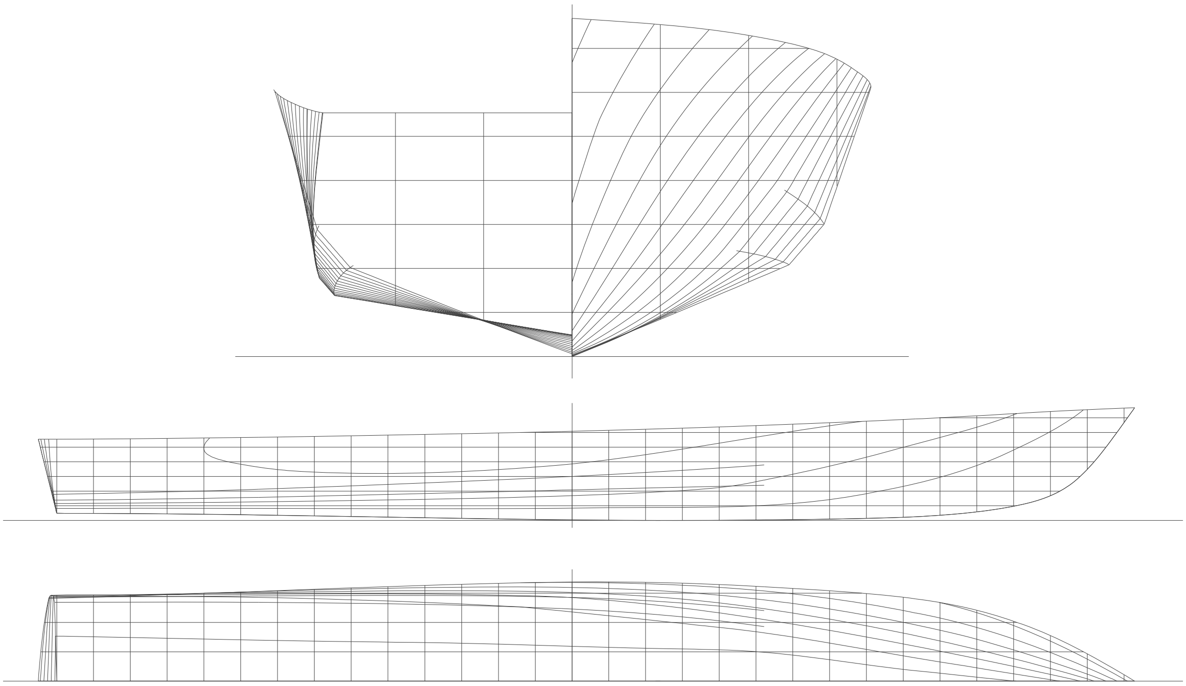

Fig.1: Lines plan of the parent hull form of the NTUA systematic series (the body plan has been scaled up by a factor of three).

In the current project, the NTUA Systematic Series was extended to a lower L/B ratio so that it is suitable also for smaller yachts in the 15 to 30 m length range. The model, denoted as 185/05, with length over breadth ratio L/B=3.25 belongs to the smaller size of the models tested within the NTUA Series. Since the realistic loading conditions for the corresponding full scale ships could be realized on that model (CDL ≥ 3.00), it was not necessary to build a second, larger model. The model was tested in calm water as well in regular and random waves. The characteristics of the model in the tested loading conditions are depicted in Table I. The experimental results are presented graphically in a convenient way.

Table I: Characteristics of the model at the tested loading conditions

C_{DL} = 3.00	**C_{DL} = 3.62**	**C_{DL} = 4.23**	**C_{DL} = 5.00**
2.079 0.842	2.091 0.909	2.101 0.963	2.114 1.024
0.569 27.003	0.569 33.139	0.569 39.216	0.569 47.215
-0.280 0.080	-0.284 0.087	-0.294 0.094	-0.297 0.103

C_{DL} = 5.62	**C_{DL} = 6.23**	**C_{DL} = 7.00**
2.122 1.065	2.129 1.102	2.138 1.146
0.569 53.764	0.569 60.159	0.569 68.386
-0.297 0.110	-0.295 0.117	-0.293 0.125

Notes:

1. Each cell of the table contains the following characteristics of the model:

L_{WL} [m]	WS [cm^2]
B_{WL} [m]	Δ [Kgr]
LCG [m]	T [m]

2. LCG is measured from amidships and is taken positive forwards.

3. Experimental setup

Since the new model was designed as an extension of the NTUA systematic series, the parameters of the tests were selected in line with the tank tests of the other models of the series.

The model was attached to the carriage via a heave rod, pitch bearing, resistance measuring assembly. Thus, it was free to heave and pitch and the respective dynamic responses in waves were recorded. In calm water the dynamic rise of C.G. and the dynamic trim were recorded. For the seakeeping tests, three strap-down accelerometers with a 0-10 g range, recommended for use in the 0.1 to 100 Hz band were fitted along the tested model at the FP, the LCG and the AP, to record the vertical accelerations in head regular and random waves. The total resistance was measured, and the added resistance in waves was derived. No turbulence stimulators were fitted.

The sampling rate was selected to 15 Hz for all tests. High rate sampling at 100 Hz, carried out at both tested speeds in waves did not reveal any indication of sharp bow-down impact accelerations, necessitating the use of special data acquisition and analysis techniques, such a technique proposed by *Zseleczky and McKee (1987)*. The absence of impact accelerations is attributed to the high deadrise angles in the bow region of the model. *Grigoropoulos and Damala (2011)* discuss this behaviour of the models belonging in the NTUA series, as well as the validity of the linearity assumption, which seems to hold to a practically sufficient level. At higher speed non-linearity effect may be enhanced. However, the operation at high speeds in severe sea conditions is of no practical interest, since the ship operators usually slow down the engines or they change course to avoid the encounter of excessive head sea waves.

3.1 Calm water performance

Model 185/05 was tested in smooth water at seven level keel loading conditions with C_{DL}=3.00, 3.62, 4.23, 5.00, 5.62, 6.23 and 7.00. For each condition the model was tested at 17 velocities in the 1-5 m/sec range using a 0.25 m/sec step.

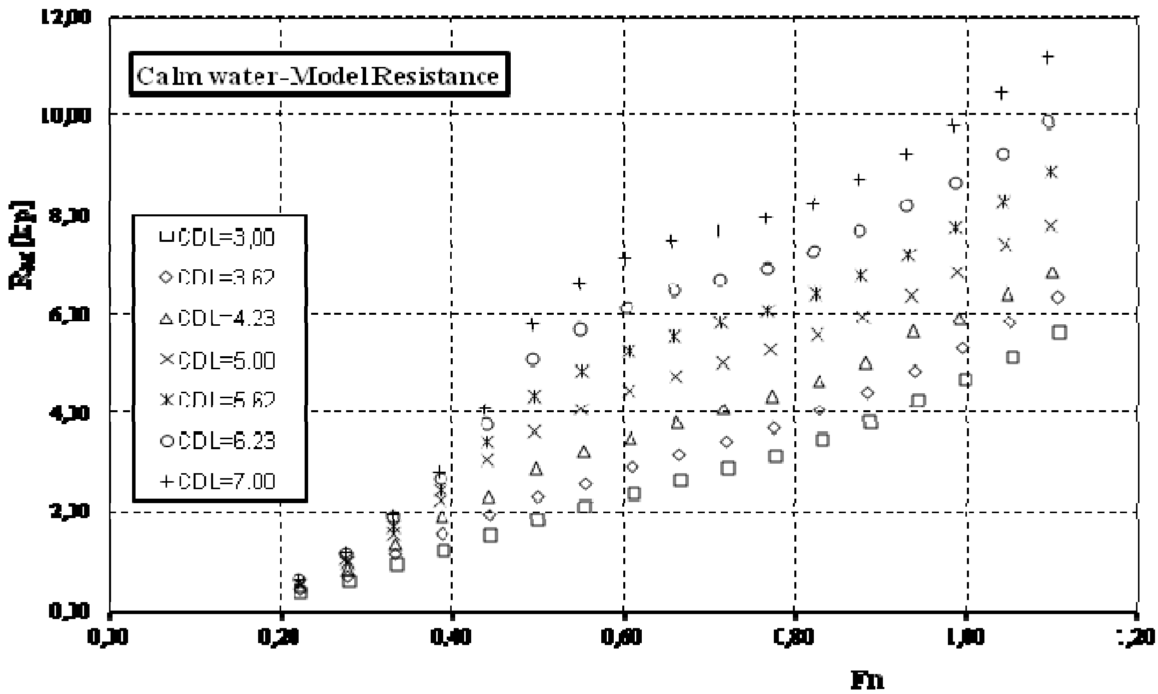

Fig.2: Model resistance R_M vs. Fn, at the tested loading conditions.

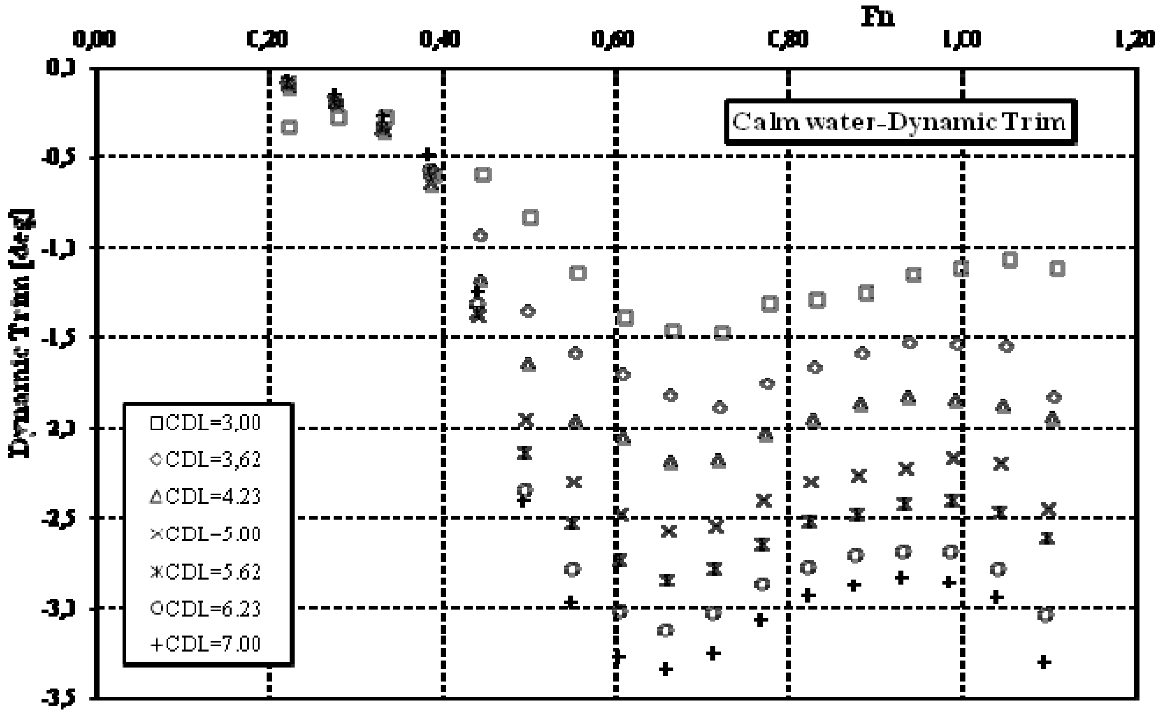

Fig.3: Dynamic trim [deg] vs. Fn at the tested loading conditions.

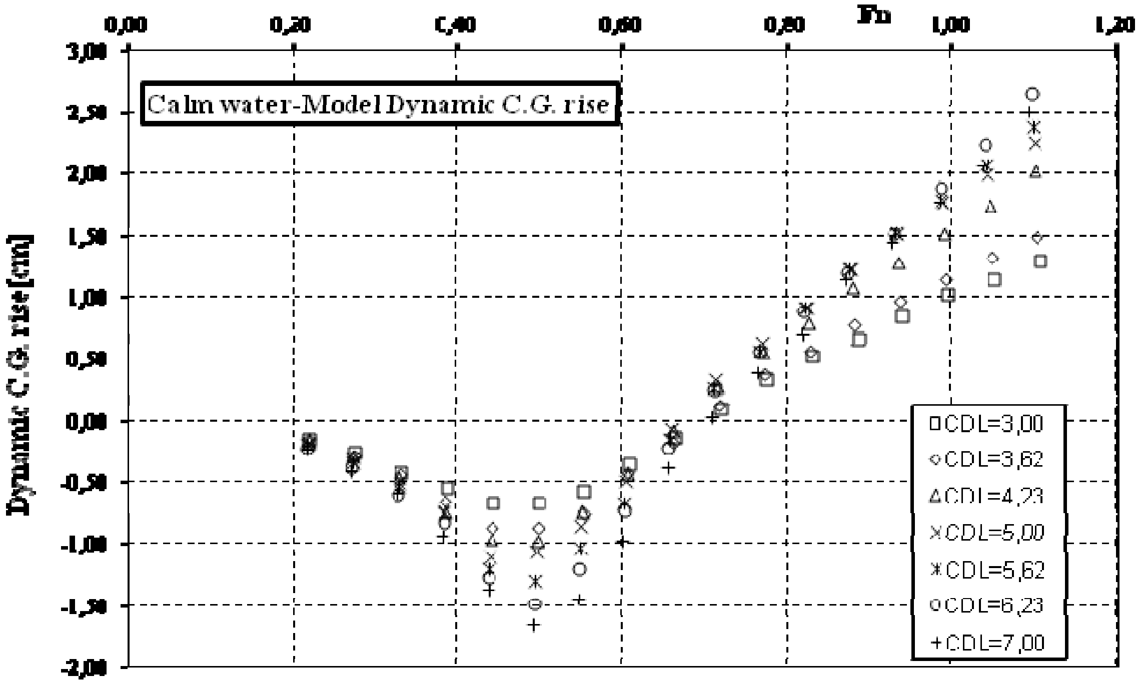

Fig.4: Dynamic C.G. Rise [cm] vs. Fn at the tested loading conditions.

The recorded quantities were resistance, dynamic trim and dynamic C.G. rise. The experimental results are plotted versus Fn along with the residual resistance coefficient C_R to be used for the extrapolation to any ship size by Froude method. The range of C_{DL} values and Fn tested were selected having in mind that this hull form is suitable for boats with length between 15 m and 30 m. Thus, higher C_{DL} values than in the original series were selected, starting from the central loading condition of the parent hull with C_{DL} = 3.00. The upper speed in the tests is set by the carriage specifications. The particulars of the tested loading conditions are depicted in Table I.

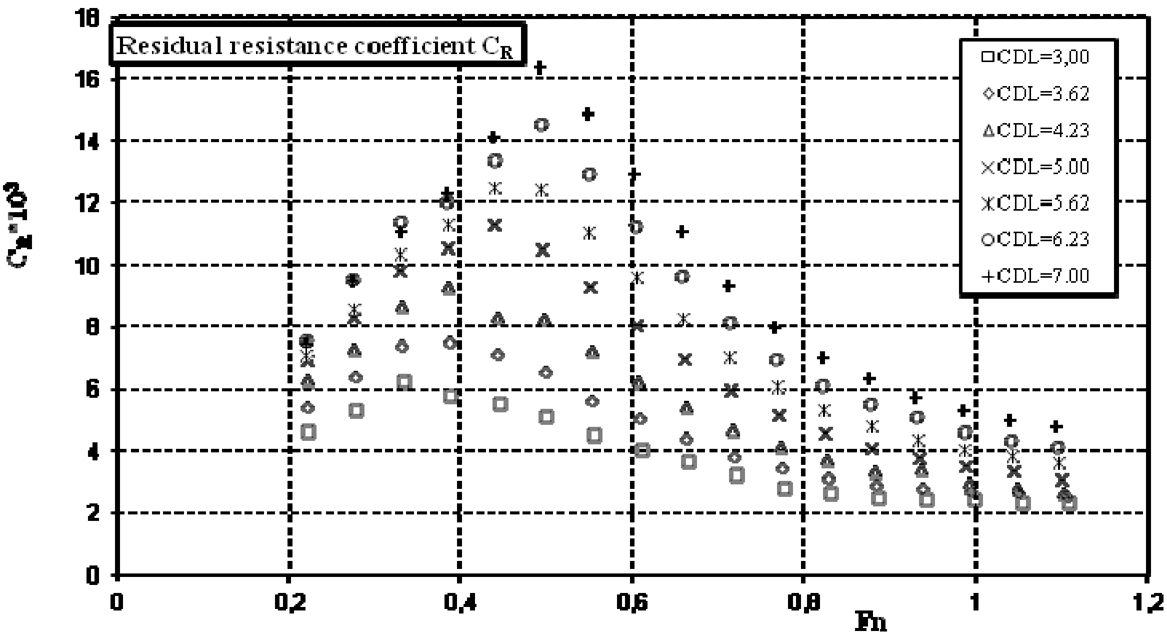

Fig.5: Residual resistance coefficient C_R at the tested loading conditions.

3.2 Dynamic responses in regular waves

Tests in regular waves provide an overview of the dynamic performance of the hull form in the full band of frequencies of the encountered monochromatic waves, as well as the frequency or wave length to which the hull form is more sensitive exhibiting maximum responses. Among the loading conditions evaluated in calm water, the two more realistic ones were selected for the tests in waves. Thus, the tests in regular waves encompass the level-keel displacements for C_{DL}=5.00 and 7.00, and two speeds corresponding to Fn = 0.68 and 1.02. Waves with amplitudes in the 3-5 cm range were used in these tests. At the lower speed (Fn = 0.68) the recorded time per run was 15 sec, while at the higher one it was only 7 sec. The sampling frequency was 15 Hz.

The derived experimental results encompass the non-dimensional Response Amplitude Operator (RAO) curves for heave, pitch, acceleration at three points along the hull (stern, LCG, and bow) with indices 1, 2 and 3, respectively, as well as added resistance in waves. The definitions recommended by the Seakeeping Committee of the *16th ITTC (1981*) to provide non-dimensional (scale-insensitive) quantities, are used in the plots (Figs. 6 to 11):

$$\mathrm{RAO}_{\xi_3} = \xi_3/\mathrm{A} \tag{1}$$

$$\mathrm{RAO}_{\xi_5} = \xi_5/(\mathrm{kA}) \tag{2}$$

$$\mathrm{RAO}_{a_i} = a_i \mathrm{L}_{\mathrm{WL}}/(\mathrm{gA}) \tag{3}$$

On the other hand, mean added resistance (AR), estimated by the difference of the mean total resistance in waves and the calm water resistance at the same speed, is proportional to the square of the wave amplitude. On the basis of this remark, following the recommendation of *17th ITTC (1984)*, the RAO of added resistance is expressed by the following non-dimensional quantity:

$$\mathrm{RAO}_{\mathrm{AR}} = \mathrm{R}_{\mathrm{AW}}\mathrm{L}_{\mathrm{WL}} \Big/ \rho g \mathrm{B}_{\mathrm{WL}}{}^2 \mathrm{A}^2 \tag{4}$$

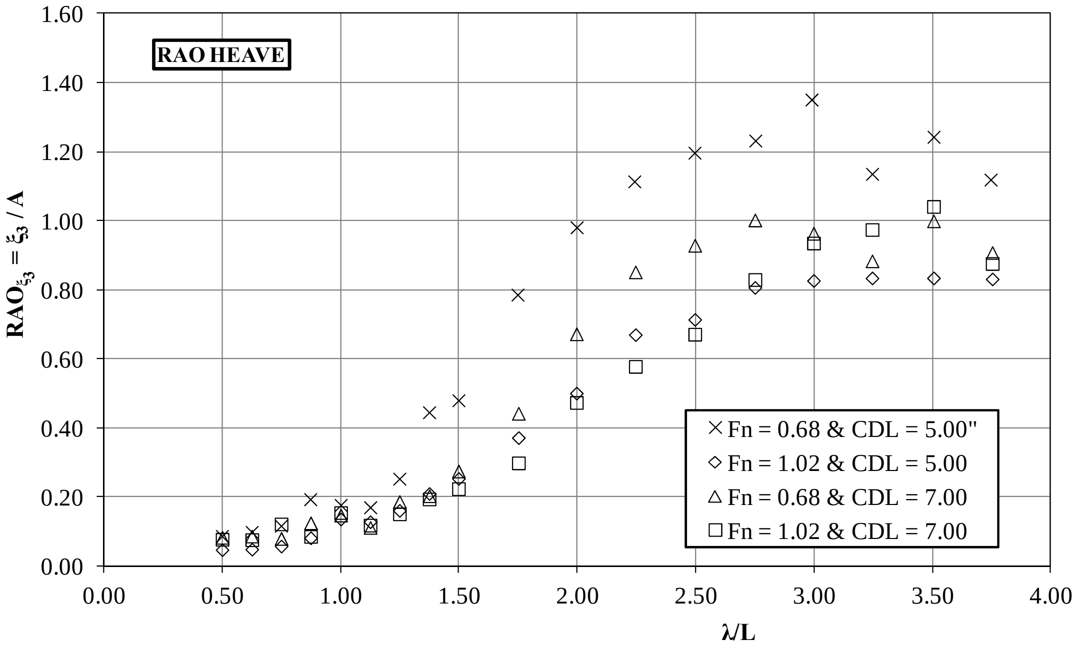

Fig.6: Heave RAO curves vs. for C_{DL}=5.00 and 7.00 at Fn=0.68 & 1.02.

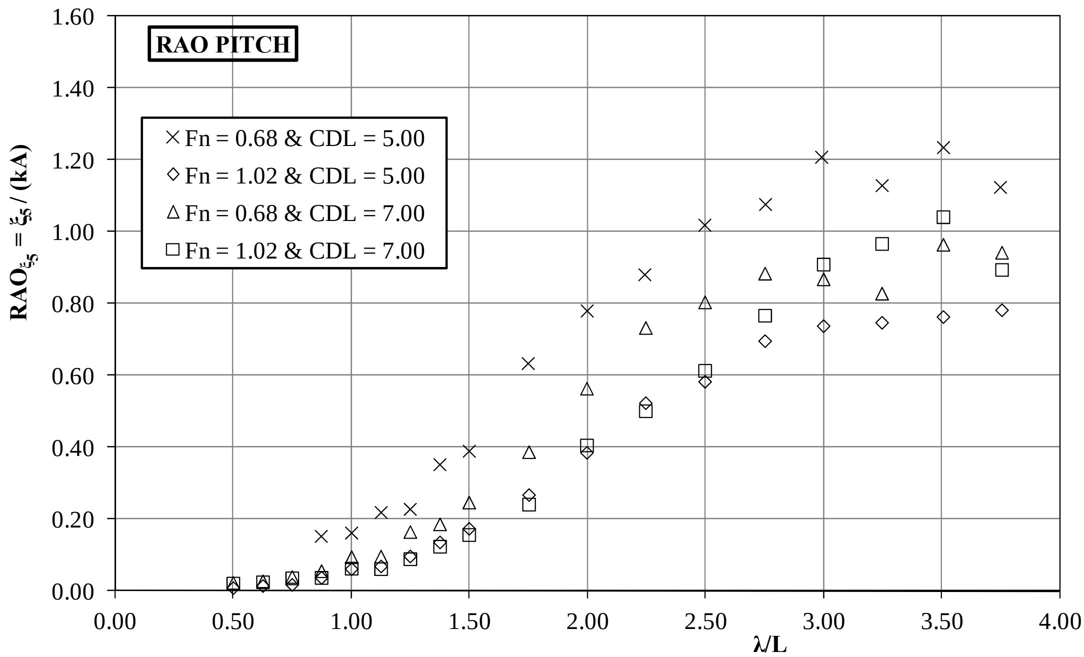

Fig.7: RAO Pitch curves for C_{DL}=5.00 and 7.00, at Fn=0.68 and 1.02.

In Tables II and III the maximum values of the RAO curves for pitch and vertical acceleration at the bow for both displacements and speeds tested are provided. In the same tables the respective λ/L values are depicted.

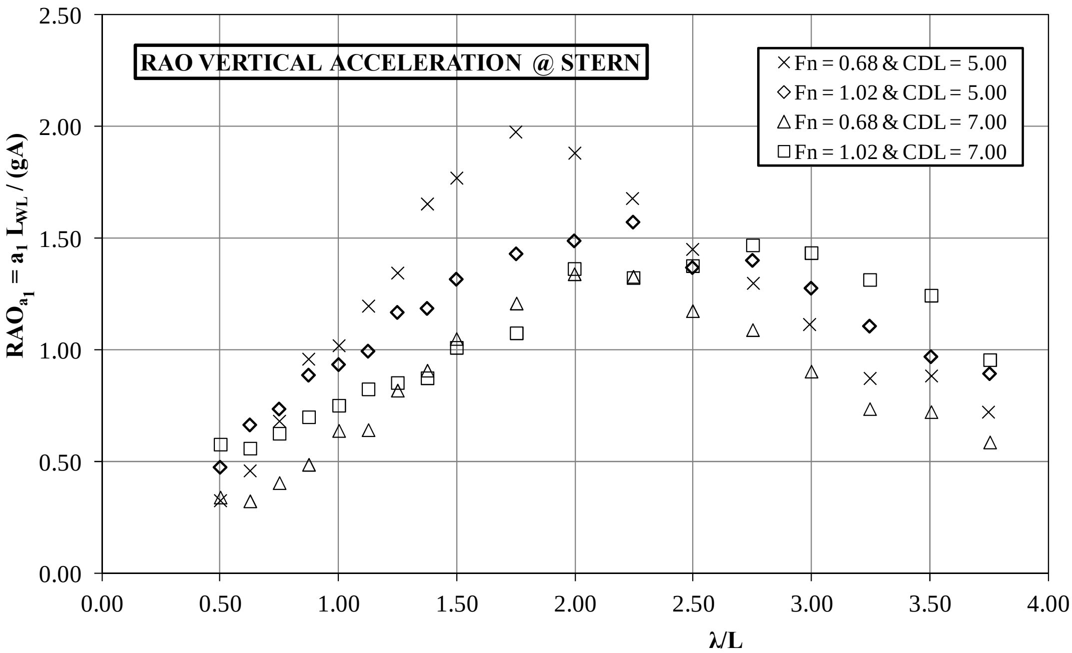

Fig.8: RAO curves of vert. accelerations @ stern for C_{DL}=5.00 and 7.00, at Fn=0.68 and 1.02.

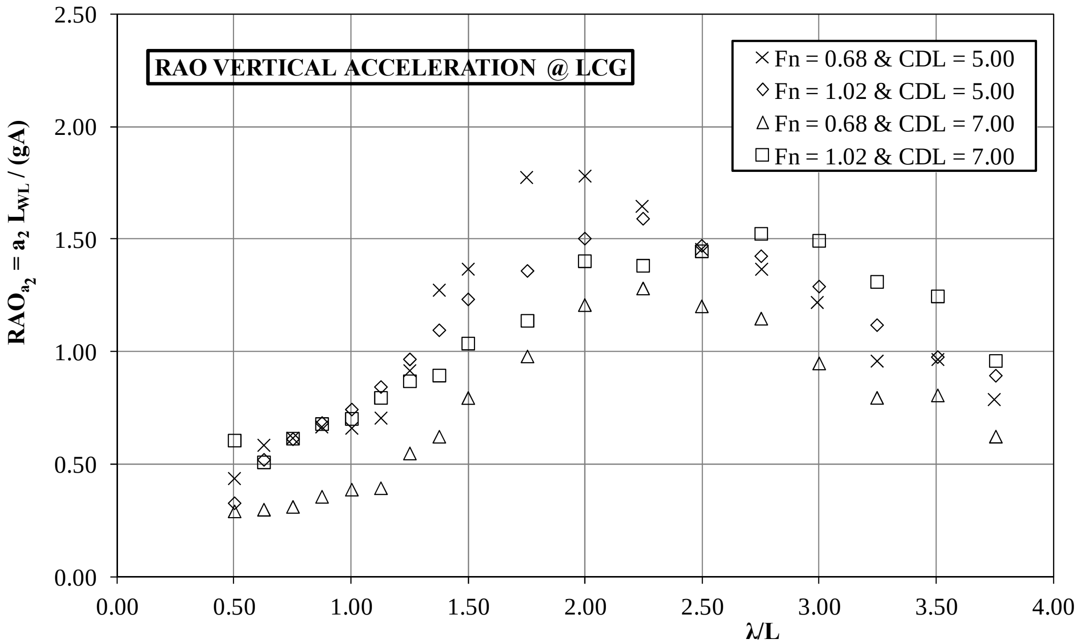

Fig. 9: RAO curve of vertical acceleration @ LCG for C_{DL}=5.00 and 7.00, at Fn=0.68 and 1.02.

Table II: Maximum values of RAO Pitch at each loading condition

C_{DL}	Fn	λ/L	MAX. RAO PITCH
5.00	0.68	3.50	1.23
5.00	1.02	3.75	0.78
7.00	0.68	3.50	0.96
7.00	1.02	3.50	1.04

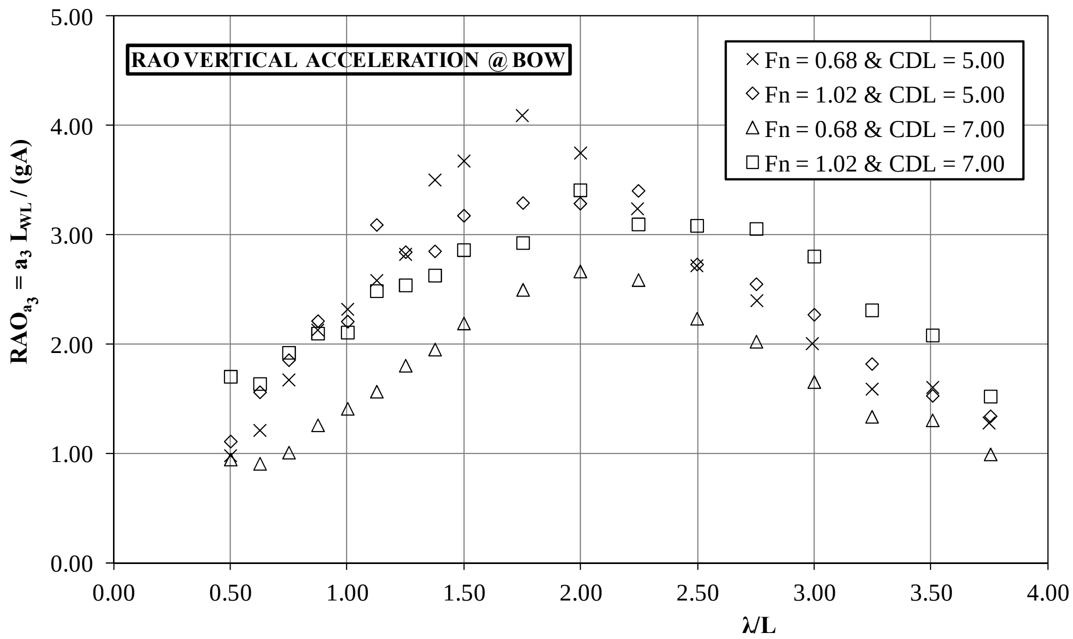

Fig.10: RAO curves of vertical acceleration @ bow for C_{DL}=5.00 and 7.00, at Fn=0.68 and 1.02.

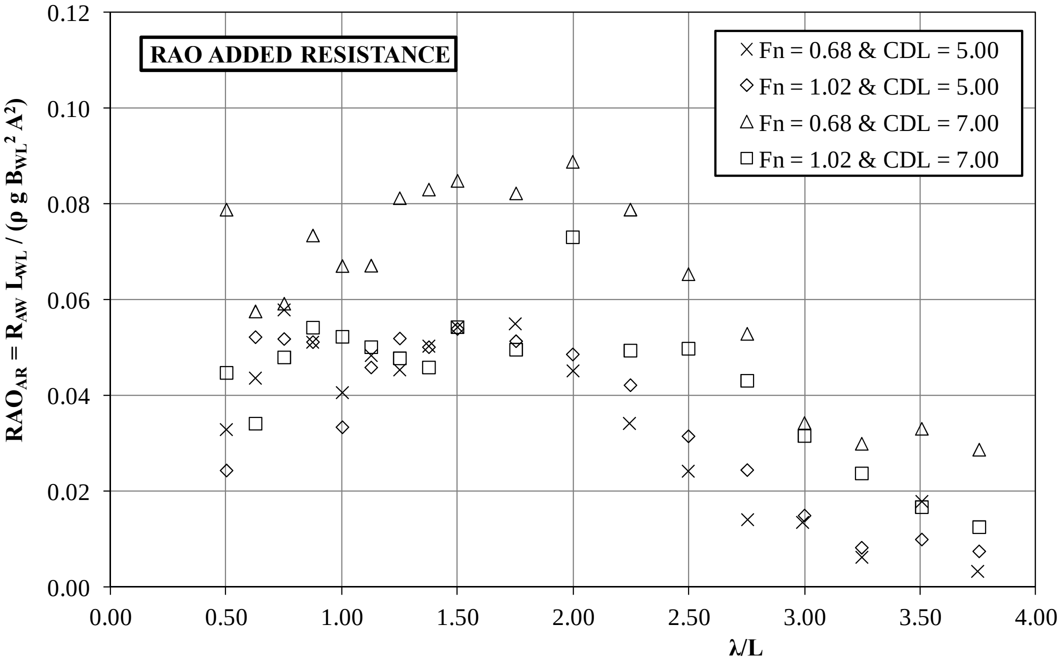

Fig.11: RAO curves of added resistance at C_{DL}=5.00 and 7.00, at Fn=0.68 and 1.02.

Table III: Maximum values of RAO Vertical acceleration @ bow (a_3) at each loading condition

C_{DL}	Fn	λ/L	MAX. RAO VERT. ACCEL. @ BOW
5.00	0.68	1.75	4.10
5.00	1.02	2.25	3.41
7.00	0.68	2.00	2.67
7.00	1.02	2.00	3.41

3.3 Performance in Sea States

Although RAO curves are very useful, as it was concluded by *Grigoropoulos & Loukakis (1995, 1998)*, carefully conducted random wave experiments are a much better yardstick for the comparative study of seakeeping behavior of high-speed semi-planing and planing hulls than regular waves.

In this section, the experimental results for the performance of the considered hull form in random waves are presented. The results encompass non-dimensional Root Mean Square (RMS) values for the same dynamic responses considered in regular waves. The followingratios have been selected to provide scale-insensitive quantities in line with the respective results presented by *Grigoropoulos and Damala (2011)* for the original NTUA series (pertinent recommendation of any ITTC Seakeeping Committees could not be found):

$$RMS'_{\xi_3} = RMS_{\xi_3} / H_{1/3} \tag{5}$$

$$RMS'_{\xi_5} = \frac{RMS_{\xi_5} * 10^2 L_{WL}}{H_{1/3}} \quad \text{[deg.]} \tag{6}$$

$$RMS'_{ai} = \frac{RMS_{a_i} \; L_{WL}}{gH_{1/3}} \tag{7}$$

On the other hand, added resistance is the difference between the mean total resistance of the model in a sea condition and the calm water resistance, at the same speed. Contrary to the other responses, the added resistance is proportional to the square of the significant wave height. On the basis of this remark, and taking into account the recommendation of *17th ITTC (1984)* for the respective RAO, the added resistance in random waves is expressed by the following non-dimensional quantity:

$$AR' = \frac{R_{AW} \; L_{WL}}{\rho g B_{WL}^2 H_{1/3}^2} \tag{8}$$

Among the quantities provided by relations (1) to (4) only RMS'_{ξ_5} for pitch response is dimensional (in degrees), while the rest ones are non-dimensional.

The Bretschneider spectral model with non-dimensional modal periods $T'_P = T_P / \sqrt{L/g}$ = 2.0 to 4.0 with step equal to 0.5 was used to model the sea states. The significant wave heights $H_{1/3}$ were selected in the 7 – 12 cm range to represent moderate waves. However, the results presented refer to $H_{1/3}$ = 1 m.

In Table IV the tested conditions are listed. On the tables the modal periods at the model scale, as well as extrapolated to an assumed full scale of 10:1, to correspond to a 23-m ship size are provided. The tests have been carried out at selected significant wave heights. For comparison the respective significant wave heights corresponding to fully developed seas (Pierson - Moskowitz spectrum) are also provided.

The tests were conducted by repetitive runs of the carriage until a total measuring period of six minutes at model scale was accumulated. This time interval corresponds to about 20 minutes sampling period at the assumed full scale. This duration is slightly shorter than the half to one hour, recommended by ITTC for sufficient statistical accuracy, when stationary stochastic processes are analyzed. Sufficient time (5-15 min) was allowed between successive runs for the water in the towing tank to calm, while its energy was continually checked. The recorded signals were passed through a low pass filter and they were carefully inspected for any spurious noise content prior to their analysis.

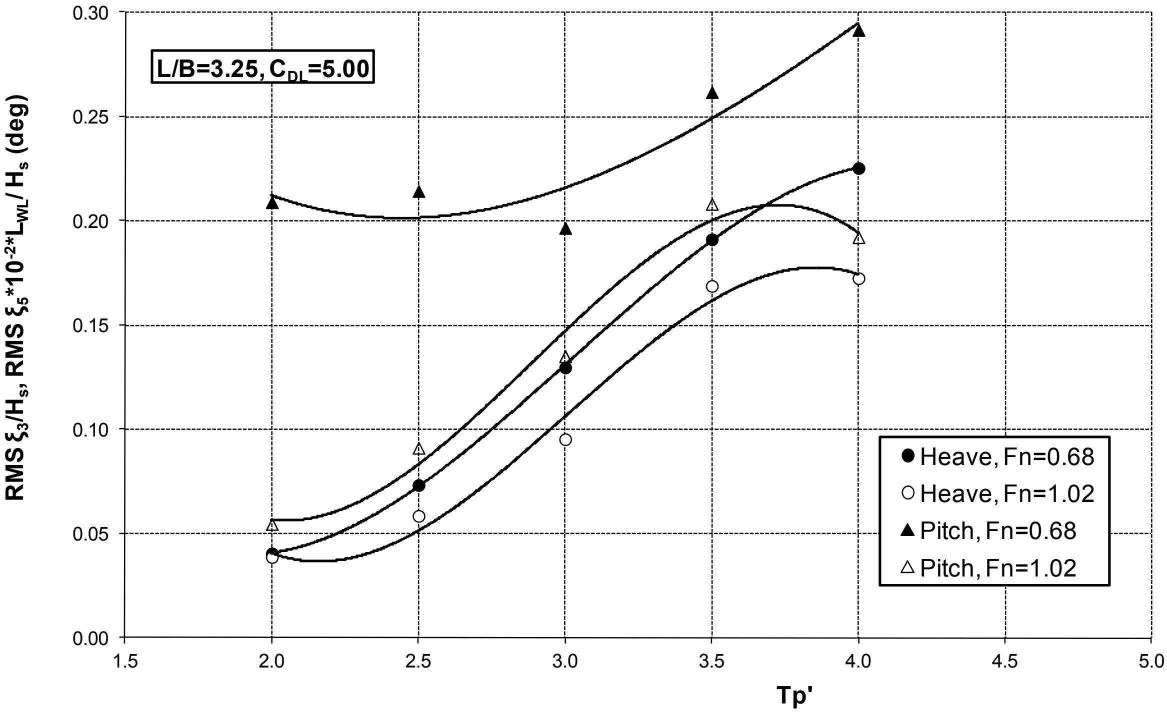

Fig.12: RMS heave and pitch responses for C_{DL} = 5.00, at Fn = 0.68 and 1.02.

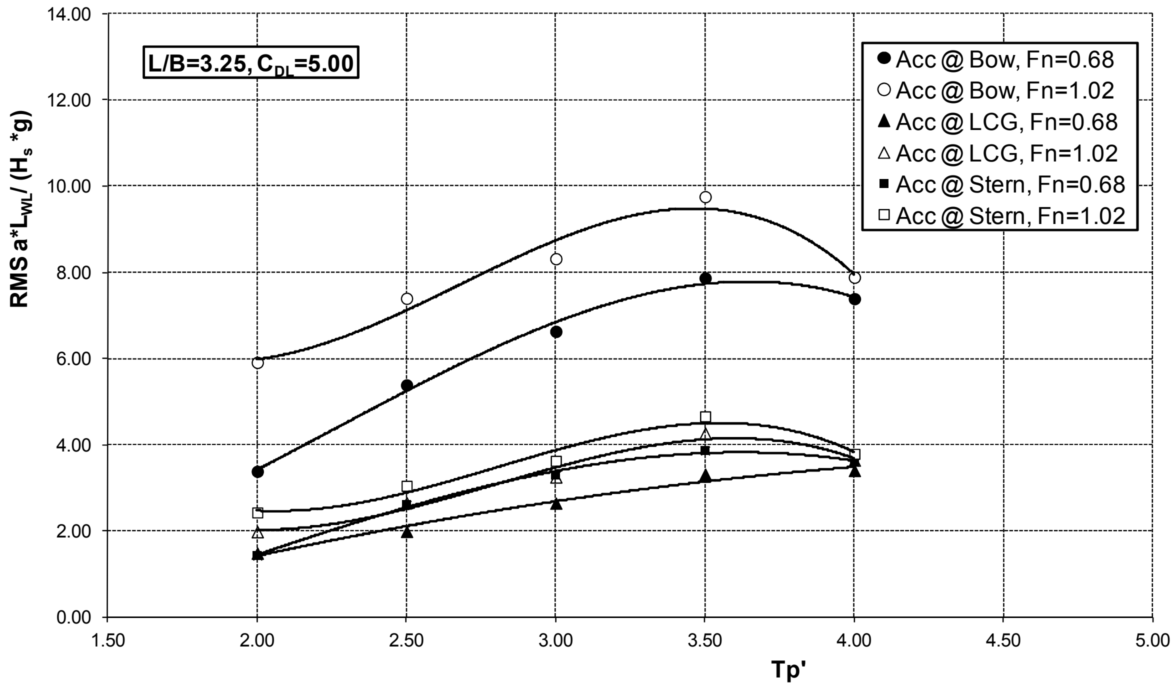

Fig.13: RMS values of the vertical accelerations at the bow, the LCG and the stern for C_{DL} = 5.00, at Fn = 0.68 and 1.02.

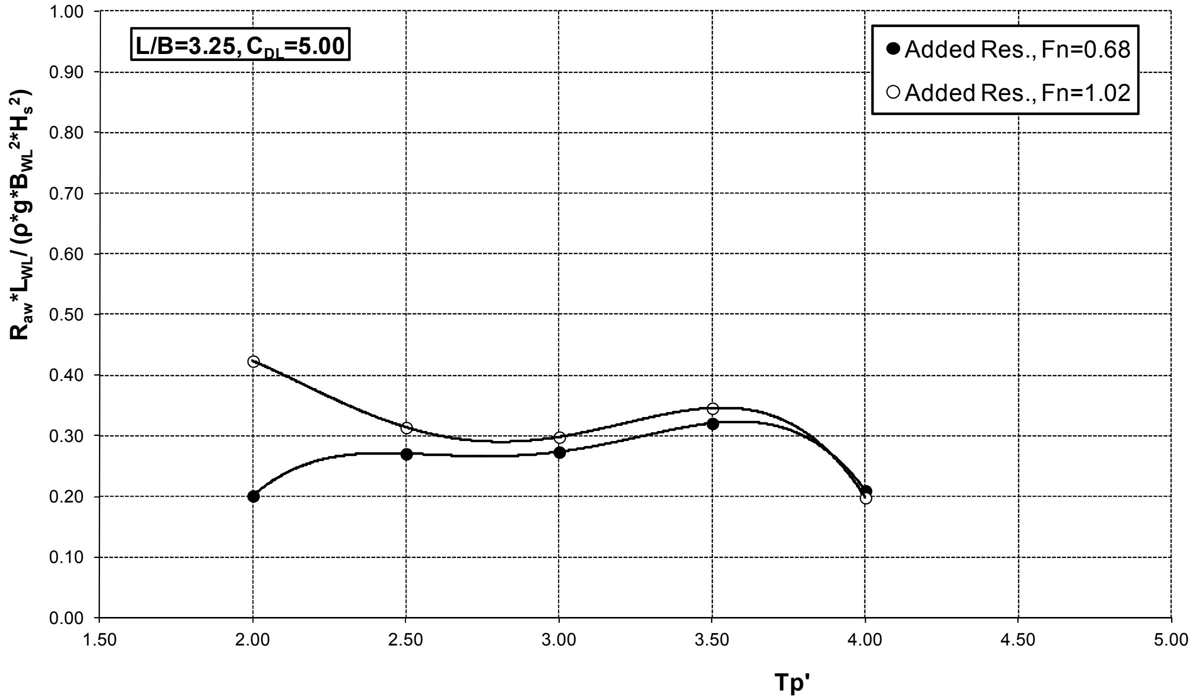

Fig.14: Added resistance for C_{DL} = 5.00, at Fn = 0.68 and 1.02.

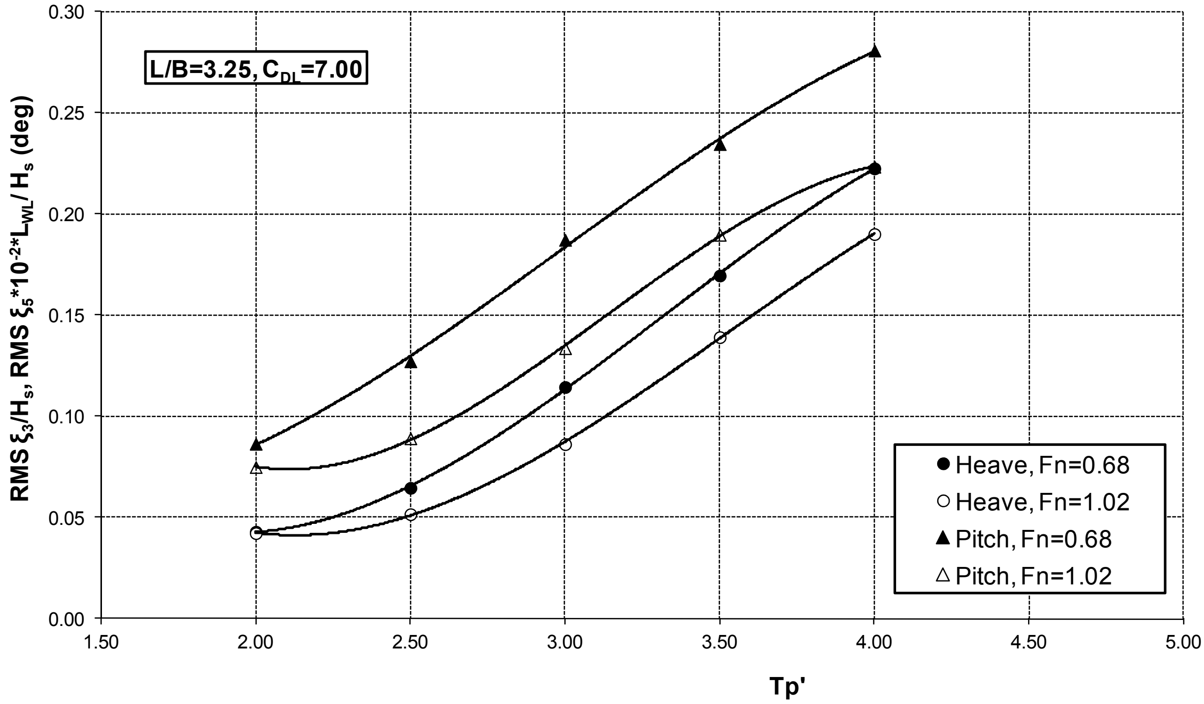

Fig.15: RMS heave and pitch responses for C_{DL} = 7.00, at Fn = 0.68 and 1.02.

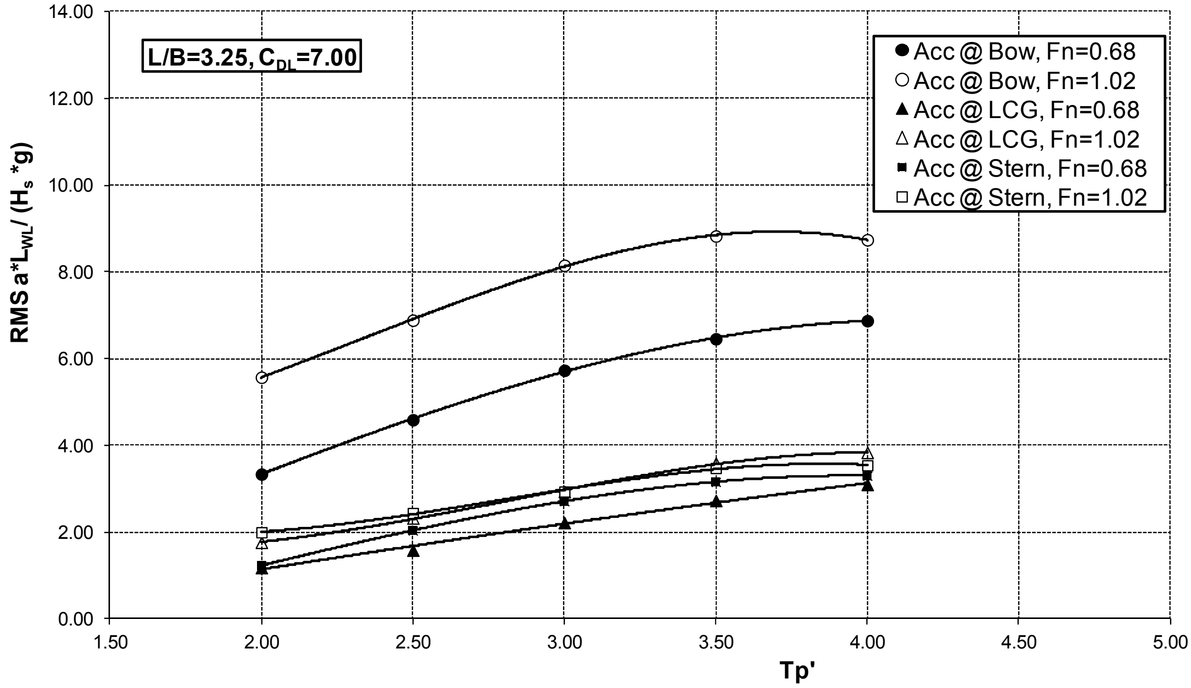

Fig.16: RMS values of the vertical accelerations at the bow, the LCG and the stern for C_{DL} = 7.00, at Fn = 0.68 and 1.02.

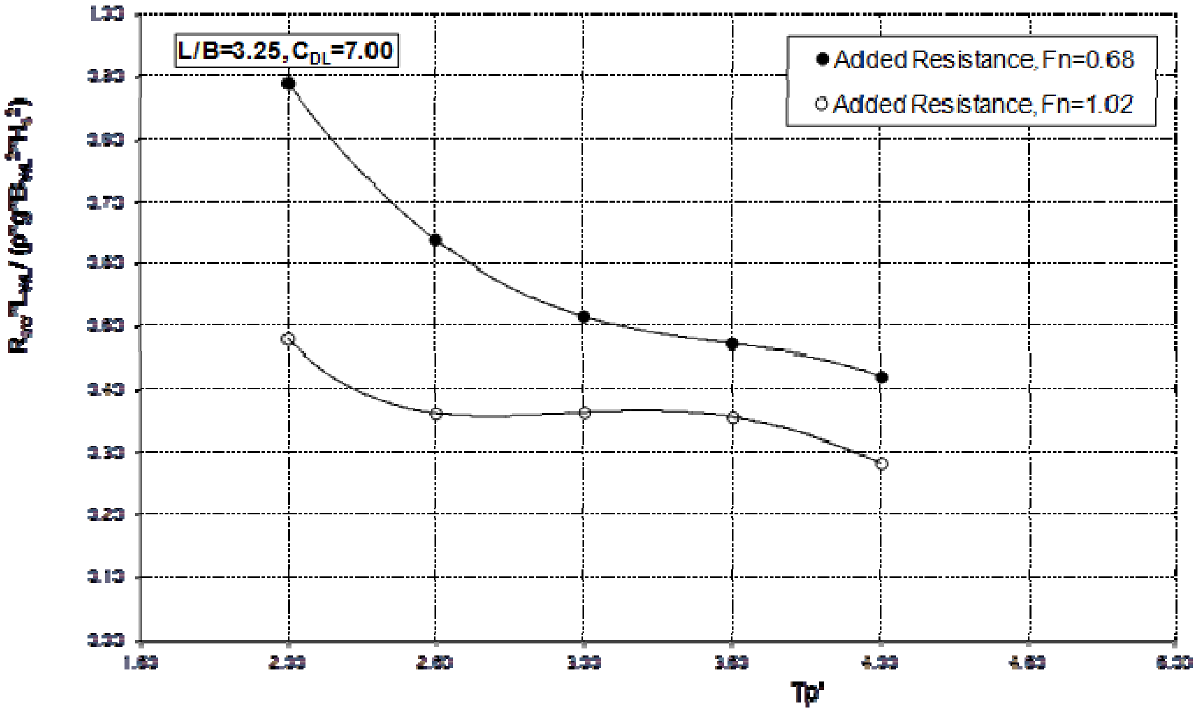

Fig.17: Added resistance for C_{DL} = 7.00, at Fn = 0.68 and 1.02.

4. Discussion and conclusions

In this paper the performance of a hull form with L/B = 3.25 extending the NTUA series of double-chine wide-transom hull forms is experimentally investigated. In Figs. 2 to 5 the calm water performance is presented. In Figs. 6 to 11 the RAO curves of the dynamic responses, based on tests in regular head waves are plotted. Finally, in Figs. 12 to 17 the respective seakeeping responses in random head waves (sea states) are presented.

Following the experimental results in calm water and extrapolating them to a 23-m yacht, Gerogiannaki (2011) demonstrated that the yacht based on the NTUA series depicts a very competitive performance compared to similar designs available in the market.

On the basis of the tests in regular waves, the variation of RAOs of the dynamic responses along the frequency band is quite smooth. This holds true even in the case of the mean added resistance in waves, which, being proportional to the square of the incident significant wave amplitude, is more sensitive to that. Furthermore, the wave lengths where the hull form exhibits maximum pitch and vertical acceleration at the bow (a_3) were estimated.

Furthermore, the curves derived by best-fitting of the irregular wave results are quite smooth and consistent in shape between the basic responses (heave, pitch) and the derived ones (vertical accelerations, added resistance). Some minor apparent discrepancies, which affect also the final shape of the best-fit curves, may be cross-checked through additional testing in intermediate T_P' values in the future. Some additional linearity tests, to further document the experimental results are also in the plan.

It should be noted here, that following Table IV, for the lower periods (respective T_P' = 2.0 to 3.0) the selected significant wave heights for the tests were higher than the respective ones corresponding to fully developed seas (Pierson-Moskowitz spectral model). This was decided because the latter were too low to receive reliable experimental results (very small waves with decreasing energy content along the towing tank). However, this correlation was reversed at the higher periods.

On the basis of the experimental results, the effect of the displacement (in terms of C_{DL} value) and speed (in terms of Fn) on the calm and rough water performance is quantified. It should be noted that the lower speed (Fn = 0.68) refers to semi-displacement mode of operation, while the higher one (Fn = 1.02) corresponds to the planing regime.

Finally, the dynamic performance of the hull form in calm water and in waves seem to be very satisfactory compared to other competitive, commercially available hull forms, that operate in the same Fn range *(Gerogiannaki, 2011)*. Thus, the evaluated hull form offers an attractive design source for vessels 15-30 m long, operating at the pre-planing and planing regime. The effect of speed is quite significant in the case of seakeeping qualities increasing the dynamic responses. On the contrary, by increasing the displacement the dynamic responses are, in general, reduced.

5. Acknowledgements

The data presented in this paper were derived during the diploma thesis of the second of the authors under the supervision of the first one. Furthermore, the technical personnel of the Towing Tank, Messrs Dionisis Synetos, Fotis Kasapis & Giannis Trachanas are responsible for the good quality of the measurements. The authors are heavily indebted to them.

References

FRIDSMA, G. (1969), *A systematic study of the rough-water performance of planing boats*, Davidson Lab. Rept. 1275, Stevens Inst. of Technology, November.

GEROGIANNAKI, A.A. (2011), *Model tests for the hydrodynamic behavior of a semi-planing hull form in calm water and in regular waves*, SNAME Annual Meeting, November 16-18, Houston, Texas, USA.

GRIGOROPOULOS, G.J.; LOUKAKIS, T.A. (1995), *Seakeeping performance assessment of planing hulls*, Intl. Conf. ODRA'95, Wessex Inst. of Technology, Szczecin, Poland, September.

GRIGOROPOULOS, G.J.; LOUKAKIS, T.A. (1998), *Seakeeping characteristics of a systematic series of fast monohulls*, Intl. Conf. on Ship Motions and Manoeuvrability SMM'98, London, February.

GRIGOROPOULOS, G.J.; DAMALA, D.P.; LOUKAKIS, T.A. (2010), *Dynamic Performance of the NTUA Double-Chine Series Hull Forms in Regular Waves*, The 2nd Chesapeake Power Boat Symposium, Annapolis, Maryland, March.

GRIGOROPOULOS, G.J.; LOUKAKIS, T.A. (2002), *Resistance and seakeeping characteristics of a systematic series in the pre-planing condition (Part I)*, SNAME Transactions, Vol. 110.

GRIGOROPOULOS, G.J.; DAMALA, D.P. (2011), *Dynamic Performance of the NTUA Double-chine Series Hull Forms in Random Waves*, 11th Intl. Conf. on Fast Sea Transportation FAST'2011, Honolulu, Hawaii, September.

16th ITTC SEAKEEPING COMMITTEE (1981), *Final Report and Recommendations to the 16th ITTC (International Towing Tank Conference),* Leningrad, USSR, pp. 185-247.

21st ITTC, HIGH-SPEED MARINE VEHICLE COMMITTEE (1996), *Final Report and Recommendations to the 21st ITTC (International Towing Tank Conference),* Trondheim, Norway, pp. 515-560.

SAVITSKY, D.; ROPER, J.K.; BENEN, L. (1972). *Hydrodynamic Development of a High Speed Planing Hull for Rough Water*, 9th Symposium on Naval Hydrodynamics ONR, Paris, p. 419.

ZSELECZKY, J. and McKee, G. (1987). *Analysis methods for evaluating motions and accelerations of planing boats in waves*, Proceedings of the 22nd A.T.T.C.

A SWATH Technology Trajectory

Karsten Fach, Abeking & Rasmussen, Lemwerder/Germany, kfach@abeking.com

Abstract

The idea of the SWATH (Small Waterplane Area Twin Hull) is older than 100 years. During the 1960s and 1970s, semisubmersibles were used in offshore oil exploration and naval architects reinvented the SWATH idea. SWATH research and military vessels were built in different countries. The Hawaiian pilots introduced their pilot SWATH. In Germany, major SWATH activities started in the early 1990s. This paper will deliver insight into the SWATH technology, today's use, and R&D projects with special focus on German developments.

1. Introduction

SWATH stands for Small Waterplane Area Twin Hull, Fig.1, a unconventional hull concept for smooth service in rough seas. The term “semi-submerged catamaran” (SSC) has been more popular in Japan, while SWATH as an acronym originated in the USA. The buoyancy of a SWATH ship is provided by its submerged torpedo-like bodies, which are connected by single or twin struts to the upper platform. The cross-section at sea surface level is minimized and thus only a minimum of the ship is exposed to the lifting forces of the waves. The idea of SWATH was taken from the principle of semi-submersible offshore rigs, which are designed to provide a working platform with minimized motions in open sea.

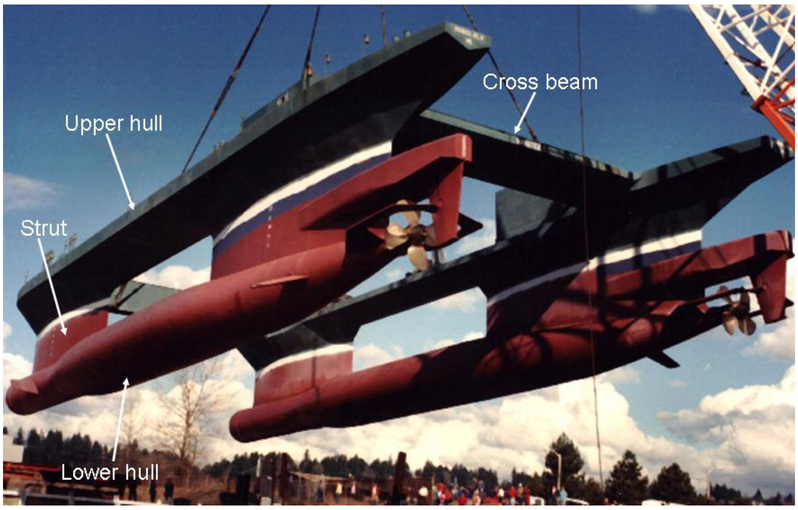

Fig.1: SWATH principle, source: A&R

SWATH advantages are seakeeping superior to similar-sized conventional and unconventional craft and a large deck area for helicopter operation. Disadvantages are its higher resistance and installed power requirements due to greater wetted surface, its sensitivity to displacement changes and to trim, large draft, increased acquisition and operating costs compared to monohulls.

2. Historical perspective on SWATH

The SWATH technology has developed for more than 100 years. Standard references on SWATH technology with survey character include *Gore (1985), Lang and Slogett (1985), Papanikolaou (1996), Andrews (2003), Bertram and Seif (2004)*. The following brief history is based on various websites, including Wikipedia and www.stabilityyachts.com/SWATH.

1880 A patent awarded to C.G. Lundborg for the single-hulled semi-submerged ship, Fig.2.

1938 Frederick G. Creed, a Canadian, presents his idea for a SWATH aircraft carrier to the British Admiralty, Fig. 4. Several years later Creed is permitted to show it to the U.S. Navy, but they do not pursue the concept. 8 years later, Creed is awarded a British patent.

1959 U.S. Navy activity in moderately high speed SWATH begins with H. Boericke proposing a monohull with largely submerged buoyancy part, for which he was awarded a patent in 1962.

1967 Dr. Reuven Leopold of Litton Industries presents to the U.S. Navy his moderately high-speed TRISEC concept, patented in June 1969, Fig. 3.

1968 The 40 m long, slow SWATH vessel "Duplus", Fig. 5, 1200 t displacement, is launched by the Boele Shipyard in the Netherlands.

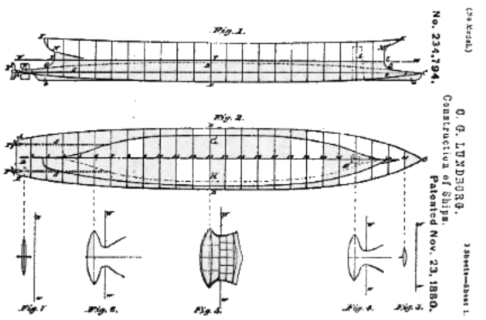

Fig.2: Lundborg SWATH (1880)

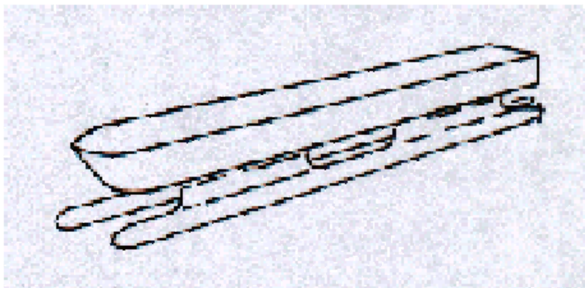

Fig.3: TRISEC concept (1967)

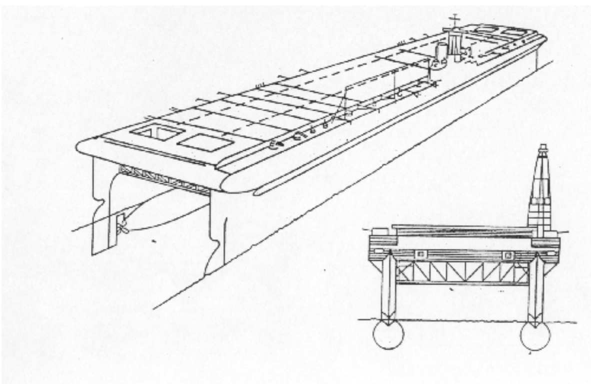

Fig.4: Creed's aircraft carrier design (1938)

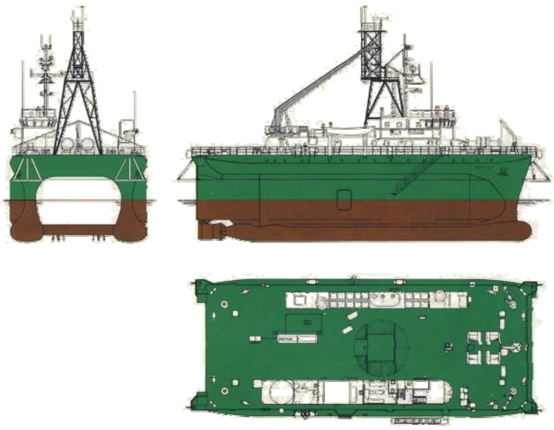

Fig.5: "Duplus" (1968)

1968 Naval Underseas Center (NUC) in San Diego develops a “high-speed ship with semi-submerged hull” concept, which is patented in 1971. The design features movable horizontal fins located aft of the vessel’s centre of gravity. The fins serve to stabilize the vessel’s trim and dampen pitch motions at higher speeds.

1970 Mitsui begins basic research in Japan on the "semi-submerged catamaran" (SSC).

1973 SWATH workboat “Kaimalino” (190 t) is launched and operated by NUC, Fig. 5.

1973 The acronym SWATH is coined by the US Navy, replacing gradually other terms such as semi-submerged catamaran.

1979 Mitsui completes the “Seagull”, the world’s first commercial SWATH ferry (26.5 kn, 446 passengers).

1992 Finnyards delivers the “Radisson Diamond”, Fig. 7, the world’s first SWATH cruise vessel.

1993 Stealth SWATH “Sea Shadow”, Fig. 8, is disclosed publicly.

1999 First SWATH pilot tender delivered by Abeking & Rasmussen, Fig. 9.

2003 SWATH research vessel PLANET delivered to German Navy, Fig. 10, *Bormann (2003).*

2008 Abeking & Rasmussen delivers 40 m SWATH yacht “Silver Cloud”, Fig. 11.

2008 Over 100 SWATH operate worldwide.

2011 SWATH offshore patrol vessel (OPV) for Latvian Navy.

Fig.6: “Kaimalino” (1973)

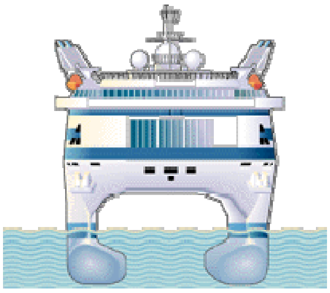

Fig.7: “Radisson Diamond” (1992)

Fig.8: “Sea Shadow” (1993)

Fig.9: A&R pilot SWATH (1999 - 2000)

Fig.10: “Planet” of German Navy (2003)

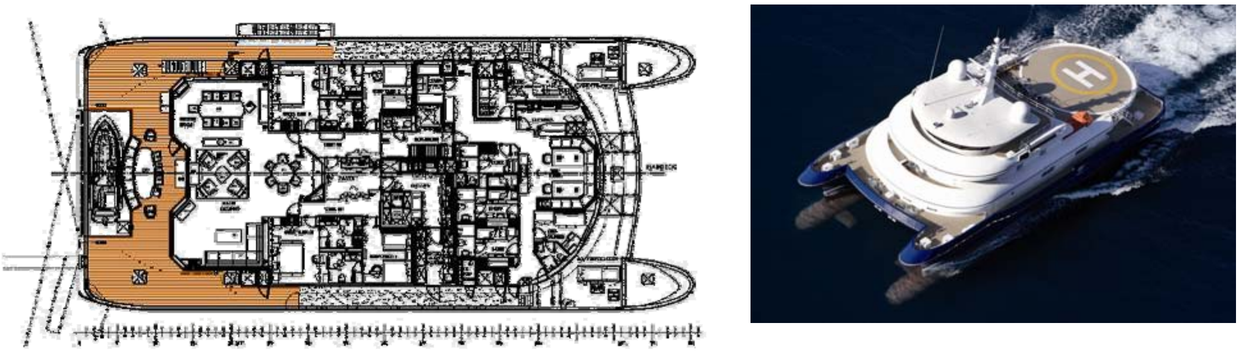

Fig.11: “Silver Cloud” luxury yacht - deck layout plan (left) and in service (right)

3. Present proliferation of SWATH

3.1. Pilot vessels

Pilot vessels should feature low motion amplitudes in waves, both for transit speed and zero speed (while the pilots board the vessel to be piloted into port). This key requirement is ideally met by a SWATH vessel. The first SWATH vessel series to be built were the pilot boats for the German pilots, designed and built by Abeking & Rasmussen, Fig.12, *Spethmann and Leue (1997)*. Table I gives the motions and accelerations (at 20 kn) in sea waves for pilot boat designs, comparing a conventional monohull and a SWATH.

Table I: Motions of pilot boats in 3.5 m significant wave height

	SWATH	monohull
heave	< 1 m	~3.5 m
roll	< 5°	< 20°
vert. acc.	0.1g	0.4g

The success of the German pilot vessels led to steady proliferation of SWATH pilot vessels, mainly along the North Sea coast. The original design developed into a SWATH family, with three sizes (25 m, 40 m, and 60 m). The modular design allowed cost effective tailored solutions and construction in parallel, distributed over several shipyards, Fig.13.

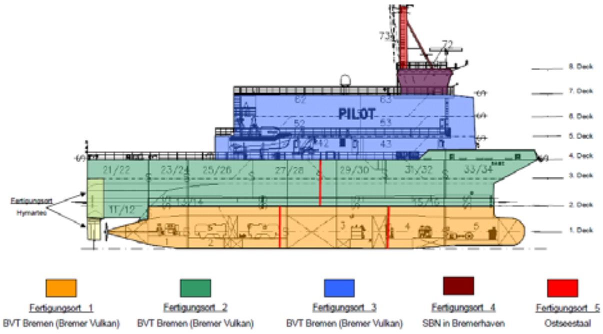

Fig.12: SWATH pilot boat built in series

Fig.13: Modular concept of SWATH family

3.2. Offshore wind farm service vessels

In the past, offshore wind farms were built near the coast. Future wind farms are envisioned for considerable deeper water and further away from the coast. Maintenance and service of such wind farms in the North Sea requires safe boarding up to significant wave heights of approximately 2.5 m. Such a limit allows virtually year-round operation in the German Bight, Fig.14, *Fach and Olschner (2011)*. Compared to conventional monohulls, the SWATH concept allows much higher utilisation rates.

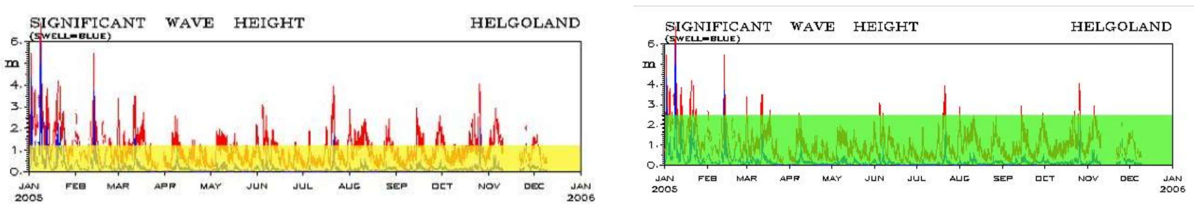

Fig.14: Seaway statistics for Heligoland with operational limit significant wave height 1.3 m (left) and 2.5 m (right)

In 2010, the first SWATH crew transfer vessel was launched, the 25 m "Natalia Bekker", Table II, Fig. 15. The design features a crescent-shaped bow with particular resilient fenders, for docking at the cylindrical structures of offshore wind farms, Fig. 16. With rapidly growing number of offshore wind farm installations in the North Sea, a significant growth of the service fleet is expected, with SWATH concepts being the most logical choice.

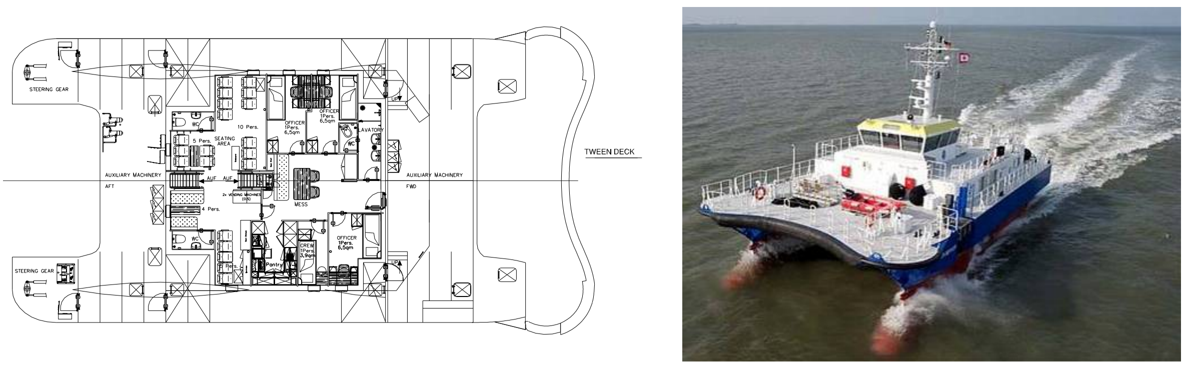

Fig.15: "Natalia Bekker" – Crew transfer vessel

Table II: Main particulars of "Natalia Bekker"

L_{oa}	26.40 m	P_B	3220 kW
B	13.00 m	V	18 kn
T	2.70 m	DWT	18 tdw

Fig.16: Crescent-shaped fenders designed for docking at cylindrical wind farm structures

3.3. Navy patrol vessels

Abeking & Rasmussen has built various naval SWATHs, Fig. 17. One of the envisioned applications is in cooperation with the Lürssen shipyard for the mine hunting improvement programme MJ2000 of the German navy, where a SWATH parent vessel acts as a control ship for at least two surface drones, *Spethmann (2001), N.N. (2002).* One of the unique advantages of SWATH vessels is the stable platform, which makes retrieval of marine drones much easier than for monohulls, Fig. 18. As drones, both air-borne and unmanned surface vessels (USVs), play an increasing role in the missions of navies worldwide, it is expected that more navies will SWATH vessels in the decades to come.

Fig.17: German navy SWATH

Fig.18: Easy launching and retrieval of drones

In 2011 and 2012, Abeking & Rasmussen delivered 25 m SWATH@A&R Patrol Boats to the Latvian Navy, Fig. 19. The vessels were constructed and delivered in co-operation with Riga Shipyard. The SWATH patrol vessel was designed and built to Germanischer Lloyd classification standards and has L_{pp} = 25.71 m, B = 13.0 m, T = 2.70 m. Different to the pilot SWATH parent design, the offshore patrol vessel's engines are placed in the lower hulls, leaving more space to accommodate the crew in the superstructure. The engine rooms are outfitted with MAN D 2842 engines (809 kW), driving Servogear controllable pitch propellers through Servogear reduction gearboxes. The design speed is 21.4 knots. The crew (up to 8 persons) can stay for one week at sea even under adverse weather conditions to fulfil the main tasks for the new vessels: patrol and surveillance of the territorial waters and in the exclusive economical zone as well as participation in international assignments. The fendering of the pilot boats was retained, facilitating all types of boarding operations for the patrol vessel. The modular design features a modular mission bay at the fore ship, Fig. 20. By fitting appropriate mission payloads (e.g. diving module, mine countermeasures module), the capabilities of the vessels can be tailored to its current mission.

Fig.19: Latvian SWATH offshore patrol vessel

Fig.20: Latvian SWATH with mission modules

4. The future starts now

The pilot tenders in SWATH design will continue to replace conventional designs. The popularity of the first prototypes for the German pilots on the Elbe river has spread along the coasts of Northern Europe, with SWATH pilot tenders introduced in the Netherlands in 2006 and in Belgium in 2011/12. It is reasonable to assume further organic growth in this segment for other countries with similarly rough waters as the North Sea.

The modular design and operation concept has also proven to be very popular, particularly for navy applications. A&R is working on further developments in this field adding a wider choice of containerized modules for the configuration of the basic platform. Concept studies have been made for larger navy vessels based on the modular SWATH concept, Fig. 21 and Fig.22. Detailed designs for a 70 m SWATH OPV will be the next step in the evolution towards larger combatants.

Fig.21: Concept study for modular navy vessel for launch and retrieval of marine drones

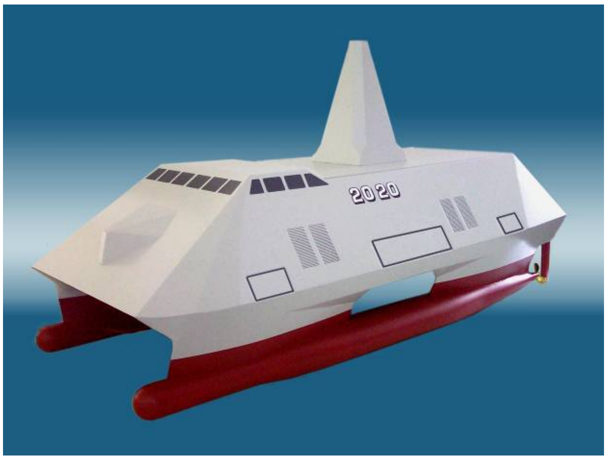

Fig.22: Concept study for SWATH frigate

Also on the basic hull design, innovations push the frontiers of hydrodynamic (and in particular seakeeping) performance. In 2012, construction work started on a SWASH (Small Waterplane Area Single Hull), Fig.23. A SWASH is like a trimaran with a single, small waterplane area central hull for buoyancy and two very thin outriggers for stability. The A&R SWASH is 20 m long; its outriggers are 8 m long. The vessel is intended for pilots, offshore wind farms, patrol boat or others.

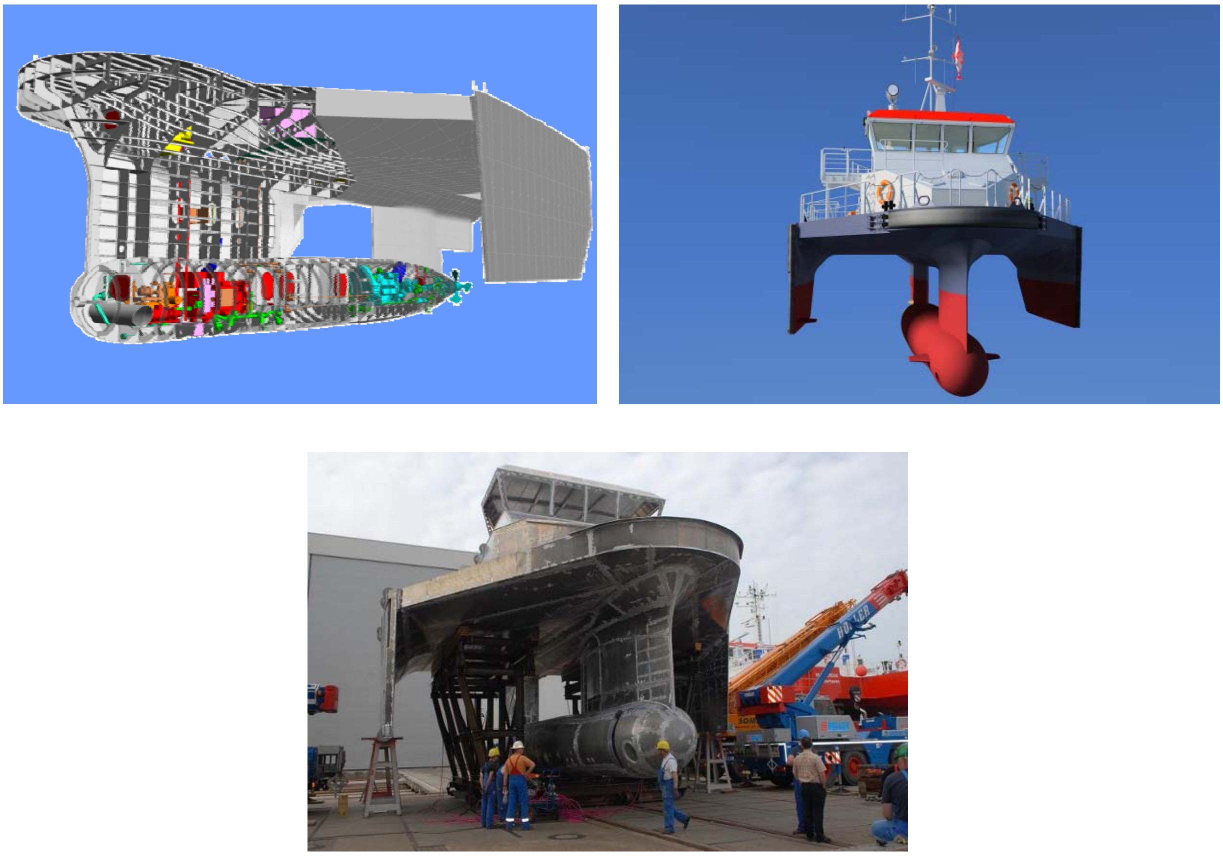

Fig.23: SWASH design (as constructed in 2012)

After the “Silver Cloud” performed very successfully, more and more interest in SWATH yachts has been received. Based on the 25 m, 40 m and 60 m SWATH@A&R designs, new yacht designs have been developed. Fig.24 shows a 62 m SWATH design study.

Fig.24: 62 m SWATH design study

Abeking & Rasmussen has projected different sizes of research vessels ranging from 25 to 70 m. SWATH vessels are a perfect platform for research. Different concepts have been developed and investigated. Fig 25 shows a 40 m research vessel project.

Fig.25: 40 m Research vessel

5. Conclusion

SWATH technology has come a long way since the first patent in 1880. It is no longer regarded an “unconventional” or even exotic concept, but has established a firm niche position whenever platforms with excellent seakeeping are required. The current developments show that research and development manages to drive the evolution of the concept with technical improvements and new applications.

6. Acknowledgement

The author gratefully acknowledges the valuable contributions by Dr Volker Bertram of FutureShip who shared his expertise generously.

References

ANDREWS, D. (2003), *Multi-hulled vessels,* Ch.46 in Ship Design and Construction, SNAME

BERTRAM, V.; SEIF, M. (2004), *New developments for fast and unconventional marine vehicles*, 4th Int. Conf. High-Performance Marine Vehicles (HIPER), Rome, pp.28-43

BORMANN, D.U. (2003), *Class 751 research and test vessel,* Naval Forces 5, pp.52-55

FACH, K.; OLSCHNER, N. (2011), *Offshore windfarm service vessel - Operational experience with the SWATH@A&R windpark tender (in German)*, Jahrbuch Schiffbautechnische Gesellschaft, Sprin-ger

GORE, J.L. (1985), *SWATH ships*, Naval Engineers Journal 97/2, pp.83-112

HYNDS, P. (2001), *SWATH designs continue to make steady headway*, Speed at Sea, Aug., pp.28-29

LANG, T.G.; SLOGETT, J.E. (1985), *SWATH developments and performance comparisons with other craft,* Int. Conf. SWATH Ships and Advanced Multi-Hulled Vessels, RINA, pp.7-23

N.N. (2002), *FLW, Specialist of naval craft*, Hansa 139/9, pp.178-183

N.N. (2005), *SWATH Technologie für kompakte Marineschiffe*, Hansa 142/2, pp.29-34

PAPANIKOLAOU, A. (1996), *Developments and potential in open sea SWATH concepts,* WEGEMT workshop Conceptual Designs of Fast Sea Transportation, Glasgow

SPETHMANN, K. (2001), *A realised SWATH-application as an example for naval purposes*, Jahrbuch Schiffbau-Technische Gesellschaft, Springer

SPETHMANN, K.; LEUE, W. (1997), *New SWATH generation of pilot-system for the German North Sea Coast*, Int. Symp. RINA SURV, Gothenburg

Parametric design tool considering integrated seakeeping, stability and wave resistance of a high speed trimaran vessel

Rafael Máximo, rafael.maximo@tpn.usp.br
Felipe Ruggeri, fruggeri@tpn.usp.br
Claudio Mueller, clasamp@usp.br

Tanque de Provas Numérico, Escola Politécnica da Universidade de São Paulo,
Av. Prof. Luciano Gualberto, travessa 3 nº 380 - CEP 05508-010 - São Paulo – SP

Abstract:

This article presents a design tool for the prediction of the main attributes of a high speed trimaran passenger vessel, intended to be integrated within an optimization procedure for rapid evaluation of various design solutions. The model is applied to the conceptual design of a trimaran vessel with capacity of 600 passengers, a design speed of 40 knots and a range of 2000 nautical miles. The design variables considered are the hulls main dimensions and coefficients and their relative positioning, and it evaluates ship total resistance, general lay-out, weights, seakeeping and stability. The ship total resistance is evaluated considering the ITTC'78 model simplified. The residuary resistance is approximated by the wave resistance and evaluated using Michell theory of slender hull extended for multihull vessels, in order to consider the potential field interaction of the waves generated by each hull. The intact stability is assured by the application of IMO rules for high speed vessels to the righting arm curve, built from the hull geometry described by NURBS. The general layout and weights are estimated considering similar vessels, empirical relations and machinery brochures from manufacturers. The seakeeping is evaluated considering the potential flow panel method code WAMIT® to obtain the body responses and the environmental conditions adopted are from Santos basin (Brazil) and the comfort index MSI (Motion Sickness Incidence) concerning passengers welfare. The model is built in Matlab® environment, with the 3D modeling using NURBS for the hull surfaces definition.

1. Introduction

Most of Brazil oil's production is offshore, requiring the transportation of personnel from the coast to the oil platforms and vice-versa with comfort and safety. Usually, helicopter are employed in this task, however, as the distance from shore increases, the cost also increases significantly, encouraging the search for alternative means of transportation to take oil rig's crew members back and forth.

For that reason, the use of a high speed vessel for passengers' transportation becomes an attractive solution for the pre-salt layer exploration in Santo basin (Brazil), which is far from the coast, 160~200 nautical miles. Employing a high speed vessel is also advantageous from the point of view of passengers' welfare during the trip, as it minimizes the exposure time to the environmental conditions, which in excess can lead to seasickness.

In this work, an alternative concept for a high speed vessel, the trimaran hull, is studied, as it may have several advantages over the monohull and catamaran forms, such as reduced ship resistance, since the hulls are thin, and better stability and seakeeping performance, as discussed by ZHANG (1997). The use of simplified computational methods (assumed here as methods that do not require a large computational time to perform an evaluation) can be used in the initial stages of the vessel design to predict the trends and tradeoffs due to the design variables variations, which is very important when there are not much similar vessels data available.

The integrated model developed considers ship resistance analysis following the thin ship theory for wave resistance, as discussed by INSEL (1991), and the frictional component considering ITTC'78 correlation line. These components are summed and compose the total ship resistance, neglecting in this first analysis the form factors.

The seakeeping performance was evaluated using WAMIT® code, which is a fast frequency domain panel method, containing simple ASCII input files for masses, moments of inertia, frequencies etc. The hull geometry can be provided in a higher order description using NURBS[1]. The hull is built using the Series 64 for the main hull and Wigley description for the outriggers, this evaluated considering the analytical expression for the surface (converted to NURBS nodes description) and the further by direct interpolation of stations in the systematic series.

The environmental conditions considered are Santos basin (Brazil), where there will be several oil platforms for the exploration of the pre-salt layer, being performed the response spectrum evaluation and the corresponding comfort index (in this work the MSI).

The stability analysis is performed considering a simplified routine that evaluates only the righting arm curve and apply the IMO 2008 rules for high speed vessels in order to verify whether the intact stability criteria are satisfied.

The ship resistance evaluation is considered of vital importance because it affects directly the required power, which defines the machinery arrangement and fuel consumption and thereof the vessel's tankage, affecting the whole ship layout, as will be presented latter. The general layout is then used for the calculation of total weight, center of gravity position and moments of inertia that, combined with the hydrostatic properties evaluated using the continuous NURBS surface definition, allows the creation of the input files for the seakeeping numerical method.

Three vessels with different sizes are created and compared with similar ones available, providing different solutions for the transportation problem. The basic idea was to implement a simplified code for design of a trimaran high speed vessel that allows several evaluations considering the design variables.

2. Synthesis model

The design variables chosen to describe a design solution of the high speed trimaran passenger vessel are the center (main) hull major dimensions and block coefficient, the side hull breath and block coefficient, the side to center hull length and displacement ratios and the position of the side hulls in relation to the center hull. Fig. 1 shows the top view of the trimaran configuration used.

The three hulls are assumed symmetric regarding their center plan (XZ) as well as the main hull center plan (XZ). The series 64 (YEH, 1965) were adopted to define the main hull section, while the side hulls were modeled as Wigley hulls.

---

[1] Non Rational Uniform Basis Spline

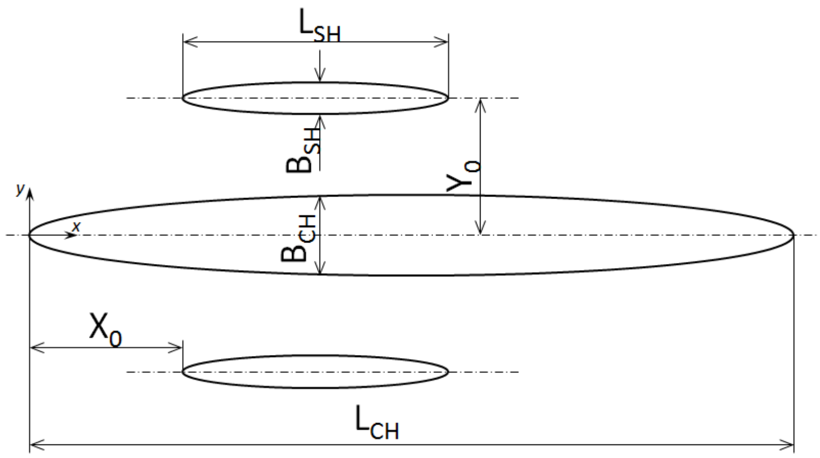

Fig. 1: Trimaran configuration (top view)

In order to help identifying typing errors and facilitate building the model in a logical way, it was built in a modular structure, and the modules considered so far are:

- Creation of hull sections
- Total resistance and effective power calculation
- Hull-propulsion system integration
- General layout and machinery
- Seakeeping response
- Intact stability evaluation and
- 3D visualization of the resulting hull.

2.1. Creation of hull sections

As stated, the main hull is derived from the series 64 for high speed displacement surface vessels. The series limitations are shown in table1.

Table 1 – Series 64 range of parameters

Parameter	Range
$\Delta/(0{,}01 \cdot L)^3$	15 – 55
B/T	2 – 4
C_b	0,35 – 0,55

The side hull is obtained from its mathematical representation, equation 1 (JOURNÉE, 2003) which gives the half-breadth as a function of the section x and elevation z. The origin being placed half-ways in longitudinal direction, in the symmetry plan in transversal direction and in the water plane level in vertical direction.

$$y = B/2 \cdot [1 - (2 \cdot x/L)^2] \cdot [1 - (z/D)^2] \cdot [1 + a_2 \cdot (2 \cdot x/L)^2 + a_4 \cdot (2 \cdot x/L)^4] \qquad (1)$$

Where:

- $a_2 = \frac{t}{2} - 1 - a_4$
- $a_4 = 105/8 \cdot (t/15 - C_P + 8/15)$

With $t = L/B \cdot tg(\alpha)$ and α being the half entrance angle on the water line. L, B and D are the main dimensions of the hull, respectively, length, breadth and depth.

Fig. 2 shows a NURBS representation of a generic trimaran vessel.

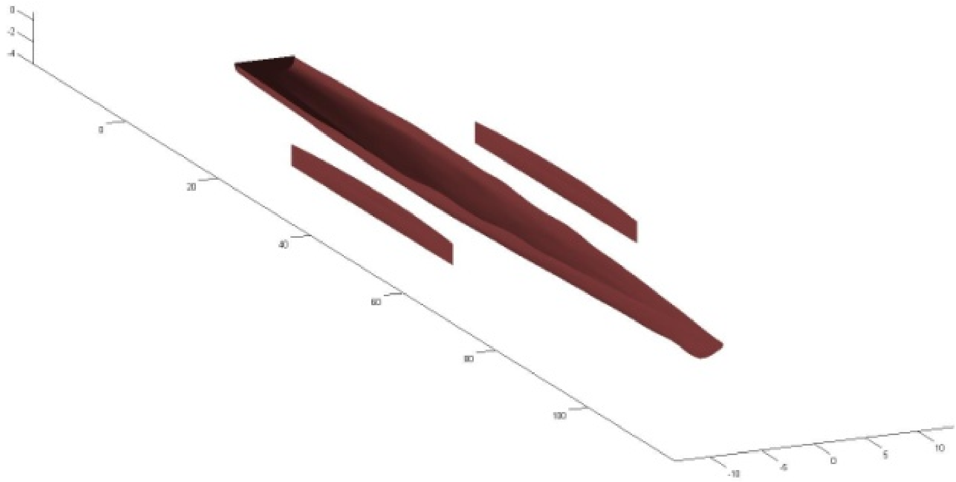

Fig.2: Generic trimaran vessel created by the model, in Matlab® environment

To describe the mathematical formulation and/or representation of the whole ship (the hulls and its systems) a right-handed coordinate system, defined by $O(x, y, z)$, was adopted.

The coordinate system is as follows:

- O → origin, in the intersection of the stern plate, symmetry plan and water plan;
- x → longitudinal axis, positive forwards;
- y → lateral axis, positive to port side;
- z → vertical axis, positive upwards.

2.2. Total resistance and effective power calculation

Total resistance is calculated according to the model proposed at ITTC'78, which divides it in viscous and residuary or wave resistances, as shown in equation 2:

$$R_T = R_V + R_W \tag{2}$$

Where R_V is given by equation 3:

$$R_V = \frac{1}{2} \cdot \rho \cdot C_V \cdot S_W \cdot V_S^2 \tag{3}$$

And C_V is approximated by the frictional coefficient calculated as a function of Reynolds number, R_n, as stated in equation 4:

$$C_V \approx C_F = \frac{0{,}075}{(log(R_n) - 2)^2} \tag{4}$$

Once the hulls are slender (high L/B ratio), it is assumed that the boundary layers are attached almost in entire hulls (the known separation occurrence in the transom stern of the center hull was neglected). Since the hulls are transversally far from each other it is assumed that the viscous interactions are small, therefore leading to the hypothesis that there is no viscous interaction between the hulls. The viscous resistance share for the whole vessel can then be expressed as in equation 5:

$$C_V = (C_V)_{CH} + 2 \cdot (C_V)_{SH} \tag{5}$$

Where the index *CH* stands for center hull, while *SH* stands for side hull.

For wave resistance evaluation, it was implemented the thin ship theory developed by MICHELL (1898) and initially extended for catamaran vessels (INSEL, 1991), and in this work applied for trimaran hulls in order to consider the wave interaction among the hulls. It is known that one of the advantages concerning trimaran vessels is that the correct positioning of the side hulls can reduce the total wave resistance, by means of destructive interactions among the waves created by each hull.

An additional consideration was that for vessels that travel on sea conditions an additional power margin of 25% due to added resistance.

2.3. Hull-propulsion system integration

The integration between the hull and the propulsion system, used to estimate the propulsion efficiency, depends on the foretold chosen system. For the present studies it was considered the use of waterjets as the main propulsion system. Since waterjets loose efficiency when working outside their designed speed range, two different solutions must be thought for low and high speeds.

The low speed systems can be design both with smaller waterjets or conventional naval propellers (single screw, variable pitch, contra-rotating propellers, etc.). In the present study, this system was not considered, given the objective of developing a design tool capable of predicting the features and attributes of a vessel intended to carry passengers along long distances at high speeds.

For the high speed system, a total of nine configurations are evaluated, resulting from the combination of 2, 3 and 4 waterjets with 2, 3 and 4 engines. The one leading to the least heavy machinery configuration is chosen.

2.4. General layout and machinery

This module is responsible for the assessment of the general layout of the vessel and all the weights, centers and moments of inertia calculations. It estimates the hull, miscellaneous and outfit weights and takes into account the following spaces:

- Machinery room, comprising the waterjets;
- Fuel tanks;
- Passenger deck;
- Luggage room;
- Superstructure (comprising crew accommodations);

The following assumptions were made for weights and centers estimation.

- Engines and waterjets weights and dimensions were taken from commercial brochures from manufacturers. Their positioning was based on similar ship's layouts.
- All superstructures were considered to be located within 70% of the length of the ship from the stern.
- Passenger deck was placed at the first deck above the hull to comprise the full breadth of the ship, and was modeled in a rectangular shape.
- Luggage room was placed on the deck above the passenger deck, also as a rectangular shape.
- Fuel tanks were located forward the engine room and were taken as the inner volume of the intersection of a rectangular shape and the hull.
- The hull weights and centers were based on an equivalent plate thickness method, as presented by HEFAZI (2005).
- Lightship weight margin of ten percent, to account for the simplifications made.

The superstructure should also account for the cross structure connecting the three hulls, but this was not yet added to the model.

The weights are divided as shown in equation 6

$$W_{total} = W_{LS} + DWT \tag{6}$$

Where W_{LS} represents the lightship weight and DWT the deadweight. Equations 7 e 9 show their subdivision.

$$W_{LS} = W_{hull} + W_m + W_o + W_{SS} + W_{misc} \tag{7}$$

Being:

- W_{hull} - hulls;
- W_m - machinery (engines plus waterjets);
- W_o - outfit;
- W_{SS} - superstructure and;
- W_{misc} - miscellaneous weights.

The hull weight is still further divided in center hull, side hulls and hull miscellaneous weights, as shown in equation 8.

$$W_{hull} = W_{ch} + 2 \cdot W_{sh} + W_{hull\_misc} \tag{8}$$

The deadweight is given by equation 9.

$$DWT = W_f + W_{pas} + W_{lug} \tag{9}$$

Where W_f represents the fuel weight, W_{pas} the passengers weight and W_{lug} the total luggage weight. The crew weight is not considered to be of relevance, regarding total displacement of the ship.

2.5. Intact stability evaluation

From the NURBS surface definition and the weights and center defined before, it is possible to determine the righting arm curve (GZ curve), represented by a Spline curve, in which the stability criteria (IMO, 2008) is applied to verify the design feasibility.

2.6. Seakeeping response

The seakeeping response is evaluated using the panel method WAMIT® for zero forward speed, with the comfort measured using the MSI (motion sickness incidence) index, considering the Santos basin conditions and the exposure time evaluated using the vessel speed.

The analysis performed evaluates the MSI index on the passenger deck, allowing the evaluation of the comfort aboard for several passenger positions. MSI index is calculated as a function of RMS vertical acceleration, frequency and exposure time, equation 10 (COLWELL, 1989).

$$MSI = 100 \cdot \Phi(z_a) \cdot \Phi(z_t^{'}) \tag{10}$$

Where $\Phi(z_a)$ is given by equation 11.

$$\Phi(z_a) = 2{,}128 \cdot log(a) - 9.277 \cdot \log(f) - 5.809 \cdot [\log(f)]^2 - 1{,}851 \tag{11}$$

And $\Phi(z_t^{'})$ is given by equation 12.

$$\Phi(z_t^{'}) = 1{,}134 \cdot log(a) - 1{,}989 \cdot \log(t) - 2{,}904 \tag{12}$$

Where a is the RMS acceleration, f is the center frequency of the 1/3 octave band and t is the exposure time.

The first 1/3 octave band is chosen as having its center frequency equal to the spectrum peak frequency and the upper and lower band limits are found by, respectively, multiplying and dividing the center frequency by $2^{1/3}$. Usually three 1/3 octave bands, one to the left and one to the right of the first band, are enough to capture the relevant acceleration spectrum area, as shown in Fig. 3 example.

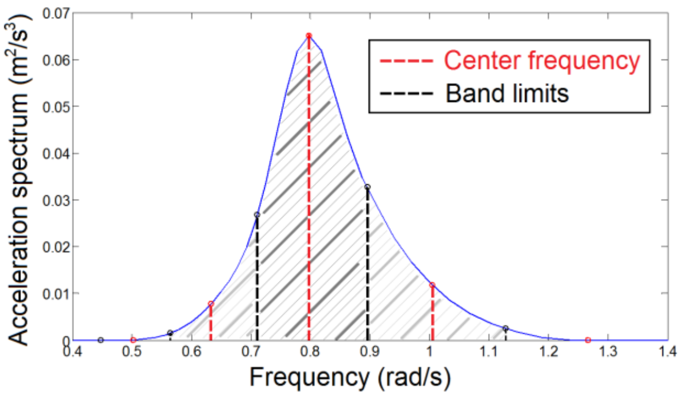

Fig.3: 1/3 octave band division of the acceleration spectrum

2.7. 3D visualization of resulting hull

The three dimension visualization of the hull is generated by plotting the NURBS surface along with the blocks representing each of the considered spaces. In that way, the solution can be compared visually with similar vessels and the spatial layout distribution can be checked. This feature is intended for the validation of the design tool under development and eventual visualization of the final solution, after an optimization process has been carried out (as described in the section *Future work*).

3. Shipowner requirements

The design requirements considered are a passenger capacity of 600 people with 40 kg luggage each, a design speed of 40 knots with a range of 2000 nautical miles and accommodation for 16 crew members. These definitions are based on similar vessels and represent a given market condition, thereby not being object of study of this work.

4. Results

For the verification of the tool prediction quality, mainly concerning power prediction, three vessels were selected for comparison with the predicted power.

4.1 Ships used for validation

Three trimaran ships with different characteristics and dimensions were chosen (Zhang, 1997) to validate the tool developed. Table 2 shows their main dimensions and coefficients. α is the transversal separation coefficient, measured by the internal distance between the side and center hull, divided by the half breadth of the center hull and β is the longitudinal positioning coefficient, measured by the distance between the stern perpendicular of the side and center hulls, divided by the center hull length minus the side hull length. The models chosen are:

A. Small Support Vessel;
B. Canadian Ferry and;
C. Fast Ferry.

Table 2 – Similar ships used for validation

Parameter	**A**	**B**	**C**
$L_{ch}\ (m)$	59,8	115,0	99,0
$B_{ch}\ (m)$	4,2	6,5	6,8
$T_{ch}\ (m)$	2,1	3,2	3,4
$\nabla_{ch}\ (m^3)$	209	1217	1014
$L_{sh}\ (m)$	19,9	30,0	35,0
$B_{sh}\ (m)$	1,06	2,0	1,5
$T_{sh}\ (m)$	0,9	1,5	2,0
$\nabla_{sh}\ (m^3)$	9,6	50,0	44,1
$\alpha\ (-)$	1,07	2,23	1,38
$\beta\ (-)$	0,3	0,3	0,3
$V_k\ (knots)$	25	36	38
$Fn_{ch}\ (-)$	0,53	0,55	0,62
$Fn_{sh}\ (-)$	0,92	1,07	1,05

In order to obtain the correct data for the center hull sections, the chosen hull must fall within the series 64 limits. Table 3 presents this compatibility check for the three selected ships.

Table 3 – Series 64 compatibility check

Parameter	A	B	C
$\Delta/(0{,}01 \cdot L)^3$	28,4	23,2	30,3
B/T	2,0	2,0	2,0
C_b	0,396	0,509	0,443

4.2. Hull surface (3D visualization)

Fig. 4 shows the visualization of the ship hull surface.

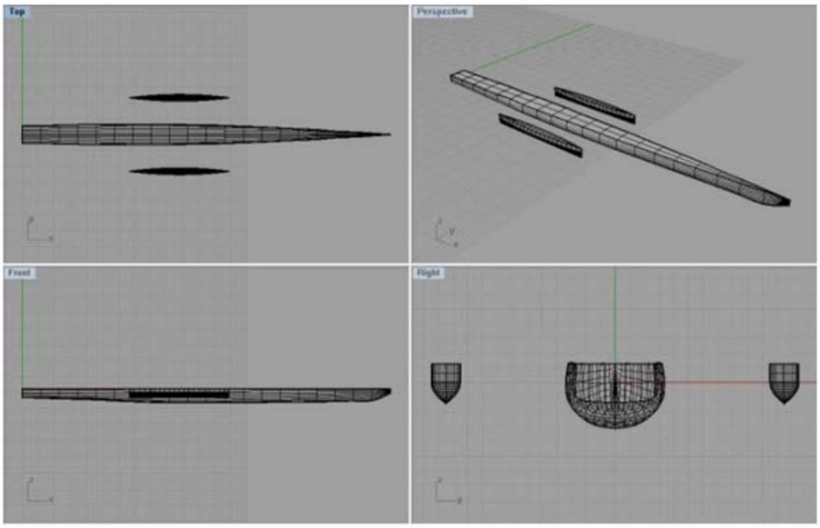

Fig.4: 3D visualization of the hull surface

4.3 Ship resistance

Table 4 shows the ship resistance and the installed power estimated and compares it with the installed power of the ships.

Table 4 – Total resistance and installed power comparison

Attribute	A	B	C
$R_W\ (kN)$	6,4	429	299
$R_V\ (kN)$	52,7	294	321
$R_{total}\ (kN)$	59,1	723	620
$P_{effet}\ (MW)$	0,76	13,4	12,1
$P_{estimated}\ (MW)$	1,72	24,2	21,8
$P_{reference}\ (MW)$	2,14	20,0	20,0

The power estimates are in good agreement with the reference values. It must be noted that no information is made available regarding the power and resistance margins considered into the reference values and thus matching the exact figures for three different ships is not possible.

4.4 Weights and centers

Table 5 shows the weights and longitudinal and vertical centers. There are no transversal centers, once all the systems modeled were assumed symmetric in relation to the mid plan of the center hull.

Table 5 – Ship weights and centers

Attribute	A	B	C
$W_{navio}\ (kg)$	187	1143	826
$LCG_{navio}\ (m)$	22,9	49,5	39,9
$VCG_{navio}\ (m)$	0,70	0,56	0,56
$LCB_{navio}\ (m)$	26,0	49,7	42,8
$VCB_{navio}\ (m)$	-0,63	-1,18	-1,17

The weights are smaller than the displacement of the original ships probably because ships B and C also transport vehicles. Ship A is not a passenger vessel, and was chosen mainly to validate its hydrodynamic performance estimation (resistance and seakeeping).

4.5. Stability evaluation

Fig.5**:** shows the stability check against IMO 2008 recommendations for vessel B, as an example used during the validation phase.

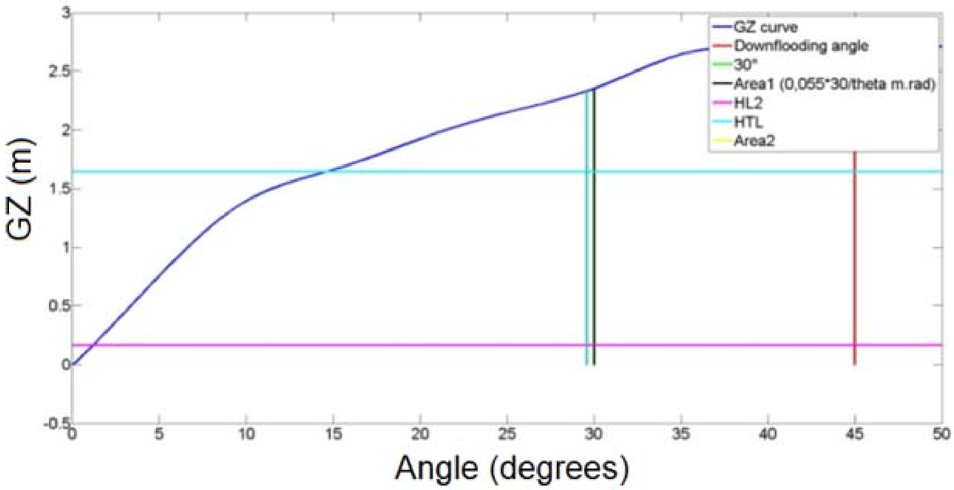

Fig.5: Stability check

The figure indicates that the foretold vessel passes all criteria applied, however, while performing and optimization process, the images displaying can be turned off, so the code works only with numerical data to check stability criteria.

4.6. Seakeeping analysis

Fig. 6 shows an example of MSI index at a specific deck height, given a peak period, Tp, a significant wave height, Hs, and a sea heading.

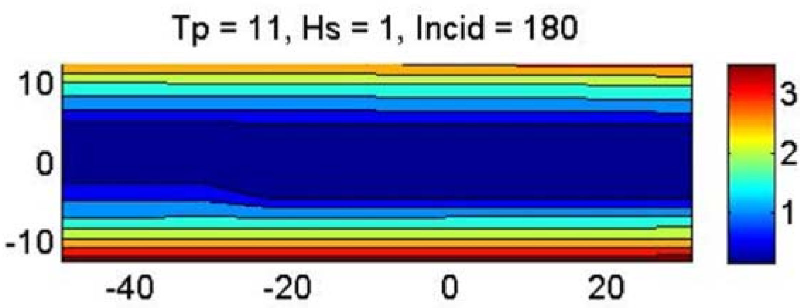

Fig. 6: MSI for a given Tp, Hs, and sea wave heading

Fig. 7 shows an example of a response amplitude operator (RAO).

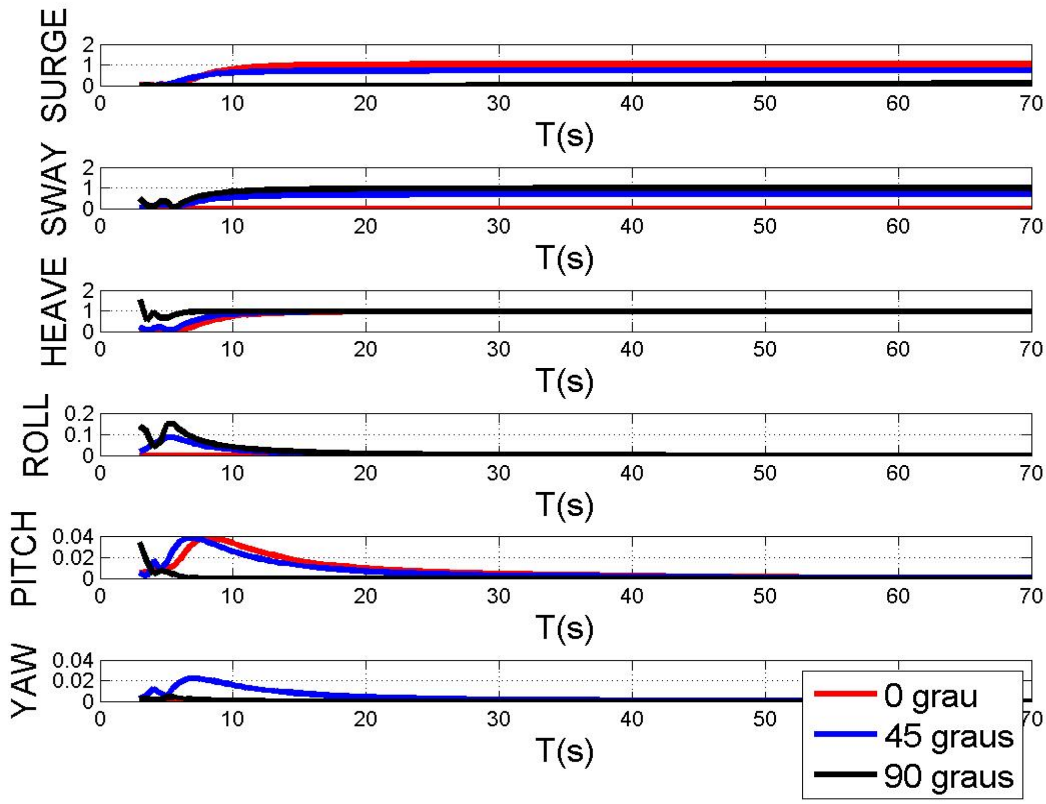

Fig. 7: RAO example

5. Conclusions

In conclusion, a robust design tool capable of predicting the main attributes concerning the early design phases of a high speed trimaran passenger vessel was created, allowing the rapid evaluation of various designs.

This design tool was validated against three reference designs, showing good agreement regarding estimated power and weights.

6. Future work

Still, this design tool must be further checked against more existing designs and extra calculation modules should be included to account for maneuverability behavior and cross-structure dimensioning.

The following step of the study would be the creation of an optimization process that, making use of the design tool here presented, should find the optimal solution (or Pareto frontier), for an specified objective function (or set of conflicting objective functions).

7. Acknowledgements

The authors would like to acknowledge the support given by all colleagues involved in the work directly on indirectly, the Department of Naval Engineering and the Numerical Offshore Tank, from Escola Politécnica of University of São Paulo.

References

COLWELL, J. L. (1989), *Human factors in the naval environment: A review of motion sickness and biodynamic problems*, Defence Research Establishment Atlantic, Canada

HEFAZI, H.; SCHIMITZ, A.; AND SHIDE, R. (2005), *Automated multidisciplinary design optimization method for multi-hull vessels*, CCDoTT Report, California State University, Long Beach foundation

IMO (2008), *International code on intact stability*

INSEL, M. (1991), *An investigation into the resistance components of high speed displacement catamarans.* Thesis, (PhD). University of Southampton

JOURNÉE, J. M. J. (2003), *Experiments and calculations on 4 Wigley hull forms in head waves*, Delft University of Technology

YEH, H. Y. H. (1965), *Series 64 resistance experiments on high speed displacement forms*, Marine Technology, pp.248-272

ZHANG, J. W. (1997), *Design and hydrodynamic performance of trimaran displacement ships*, Thesis, (PhD), University College London.

Fast ship hydrodynamics on shallow water

Lars Lübke, Potsdam Ship Model Basin (SVA), Potsdam/Germany, luebke@sva-potsdam.de

Abstract

Numerical investigations were conducted with a small fast going vessel in shallow water. In the course of the investigations the ship resistance and the dynamic sinkage and trim were determined for three ship speeds (Fr = 0.8–1.2) and eight water depth. The results show the impact of shallow water on the ships performance. The hull resistance was found to increase or decrease in shallow water in dependency of the speed. The latter was not expected. As explanation for this finding the "wing in ground" effect is considered to be a possible reason. The results have to be further validated and verified. The calculations were conducted for model scale with the scale ratio being λ = 16. For the numerical calculations the RANSE-solver ANSYS-Fluent and CFX were employed.

1. Introduction

The water close to the German shore in the North- and Baltic-sea is relatively shallow, with varying water depth. This circumstance makes it often necessary to take shallow water effects into account for speed prediction of fast going ships.

During experimental investigation of high speed vessels in shallow water, the following restrictions have to be taken into account:

- The carriage speed puts limits to the scale ratio of the investigated vessel (Froude identity). In case the requested speeds exceeds the carriage speed the scale ratio has to be reduced, which increases the prediction uncertainty.
- The investigation for varying water depth requires special facilities, such as an adjustable floor.

The above limitations can be overcome with the use of numerical methods; however other uncertainties and constraints are introduced. The water depth in numerical simulations can be adjusted with little effort and the speed can be simply redefined, but particularly the grid uncertainty is high. In addition the simulation time for these kinds of calculations is considerable, due to the transient oscillation of the dynamic floating position of the ship. The intention of the investigation was to predict the qualitative differences caused by speed and water depth on the ships performance.

2. Geometry and numerical grid

For the investigations a fast monohull was chosen. The main particulars of the hull are given in Tab. 1. In Fig. 1 the geometry of the hull is shown. The hull was investigated without appendages.

Table I: Main particulars

	L_{OA} [m]	B [m]	T [m]	∇ [m³]	L_{CB} [m]
λ = 1.0	37.69	7.65	1.86	267.9	16.21
λ = 16	2.356	0.478	0.116	0.065	1.01

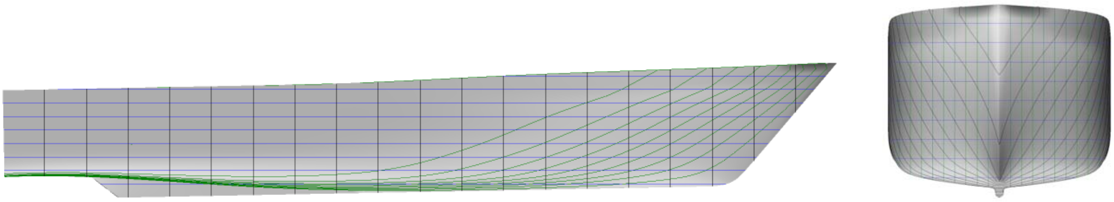

Fig.1: Hull

In the solution domain a block-structured numerical mesh was generated with ANSYS ICEM HEXA. The numerical mesh around the ship is identical for all calculations. In order to simulate different water depth, additional mesh blocks were appended to the ship mesh.

The spatial discretization error was studied on three different numerical meshes for one water depth (h = 8m) only. A refinement ratio of $\sqrt{2}$ was chosen for all grid dimensions. In Tab. 2 the mesh sizes are given, while in Fig. 2 the surface meshes of the hull for the three grid densities are shown. For the investigation the coarse mesh was chosen, with the number of grid cells ranging between 0.65 – 0.75 Million in dependency of the water depth.

Table II: Mesh size

	coarse	medium	fine
Refinement ratio	1	$\sqrt{2}$	2
No. of elements [10^6]	0.65-0.750	1.83	5.16

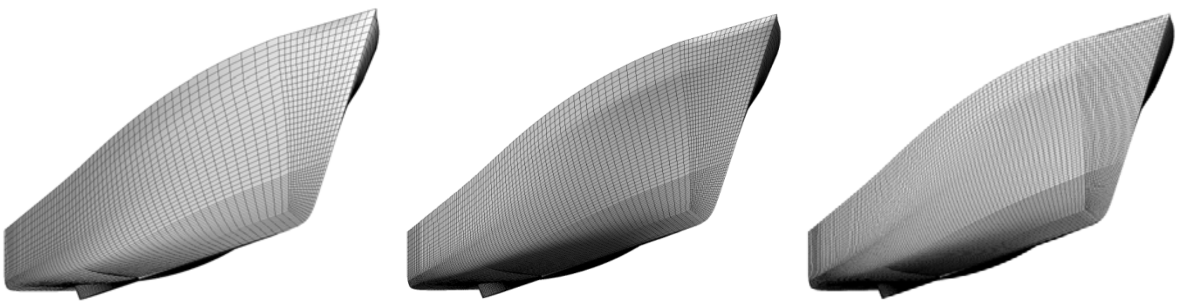

Fig.2: Numerical mesh, coarse (left), medium (middle), fine (right)

3. Results

The calculations were conducted for different ship speeds and different water depth, for a scale ratio of λ = 16. In Tab. 3 the operation points are given.

Table III: Operation points

		OP1	OP2	OP3
Fr		0.8	1.0	1.2
V [kts] (λ = 1)		29.9	37.4	44.9
V [m/s] (λ = 1)		15.38	19.2	23.1
V [m/s] (λ = 16)		3.85	4.81	5.77
Re		4.88E+08	6.10E+08	7.32E+08

Tab. 4 gives the Froude depth number for the investigated operation points and water depth.

Table IV: Froude depth number

		Fr_h		
***h* [m]**	***h/T***	**OP1**	**OP2**	**OP3**
8	4.3	1.74	2.17	2.60
16	8.6	1.23	1.53	1.84
32	17.2	0.87	1.09	1.30
48	25.8	0.71	0.89	1.06
64	34.4	0.61	0.77	0.92
72	38.7	0.58	0.72	0.87
80	43.0	0.55	0.69	0.82
96	51.6	0.50	0.63	0.75

The vertical center of gravity was chosen to lie in the design water line (*T*). A variation of the vertical center of gravity position has shown that the impact on the resistance is negligible, while only minor differences in trim and sinkage were observed. The investigation was carried out with the center of gravity being placed at 100%, 80% and 65% of the ships draught. For the $0.65 \cdot T$ case trim and sinkage increased by about 2.5% and 3.5% respectively, in comparison to the $1.0 \cdot T$ case.

For the calculations the RANSE solvers ANSYS Fluent and CFX were used. The dynamic sinkage and trim angle were determined by solving the motion equations for a rigid body with 2 degrees of freedom (2DOF). The motions of the ship (rigid body) were controlled within an additional iteration loop with under-relaxation of the motion behavior. For the calculations with Fluent the equations were solved segregated, while for CFX a coupled approach was chosen.

In the following a positive squad, sinkage means that the hull is immerging into the water, while negative values mean that the hull is emerging, coming out of the water. Positive trim angles mean that the hull trims down to the stern.

3.1 Verification

For a water depth draught ratio of h/T = 4.3, a Froude number of Fr = 0.8 and a scale ratio of λ = 16 the spatial discretization error was studied. For this purpose the medium and fine mesh were trimmed according to the coarse mesh results. The dynamic position of the ship may also dependent on the spatial discretization, but with this approach the differences in resistance can be solely related to the spatial discretization.

In Tab. 5 the resistance for the investigated operation point is given for the three numerical meshes. The total resistance (R_T) is splitted in a frictional (R_F) and a pressure (R_P) component. The difference between the coarse and the medium grid is denoted ε_{23}, while the difference between the medium and the fine mesh is referred to as ε_{12}. The difference in percent between the medium and fine grid with respect to the fine grid results is named ε_{12}%S1. The convergence ratio is defined as $R = \varepsilon_{12}/\varepsilon_{23}$. For the total resistance a monotonic convergence can be attested ($0<R<1$). However for the pressure and frictional resistance monotonic divergence ($R>1$) and oscillatory convergence ($R<0$, $|R|<1$) can be found. Therefor the grid uncertainty on basis of a generalized Richardson extrapolation cannot be determined. The iterative uncertainty for the total resistance, due to the oscillatory iterative convergence, was determined to be U_I = 0.1 N for the coarse, U_I = 0.8 N for the medium and U_I = 1.2 N for the fine mesh. The iterative uncertainty defined as $U_I = 0.5*(S_U-S_L)$ was calculated with the upper S_U and lower S_L bounds.

Table V: Verification, λ = 16

Fr = 0.8	coarse (3)	medium (2)	fine (1)	ε_{23}	ε_{12}	ε_{12}%S1
R_F	28.7	27.2	28.3	1.5	-1.1	-4.1
R_P	34.7	34.1	31.8	0.6	2.3	7.1
R_T	63.4	61.3	60.1	2.1	1.1	1.9

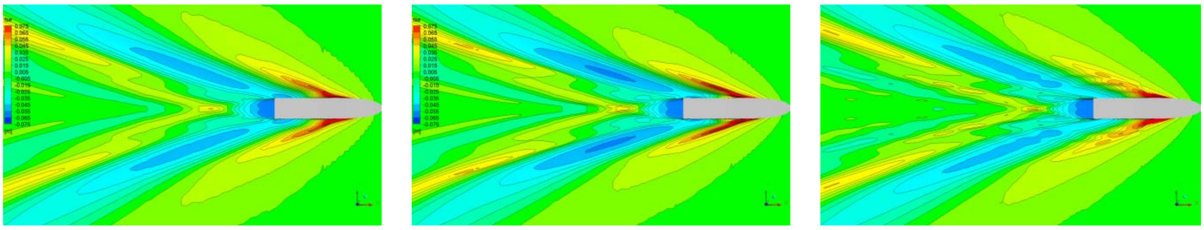

Fig.3: Free surface elevation, h/T = 4.3, Fr = 0.8, λ = 16, coarse mesh (left) medium mesh (middle) and fine mesh (right)

The difference in total resistance between the coarse and the fine mesh amounts to about 5% of the fine mesh results. The coarse grid results are considered accurately enough to determine the qualitative differences between the different operation points. For this reason the consecutive investigations were continued on the coarse mesh.

In Fig. 3 the free surface elevation calculated on the coarse (left), the medium (middle) and the fine mesh (right) is shown for the investigated operation point. The comparison of the wave elevation around the hull, reveals that the wave crest and trough around the hull gain elevation from the coarse to the medium mesh, however decrease in size again between the medium and fine grid. This is due to the circumstance that with the grid spacing of the fine mesh the wave steepness could be resolved to an extent that triggers wave breaking, which also explains the unsteady wave pattern for the fine mesh.

3.2 Validation

The ship was also investigated in the towing tank of the SVA Potsdam. Since in the towing tank no adequate facility to adjust the water level was available, the tests were carried out for the water depth draught ratio of $h/T = 38.7$ only. The experimental results were used to validate the CFD computations on the coarse mesh for $h/T = 38$.

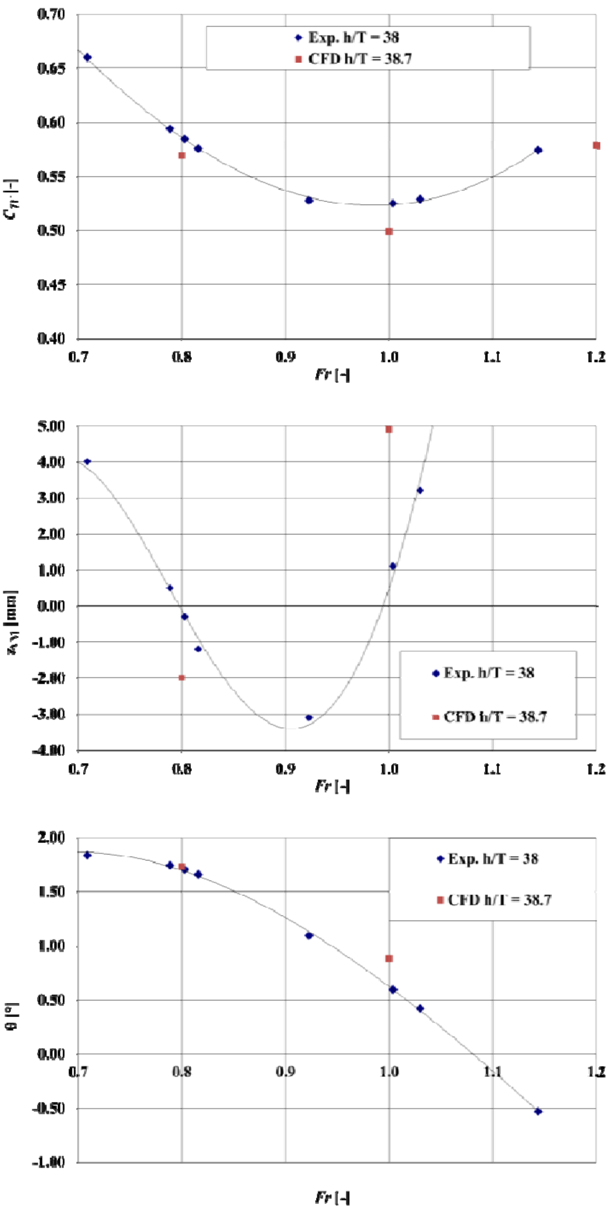

Fig.4: Comparison of measured and calculated resistance, trim and sinkage of the hull

In Fig. 4 the measured and computed resistance displacement coefficients (top), the sinkage (middle) and trim (bottom) are given for the investigated speed range.

The measured values are given in blue, while the calculated values are given in red.

It shows that the resistance coefficient (top) has a local minima for Froude numbers around $Fr = 0.9$-1.0. For $Fr = 0.8$ the computed resistance coefficient is approximately 3% lower than the measured value, while for $Fr = 1.0$ the discrepancies amount to about 5%. For the $Fr = 1.2$ case no measurements were available.

The middle graph in Fig. 4 shows the measured and computed dynamic sinkage of the hull at midships. Between Froude number $Fr = 0.8$ and $Fr = 1.0$ the hull is coming out of the water. For the rest of the investigated speed range the hull has squad. The agreement between measurements and computations is reasonable, if the magnitude of the squad is considered.

The dynamic trim is given in the bottom graph of Fig. 4. For Froude numbers greater than roughly $Fr > 1.1$ the hull trims down to the bow.

The comparisons were conducted with the coarse mesh results, achieving a good agreement between measured and computed values, with increasing discrepancies for higher Froude numbers. It is expected however, that the discrepancies between measured and computed values is slightly larger for finer meshes.

3.3 Shallow water effects

In course of the simulations the resistance and the dynamic trim and sinkage were determined for different water depth and speeds. In order for the ships to reach a kind of steady state, the dynamic floating position (trim and sinkage) has to be calculated. The oscillating motion of the free floating hull at the beginning of the simulation has to be damped out. This requires long calculation times, as shown in the following figure, illustrating the time history of the resistance, the trim angel and the motion of the vertical center of gravity of the ship during the simulation, for a calculation starting with an untrimmed hull but with converged flow field (first 2.5s simulation time). In course of the project the approach was altered towards a pre-trimmed hull with corresponding converged flow field, taken from a calculation with similar water depth-draught ratio.

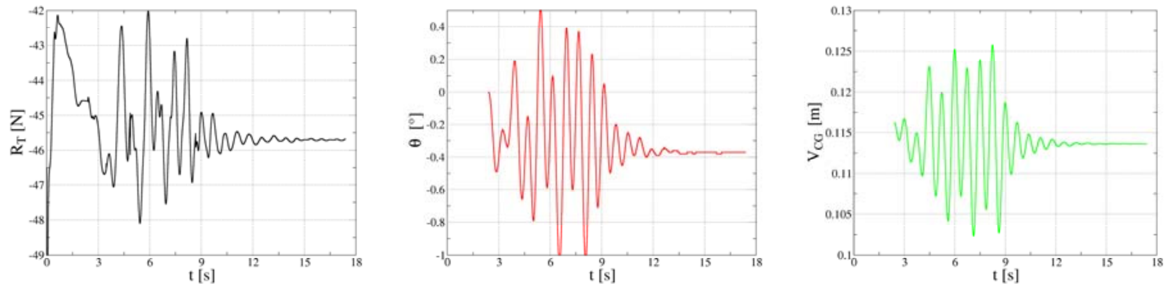

Fig.5: Time history of total resistance (left), trim angle (middle) and dynamic position of the vertical center of gravity (right)

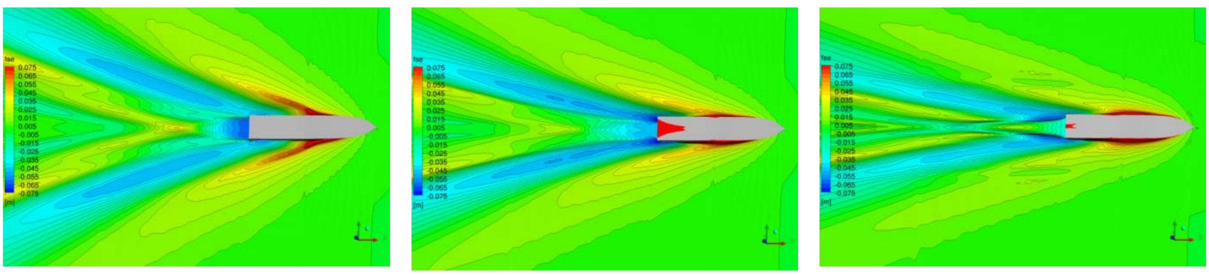

Fr = 0.8, *h/T* = 4.3 | *Fr* = 1.0, *h/T* = 4.3 | *Fr* = 1.2, *h/T* = 4.3

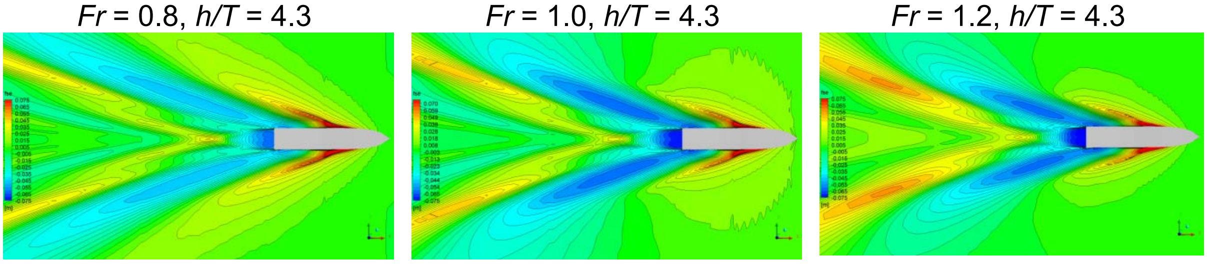

Fr = 0.8, *h/T* = 4.3 | *Fr* = 0.8, *h/T* = 17.2 | *Fr* = 0.8, *h/T* = 51.6

Fig. 6: Free surface elevation for different Froude numbers but the same water depth (top) and different water depth but the same Froude number (bottom)

In top of Fig. 6 the free surface elevation is shown for the Froude numbers $Fr = 0.8$ (left), $Fr = 1.0$ (middle) and $Fr = 1.2$ (right) for a water depth-draught ratio of $h/T = 4.3$. With increasing speed the ship's bow is covered entirely with water. For the Froude number $Fr = 1.0$

and 1.2 splash water can be detected on deck of the aft ship. In the bottom row of Fig. 6 the wave field is shown for a Froude number of $Fr = 0.8$ and water depth-draught ratios of $h/T = 4.3$ (left), $h/T = 17.2$ (middle) and $h/T = 51.6$ (right). The difference in free surface elevation between the different water depths is large, with an increase in spreading angle of the wave contours and an elongation of the wave length.

In Fig. 7 the resistance coefficient (top), the sinkage (middle) and trim (bottom) are given for different water depth and Froude numbers. The values for a Froude number of $Fr = 0.8$ are given in blue, while the data for $Fr = 1.0$ and $Fr = 1.2$ are colored in red and green respectively.

It shows (top graph of figure) that for a Froude numbers of $Fr = 1.2$ the resistance of the hull is increasing with decreasing water depth, as is expected. However for $Fr = 0.8$ and 1.0 the relation is reversed and the hull resistance decreases with decreasing water depth. It is also shown that the resistance coefficient for $Fr = 1.0$ is smaller than for the other two speeds, as already shown during validation in Fig. 4. The shallow water affects the resistance of the hull in dependency of the ship speed.

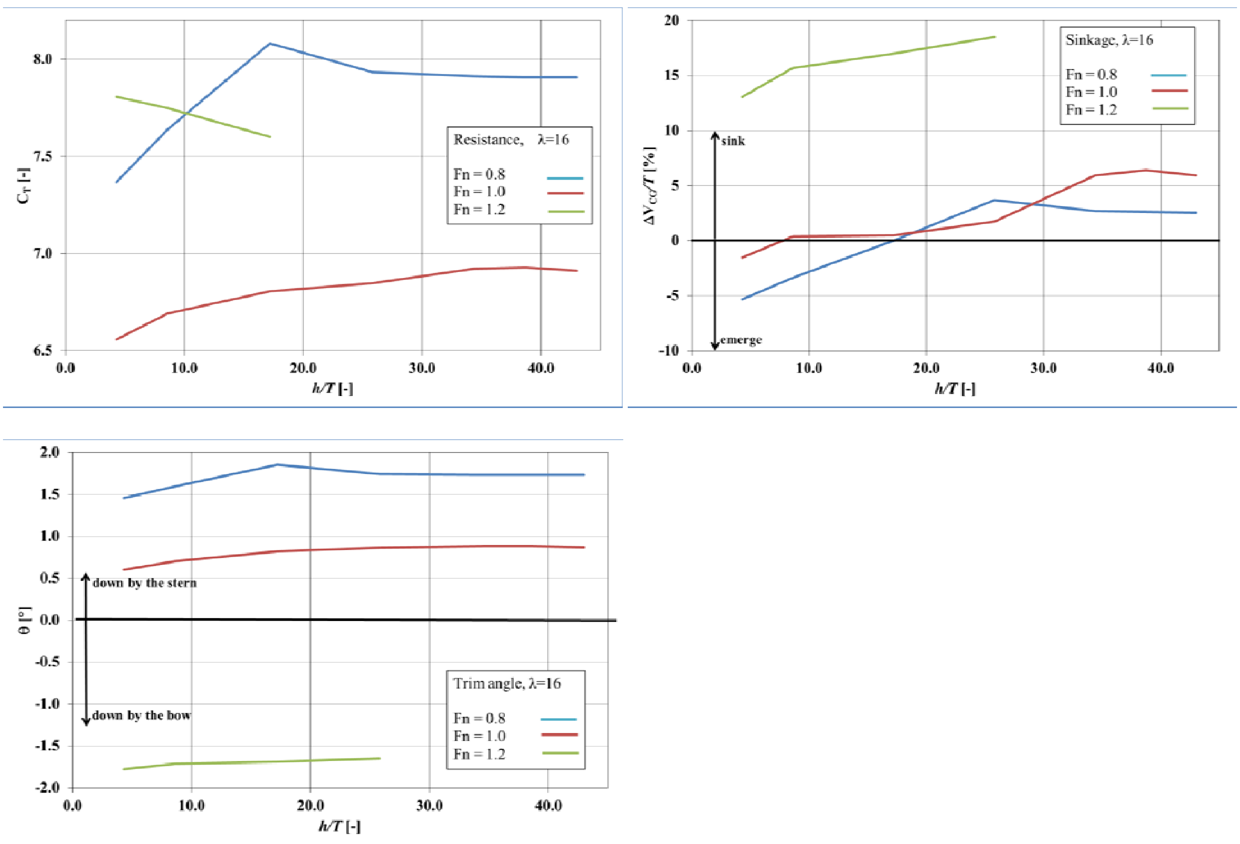

Fig. 7: Total resistance coefficient, sinkage and trim angle

- For $Fr = 0.8$ the resistance is affected by shallow water beginning from a water depth draught ratio of about $h/T < 25.8$.
- For $Fr = 1.0$ the resistance is affected by shallow water beginning from a water depth draught ratios of about $h/T < 34.4$.
- For $Fr = 1.2$ the water depth for which the resistance of the hull is affected cannot be determined yet.

In the middle graph of Fig.7, the sinkage of the center of gravity (slightly aft of amidships) is shown. Only in case of the smallest water depth and Froude numbers of *Fr* = 0.8 and 1.0 the hull comes out of the water. For the rest of the investigated operation points the hull has squad. This circumstance would give an explanation for the lower resistance of the hull in shallow water for the lower Froude numbers.

The trim angles for the different water depth and speeds are shown in the bottom graph of Fig.7. For Fr = 0.8 and 1.0 the hull trims to the stern, while for Fr = 1.2 to the bow. For all investigated operation points the trim angle decrease with decreasing water depth.

The finding that the resistance can also decrease in shallow water is at first a surprise and stands in contradiction to the general performance of ships in shallow water. To explain this circumstance a kind of “wing in ground” effect is considered to cause this finding. In this case, the hull experiences additional lift, caused by a pressure build up between bow and ground. This would also explain why the hull is lifted out of the water in these conditions, see Fig.7.

Further studies have to be conducted in order to verify this finding and to determine whether this also applies for other hull forms.

4. Conclusion

The effect of shallow water on the resistance of a fast going vessel was investigated numerically. The results show a large impact of shallow water on the ships performance.

The ship showed for a Froude number of *Fr* = 1.2 an increase in resistance in shallow water, while for the lower investigated speed range a decrease in resistance in shallow water was detected. This later is not what is generally expected. As explanation the “wing in ground” effect is considered. In order to verify this finding further investigations are being conducted.

The validation of the computed results with the corresponding measurements shows in general a good agreement. With increasing speed the discrepancies between experimental and computational data get larger. The comparisons could only be carried out for one water depth.

5. Acknowledgements

The author would like to express his gratitude for the support granted by the “Federal Ministry for economy and technology” under the registration number MF090192 of the project management of EURONORM.

References

LU ZOU, LARS LARSSON (2011), *A Verification and Validation Study Based on Resistance Submission to the Gothenburg 2010 Workshop on Numerical Ship Hydrodynamics*, 14^{th} Numerical Towing Tank Symposium, Poole, England

DUDSZUS, DANCKWARDT (1982), *Schiffstechnik, Einführung und Grundbegriffe,* VEB Verlag Technik Berlin

On Structural Design of High-Speed Planing Craft with Respect to Slamming

Mikael Razola, KTH Royal Institute of Technology, Stockholm/Sweden, razola@kth.se
Anders Rosén, KTH Royal Institute of Technology, Stockholm/Sweden
Karl Garme, KTH Royal Institute of Technology, Stockholm/Sweden
Ivan Stenius, KTH Royal Institute of Technology, Stockholm/Sweden
Alexandros Antonatos, KTH Royal Institute of Technology, Stockholm/Sweden

Abstract

In this paper a methodological framework that enables detailed studies of the loading conditions and structure responses for planing craft in waves is presented. The methodology is demonstrated by analysis of an aluminum and a sandwich version of a 10-meter high-speed craft during a slamming event. The results are used to discuss the abilities and limitations of the framework, various aspects of the slamming phenomena and the related responses, and the prevailing design principles for high-speed craft. The methodology is concluded to be useful in evaluation and development of the prevailing design methods and in establishment of a method for direct calculation.

1. Introduction

High-speed planing craft in irregular waves is a complex problem where the craft motions, acceleration, pressure distribution and structure response are closely interlinked. The slamming pressure distribution is transient, non-uniform and peaked, and each impact between the craft and the wave surface is unique. Due to the complexity of both the hydromechanic and the structural mechanic problem, methods for direct calculation of loads and responses are presently few. Moreover, experimental measurement of, for example, pressure loading and structure response is not trivial. Hence, the detailed loading conditions for high-speed planing craft structures exposed to slamming, are not yet fully mastered.

Today, structural design of high-speed planing craft is typically based on design loads derived using scantling codes such as *DNV (2011)* and *ISO (2008).* The load formulation used in these regulations is essentially based on a semi-empirical method developed during the 1970s by *Allen and Jones (1978)*. The slamming pressure distribution is here modeled as static and uniform, treating each structural component independently of others. These methods were derived with, at the time being, state-of-the-art experimental and numerical procedures, using contemporary craft. Since then, the technological advances in materials, production, and analysis techniques, have changed the way craft are designed and built. Modern material concepts, such as sandwich structures with fiber-reinforced laminates, have for exampled enabled development in structural layout with less secondary stiffening and larger panels. The validity of the semi-empirical design methods for such structures may therefore be questioned.

This paper presents a framework of interlinked methods that enables detailed studies of the loading conditions for planing craft in waves, with high resolution in both time and space. In an ongoing research project these methods are applied to perform phenomenological studies of the loading conditions for high-speed craft, to evaluate and challenge the prevailing semi-empirical design methods, and to establish alternative design methods based on direct calculation of loads and responses. The framework consists of four modules, the Rule-based scantlings module, the Slamming load module, the Finite-element module and the Signal-processing module, as shown in Fig.1. The Rule-based scantlings module is used to efficiently develop initial scantlings and enables parametric studies of different material concepts and structural arrangements. The slamming load module contains a numerical approach for simulation of the detailed slamming pressure distribution, and an experimental approach, where the slamming pressure distribution sequences are determined based on discrete point measurements. In the Finite-element module momentary slamming pressure distributions are applied on a fully parameterized model of the craft hull based on results from the scantlings module, and detailed structure responses are calculated in the time-domain. The signal-processing module is used to study the complete stochastic load and response processes for example containing methods for signal peak identification, and methods for calculating extreme response values. The different modules are here presented and calculations are demonstrated for one typical slamming event for one aluminum and one sandwich version of a 10-meter high-speed craft. The results are used to discuss various aspects of the slamming phenomena, the related structure response, and principles of high-speed craft design.

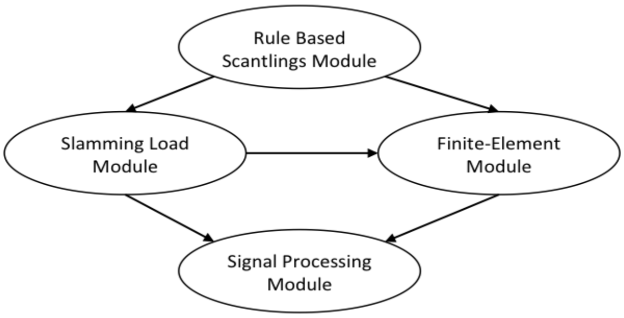

Fig.1: Schematic outline of methodological framework.

2. Methodological framework

The modules contained within the framework in Fig.1 are here presented using a 10.5-meter high-speed planing craft. The craft has a displacement of 6500 kg, and a deadrise angle of 22 degrees at the stern, which is increasing towards the bow. The focus in this particular study is on a section of the craft between 5≤*x*≤8 meters as shown in the linesplan in Fig.2, which is typically subjected to large slamming loads.

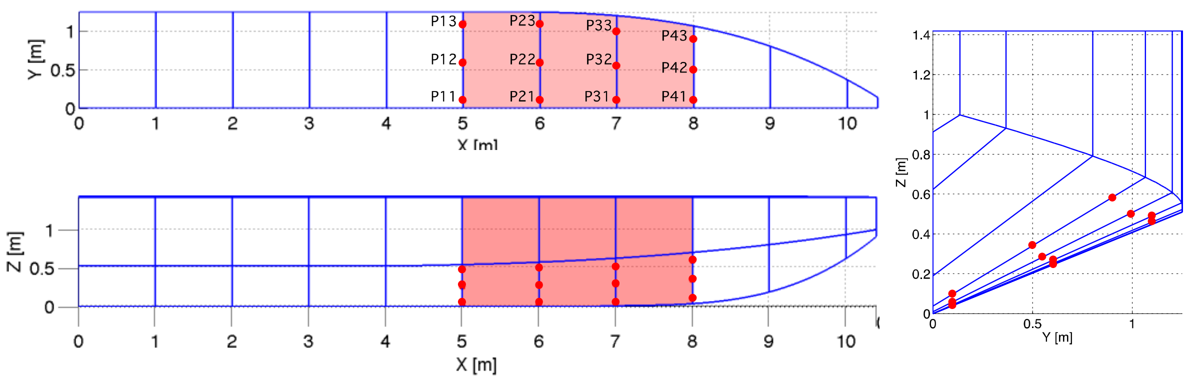

Fig.2: Linesplan of the studied craft with the studied section highlighted. Pressure transducer locations used for load derivation are marked ‘o’.

2.1. Rule based scantling module

The rule-based scantling module consists of a tool presented in *Stenius et al (2011a)*, which enables efficient parameterization of the craft structural arrangement, structural hierarchy and structural component cross-sections; automatic determination of scantling requirements regarding strength, stiffness or minimum thickness, for each individual structural element; rational evaluation of the structure efficiency; and iterative modification of the structure towards maximized efficiency and minimized weight. At present the automatic determination of scantling requirements are made based on *DNV (2011)*, but any scantling code could be implemented.

In this study the example craft is designed according to the rules and regulations of *DNV (2011)* for a service restriction R3 patrol, using a design acceleration of 5*g*, which is representative for a small, highly loaded patrol craft (*Koelbel 2001*). Two different versions of the craft are studied: an aluminum version and a carbon sandwich version. To simplify the analysis, the same displacement is used for the two craft versions even though the composite version probably would be lighter in a real case. The structure arrangement in the studied section is governed by a continuous primary girder at y=0.47 m which support engine and waterjet units at the stern.

The aluminum version is developed using an NV-5083 aluminum alloy with material properties according to Table 1. The rule-based scantlings module is used to iteratively refine the structural arrangement and, as seen in Fig. 3, within a few iterations a local minimum is typically found. In the final structural arrangement, displayed in Fig. 4, the craft bottom is divided longitudinally by three web frames, and transversely by three stiffeners and the girder. As seen the result is a densly stiffened structural arrangement with small panels. The stiffeners are L-profiles, while the webframes are simple flat bars. As usual, application of the handbook type formulas in the scantling code require rather drastic idealizations of the structural hierarchy. Here it is assumed that the stiffeners carry the loads from the plate fields, the webframes carry the loads from the stiffeners, and that the girder, keel and chine carry the loads from the webframes. The basic stiffener spacing in the bottom is between 235 and 280 mm, the girder web height is 190 mm and the webframe height 85 mm. The thickness of the bottom plating is 5.5 mm, for the girder web and flange 4.4 mm and for the stiffener web and flange the thickness is typically 4-5 mm.

Table 1: Mechanical properties for aluminum NV-5083.

Material properties NV-5083		
Tensile yield stress	205	MPa
Ultimate tensile strength	303	MPa
Shear yield stress	79	MPa
Young’s modulus	70	GPa

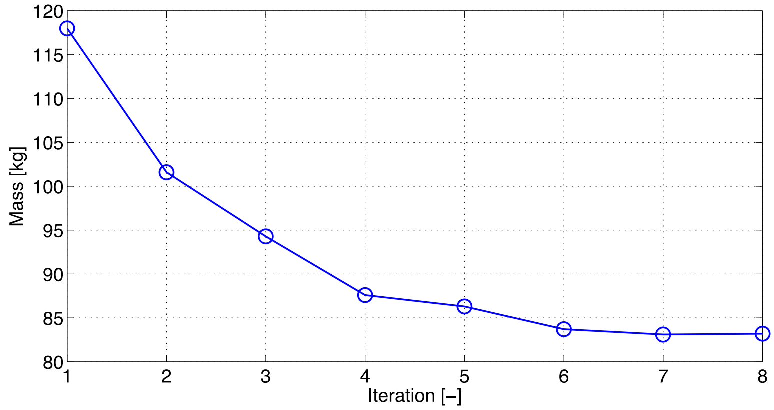

Fig.3: The mass of the hull bottom structure of the studied section of the aluminum version for successive design iterations.

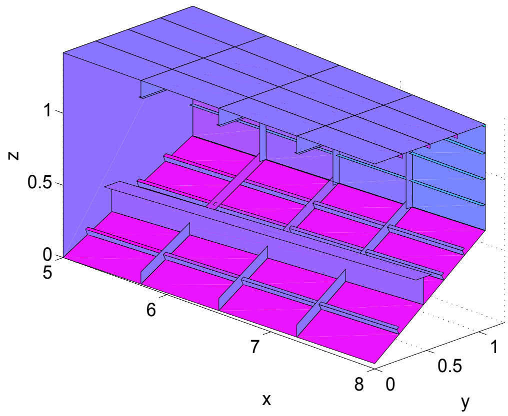

Fig.4: The structural arrangement of the aluminum version of the craft.

The composite version is designed using sandwich panels with a medium density foam core and quasi-isotropic carbon-fiber/vinylester laminates with material properties according to Table 2. The primary girder is of top-hat type with fibers aligned mainly in the ±45° direction in the webs and in the 0° direction in the flange. The final structural arrangement is, as expected, significantly different from that of the aluminum section. No secondary stiffening is used which result in large panels and a more obvious structural hierarchy, as seen in Fig. 5. The girder web height is 300 mm, and typical face laminate thicknesses are in the order of 1 mm, while the core thicknesses are 22mm.

Table 2: Mechanical properties of sandwich materials.

	Panel	*Web*	*Flange*	*Core*
Layup	[0°=25% 90°=25% ±45=25%]	[0°=10% 90°=10% ±45=40%]	[0°=72% 90°=14% ±45=7%]	Divynicell H-130
v_f	0.6	0.6	0.6	
E_{11} GPa	38	23	77	38
E_{22} GPa	38	23	-	-
σ_u MPa	300	184	616	3
τ_u MPa	115	168	48	2.2

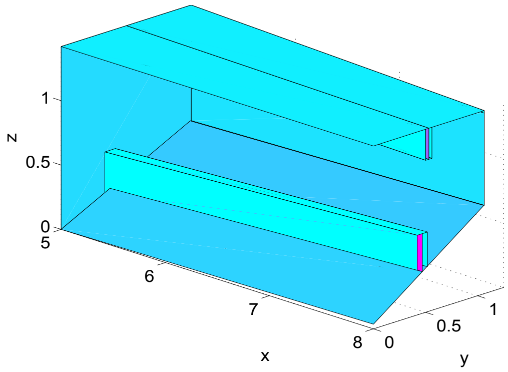

Fig.5: The structural arrangement of the sandwich version.

2.2. Slamming load module

The slamming load module contains two principally different load prediction methods: an experimental and a numerical approach. The numerical approach is based on a non-linear strip method which is used to simulate craft motions, accelerations and hydrodynamic section forces in irregular seas (*Garme&Rosen 2003, Garme 2005*). The momentary slamming pressure distribution is then modeled by scaling a pressure shape function with the simulated section forces. This approach has been shown promising as an efficient alternative to more extensive hydromechanics simulations (*Rosén 2004*). Fig. 6 exemplifies the modeled momentary slamming pressure distribution on the example craft in irregular waves. Clearly the approach captures the principal non-uniform and large gradient characteristics of the slamming pressure distribution in the chines dry region. In the chines wet region the pressure is modeled as uniform.

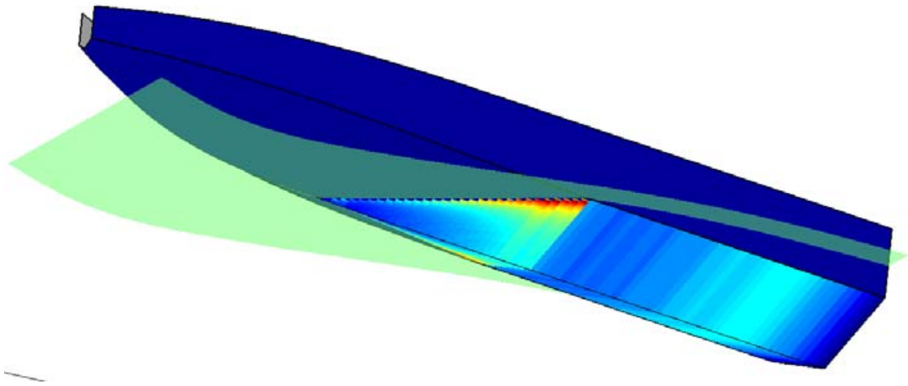

Fig.6: Modeled momentary slamming pressure distribution for the studied high-speed planing craft running in irregular waves.

Alternatively to numerical predictions, the momentary slamming pressure distribution can be determined based on model or full-scale experiments. The bottom of the craft is then instrumented with a matrix of high frequency pressure transducers and a method of Pressure Distribution Reconstruction (PDR) is then used to resolve the complete spatial pressure distribution (*Rosén 2005*). In short the PDR-method is based on a set of assumptions and interpolation techniques that relate measurements of the propagating pressure pulse in one position of the hull at a particular time instant to measurements in other positions at other time instants.

In the present study the slamming pressure distribution sequences are derived from measurements on a 1:10 scale model of the craft. The section is instrumented with 12 diaphragm pressure transducers according to Fig. 2 where a sampling frequency of 2500 Hz in model scale is used. The following results are however presented in full-scale. The model was towed in different speeds, wave heights and wave periods and the runs were repeated to obtain sufficiently large samples for statistical evaluation of global response. In this study the focus is on one severe slamming event, occurring during the period $51.220 \leq t \leq 51.386$ s, in the conditions outlined in Table 3.

Table 3: The full-scale conditions represented in the model experiments.

Speed	*Wave height*	*Wave period*	*Wave spectrum*
14.2 m/s	1 m	3.8 s	ITTC

In Fig.7 the measured acceleration time-series for the studied slamming event is displayed. The acceleration signal is low-pass filtered to 50 Hz, ensuring that only rigid body accelerations are present. As seen, the peak acceleration value for this particular slamming event is 3*g*.

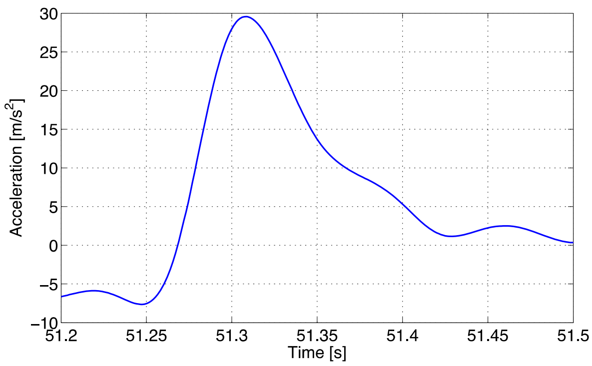

Fig.7: Acceleration time-series during the studied slamming event.

In Fig.8 the measured pressure magnitude time-series for each pressure transducer are displayed, and in Fig. 9 the corresponding reconstructed momentary slamming pressure distribution at three different time instants. The peaked and transient character of the slamming pressure distribution is clearly captured, were the largest pressures occur close to the keel during the initial phase of the impact. During this particular slamming event the peak pressure reaches 224 kPa at t=51.2656 s and as the pressure pulse propagates towards the chine the magnitude decreases due to craft deceleration.

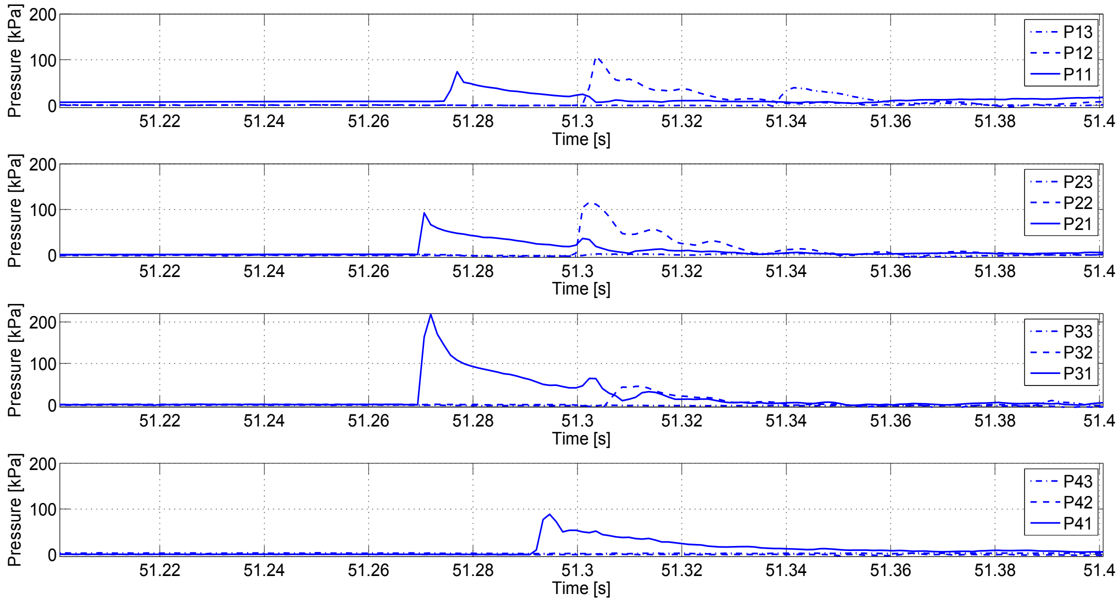

Fig.8: The measured pressure time-series. Transducer locations displayed in Fig.2.

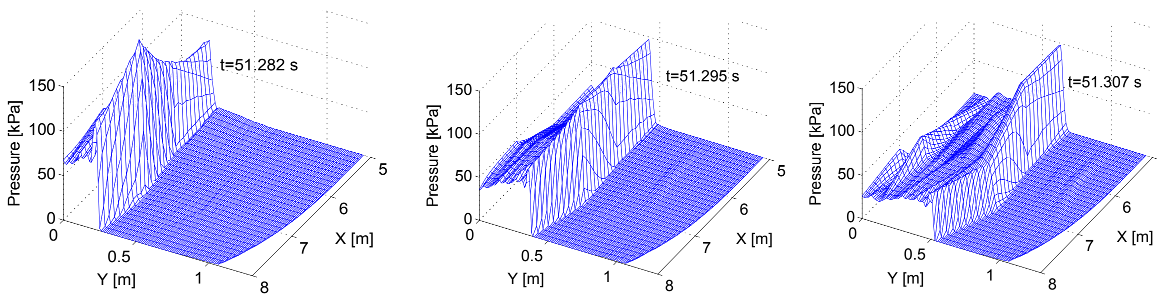

Fig.9: The reconstructed slamming pressure distribution at three different time-instants.

As stated, the two craft versions in this paper are design using a design acceleration of 5*g*. This acceleration measure is according to DNV (2011) that value with a 1% probability of being exceeded. Assuming a 3-hour stationary sea state, the extreme acceleration value for the studied running conditions is 6.8*g*, while the average of the upper $1/10^{th}$ and $1/100^{th}$ peak acceleration values are 4.4*g* and 5.2*g* respectively. It is therefore clear that the present running conditions are severe, and resulting stress levels close to or even above allowable limits should be expected.

2.3. Finite-element module

The finite-element module is developed based on the fundamental assumptions that the structure deformation does not affect the pressure loading, and that that the natural frequencies of the structure are large compared to the loading frequencies. The assumption of no hydroelastic interaction enables the pressure distribution to be applied on the FE-representation of the craft quasi-statically in each time-step. Using the python scripting capabilities of the standard FE-software ABAQUS, a fully parameterized finite-element model of the studied craft is generated based on a geometry offset file and the results from the rule-based scantlings module (*Antonatos 2012*). The craft structure is modeled using a combination of shell and beam elements. Either the complete craft may be studied, where the boundary conditions are enforced through inertia relief, such as in Fig. 10, or a section of the craft may be studied in greater detail.

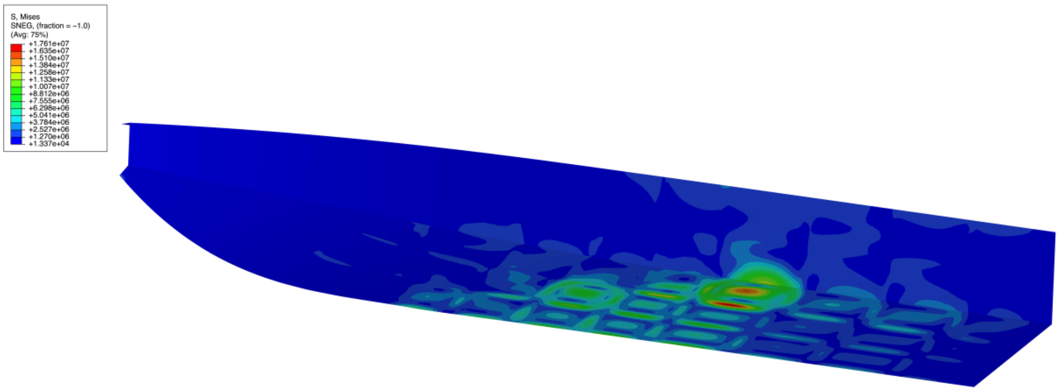

Fig.10: An example of calculation of equivalent stress distribution due to the momentary slamming pressure distribution in Fig.6.

In this study the two craft versions are modeled using a combination of 8-node quadratic shell elements (S8R) for the plating and primary girder webs, where the through thickness shear stresses are estimated for the sandwich components, and 3-node quadratic beam elements (B32) for secondary stiffening and girder flanges. The sandwich panels are modeled using three laminas, where the faces are represented by one lamina each and the core by one lamina, using material properties from Table 2. The FE-models of the two different craft versions are displayed in Fig.11. Of primary interest is the structure response in the bottom of the craft due to slamming, however, for proper modeling of the chine stiffness, the model also incorporates the side structure. Symmetry boundary conditions are applied along the centerline of the section, while the aft, forward and deck edges of the section are modeled as fixed. Based on nearest neighbor interpolation of the highly resolved pressure distribution from the slamming load module, the pressure load for each element on the craft bottom is calculated in each time-step. The mesh density is selected based on a convergence study that considers both the FE-solution itself, but also the ability of the mesh to resolve the peaked slamming pressure distribution. A transverse element length of 25 mm gives convergence within a few percent.

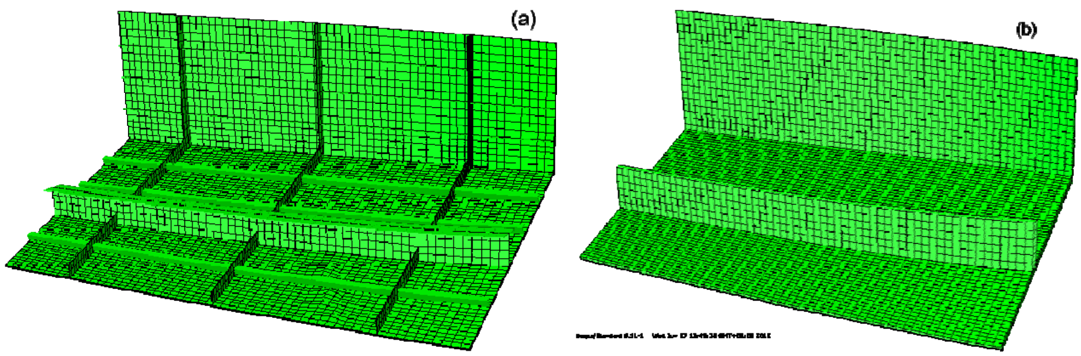

Fig.11: Finite-element models of the aluminum (a) and the sandwich (b) versions.

2.4. Signal processing module

Performing the fluid-structure interaction modeling with the non-linear strip method and the quasi-static load application require relatively limited computational efforts. Hereby long simulations in irregular waves are feasible. Due to the stochastic and irregular character of the waves, global craft response as well as the local structure response, these processes must be described using statistics. The signal-processing module contains methods for peak characterization and identification in both global craft response and in structure response signals. It also contains methods to calculate statistical measures such as averages of a certain fraction of peak values and extreme response values. Instead of studying a large number of impacts and applying statistics, the main focus of the present study is on a single slamming event that is used to demonstrate in-depth studies of the loading conditions for high-speed craft in both time and space. Therefore this module is not covered in detail in this paper.

3. Results

Here the potential of the outlined methodology is demonstrated by presenting a selection of results from the analysis of the two craft versions. These results will then be used in the following section to discuss various aspects of the methodological framework and its application within the present research project.

In Fig.12 the momentary slamming pressure distribution at two time instants during the studied slamming even are displayed together with the corresponding deflections for the aluminum and sandwich structures. It can be observed that the non-uniform pressure distribution is clearly resolved by the selected mesh density. Typical maximum plate deflections for the aluminum version are 4.7 mm, and for the sandwich version 10.0 mm, while the maximum girder deflection is 2.5 mm and 5.7 mm for the aluminum and sandwich versions respectively.

As stated, the studied running conditions are rather severe. During the studied impact, the maximum panel bending stress is 200 MPa for the aluminum version and 116.7 MPa for the sandwich version, found in panels adjacent to the keel. For the aluminum version this stress level coincides with the yield stress of the material and is hence above the allowable stress limits. The maximum panel bending stresses occur at a time-instant when the pressure pulse has traversed the complete inner panel, both for the aluminum and sandwich craft versions. For the sandwich version, the maximum core shear stress occurs at the keel, before the pressure pulse has reached the midpoint of the panel, and reaches a magnitude of 1 MPa, approximately 50% of the core shear failure stress as seen in Fig.13. For panels between the girder and chine, the maximum bending stresses at the panel midpoint, and the maximum core shear stresses at the girder joint, occur at a time-instant when the pressure pulse has only traversed half the panel. This is likely due to the lower stiffness of the joint between the plating and girder compared with the keel. Also, due to craft deceleration, loads and consequently stress levels typically decrease closer to the chine.

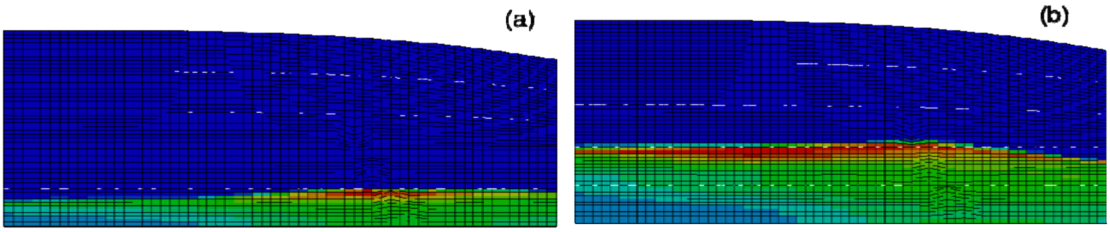

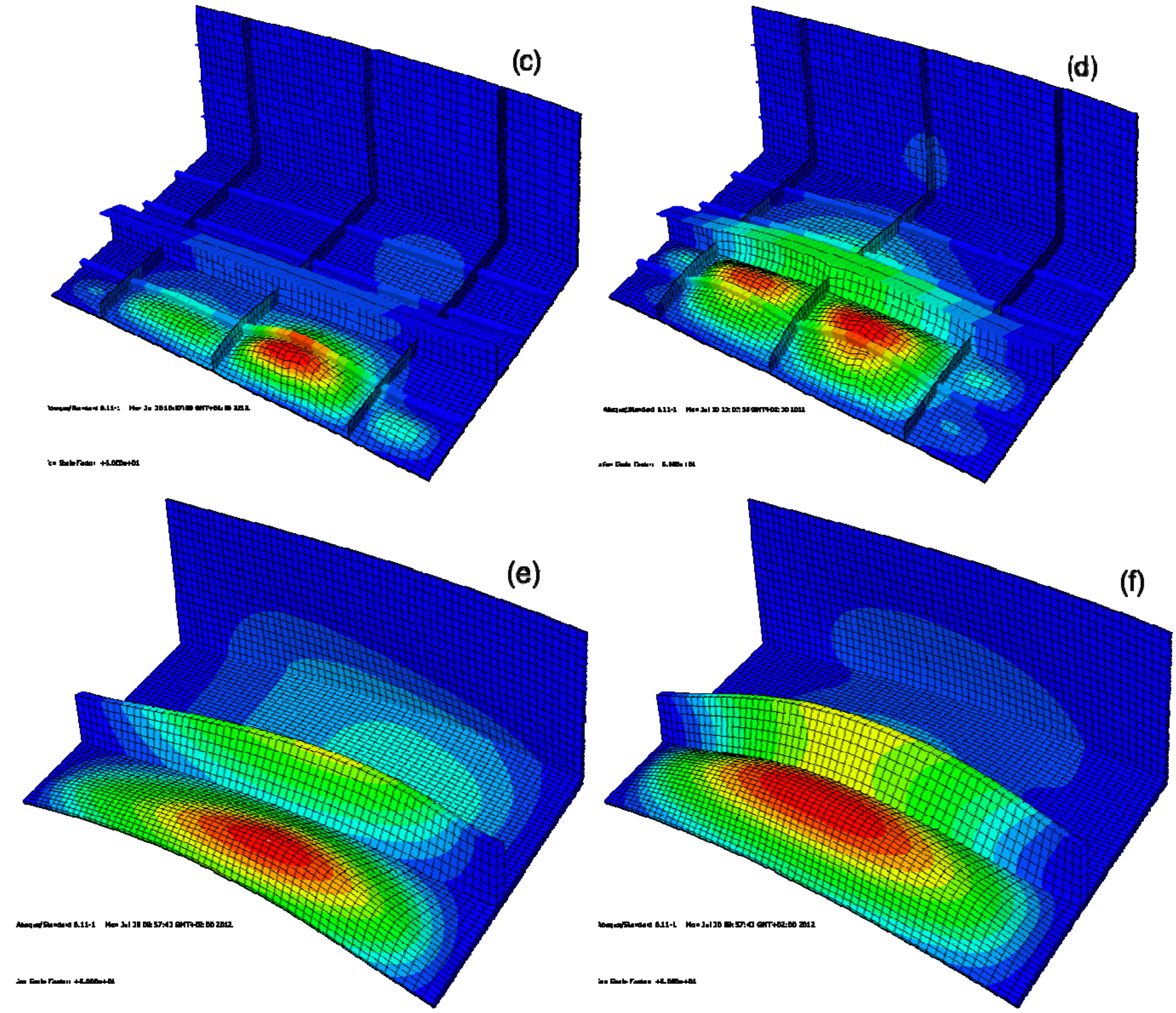

Fig.12: Deflection magnitude of the aluminum structure (c-d) and the sandwich structure (e-f) due to the momentary slamming pressure distribution (a-b). For illustrative purposes the structure responses are scaled using a factor of 50.

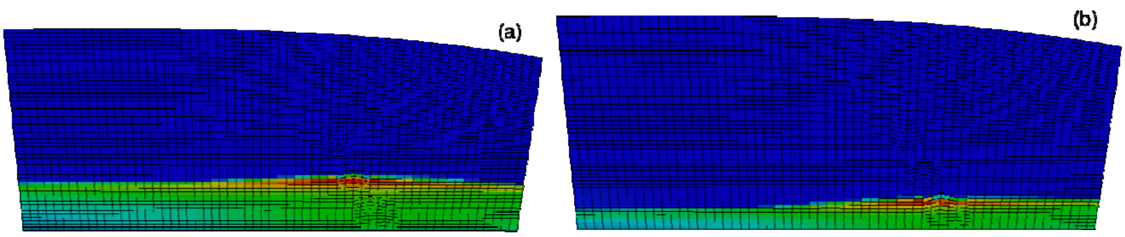

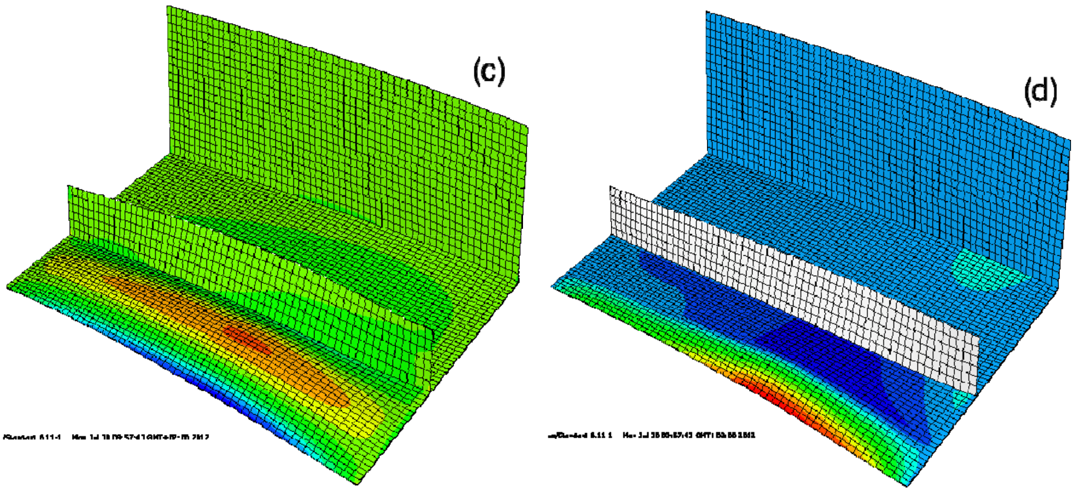

Fig.13: Pressure and shear stress distribution at maximum bending stress (t=51.287 s) (a and c) and at maximum core shear stress (t=51.277) (b and d) for the sandwich version of the craft.

Fig.14 displays time-series of bending stresses in the flanges at the aft and fore end of the girders for both the aluminum version and sandwich version. The maximum stresses occur at a time-instant when the pressure pulse has traversed across half the bottom, this time instant also corresponds well to the instant of total maximum load. Further, the time-instant of maximum bending stress in the girder corresponds well between the aluminum and sandwich versions of the craft. It is however clear that the loading situation is more complex for the aluminum version where there are larger differences in maximum stress values at the forward and aft end of the girder due to the non-uniform load distribution also in the longitudinal direction. In Fig.15 the time-series of bending stress for the panels where the largest stresses are found, are displayed. The maximum stresses are for this particular slamming event found in the panels adjacent to the keel, for both craft versions. The load rise time is as seen significantly shorter for the smaller aluminum panel compared to the larger sandwich panel.

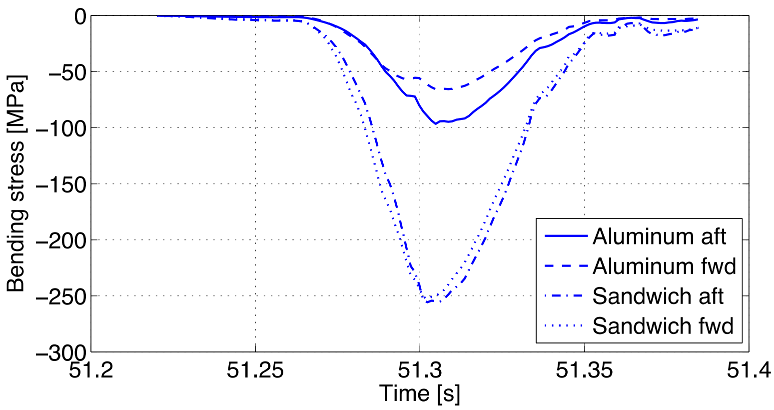

Fig.14: Time-series of bending stress in the flange at the aft and forward end of the primary girder for the two craft versions.

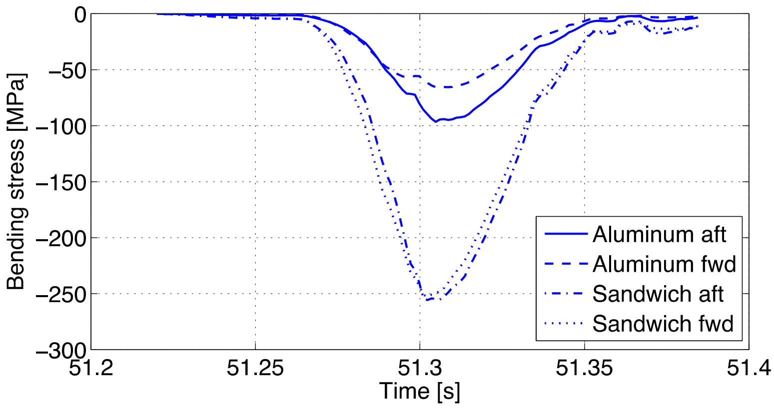

Fig.15: Time-series of panel bending stress for the highest loaded panels for the two craft versions.

In Fig.12 it can be seen that a large twisting moment is inferred on the primary girder due to the non-uniform character of the slamming pressure loading. Such deformations of course affect the effective boundary conditions of the surrounding structure. The developed methodology can be used for detailed studies of such effects. As an example the stiffener effective boundary conditions are highlighted through Fig. 16 where the deflection and rotation about the y-axis along the stiffener closest to the keel in the aluminum craft version at the instant of maximum deflection are displayed. It can be seen that due to the non-uniform character of the pressure loading in the longitudinal direction the effective boundary conditions for the different segments of the stiffener varies significantly as the slamming load propagates across the bottom.

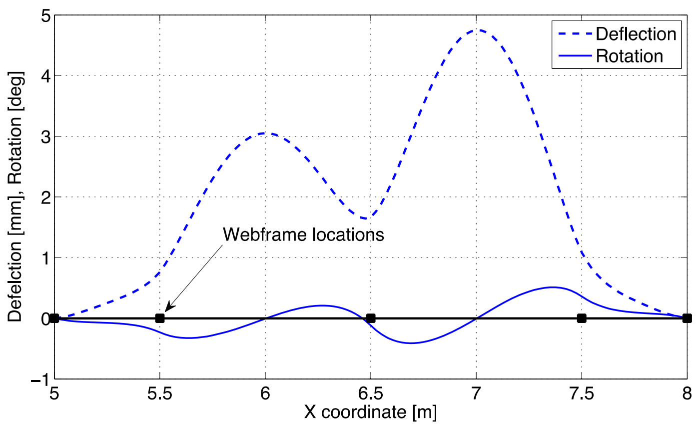

Fig.16: Deflection and rotation about the y-axis along the stiffener closest to the keel at the instant of maximum deflection.

4. Discussion

The results presented in the previous section demonstrate some of the potential in the developed methodology regarding detailed studies of the loading conditions and structure responses for high-speed planing craft. Several of the methods contained within the methodological framework have been verified and validated. The nonlinear strip-method is for example extensively validated in *Garme&Rosen (2003)* and *Garme (2005),* while the pressure modeling technique has been studied in *Rosén (2004)* and *Razola et al (2012).* The alternative pressure reconstruction method based on experimental measurements has been validated in *Rosén (2005).* There are however parts of the methodology that require further development and evaluation in the pursue of establishing a method of direct calculation. For example the FE-module and the signal-processing module are currently under further development, and future work also include full-scale validation of the predicted structure responses. Here some of the assumptions and idealizations in the developed methods and in the present study will be discussed, along with application of the methodological framework in the evaluation and development of the prevailing semi-empirical design methods and direct calculation methods.

4.1. Quasi-static assumption

One fundamental assumption that enables the presented analysis is, as stated, that the hydroelastic interaction between the hydrodynamic loading and the structure response may be neglected. In for example *Stenius et al (2011b)* and *Bereznitski (2001)* methods for characterization of the importance of hydroelastic effects are presented. According to *Bereznitski (2001)* the hydroelastic effects can be characterized by the ratio, R, between the natural frequency of the dry structure and the loading frequency, where the loading frequency is defined as twice the time for the stress level to rise from zero to its maximum value. For $R>2$ limited effects of hydroelasticity are to be expected. Based on the results from Fig. 14 and Fig.15, the loading frequency of the girders is found to be ~15 Hz for both craft versions. The highest panel loading frequency is 36 Hz for the aluminum version and 21 Hz for the sandwich version. In this study the first natural frequency of the dry aluminum bottom structure is 105 Hz and 90 Hz for the sandwich structure.. This implies an R-value of ~3 for the aluminum structure, and R-value of ~4 for the sandwich structure. This infers that the assumptions regarding quasi-static loading conditions are indeed reasonable, at least for this particular slamming event.

4.2. Semi-empirical design methods

As stated, the rules and regulations governing design of high-speed craft with respect to slamming loads, rely to a large extent on methods developed during the 1960’s and 1970’s based on analysis of densely stiffened aluminum or steel craft from that time. The validity of those methods for modern fiber-reinforced sandwich craft may therefore be questioned. The simulations presented in the previous section will here be used to highlight some questionable aspects.

A fundamental modeling assumption in the semi-empirical methods is that the slamming pressure may be modeled by a uniform pressure, which in some sense should be equivalent to the real slamming load for example regarding the total load or the bending moments. In Table 4 the maximum stresses in a panel adjacent to the keel in the two craft versions during the studied slamming event, are presented together with the stress levels due to a force equivalent uniform pressure applied quasi-statically to the same panels. The force equivalent pressure is here calculated as the maximum value of the integrated slamming pressure distribution on each of the considered panels. Due to the peaked character of the pressure distribution, the maximum average pressure is larger on the smaller aluminum panel at 96.7 kPa, compared to the larger sandwich panel where the maximum average pressure is 51.4 kPa. As seen the force equivalent uniform pressure results in an 11% underestimation of the bending stresses for the smaller aluminum panel and an underestimation of as much as 25% for the larger sandwich panel. Similarly, in Fig.17 the shear stress distribution across the sandwich panel adjacent to the keel is displayed due to the uniform pressure and due to the real reconstructed pressure at the time-instants of maximum shear stress at the keel and at the bottom girder joint. The shear stresses in the panel both at the keel and at the girder are underestimated by as much as 30% by representing the actual slamming pressure distribution by a uniform pressure.

Table 4: The maximum stress levels due to the reconstructed slamming pressure distribution and due to a force equivalent uniform pressure.

	Aluminum version	*Carbon version*
Max panel bending stress (reconstructed pressure)	200 MPa	117 MPa
Max panel bending stress (uniform pressure)	179 MPa	88 MPa
Max core shear stress (reconstructed pressure)		1 MPa
Max core shear stress (uniform pressure)		0.7 MPa

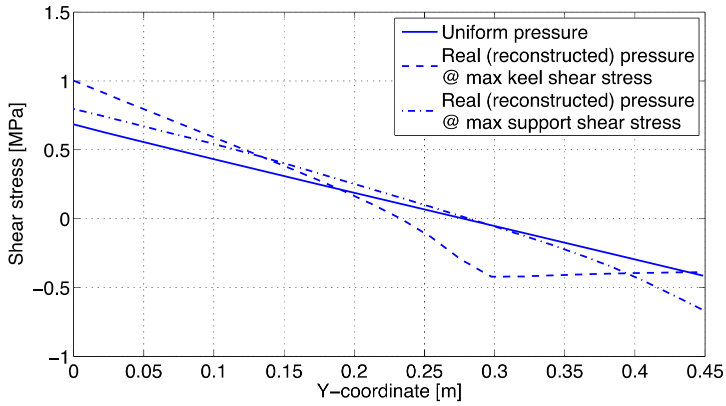

Fig.17: Shear stress distribution across the sandwich panel adjacent to the keel.

In the prevailing semi-empirical design methods, handbook formulas based on basic mechanics are used for calculation of deformations and stresses in common structural members such as beams and plates. Naturally, simplifications and assumptions follows, such as using simplified boundary conditions where the recommendations typically vary between fixed and partially fixed depending on structure member and load case (e.g. *DNV 2011*). However, as noted in Fig.12 the structural behavior due to slamming for the present craft violates some of these basic assumptions. In the aluminum version the stiffeners are instead of transferring the load to the webframes, deflecting with the plating, resulting in that the plate fields between girder, keel and webframes in principle act as a single structural component. The webframe and girder beam system also in principle deflects as a single unit, and it would therefore be more appropriate to idealize the web frame span as the full distance between keel and chine in the rule-based scantling calculations in this case. It is also shown in Fig. 16 that the stiffener boundary conditions for cases where fixed boundaries typically are assumed due to structure and load symmetry, may indeed be questioned.

In the ongoing research project the presented methodological framework is used to perform an extensive evaluation and development of the prevailing semi-empirical design methods for more conventional densely stiffened metal craft as well as for modern sandwich craft. Besides the issues highlighted here, the research project also considers other aspects, such as the rationale behind using statistical measures of the vertical acceleration at the craft center of gravity to express local design loads, and the effects of panel or load carrying area aspect ratio on the design pressure levels.

4.3. Direct calculation of loads and responses

Due to the complexity of the loading and response situation for high-speed craft in irregular waves, refinement and optimization of high-speed planing craft structures will require direct calculations. In the ongoing research project the presented methodological framework forms the basis for establishing a direct calculation design method. This work for example includes further evaluation of the slamming load module, further development of the signal processing module, material modeling and development of related design criteria.

Along with the here presented research project it is also worth mentioning some other ongoing efforts by other research groups on establishing direct calculation methods for high-speed craft. Regarding the hydromechanic problem of planing craft in waves there are examples of detailed CFD approaches such as those in *Campanetto (2004)* and *Fu et al (2011)* and less complex strip-methods similar to that applied here such as *Akers (1999).* There are also approaches that take a more complete grasp on both loads and response prediction such as the design methodology presented in *Phillips et al (2004),* where a simplified numerical procedure is used to derive the hydrodynamic forces which are then applied on a FE-model of the craft to derive structure responses, and in *Gupta et al (2003)* a methodology for prediction of route/mission dependent rational design loads is presented. Hopefully these collective efforts will enable a leap forward in structural design of high-speed planing craft.

5. Conclusions

This paper gives insight into an ongoing research project aiming at challenging and further developing the structural design methods for high-speed planing craft. Within this project a methodological framework has been developed that enables detailed studies of the loading conditions and responses for high-speed planing craft in arbitrary wave systems. The paper gives a brief account of the different modules in this framework and demonstrates the abilities of the framework in calculation of loads and structure responses for an aluminum version and a sandwich version of a typical 10-meter high-speed craft.

The efficiency of the presented methodology enables long simulation times where statistics can be applied to study the load and response phenomena. In this study the focus is however on one single slamming event to demonstrate the level of detail the can be studied, and to discuss various aspects of the prevailing design principles for high-speed planing craft. The complexity of the loading and responses for planing craft structures and some of the questionable aspects of the prevailing semi-empirical design methods are highlighted. It is for example shown that the panel fields in the aluminum version of the craft in principle behave as one unit, and that the function of the stiffeners, as well as the assumptions regarding structural hierarchy in the rule-based scantling calculations, can be questioned. It is also shown that modeling of the actual slamming pressure distribution as a uniform pressure may under-predict structure response by as much as 30%, and that the use of a uniform design pressure might be differently valid for different material concepts.

The presented methodological framework is concluded to have a large potential, enabling detailed and extensive parametric studies of loading conditions and structure interaction for high-speed craft in waves. Future and ongoing work involves further development and evaluation of the methods in the framework, and application of the framework in the evaluation and development of the prevailing semi-empirical design methods, and in establishment of a method of direct calculation of loads and responses for high-speed craft in waves.

6. Acknowledgements

This research has been financially supported by FMV (the Swedish Defense Materiel Administration) and the U.S. Office of Naval Research Solid Mechanics Program grant no. N00014-07-1-0344.

References

AKERS, R.H. (1999), *Dynamic Analysis of Planing Hulls in the Vertical Plane*, presented at SNAME New England Section Meeting, April 29.

ALLEN, R. G.; JONES, R.R. (1978), *A Simplified Method for Determining Structural Design Limit Pressures on High Performance Marine Vehicles*, AIAA/SNAME Advanced Marine Vehicle Conference, April.

ANTONATOS, A. (2012), *Parameteric FE-modeling of High-speed Craft Structures*, Master Thesis, Royal Institute of Technology, Stockholm, Sweden.

BEREZNITSKI, A. (2001), *Slamming: The Role of Hydroelasticity*, International Shipbuilding Progress 40/4.

CAPONNETTO, M. (2002), *Seakeeping Simulation of Fast Hard Chine Vessels using RANSE*, 5th Numerical Towing Tank Symposium, NuTTS, Pornichet, France.

PHILLIPS, H.J.; CRIPPS, R.M.; REES, S.J.; VAUGHN, L.F. (2004), *The Development and Validation of a Hydrodynamic and Structural Design Methodology for High-Speed Rescue Craft*, RINA International Conference on High-Speed Craft.

DNV (2011), *Rules for Classification of High Speed, Light Craft and Naval Surface Craft*, June.

FU, T.C.; AKERS, R.; O'SHEA, T.; BRUCKER, K. (2011), *Measurements and Computational Predictions of a Deep-V Monohull Planing Hull*, 11th International Conference of Fast Sea Transportation, FAST, Honolulu, Hawaii, USA, September.

GARME, K.; ROSÉN, A. (2003), *Time-Domain Simulations and Full-Scale Trials on Planing Craft in Waves*, International Shipbuilding Progress 50/4.

GARME, K. (2005), *Improved Time-Domain Simulation of Planing Hulls in Waves by Correction of the Near Transom Lift*, International Shipbuilding Progress 52/3.

GUPT, A M.; MCCAIN, M.; EISELE, D. (2003), *A Route or Mission-Dependent Approach for the Calculation of Rational Structural Dynamic Loads for High-Speed Multihulls*, SNAME Annual Meeting, San Francisco.

ISO (2008), *Part 5: Design Pressures for Monohulls, Design Stresses, Scantling Determination*, ISO 12215-5:2008 Hull Constructions and Scantlings.

KOELBEL, J.G. (2001), *Structural Design for High Speed Craft Part II*, Professional Boatbuilder 68, December/January.

RAZOLA, M.; ROSÉN, A.; GARME, K. (2012), *Experimental Evaluation of Slamming Pressure Models used in Structural Design of High-Speed Craft*, submitted for publication.

ROSÉN, A. (2004), *Loads and Responses for Planing Craft in Waves*, PhD Thesis, Royal Institute of Technology, TRITA-AVE 2004:47, Stockholm, Sweden.

ROSÉN, A. (2005), *Impact Pressure Distribution Reconstruction from Discrete Point Measurements*, International Shipbuilding Progress 52/1.

STENIUS, I.; ROSÉN, A.; KUTTENKEULER, J. (2011a), *On Structural Design of Energy Efficient Small High-Speed Craft*, Marine Structures 24/1.

STENIUS, I.; ROSÉN, A.; KUTTENKEULER, J. (2011b), *Hydroelastic Interaction in Panel-Water Impacts of High-Speed Craft*, Ocean Engineering 38/2-3, February.

Study of WIG Dynamics under Different Perturbations

Nikolai Kornev, Andreas Groß, N.Danh Dang, Ravi Pendyala
Chair of the Modelling and Simulations, University of Rostock,
A. Einstein Str.2, 18059 Rostock, Germany

Abstract

The paper presents the motion time domain simulation of WIG craft of the Lippish type under wind and wave perturbations. The aerodynamic characteristics were obtained using the vortex lattice method. The motion is considered in the longitudinal plane. A novel approach is proposed to generate artificial wind turbulence with prescribed kinetic energy and spectra. The wave surface is modeled by the plane performing linear and angular oscillations. The motion simulation was performed to show the limitations of flight safety analysis based on the classical stability theory. Simulation of the take-off motion was carried out to determine the conditions for safe transition from the skimming mode to the flare one. It was shown that the application of the flight control is necessary for the safe flight near the ground.

1. Introduction

WIG craft are still considered as a very promising transport. They are much faster than any other high speed ships and possess amphibian properties. The lift to drag ratio L/D of wings near the ground can attain values over 30. For comparison, the L/D ratio of modern airplanes is around 20 and the possibilities to improve it have been sufficiently exhausted. That is why the WIG craft attract attention of both aviation industry and shipbuilding. The efficiency of the WIG craft depends on the size. To utilize the ground effect in a full manner the relative height of flight referred to the wing chord should be as small as possible and not exceed 0.2-0.3. However, the minimum height of flight near the free surface is limited by waves and safety considerations. Therefore only large craft can fly at small relative heights of flight and completely utilize the ground effect attaining high L/D ratio. Development of ultra large WIG craft like Pelican designed by Boeing, *Rawdon and Hoisington (2003)*, is getting probable with the appearance of modern light materials. Most of WIG craft in use today are relatively small machines which have modest L/D ratios and are attractive because of their amphibian properties.

The development of WIG craft started at the end of fifties is still not resulted in the creation of any serially manufactured machine. The weights of prototypes are ranged from around 500 ton (Soviet KM) to a few hundred kilograms. There is the opinion that the three following problems prevent the WIG development: Overpowering necessary to perform the take-off at rough sea condition, strengths problems associated with the water impact of wing elements, especially flaps and stability. The stability problem is a very serious one and this is the reason of almost all accidents happened with the WIG craft. This problem is in focus of the present paper.

The linear WIG stability theory was developed in the sixties by Irodov in the Soviet Union, *Irodov (1970)*, and Staufenbiel in Germany, *Staufenbiel und Yeh (1976)*. Most detailed description of the dynamics, stability and control of WIG craft is given by *Zhukov (1997)* and *Diomidov (1996)* who made serious contribution to the design of all famous Soviet ekranoplanes. Overview of some results can be found in the book of *Rozhdestvensky (2000)* and in the SNAME handbook, *K.Fach, H.Fischer, N.Kornev and U. Petersen (2004)*.

The stability can be secured by the proper design of wing arrangement and application of the automatic control. The requirements for the design were formulated by specialists of Alexeyev Burea and TSAGI on the base of analytical investigations, numerous tests with models and large scale craft. They are partly presented, for example, in *N.V.Kornev and K.Matveev (2003).* There are two very efficient design rules to improve stability by use of S-shaped profiles and tail units placed relatively far from the main wing. According to the experience gathered by the authors (NK), all other design measures are not efficient and their effect on stability and aerodynamics is often contradictory.

WIG craft designed by Russian and German specialists were thoroughly proved using the linear stability theory and nonlinear motion simulations. Although all famous craft satisfy the criteria of both static and dynamic stability, the trial tests and operation of WIG craft has been accompanied by stability problems. One possible reason is the fact, that the classical stability theory is based on linear representation of forces which are strongly nonlinear near the ground. Also the prediction from the classical stability theory is valid for the case of small perturbations. *Avvakumov (2000)* introduced the term of the stability “in small” meaning the stability predicted by the linear stability analysis to differentiate it from the stability “on the whole”. The realistic perturbations cannot be considered as small ones and the conclusions drawn from the linear stability theory are not sufficient to guarantee the safe flight.

One of the authors (NK) was involved in stability evaluation of a certain number of WIG craft. Despite the stability “in small” the behavior of these craft was not always quite satisfactory under real flight conditions. The reason for this contradiction is perhaps that the WIG craft considered as a dynamic system possesses substantially nonlinear properties, *Avvakumov (2000)*. Therefore, the safety of the stable “in small” WIG craft without the flight control can be guaranteed only for a certain level of perturbations which is sufficiently limited in ground effect.

The idea of this study was to take a WIG craft which is faultless from the point of view of the classic stability analysis and simulate its motion under perturbations of different level to show the limitations of the linear stability theory for the prediction of the flight safety. The hypothetical WIG craft of the Lippish type is studied with and without flight control system. In this paper we consider only the motion with three degree of freedom in the longitudinal plane.

In the theoretical part (sections 2 and 3) we present the mathematical models used for the calculations of aerodynamics and time domain simulation of the WIG motion. A novel method for generation of wind perturbations with prescribed spectra and turbulent kinetic energy depending on the flight height is described in the section 2.3. The study of nonlinear motion (section 4) was performed as the time domain simulation in cruise regime and in the transition from the water born to the flare mode. The impact of wind and waves is investigated in the cruise using the models developed in the sec. 2.3 and 2.4. The conclusion ends the paper.

2. Mathematical model

2.1. Aerodynamics

The aerodynamic model is based on the representation of forces in a form of truncated Taylor series. This idea taken from the aviation has sufficiently been modified by Prof. Valentin Treshkov in the late of sixties. The original force coefficient C representation used in aviation reads

$$C(\alpha,t)=C^0\left(\alpha_0\right)+\frac{\partial C}{\partial\alpha}(\alpha_0)\left(\alpha(t)-\alpha_0\right)+\frac{\partial C}{\partial\dot{\alpha}}(\alpha_0)\frac{\dot{\alpha}(t)b}{U_a}+\ldots \qquad (1)$$

where α is the angle of attack. In the proximity to the ground the force coefficient depends additionally on the height of flight *h*. A formal extention of (1) to the ground effect aerodynamics is

$$\begin{gathered}C(\alpha,h,t)=C^0(\alpha_0,h_0)+\frac{\partial C}{\partial\alpha}(\alpha_0,h_0)\left(\alpha(t)-\alpha_0\right)+\frac{\partial C}{\partial h}(\alpha_0,h_0)\left(h(t)-h_0\right)+\\ \frac{\partial C}{\partial\dot{\alpha}}(\alpha_0,h_0)\frac{\dot{\alpha}(t)b}{U_a}+\frac{\partial C}{\partial\dot{h}}(\alpha_0,h_0)\frac{\dot{h}(t)}{U_a}+\ldots\end{gathered} \qquad (2)$$

Treshkov noted that the representation (2) is not convenient for WIG craft because of ambiguous definition of the angle of attack. In the aviation the angle of attack can be produced either by the craft pitching rotation $\alpha=\vartheta$ or by the vertical motion $\alpha=\frac{\dot{h}(t)}{U_a}$. There is no difference between two ways of the angle of attack production and $\frac{\partial C}{\partial\alpha}(\alpha_0,h_0)=-\frac{\partial C}{\partial\dot{h}}(\alpha_0,h_0)$. Both motions are steady if $\dot{\vartheta}=0$ and $\ddot{h}(t)=0$. The vertical motion close to the ground is principally unsteady and it is not similar to the pitching rotation $\frac{\partial C}{\partial\alpha}(\alpha_0,h_0)\neq\frac{\partial C}{\partial\dot{h}}(\alpha_0,h_0)$. To escape the ambiguous definition of the angle of attack it was excluded from the force consideration and replaced by the pitch angle ϑ. The modified force representation reads:

$$C(\vartheta,h,t)=C(\vartheta,h)+\frac{\partial C}{\partial\dot{\vartheta}}(\vartheta,h)\frac{\dot{\vartheta}(t)b}{U_a}+\frac{\partial C}{\partial\dot{h}}(\vartheta,h)\frac{\dot{h}(t)}{U_a}+\ldots \qquad (3)$$

The steady force coefficients $C(\vartheta,h)$ and their unsteady derivatives $\frac{\partial C}{\partial\dot{\vartheta}}(\vartheta,h),\frac{\partial C}{\partial\dot{h}}(\vartheta,h)$ are calculated using the Vortex Lattice Method (VLM) implemented in the code Autowing, *http://www.lemos.uni-rostock.de/cfd-software/* and *N.V.Kornev and V.K.Treshkov (1992)*. The total number of vortex elements was around two thousands. The most important advantage of the formalism utilized in the Autowing is the consideration of nonlinear effects. Within the classical unsteady wing theory the unsteady derivatives are calculated with respect to the zero angle of attack delivering the values $\frac{\partial C}{\partial\dot{\vartheta}}(0,h),\frac{\partial C}{\partial\dot{h}}(0,h)$. It was early realized that these derivatives are sufficiently depend on the mean pitch angle. According to this the wing should oscillate around the actual pitch angle. Description of the VLM method and its thorough validation are given in *N.V.Kornev and K.Matveev (2003)*, *N.V.Kornev and V.K.Treshkov (1992*), and *K.Benedict, N.V.Kornev, M.meyer and J.Ebert (2002).*

The calculations of the coefficients in (3) were performed for the small frequencies and amplitudes of oscillations. These two assumptions are quite proper for the sake of the classical stability analysis and were usually used in the practice for design of Soviet WIG craft. For the large motions they are not valid. The only proper approach for the large motions is the six degree of freedom (DOF) simulations coupling the viscous flow computations with motion calculations which allows one to take, for instance, the flow separations into account. Although such an approach is becoming more and more popular, it is extremely time consuming and still cannot be applied for serial investigations. In this paper, it is assumed that the crash tendency at large perturbations can reliably be predicted with simplifications mentioned above.

The influence of different steering elements (flaps on the main wing and flaps on the tail unit) is taken into account by introduction of additional linear terms into (3)

$$\Delta C(\vartheta,h,t)=\frac{\partial C}{\partial\delta}(\vartheta,h)\delta, \qquad (4)$$

where δ is the flap deflection. The coefficients $\frac{\partial C}{\partial\delta}(\vartheta,h)$ were calculated using the Autowing software.

2.2. Equations of the longitudinal motion

Although the representation (3) is usually used in the frequency domain simulation formalism, it is utilized here within the three DOF time domain simulation based on the system of three ordinary differential equations:

$$m\dot{U}_{xcg}=Thrust-\frac{\rho U_{\alpha}^{2}S}{2}C_{D}$$

$$m\dot{U}_{ycg}=\frac{\rho U_{\alpha}^{2}S}{2}C_{l}-mg \qquad (5)$$

$$J_{z}\dot{\omega}_{z}=\frac{\rho U_{\alpha}^{2}Sb}{2}C_{n}$$

$$\dot{h}_{cg}=U_{ycg},\dot{\vartheta}=\omega_{z,}U_{y}=U_{ycg}-w_{y}(t),U_{a}=U_{d}+w_{x}(t)$$

Here the index cg stands for the center of gravity, $w_x(t),w_y(t)$ are wind fluctuations (see the next section), ρ is the air density, *m* is the mass, J_z is the inertia moment, S and b are the reference area and chord. The lift component and the pitching moment produced by the engine are neglected. The coefficients C_D, C_l and C_n are represented in forms (3) and (4).

The automatic control system used in the paper is of the PD type, *Brockhaus (1994)*.

$$\delta_{flap} = -K_1(h_{cg} - h_{cgdesirable}) - K_2\dot{h}_{cg} \tag{6}$$

$$\delta_{tail} = K_3\vartheta + K_4\dot{\vartheta}_{cg}$$

Here δ_{flap} is the deflection of the flap on the main wing used to control the height of flight, δ_{tail} is the deflection of the flap on the tail unit used to control the pitch angle, $h_{cgdesirable}$ is the desirable height of flight and K_i are the coefficients of the control law (6). The delay of the flaps action was not considered.

2.3. Synthesis of wind turbulent fluctuations $w_x(t), w_y(t)$ in the earth boundary layer

The synthesis of turbulent fluctuations is one of the important problems for Large Eddy Simulations (LES) and Direct Numerical Simulations (DNS) which both demand temporal and spatially resolved velocity fields at the inlet of the computational domain. In this paper we apply the procedure proposed by *Kornev N., Hassel (2007)* capable of generating the unsteady three dimensional divergence free fluctuation fields with prescribed root mean square (r.m.s) and energy spectra of velocity fluctuations.

2.3.1. Statistical data for the earth boundary layer turbulence

The mean velocity within the earth boundary layer has the following form (see *John D.Holmes (2007)*):

$$U(z) = U_{10}\left(\frac{z}{10}\right)^{1/\ln(50/z_0)} \tag{7}$$

where U_{10} is the reference mean velocity at the height of 10 meters over the ground, *z* is the distance from the ground and z_0 is the surface roughness approximated from the real observation data:

$$z_0 = \left(\frac{U_{10}}{232.617}\right)^{1/0.322651} \tag{8}$$

The r.m.s. of the full velocity fluctuation $u' = \sqrt{\overline{u_x'^2} + \overline{u_y'^2} + \overline{u_z'^2}}$ is estimated as (see *John D.Holmes (2007)*):

$$u' = U_{mean}\left(\frac{1}{\ln(z/z_0)}\right) \tag{9}$$

The spectrum for wind turbulence $S_u(f)$ was proposed by Kaimal, *Pena, Gryning and Mann J. (2010)*:

$$S_u(f) = \frac{102\frac{fz}{U}u_*^2}{f\left(1+33\frac{fz}{U}\right)^{\frac{5}{3}}} \tag{10}$$

where *f* is the frequency in Hz, *n = fz/U* is the dimensionless frequency and u_* is the surface friction velocity. The total velocity is the sum of the fluctuations and the mean velocity:

$$\vec{U} = \vec{u}' + U(z)\vec{w} = \vec{u}' + U_{10}\left(\frac{z}{10}\right)^{1/\ln(50/z_0)}\vec{w} \tag{11}$$

where the unit vector $\vec{w}$ shows the wind direction. The integral length L can be calculated from the approximation (see *Pena, Gryning and Mann J. (2010)*):

$$L = \frac{1}{\sqrt{2\pi}}(46.36\kappa z - 0.46(\kappa z)^2) \tag{12}$$

Here κ =0.41 is the Karman's constant.

2.3.2. Artificial generation of wind turbulent fluctuations

The idea is based on the modeling of turbulence by a set of vortex elements randomly distributed within the space. It is assumed that the vortex elements are carriers of the spherically symmetric vector potential $A(r)$. The velocity taken as the curl of the vector potential $u(\vec{r}) = \nabla \times A(r)$ satisfies the divergency free condition automatically $\nabla u(\vec{r}) = \nabla(\nabla \times A(r)) \equiv 0$. The relation between the potential $A(r)$ and the three dimensional velocity spectrum is determined in *Kornev N., Hassel (2007)* as:

$$A(r) = \int_0^\infty \sqrt{S_u(f)}\frac{Sin(fr)}{fr}df \tag{13}$$

Application of the original Kaimal spectrum results in the singularity of the velocity because of weak decay of $S_u(f)$ at high frequencies. To avoid this problem the Kaimal spectrum is corrected in the range of large frequencies by multiplying with the exponential term $Exp\left[-2.5\left((\eta f)^4 + 0.4\eta^4\right)^{1/4} - 0.4)\right]$ in the same manner like it done for the spectrum of the full developed turbulence:

$$S_u(f) = \frac{102\frac{fz}{U}u_*^2}{f\left(1+33\frac{fz}{U}\right)^{\frac{5}{3}}} Exp\left[-5.2\left((\eta f)^4 + 0.4\eta^4\right)^{1/4} - 0.4)\right] \tag{14}$$

The parameter η is the Kolmogorov microscale. Since the velocity field is rescaled to achieve the desirable r.m.s the friction velocity can be taken equal one, i.e. $u_* = 1$. Substitution of (14) into (13) results in the integrals which have no analytical representation. Following *Kornev N., Hassel (2007)* we calculated the integral (13) numerically and approximated the derivative $\frac{\partial A}{\partial r}$:

$$\frac{\partial A}{\partial r}=u_*\frac{-0.239}{\left(z/U\right)^{0.331}}r^{-7/6}\frac{1}{1+\frac{0.134}{\left(z/U\right)^{0.416}-0.135}r^{9/6}}\left(\frac{r/\eta}{\left(\frac{139.865\left(z/U\right)^{0.021}}{\left(z/U\right)^{0.148}+5.397}+\left(r/\eta\right)^{2.560}\right)^{0.396}}\right)^2$$

depending on the distance from the vortex *r,* Kolmogorov microscale η and the ratio (z/U).

The velocity at the arbitrary point $\vec{r}$ can be calculated using the Biot- Savart law, *Kornev N., Hassel (2007).*

$$\vec{u}=(\vec{r}\times\vec{\gamma})\frac{\partial A}{\partial r}\frac{1}{r} \tag{15}$$

The vortices are randomly generated in front of the computational domain with a certain overlapping and move with the mean velocity *U* depending on the distance from the ground. The magnitude of the strength vector can be taken the same for all vortices $|\vec{\gamma}|=1$. For the isotropic turbulence the orientation of the vector $\vec{\gamma}$ is uniform in space. For the anisotropic turbulence the vector $\vec{\gamma}$ has to have a preferential direction prescribed by the Reynolds stresses:

$$R_{ii}=k(1-\gamma_i^2),R_{ij}=-k\gamma_i\gamma_j$$

Here k is the total turbulent kinetic energy. The vortices induce the fluctuations according to (15) which possess the prescribed energy spectrum. The total velocity is found as the sum of the mean velocity (7) and fluctuations induced by all vortices populating the computational domain.

In this paper we use the assumption of the isotropy $\overline{u_x^{/2}}=\overline{u_y^{/2}}=\overline{u_z^{/2}}$ although the method is capable of generating the anisotropy velocity fluctuations as well. To get the desirable r.m.s. $u^/$ the generated velocity components $u^/_{igenerated}$ are rescaled at each time instant $m\Delta t$ using the recurrent formula:

$$\begin{aligned}
&u^/_{icorrected}(m\Delta t)=\chi u^/_{igenerated}(m\Delta t),\\
&\chi=\frac{u^/}{\sqrt{(\overline{u_x^{/2}}+\overline{u_y^{/2}}+\overline{u_z^{/2}})/3}},\\
&\overline{u_i^{/2}}=\frac{1}{m}((m-1)\overline{u_i^{/2}}+u_i^{/2}(m\Delta t)).
\end{aligned} \tag{16}$$

Another spectrum which can be used for turbulent fluctuation synthesis is the spectrum of the decaying turbulence $S(f)=f^4Exp[-f^2/(\pi L^2)]$, where the integral length *L* is determined from (12).

2.3.3. Calculation of the wind fluctuations effect on WIG aerodynamics

The aerodynamic force is proportional to the relative speed squared and the force coefficient which depends on Re number and the distribution of the wind velocity along the craft. To consider the latter effect in a full manner one has to perform real time domain simulation solving coupled aerodynamic problem (determination of forces) and motion equation at each time instant. Generally, the use of the representation (3) becomes senseless especially if the potential theory cannot be applied for force determination because the wind fluctuations filed is not irrotational. To avoid the solution of a very complicated problem and to draw conclusions of qualitative character, it is supposed in this paper that the integral length *L* are much larger than the size of the craft. In this case the variation of the wind velocity along the craft can be neglected and the incident flow calculated at the centre of gravity is assumed to be uniform. Herewith the worst case is considered because the effect of wind is generally stronger if the velocity is changed at once on the whole wing arrangement. We can then use the representation (3) and precompute the coefficients before motion simulation.

2.4. Simulation of wave perturbations

Prof. Treshkov proposed in seventieth a very interesting approach to calculate easily the wave perturbations using steady and unsteady derivatives determined without waves. Unfortunately being directly involved in the design of Soviet ekranoplanes he had no permission to publish his results. Treshkov's method (see short description in *N.V.Kornev and V.K.Treshkov (1992*)) is based on the assumption that the wave has the length L_w much larger than the wing chord *b*. At large Froude numbers typical for WIG craft the water surface deformation due to the aerodynamic pressure caused by the craft can be completely neglected. For this case the water surface can be replaced by the plane which is tangential to the wave surface below the center of gravity. The plane performs linear and angular oscillations as shown in Fig.1. Additional force caused by waves is calculated as the Taylor series with respect to the wave ordinate $y_w = Y_w \cos(\sigma t)$, where $\sigma = \frac{2\pi}{L_w}(U_{xcg} - U_{wave})$ is the encounter frequency, and its time dimensionless derivative $\dot{y}_w = -Y_w \sin \sigma t \frac{2\pi}{L_w}$:

$$\Delta C_{wave} = \frac{\partial C}{\partial y_w} y_w + \frac{\partial C}{\partial \dot{y}_w} \dot{y}_w, \tag{17}$$

For small ratio b / L_w the derivatives (17) are expressed through the common derivatives on h, ϑ and $\dot{h}$:

$$\frac{\partial C}{\partial y_w} = -\frac{\partial C}{\partial h}, \frac{\partial C}{\partial \dot{y}_w} = -\left(57.3\frac{\partial C}{\partial \vartheta} + \frac{\partial C}{\partial \dot{h}}\right) \tag{18}$$

The representation (17) and relations (18) are valid for C_D, C_l and C_n coefficients. Treshkov's method is applicable for the regular waves of large lengths referred to the wing chord. Since the eigenfrequency of real WIG is small this approach is practically useful for estimations of resonance cases. The experience also shows that the reaction of WIG to short waves is negligible.

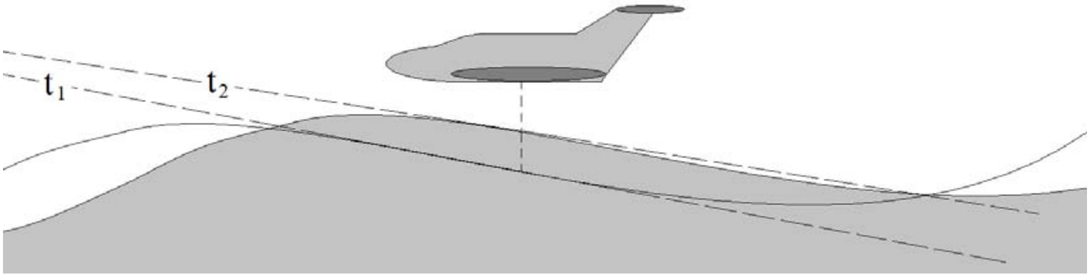

Fig.1: Simulation of the wave perturbation effect by replacing the free surface (solid line) with the plane (dashed line) performing linear vertical and angular oscillations. Two different time instants t_1 and t_2 are shown.

3. Results

3.1. Object of the study

The subject of investigations is the WIG configuration of the Lippish type (Fig.2). The fuselage and the side rudders were neglected. The configuration consists of the central wing which models the aerodynamic influence of the fuselage, main wing, tail unit, endplates and winglets. The main geometric parameters are listed in the table 1. All sizes are referred to the root chord of the central wing *b*. The mass of the craft in the basic case is 1.7 ton. The WIG craft is faultless from the point of the classical stability analysis. It possesses both static and dynamic stability up to the height of flight of 2.5 meters at zero pitch angle. At the height of 0.5 meters the Irodov criterion referred to *b* is about 0.13. The speed of the craft if not explicitly mentioned further is 40 m/s. The binding criterion

$$\frac{dh}{dV} = \frac{2}{V} \frac{C_l}{\partial C_l / \partial h} \frac{X_\vartheta}{X_h - X_\vartheta}$$

calculated at this speed and height of flight of 0.5 m is 0.05 and can be considered as quite satisfactory.

Table 1. Main geometrical characteristics of the WIG craft used in calculations.

	Chord	Aspect ratio	Taper ratio	Sweep angle (deg)	Pitch angle (deg)	V-angle (deg)
Central	1.0	0.3	1.0	0	6.0	0
Main wing	1.0	0.5	0.3	-20	6.0	-12
Tail unit	0.2	4.0	1.0	0	2.0	0
Winglet	0.2	1.4	0.7	25	6.0	35

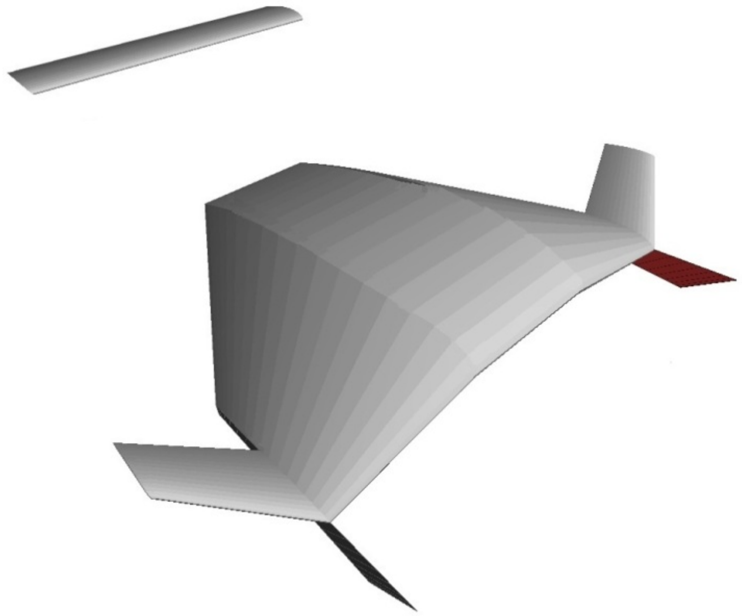

Fig.2: Hypothetical WIG craft used for the study

3.2. Stability in cruise mode

3.2.1. Influence of nonlinear aerodynamic effects on the WIG motion

In this study the forces were represented in the form used in the classical stability theory:

$$C(\vartheta,h,t)=C(\vartheta_c,h_c)+\frac{\partial C}{\partial\vartheta}(\vartheta_c,h_c)(\vartheta-\vartheta_c)+\frac{\partial C}{\partial h}(\vartheta_c,h_c)(h-h_c)+$$
$$+\frac{\partial C}{\partial\dot{\vartheta}}(\vartheta_c,h_c)\frac{\dot{\vartheta}(t)b}{U_a}+\frac{\partial C}{\partial\dot{h}}(\vartheta_c,h_c)\frac{\dot{h}(t)}{U_a}+\ldots \tag{19}$$

to see the difference in the dynamics with and without account for nonlinearity in aerodynamic characteristics. The index *c* in (19) stands for the cruise mode. The craft has initial pitch angle of -3 deg with other parameters corresponding to the cruise mode at zero pitch angle. The damping is larger and decay of oscillations is faster at small heights of flight because of strong restoring forces (Fig.3). Due to strong restoring forces the oscillation magnitude decreases when the height of flight is getting smaller and it is sufficiently larger when the forces are represented with consideration of nonlinear effects. This can be explained by the positive contribution of nonlinear terms $\frac{\partial^2 C_l}{\partial h^2} > 0$ to the lift coefficient which is neglected in the representation (19). The decay of oscillations is approximately the same for both cases of force representation although the unsteady derivatives in (3) depend sufficiently on height of flight. Neglect of nonlinear terms in force representation results in the underestimation of the oscillation magnitude.

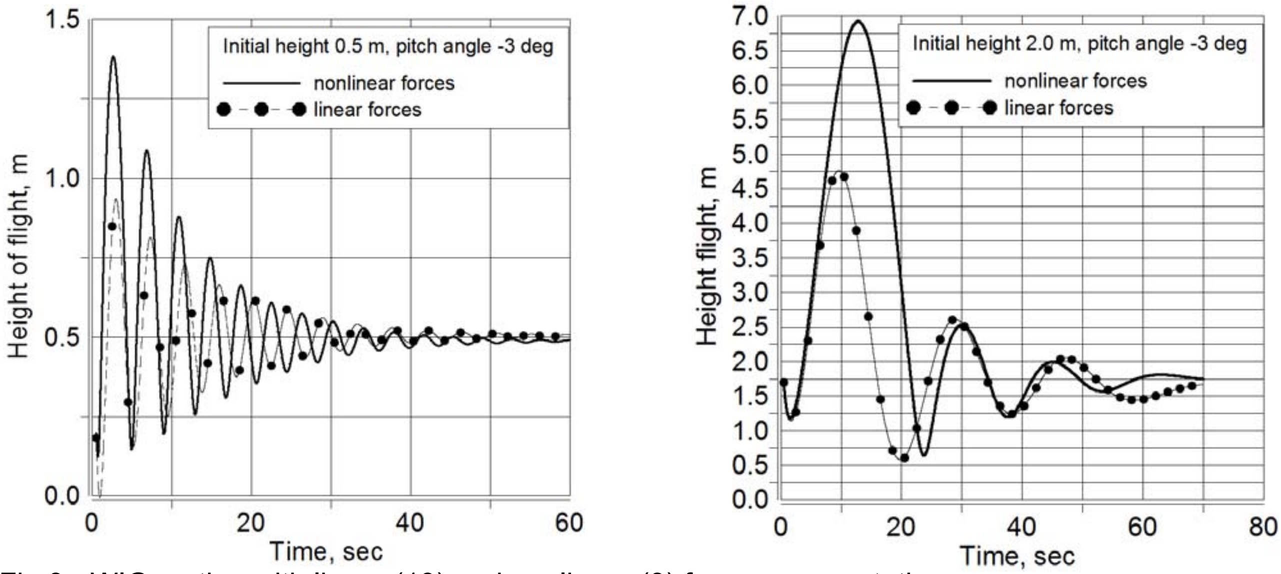

Fig.3**:** WIG motion with linear (19) and nonlinear (3) force representations.

3.2.2. Influence of the wind and waves on the WIG motion

Influence of the height of flight on the flight safety is contradictory. From one side the stability is improved when the WIG approaches to the ground due to increase of the natural restoring forces and damping caused by the ground effect. From the other side the gap between the free surface and craft is getting smaller. As result, even small perturbations can cause the water impact. The flight safety can be sufficiently affected. This fact is illustrated in Fig.4. The calculations were performed with the wind fluctuations and wave models described in the sec. 2.3 and 2.4. Because of huge amount of calculations the investigations were performed for wind speeds of 0, 5, 7.5, 10 and 15 m/s. The intermediate values were not studied. The wave was regular with the amplitude corresponding to the significant wave height chosen for the given wind speed from empirical correlations of *NASA (2000).* The wave length to the height ratio is 25.

The WIG motion was defined as the safe one if the height of flight doesn't exceed 10 meters and the craft has no impact with the water surface. The results are summarized in Fig. 4 for the headwind (upper picture) and following wind (lower picture). The maximum allowed wind speed is presented depending on the cruise height of flight without and with flight control. In the latter case all coefficient K_i were taken equal to four, i.e. $K_i = 4$. The craft speed was chosen from the condition that the speed relative to the air is equal to the craft speed at calm conditions. In this case the craft weight and the thrust are the same for all simulations.

The flight at small height of 0.5 m is proved to be fully impossible at weak wind of 5 m/s due to the water impact. The flight in the working range of the flight heights from 1 m to 2 m is possible only up to the wind speed of 5 m/s (12.5 percent of the cruise speed at calm condition). The effect of the flight control is negligible because the coefficients $K_i = 4$ are small.

With the application of the strong control with $K_i = 114$ the safe flight becomes possible up to the strongest wind which induces waves with the amplitude equal to the cruise height of flight.

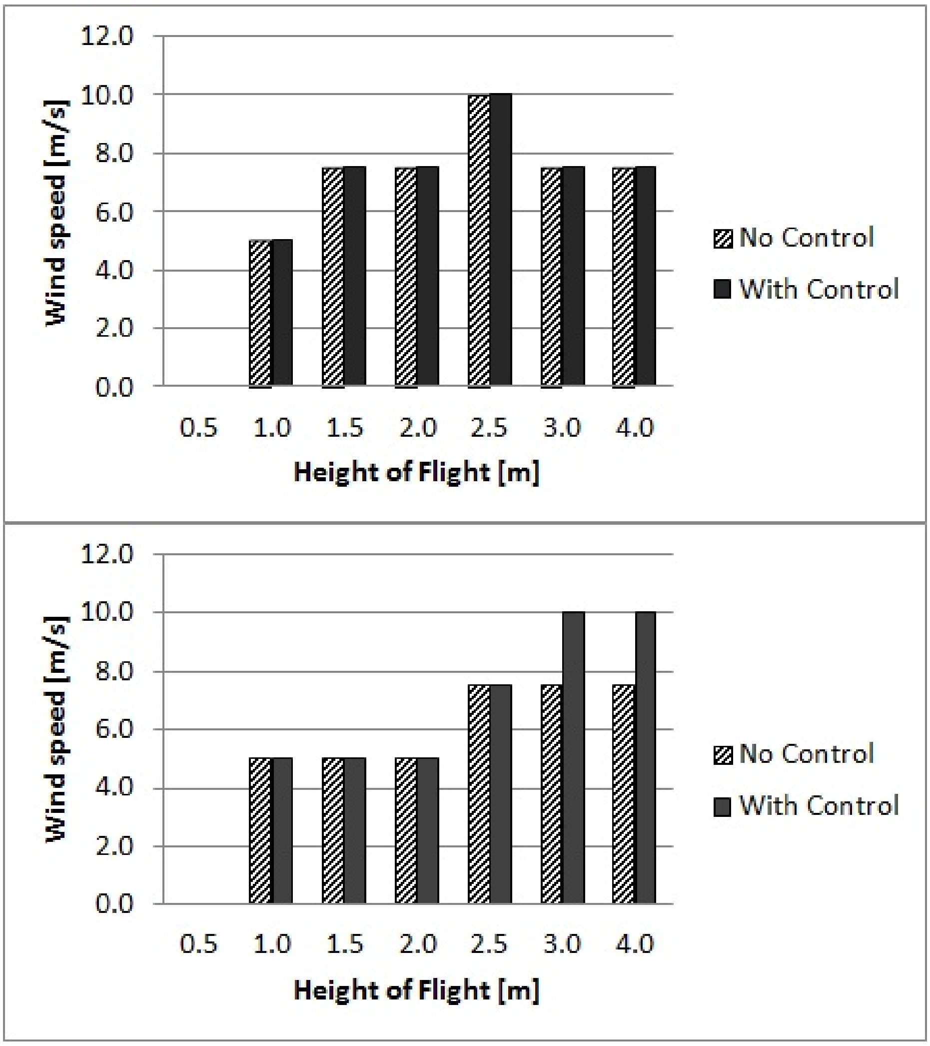

Fig.4: The maximum allowed wind speed for the WIG craft under headwind (upper picture) and following wind (lower picture).

3.2.3. Influence of the step like wind gust on the WIG motion

This study replicates the real situation which happened when the WIG flew from any river or harbor into the open water basin with a strong steady wind (Fig.5). The trajectories are presented in Fig.6 for wind speeds of ± 1 m/s and ± 3 m/s. The wind was switched on after 2 sec of flight in cruise at the height of 0.5 m. For the head wind the craft experiences first jump in height, losses the aerodynamic lift due to weakening of the ground effect and then approaches the free surface. If the wind gusts are larger than 3 m/s (around eight percent of the cruise speed) the water impact happens at this stage of the motion resulting in the crash. Therefore, the wind gusts larger than 3 m/s are not admissible. It should be noted that the pitch angle is kept within the acceptable range in all simulations. There were documented no pitch up tendency and the only reason for the crash was the water impact. In the case of the following wind gust the water impact can happen already in the first stage of the perturbed motion due to a sudden loss of the relative speed resulting in a drop of the lift. The maximum admissible gust is -3 m/s.

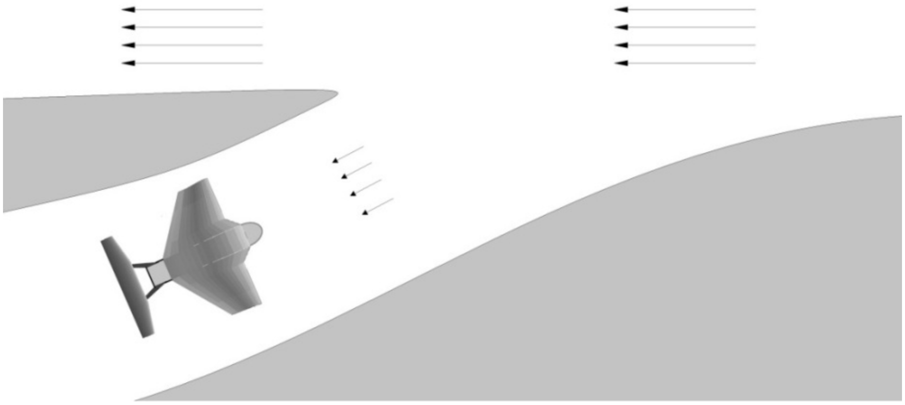

Fig.5: Illustration of the situation when the WIG craft flying into the open water basin with a strong steady wind.

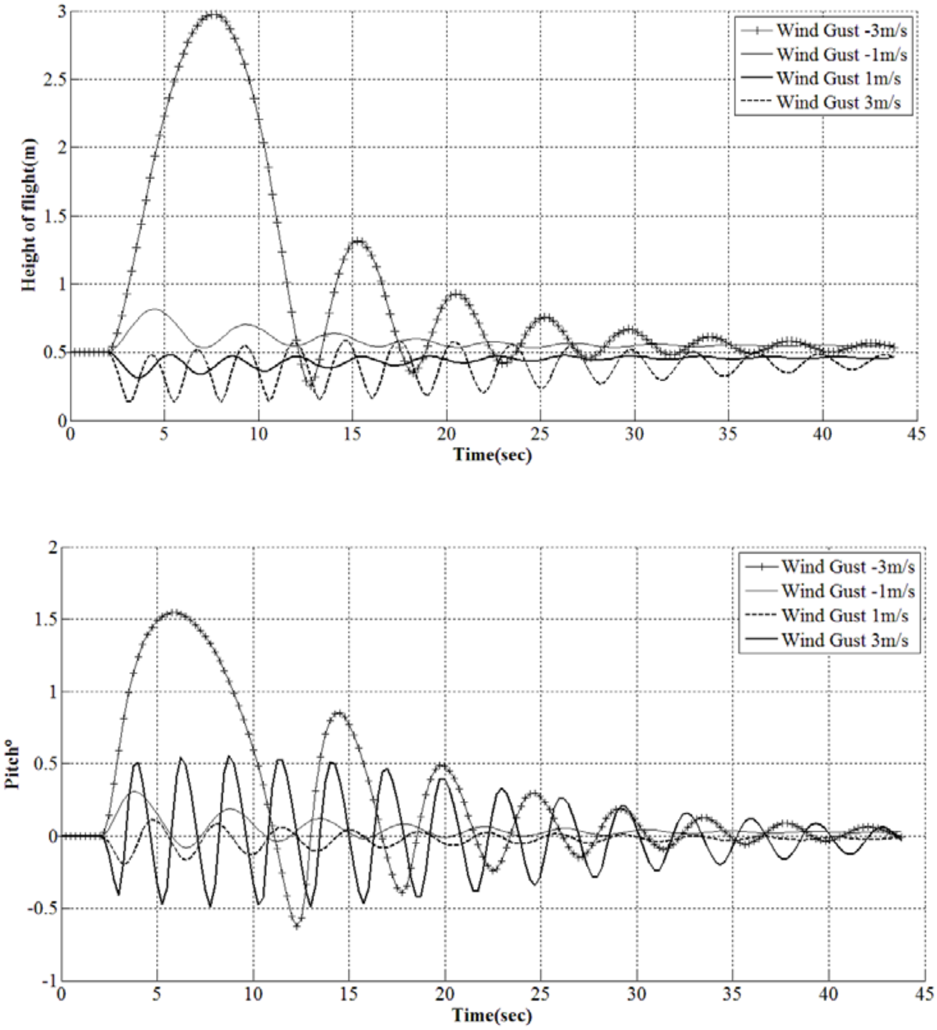

Fig.6: Trajectory (upper picture) and pitch angle (lower) of the WIG craft under step like wind gust perturbation.

3.3. Motion in the transition from the skimming mode to the flare mode

Most of WIG crashes especially crashes of small machines in the last time happened during the take-off. Very often, by speaking about WIG stability one means the safety of the transition from the skimming mode to the flare one. This type of the motion is the transitional one and its safety cannot be evaluated using the classical stability analysis. The transitional motion should be studied within time domain simulation.

Since the water born regime is outside of the scope of the present work, the motion is studied starting from the height of 0.1 m with different initial speeds, pitch angles and thrusts. The task is to attain the cruise height of 0.5 m without water impact and not exceeding the height of flight of 10 meters. Fig. 7 presents the maximum height of flight attained during the flight starting from the different initial pitch angles (left) for the original craft (solid line) and the craft with doubled weight (dashed line). The initial speed and thrust correspond to these of the cruise mode. The speed of the heavy machine was 56.6 m/s. The influence of the weight and cruise speed is unsubstantial (Fig.7). If the craft has the absolute initial pitch angle more than three degrees the craft experiences the water impact resulting in the crash.

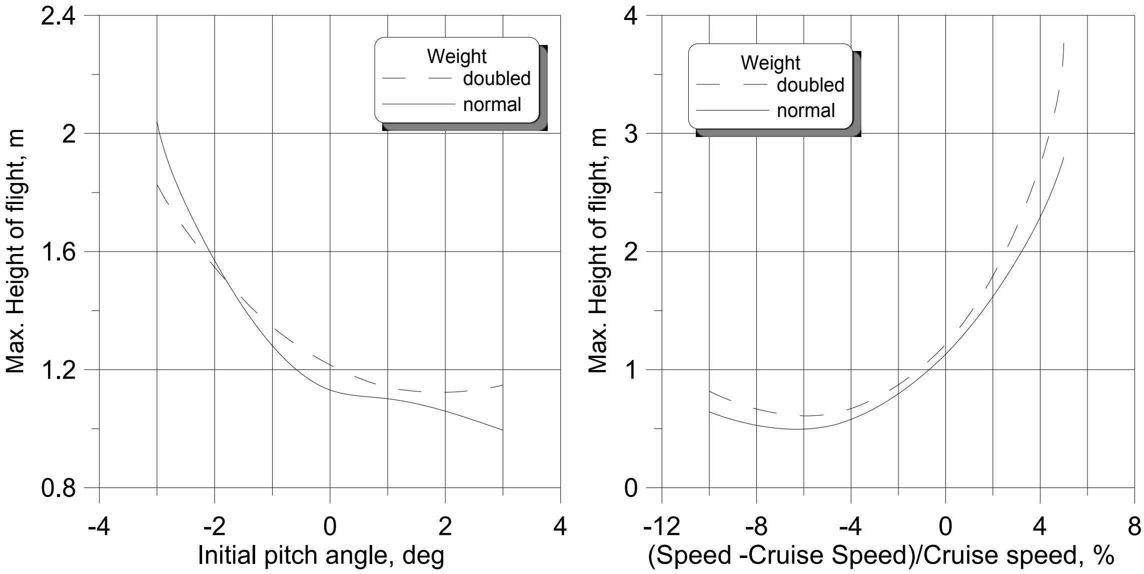

Fig.7: Maximum height of flight attained during the flight starting from the height of 0.1 m at different initial pitch angles (left) and speeds (right).

Fig.7 (right) illustrates the fact that the initial over speed at the beginning of the flight is not acceptable to perform the safe transition. In this calculation the initial pitch angle and the thrust correspond to these of the cruise mode. If the over speed is ten percent larger than this in the cruise regime the WIG craft experiences the pitch up tendency leading to the crash situation. There is no big difference in the motion behavior of basic and heavy machines. On the contrary, the initial over thrust is proved to be not critical for the flight safety. The calculations performed with the initial speed, zero pitch angle and the initial doubled thrust reduced after 5 sec to the cruise thrust doesn’t cause the crash and the transition runs quite safely. Concluding, the safety of the transition phase can be guaranteed by the control of the pitch angle and the speed during the take-off.

4. Conclusions

The stability theory of WIG craft developed by *Irodov (1970)*, *Staufenbiel und Yeh (1976)* and *Zhukov (1997)* established principles of design of wing arrangements for the flight close to the ground. This classical theory derived from the Hurwitz formalism is based on the linear representation of forces and assumption of small perturbations. In reality the WIG craft is a nonlinear dynamic system because of strong nonlinear dependency of forces both on the pitch angle and especially on the flight height. That is why the conclusions drawn from the stability theory are not sufficient for the flight safety evaluation. The stability theory requirements should be considered in design process as necessary but not sufficient ones. The nonlinear time domain simulation of WIG motion at different perturbations should be inevitable part of the stability analysis.

As shown in this paper the motion of the WIG craft which is optimal from the point of the classical stability theory (with respect to the Irodov criterion, position of the center of gravity, binding criterion, etc.) can become unstable under relatively weak perturbations (wind gust of eight percent of the cruise speed, air fluctuations at the wind speed about twelve percent of the cruise speed). There is a certain kind of contradiction of ground effect influence on the stability. From one side the restoring forces contributing to the natural stability of WIG craft increase when the height of flight decreases. From the other side the gap between the craft and the free surface is getting smaller. Even small perturbations can cause the water impact. Therefore the minimal height of flight should be restricted. This improves the safety but diminishes the operation efficiency. The flight in extreme ground effect to increase the efficiency seems to be impracticable idea.

There is also no guarantee that the WIG craft well designed according to the stability theory can perform the take-off safely. For that the pitch angle and the speed should be strongly limited in the take-off phase of the motion. An important conclusion drawn from the presented time domain simulation is the necessity of application of an efficient flight control system for WIG craft. The operation of the WIG craft without the flight control system is very risky according to our simulations.

5. Acknowledgements

This work was partially supported by the Deutsche Forschungsgemeinschaft under project KO3394/3-1.

References

RAWDON, B., HOISINGTON, Z. (2003), *Vehicle Design for Mass-Market Cargo Transport*, AIAA Paper 2003-555, pages 1 – 11.

IRODOV, R. D. (1970), *Criteria of longitudinal stability of ekranoplan*, Technical Note of the Central Hydro-Aerodynamical Institute (TSAGI) (in Russian), volume 1, number 4.

STAUFENBIEL R., YEH, B.T. (1976), *Flugeigenschaften in der Längsbewegung von Bodeneffekt- Fluggeräten: Teil 1 und 2*, Zeitschrift für Flugwissenschaften 24, Hefte 1 und 2.

ZHUKOV, V.I. (1997), *Peculiarities of the WIG's aerodynamics, dynamics and stability*, TSAGI Press (in Russian).

DIOMIDOV, V.B. (1996), *Automatic control of ekranoplan motion*, Elektropribor publisher, St. Petersburg (in Russian).

ROZHDESTVENSKY, K. (2000), *Aerodynamics of a lifting system in extreme ground effect*, Springer.

FACH, K., FISCHER, H., KORNEV, N., PETERSEN, U. (2004), *Wing in ground effect craft, Ship Design and Construction*, SNAME, Chapter 48.

KORNEV, N.V., MATVEEV, K. (2003), *Numerical modeling of dynamics and crashes of wing-in-ground vehicles*, AIAA Paper 2003-600, pages 1 – 9.

AVVAKUMOV, M.N. (2000), *Requirements for aerodynamic characteristics of ekranoplan from viewpoint of stability, linear estimates of dynamic properties of the craft and modeling of its motion*, Proc. Conf. GEM, St. Petersburg, Russia, pages 25 - 34.
http://www.lemos.uni-rostock.de/cfd-software/

KORNEV, N.V., TRESHKOV, V.K. (1992), *Numerical Investigation of Nonlinear Unsteady Aerodynamics of the WIG Vehicle*, Proc. Intersociety High Performance Marine Vehicle Conference, Arlington, VA, USA, pages 38 – 48.

BENEDICT, K., KORNEV, N.V., MEYER, M., EBERT, J. (2002), *Complex mathematical model of the WIG motion including the take-off mode*, J. Ocean Engineering, volume 29, number 3, pages 315 – 357.

BROCKHAUS, R. (1994), *Flugregelung*, Springer.

KORNEV N.V., HASSEL, E. (2007), *Synthesis of homogeneous anisotropic divergence free turbulent fields with prescribed second-order statistics by vortex dipoles*, Physics of Fluids, Vol. 19, No.5.

HOLMES, JOHN D. (2007), *Wind Loading of Structures*, Second Edition, Chapter3, Taylor&Francis.

PENA A., GRYNING, S.E, MANN, J. (2010), *On the length-scale of the wind profile*, Quarterly Journal of the Royal Meteorological Society. 136: 2119–2131, October 2010 Part B.

NASA (2000), NASA *handbook 1001 "terrestrial environment (climatic) criteria handbook for use in aerospace vehicle development"*, chapter 14.

Conceptual Design of a Zero-Emission Open-Top Container Feeder

Fridtjof Rohde, FutureShip, Hamburg/Germany, fritjof.rohde@GL-group.com
Pierre Sames, Germanischer Lloyd, Hamburg/Germany, pierre.sames@GL-group.com

Abstract

This paper describes a concept design for a zero-emission container feeder, based on existing technologies. The vessel uses liquid hydrogen as fuel to generate power with a combined fuel cell and battery system. After outlining the general requirements, technical and commercial aspects of the design are discussed. The open-top concept for short port turnover times, the large width for extra container stowage and minimum ballast, fuel cells, and the unconventional bow design are key features of the design that may influence future ship designs well before liquid hydrogen is used on cargo ships.

1. Introduction

The world's shipping fleet will continue to grow to meet the global transport demand. With the expected fleet growth for the next decades, emissions from shipping will increase.

MARPOL Annex VI restricts SOx and NOx emissions already severely for so-called "Emission Control Areas" (ECAs). By 2012, the Baltic Sea, the North Sea and the coast of Northern America (USA and Canada) were ECAs. By 2020, current standards for emission control areas (ECA) should be globally imposed. This will impose a universal change towards much cleaner (and more expensive) fuels than currently in use, but also promote research into abatement techniques and improving fuel efficiency per se.

There are many options to make ships more fuel efficient, as discussed e.g. in *Buhaug et al. (2009)*. The attractiveness of individual options depends on ship type and whether the ship is being designed or in service. For example, Germanischer Lloyd developed a marginal abatement cost curve for measures improving the energy efficiency of the world's container fleet, Fig. 1, *Köpke and Sames (2011)*. The curve was based on a price of 700 USD/t HFO (heavy fuel oil). Estimates for improvement potential and costs for the individual measures were validated with selected German ship operators. The analysis yielded a theoretical abatement potential of 24% for profitable measures (i.e. measures that pay for themselves by saving fuel, assuming 5% interest rate on the capital). This may appear a lot, but still falls short by a wide margin of the targets. For global shipping, the EU targets to bring down CO2 emissions to 80% of the 2005 levels by 2020, and 20% of the 1990 levels by 2050.

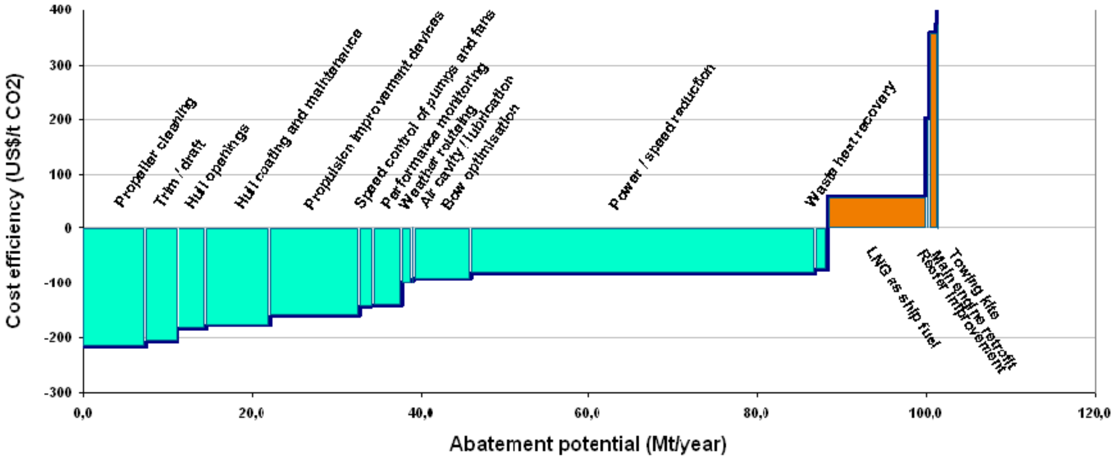

Fig.1: Marginal abatement cost curve for container vessel fleet

Even if known and available measures are implemented, there is wide consensus that shipping will not meet the discussed emission targets. Therefore, we should start investigating more radical solutions to enable future shipping with low (and ultimately zero) emissions. Using liquid hydrogen as a fuel is a key concept in this regard.

2. Hydrogen as a fuel

The 2020 generation target for offshore wind farms operating in the German Exclusive Economic Zone (EEZ) is an installed capacity of 3 GW. One of the disadvantages of renewable energy in its current form, however, is the problem of matching the intermittent nature of the supply with consumer demand. Insufficiencies in the grid and underdeveloped storage technologies mean that wind turbines are often not turning when they could be. Studies have estimated that as much as 30% of an offshore wind farm's potential energy generation cannot be fed into the grid. Liquid hydrogen (LH2) is an attractive option to store this excess energy, as it features more than 60 times the energy density than alternative energy storage technologies, *Schindler et al. (2009)*.

Using LH2 as storage technology for excess energy is by no means a new idea. There are countless studies using LH2 as clean energy in some form or another. The typical scenario involves hydrogen generation in some part of the world where there is an excess supply in energy (e.g. water power in Canada, thermal power in Iceland, solar power in desert regions) and transport to areas with high energy demand and strict air pollution criteria, e.g. *Petersen et al. (1993)*. *Mathur et al. (2008)* apply this generic scenario to offshore wind farms, albeit still having in mind to use the hydrogen fuel then on land. A logical further step is to use the hydrogen directly on ships as a fuel. The concept consists then of large offshore wind farms which convert locally the excess energy into LH2 with local storage and docking stations for transferring the LH2 (as cargo or fuel), Fig. 2 (left). A typical 500 MW wind farm could produce 10,000-12,000 t LH2 using its generation surplus. This could serve the bunkering needs of five feeder vessels of the size presented below and shown in Fig.2 (right).

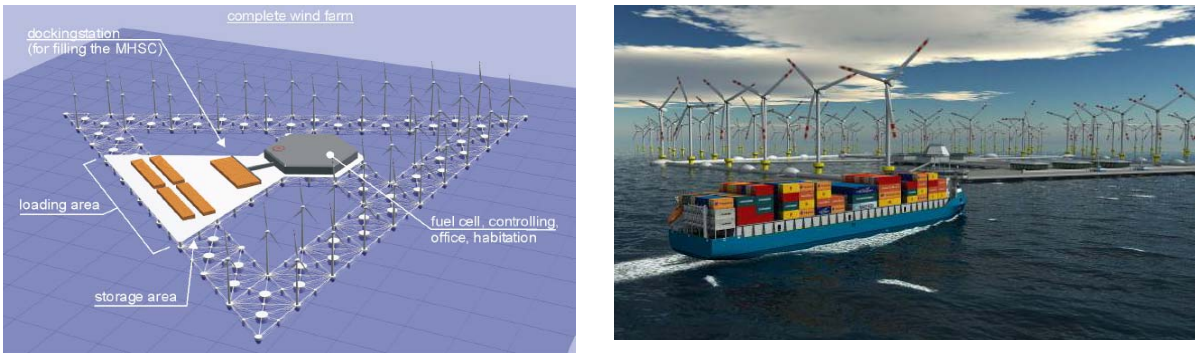

Fig.2: Offshore wind farm with hydrogen docking station, source: EU network of excellence VISIONS (2006), Germanischer Lloyd

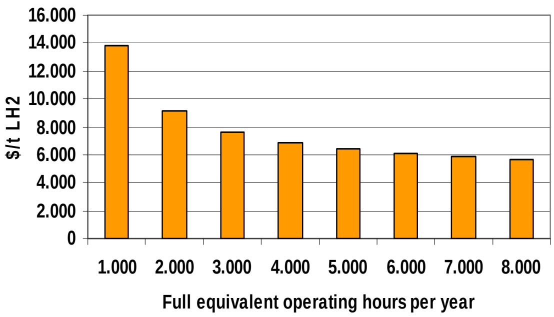

Fig.3: Cost of offshore generated liquid hydrogen, *Altmann et al. (2004)*

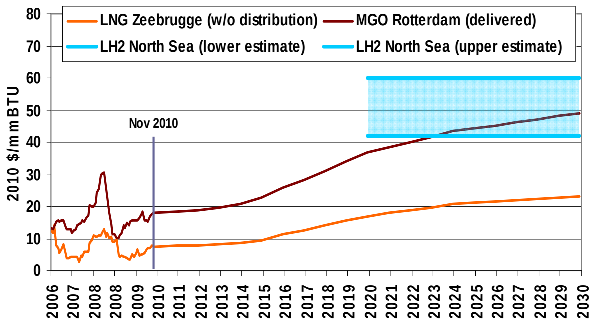

Fig.4: Prediction of fuel prices based on calorific value

The cost for LH2 produced offshore is several times higher than currently used marine gas oil (MGO). At 4000 h per year production, we expect a price of up to 7000 USD/t LH2 (including production, liquefaction and intermediate storage on-site), Fig.3. This may appear prohibitively high. However, considering the higher calorific value of hydrogen (kW/t), LH2 may become cost competitive in the mid-2020, taking surcharges for emissions into account.

3. An idea is born - Functional requirements

Sketching has been used in the early stages of ship design, both as an aid to the development of the design itself and as a communication medium, *Pawling and Andrews (2011)*. In line with this time-honoured tradition, our design started with a rough idea and a sketch, Fig.5. The sketch captured already several of the prominent features of the later design, such as the propulsion concept and the bow combining wave resistance and seakeeping aspects.

The key data outlining the design were summarised as follows:

- Area of operation: Northern Europe (North Sea, Baltic Sea); hence an area of strict emission regulations and a forerunner in using gas as a fuel in shipping
- Design speed: 15 knots. The relatively slow speed reflects general trends towards lower speeds and is compensated in part by faster handling in port.
- Keep ballast water as low as reasonably possible.
- Good manoeuvring for fast handling in port and estuaries, as the vessel will have frequent calls in ports
- Open-top design for fast cargo handling in port
- Fuel: liquid hydrogen; for zero CO2, SOx, NOx and PM emissions

- main propulsion: fuel cells with battery systems; battery systems allow faster changing of power than fuel cells
- C-type tanks to hold liquid hydrogen for a ten-day roundtrip range

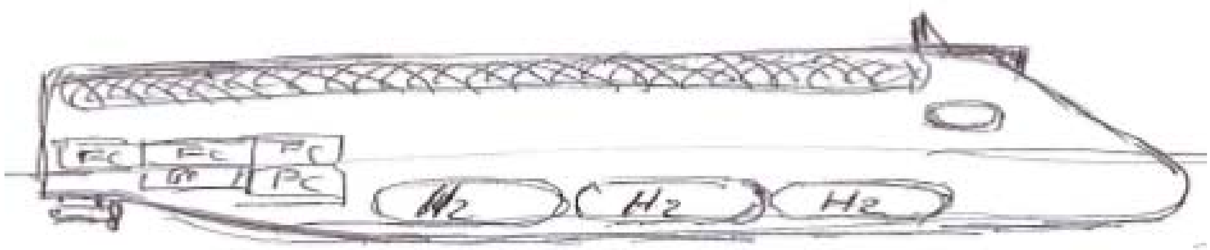

Fig.5: First design sketch

4. Design description

4.1. Main dimensions and general arrangement

Table I gives the main dimensions. The design used FORAN as supporting design software (hull shape description, stability calculations, etc.). The general arrangement plan, Fig.6, was drawn in AutoCAD.

"Modern" feeder ships now in service are based on designs which are typically 5 to 10 years old and do not yet reflect the significant increase in fuel prices of the year 2008 and after. Most recent designs feature already lower design speeds in reaction to the higher fuel cost. For our design, the selected design speed is some 15% lower than found in modern feeder ships with similar cargo capacity. The lower design speed reduces Froude number and makes shorter and wider ships hydrodynamically more attractive.

Table I: Main particulars of LH2 feeder ship

Length between perpendiculars	131.25 m	Trial speed at design draft	15 kn
Length overall	137.22 m	Deadweight	11000 tdw
Breadth moulded	24.40 m	Container intake	1000 TEU
Depth	14.00 m	Container at 14 t/TEU	700 TEU
Draft loaded	8.50 m	Reefer slots	150
Draft design	8.00 m		

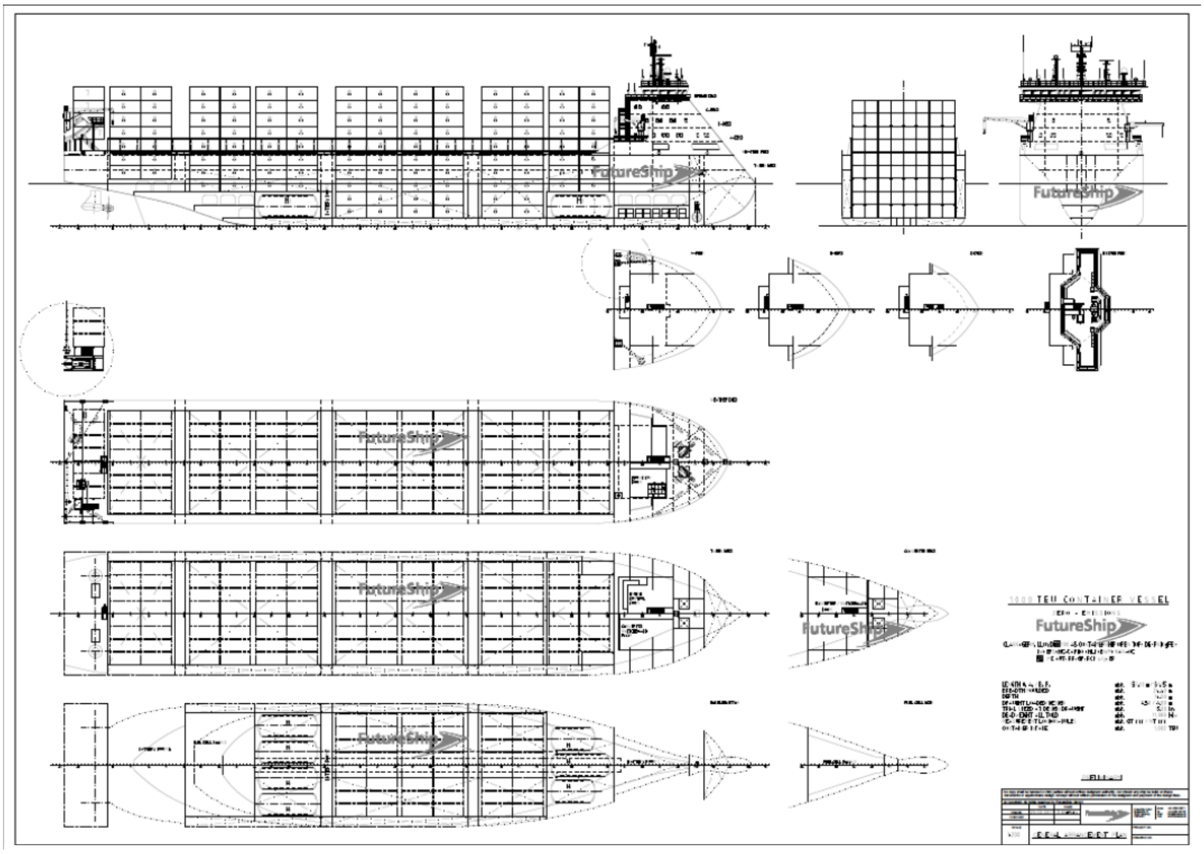

Fig.6: General arrangement plan

The increased width adds cargo capacity and reduces required ballast. This improves the ratio of payload/deadweight compared to typical “modern” feeder ships. The increase in width stays moderate enough to avoid natural roll periods below the critical threshold of 10 s for the ship in partial load.

The open-top design supports short turn-around times in port, as no hatch covers need to be moved. Also, stowage space for (hydraulic) hatch covers is saved. In addition, the open-top design adds more flexibility in container stowage and port logistics, as it allows access to individual stacks, not just cargo holds. The increased flexibility allows adapting stability, e.g. by arranging heavy containers on bottom as needed. Also, ventilation of refrigerated containers is facilitated.

The deckhouse is located forward, integrated in the bow structure, similar to many modern offshore supply vessels. The ship operates frequently in the Baltic Sea (an area with low to moderate sea states) and the chosen bow design gives above-average seakeeping performance, making the forward arrangement acceptable from a seakeeping point of view. The chosen arrangement has several advantages:

- It gives excellent visibility. There is no line-of-sight limitation which increases the nominal container slot capacity.
- It allows large rectangular cargo area. The fuel cells do not need a funnel for exhaust gas. Thus there is no obstruction for container bridges aft of the deckhouse, making container handling straightforward and rapid.
- It protects the open-top cargo area from spray water.

4.2. Hydrodynamics

The operational profile involves significant time in port approach and berthing, as typical in short sea shipping. High manoeuvrability saves time in this respect. Thus podded drives (combining electric motors and excellent manoeuvrability) were a logical choice for the propulsors. The typical twin-drive arrangement in combination with electric drive gives en passant redundancy in propulsion. The lines in the aftbody were designed for good inflow to the propellers with a central skeg for improved course-keeping in regular transit operation.

In addition to the two podded drives, a bow thruster provides extra manoeuvrability. The bow thruster is retractable and can be turned 360° when lowered. It serves as additional "take-me-home" device.

Fig.7: Aftbody of zero emission design

Fig.8: Bow of zero-emission design

The bow was designed incorporating elements of an Ulstein X-bow (or axe-bow) and a conventional bulbous bow, Fig.8. The X-bow features good seakeeping performance for shorter ships, e.g. *Keuning and van Walree (2006)*. Conventional bulbous bows are designed for minimum calm-water resistance. The chosen design features a good compromise between calm-water resistance and seakeeping performance. Formal multi-criteria optimisation considering both resistance and seakeeping yields similar shapes. In our case, there is the added feature of a streamlined knuckle line to make production of the foreship easier.

4.3. Machinery, equipment and outfit

The vessel is equipped with a 5 MW fuel cell system for propulsion and on-board energy supply. The system consists of ten linked 0.5 MW modules. There are two power generation rooms, situated forward and aft. One known drawback of fuel cells is the slowly changing current and power output. In layman's terms, fuel cells are too slow to follow any fast changing loads. The slow dynamics of fuel cells poses a fundamental problem for vessel control. Therefore, the design features a 3 MW battery system, charged by the fuel cell system, to provide rapid additional power for peak usage.

The ship is fuelled by liquid hydrogen (LH2), stored in multiple pressurised IMO Type C tanks. The short transit times allowed keeping the bunker stores small, using a total LH2 tank capacity of 920 m^3. This capacity is enough to power the ship over a typical 10-day round-trip journey. Based on GL's study for a gas-fuelled container feeder, *Scholz and Plump (2010)*, an estimated 6% of the TEU capacity of the vessel needs to be sacrificed for the hydrogen fuel tanks. As the basic stability was already very good, the fuel tanks could be arranged according to easy fuel distribution and redundancy, rather than stability aspects. With tanks feeding the fuel cells both forward and aft, the refuelling time in dual bunkering is estimated to be three hours.

Table II: Typical efficiencies for energy generation and transformation in marine engineering

Mechanical		Electrical	
Medium-speed diesel	48%	Fuel cells	
Low-speed diesel	51%	Generator	97%
Single-stage gear	98%	Electric motor	97%
Two-stage gear	97%	Transmission (high-voltage)	99%
Shaft bearing	99%	Frequency converter	91%
Propeller	68%	Podded drive	72%

Diesel mechanical: $0.48{\cdot}0.98{\cdot}0.99{\cdot}0.68 = 0.32$

Fuel-cell electrical: $0.40{\cdot}0.97{\cdot}0.99{\cdot}0.97{\cdot}0.91{\cdot}0.72 = 0.25$

Table III compares the main weight groups for the LH2 design and a conventional open-top feeder ship of same capacity. In this context, “conventional” means equipped with a two-stroke diesel engine and single propeller.

Table III: Weight composition as compared to conventional open-top container vessel

	LH2	Conv.	Diff.	comment
steel + tanks	3442 t	3255 t	-5.4 %	Due to tanks
equipment & outfit	723 t	732 t	0.0 %	
machinery	526 t	511 t	-2.85 %	Minus fuel cells and batteries, plus diesel
SUM	4750 t	4550 t	-4.21 %	
KG	9.98 m	10.03 m	0.50 %	

Fig.9: Power generation rooms forward and aft; fuel cells (yellow), battery packs (red); tanks (grey)

5. Further aspects

The LH2-fuelled container vessel has significantly higher investment costs than a similarly sized vessel of traditional design. Based on data from a GL market study on fuel cell systems and the gas-fuelled container feeder study, *Scholz and Plump (2010)*, the cost of the LH2-fuelled vessel is estimated at 35 mUSD, 60% higher than an HFO/MGO fuelled vessel (22 mUSD). The largest part of this increase is associated with the fuel cell system (7.4 mUSD), the Type C tanks (4.8 mUSD) and the battery system (0.8 mUSD). This estimate assumes that the costs associated with fuel cells production will continue their steady decline, with an expected drop in investment cost by 2020 to 1500 USD/kW.

Based on GL estimates, liquid hydrogen produced through wind power could become commercially attractive as an alternative to MGO in the 2020s, if MGO prices increase to 2000 USD/t. To arrive at this estimate, annual costs (including fuel costs, other operating costs and annualized capital costs) were compared for a LH2-fuelled feeder vessel and a standard container feeder vessel, using MGO as fuel and operating inside of an emission control area (ECA). The difference between current MGO prices and the required 2000 USD/t to make LH2 commercially attractive should be considered in light of MGO prices over period 2000 to 2010. During this decade, MGO prices increased from 250 to 650 USD/t, with an intermediate peak value of 1300 USD/t in June 2008.

6. Conclusion

The pressure to reduce greenhouse gases will only increase over the coming years and 2020 is a date within the lifetime of many vessels currently operating. To reach the target of reducing CO2 levels against historic levels, new technologies must be implemented. This vision of a zero emission vessel shows how new technology can contribute to meeting such targets and propel the industry into the future.

7. Acknowledgements

Many colleagues at Germanischer Lloyd have supported this paper with their special expertise, supplying text and/or figures, namely (in alphabetical order) Simon Adams, Volker Bertram, Bettar El Moctar, Martin Köpke, Rainer Martens, Björn Pape, Gerd-Michael Würsig. We are grateful for the computer-generated art work of Bernd Sadler (Sadler-Imageworks), who gave life to our technical concept.

References

ALTMANN, M.; SCHMIDT, P.; WURSTER, R.; ZERTA, M.; ZITTEL, W. (2004), *Potential for hydrogen as a fuel for transport in the long term (2020 - 2030),* Report Ludwig Bölkow Systemtechnik, München
http://www.lbst.de/ressources/docs2004/LBST-study-IPTS_2004_eur21090en.pdf

BUHAUG, Ø.; CORBETT, J.J.; ENDRESEN, Ø.; EYRING, V.; FABER, J.; HANAYAMA, S.; LEE, D.S.; LEE, D.; LINDSTAD, H.; MARKOWSKA, A.Z.; MJELDE, A.; NELISSEN, D.; NILSEN, J.; PÅLSSON, C.; WINEBRAKE, J.J.; WU, W.Q.; YOSHIDA, K. (2009), *Second IMO GHG study 2009,* Int. Maritime Organization (IMO), London

KÖPKE, M.; SAMES, P. (2011), *Outlook on CO2 emissions of the container world fleet and possible reduction targets*, 8th Annual Green Ship Conf., Oslo

KEUNING, J.A.; WALREE, F. Van (2006), *The comparison of the hydrodynamic behaviour of three fast patrol boats with special hull geometries,* 5th Int. Conf. High-Performance Marine Vehicles (HIPER), Launceston, pp.137-152.

MATHUR, J.; AGARWAL, N.; SWAROOP, R.; SHAH, N. (2008), *Economics of producing hydrogen as transportation fuel using offshore wind energy systems*, Energy Policy 36/3, pp.1212-1222.

PAWLING, R.; ANDREWS, D. (2011), *Design sketching – The next advance in computer aided preliminary ship design?,* 10th Conf. Computer and IT Applications in the Maritime Industries (COMPIT), Berlin, pp.426-441.

PETERSEN, U.; WÜRSIG, G.; KRAPP, R. (1993), *Design and safety considerations for large-scale sea-borne hydrogen transport,* Int. J. Hydrogen Energy 19/7, pp.597-604.

SCHINDLER, J.; WURSTER, R.; ZERTA, M.; LANDINGER, H.; SCHMIDT, P.; WEINDORF, W.; BLANDOW, V. (2009), *Hydrogen and fuel cells as strong partners of renewable energy systems*, Report Ludwig Bölkow Systemtechnik, München
http://www.lbst.de/ressources/docs2009/eha_study_h2re_en.pdf

SCHOLZ, B.; PLUMP, R. (2010), *Gas-fuelled feeder container vessel*, Hansa 147/8, pp.144-145.

Maneuvering Simulation of High Speed Fast Rescue Craft

Karan Bhawsinka[1], Heather Peng, Brian Veitch
Faculty of Applied Science and Engineering, Memorial University of Newfoundland, Canada
hpeng@mun.ca

Abstract

When small marine crafts are launched from platforms in rough seas or used for search and rescue or law enforcement, proper training is required to ensure crews can execute these operations successfully and safely. Simulation has been used for decades to enhance personnel training. However the quantity and distribution of crews combined with variations in vessel design and equipment have limited the use of simulation for high speed craft (HSC) training. To overcome these limitations and address HSC training requirements, a maneuvering simulation model for high speed planing hull crafts was developed to simplify fast rescue craft (FRC) maneuvering simulation. A PC based maneuvering simulation program was developed by using 6 DOF mathematical models. In this paper, a simulation of a 7.5m rigid hull inflatable boat is presented. The maneuvers were visualized in real-time by plugging the program into a commercial FRC simulator and satisfactory results were found.

1. Introduction

In the past few years, significant improvements have been made in vessel performance of high speed planing hull crafts. Naval, coast guard and law enforcement agencies task them to complete a growing range of operational objectives. Because of this, there is a continuous demand to enhance personnel training. As we improve our understanding of planing hull hydrodynamics, the use of maneuvering simulation technology for this purpose is becoming more and more attractive. While developing a displacement hull maneuvering simulation program, it can be assumed that the wetted hull surface is constant. For planing hull maneuvering simulation, this cannot be assumed as the shape of the hull under water will change with some motions (for example forward speed and drift angle). Some of the consequences are:

- Hydrodynamic coefficients cannot be considered constant throughout the maneuvering motion
- There is strong coupling between longitudinal, lateral and vertical motions

Also, many planing hull vessels use waterjets and outboard motors as their propulsion and control devices, whereas most displacement hull maneuvering simulation programs only incorporate conventional rudders and propellers in their mathematical models. Thus these programs cannot be used for simulating planing hull maneuvering motions.

The influence of speed on the hydrodynamic derivatives of a high speed craft has clearly been demonstrated by Ishiguro (Ishiguro et al., 1993). The paper shows that for the vessel considered (SSTH), the difference between values at Froude numbers 0.184 and 0.735 can be as much as 40% for Yr for instance. The influence of speed should therefore be taken into account in maneuvering models of high speed crafts.

A program (known as 'VESSIM') for maneuvering simulation of hard-chine craft in planing mode was developed in MARIN and Delft University. Based on 6 DOF formulations, this program takes into account all the interactions between the motions. Plante et al. (1998) presented the results from extensive tests.

Katayama and Ikeda have published a series of papers on planing craft hydrodynamics (Katayama et al., 2005; Tajima et al., 1999) in which they investigated the effect of maneuvering motions on running attitude (rise, trim angle and heel angle) and the effect of change of running attitude on maneuvering hydrodynamic forces. The results in these papers demonstrated that the effects of change of running attitude on the maneuvering derivatives are significant. These effects should be taken into account in order to evaluate the maneuverability of high speed crafts. For planing hull maneuvering analysis 6 DOF motion equations must be solved rather than 3 or 4 DOF motion equations. In 2006, Katayama proposed a mathematical maneuvering model for planing hulls using 3 DOF motion equations, which takes into consideration the change of running attitude caused by maneuvering motion (Katayama et al., 2006, 2009).

In this paper, a simplified maneuvering simulation of a Fast Rescue Craft is developed. It solves 3 degree of freedom (surge, sway and yaw) motion equations in the time domain. The hydrodynamic coefficients in these equations are defined as functions of Froude number and drift angle. These coefficients are estimated through the full scale maneuvering measurements. This method of creating the coefficient database is approximate, but it is much less time consuming and is a practical choice. For simulating the other 3 DOF motions, i.e. roll, pitch and heave, a method developed by Katayama was used. In this method, instantaneous running attitude is defined as a function of Froude number and drift angle. It is calculated at every time step by two dimensional linear interpolations of the measured data in the running attitude database rather than by solving the motion equations. Further, the program is tested by running it on a commercial fast rescue craft simulator.

2. Mathematical model

In order to simulate planing hull maneuvering, two right-handed coordinate systems were employed to derive motion equations. In the earth fixed coordinate system OXYZ, the OXY plane coincides with the waterplane surface and Z-axis points vertically downwards. In the ship fixed coordinate system oxyz, the origin is at the midship section and intersects the longitudinal plane of symmetry at the waterplane.

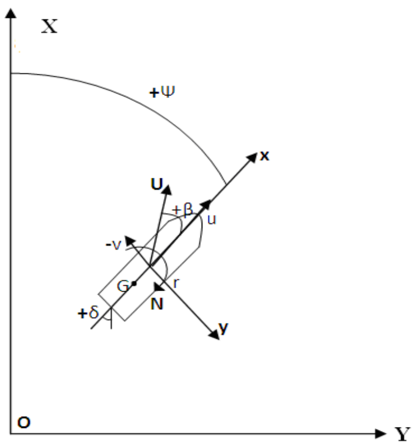

Fig.1: The Coordinate System

The 4-degree general maneuvering motion equations (surge-sway-roll-yaw) in ship fixed coordinate system are expressed as:

$$m[\dot{u} - vr - x_G r^2] = -X_{\dot{u}}\dot{u} + (Y_{\dot{v}} + X_{vr})vr + X(u) + X_P + X_R - R + X_E$$

$$m[\dot{v} + ur + x_G \dot{r}] = -X_{\dot{u}}ur - Y_{\dot{v}}\dot{v} - Y_{\dot{r}}\dot{r} + Y_v v + Y_r r + Y_{vr}vr + Y_{vv}v|v| + Y_{rr}r|r| + Y_P + Y_R + Y_E$$

$$I_{XX}\dot{p} - z_G[\dot{u} + ru] = -K_{\dot{p}}\dot{p} + K_p p + K_\phi \phi + z_G(Y_v v + Y_r r + Y_{vr}vr + Y_{vv}v|v| + Y_{rr}r|r|) + K_P + K_R + K_E$$

$$\begin{aligned} I_{zz}\dot{r} + mx_G[\dot{v} + ur] = & -N_{\dot{r}}\dot{r} - N_{\dot{v}}\dot{v} + N_v v + N_r r + N_{vr}vr + N_{vv}v|v| + N_{rr}r|r| + N_{vvr}v^2 r + N_{vrr}vr^2 \\ & + N_\phi \phi + N_{v\phi}v\phi + N_{r\phi}r\phi + x_G(Y_v v + Y_r r + Y_{vr}vr + Y_{vv}v|v| + Y_{rr}r|r|) + N_P + N_R + N_E \end{aligned}$$

where u, v, p, r are surge, sway, roll and yaw velocities relative to the water at the center of gravity; ϕ, ψ are roll and yaw angles respectively; R is the resistance of the ship; x_G, z_G are coordinates of the center of gravity. The terms with subscripts P, R and E represent propeller, rudder and environmental forces, respectively.

The total external forces and moments in these equations were modelled to simulate a planing hull moving in unbounded, calm, and deep water. Forces and moments caused due to wind, waves and current, and any influence of shallow water and bank suction were neglected. Also, the dynamics of the propulsion and control system were not included in the external force and moment model. Rather, it was assumed that the propellers (either outboards, water-jets or screw propellers) produce a constant thrust that compensates for the calm water resistance (magnitude of thrust force is fixed in steady running condition) and the direction of this thrust is changed to steer the ship.

3. Simplifying FRC maneuvering simulation

For planing hull maneuvering simulation, the running attitude (rise, trim angle and heel angle) is function of forward speed and drift angle. The maneuvering hydrodynamic forces related to velocity and accelerations are dominant. All the other terms can be neglected. Therefore the motion equations in the planing hull simulation are reduced to surge-sway-yaw three degree of freedom systems.

$$m'[\dot{u}' - v'r' - x_G' r'^2] = -X_{\dot{u}}'\dot{u}' + X'(u') + thrust' \times \cos\delta$$

$$m'[\dot{v}' + u'r' + x_G'\dot{r}'] = -Y_{\dot{v}}'\dot{v}' - Y_{\dot{r}}'\dot{r}' + Y_v'v' + Y_r'r' - thrust' \times \sin\delta$$

$$I_{zz}'\dot{r}' + m'x_G'[\dot{v}' + u'r'] = -N_{\dot{r}}'\dot{r}' - N_{\dot{v}}'\dot{v}' + N_v'v' + N_r'r' - x_p' thrust' \times \sin\delta$$

Where $'$ denotes the non-dimensionalized parameters. δ is the direction of the outboard engine and x_p' is the distance between the propeller and center of gravity.

For modeling external force and moment acting on hull, a simple linear mathematical model was used. In this model, the maneuvering hydrodynamic forces vary at each time step and are defined as follows:

- $X'(u), Y_v', N_v', Y_r', N_r'$ = function of Froude number (F_n) and Drift angle (β)
- $X_{\dot{u}}', Y_{\dot{v}}, Y_{\dot{r}}', N_{\dot{r}}', N_{\dot{v}}'$ are estimated from Motora's (1960) chart and Toxopeus' (1996) method.

By solving the above mentioned motion equations using this new definition of hydrodynamic coefficients, one can obtain X, Y and heading angle values at every time step. For calculating the other 3 DOF motions, i.e. roll, pitch and heave, instantaneous running attitude is defined as a function of Froude number and drift angle. It is calculated at every time step by two dimensional linear interpolations of the measured data in the running attitude database rather than by solving the motion equations.

4. Validation on TB45 craft

The turning circle of a planing crafts TB45 was simulated by using the planing hull maneuvering simulation program developed based on the above mentioned method. In this case, Y_r' is assumed to be dependent on forward velocity and trim and N_r' is assumed to be dependent on forward velocity and rise. The simulation results were compared with full scale sea trials results. The craft, whose principal particulars are shown in Table 1, is the one tested by Katayama (Katayama et al., 2006).

Fig.2 shows the simulated trajectories of the TB45 planing craft in deepwater for the following turning circle maneuvers: Initial Froude number, Fn = 0.7 and thrust angle = 14.6 degrees. The comparison with sea trial results and Katayama's simulation results (Katayama et al., 2009) is also presented. It shows the agreement between the present simulation and the trials data.

Table 1: Principal Particulars of TB45 (Katayama et al., 2006)

Length over all: L_{OA} (m)	0.9366
Breadth: B (m)	0.1833
Depth: D (m)	0.11
Draft: d (m)	0.0302

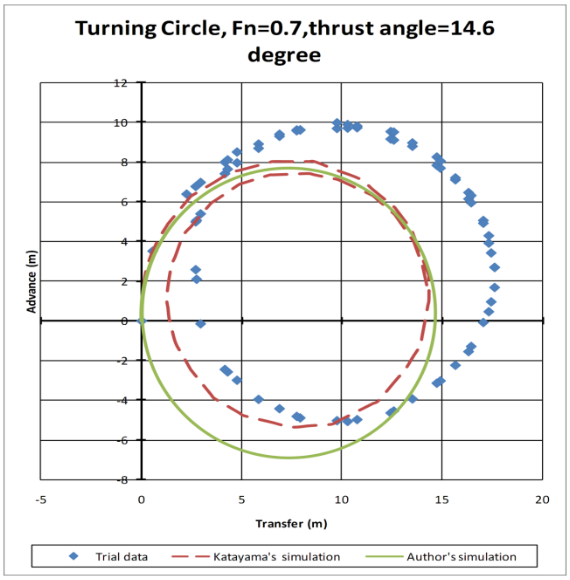

Fig.2: Turning circle trajectory for 14.6° starboard turn, Fn = 0.7

To obtain these maneuvering hydrodynamic forces at every time step, a database of hydrodynamic coefficients is required, which can only be created by conducting specially designed model tests that take into account the coupling between horizontal and vertical motions. Because of this requirement, this method can only be used for craft for which model test data from specially designed model tests is available. To create a more general program that is suitable for the marine simulation industry, there is a need to redesign the mathematical model for the planing hull maneuvering simulation to overcome the limited availability of sea trial data.

5. Modified Katayama's method for a 7.5m rigid hull inflatable boat

In order to conduct the manoeuvring simulation of the twin outboard 7.5m rigid hull inflatable boat, Katayama's model was modified. Based on the available full scale turning circle information, an input dataset was developed.

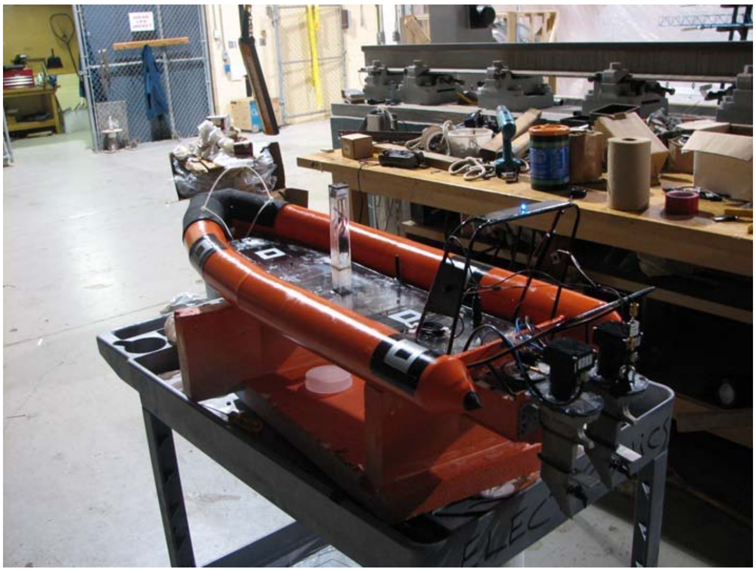

Fig.3: Twin outboard 7.5m rigid hull inflatable boat (Power and Simões Re, 2007)

The new sea trial results required for simulation included the experimental turning diameter values as shown in Table 3. Using this turning diameter data, the hydrodynamic coefficients were calculated at various Froude number and drift angle combinations. This was done using trial and error method.

It should be noted that the first guess of non-dimensionalized maneuvering derivatives data in the dataset are taken from the published results of extensive model tests conducted by Katayama on the model TB45 (Katayama et al., 2005; Katayama et al., 2006). Although the hull of TB45 model was different from the hull used in the new sea trials, TB45's non-dimensionalized hull force dataset was used to obtain hull forces because this was the only hull force dataset found in the literature for planing hulls. The simulated turning diameter results were then compared with the new sea trials turning diameter data. If the results did not compare well, hydrodynamic coefficients were slightly altered and turning circle was simulated again. This was done iteratively until the simulation results matched the sea trial results. Through this procedure, optimal hydrodynamic coefficients were obtained for the chosen Froude number and drift angle combination.

Table 2: Experimental Turning Diameter of a 7.5m Rigid Hull Inflatable Boat

Steering Wheel Rotation (deg)	RPM	Experimental Turning Diameter (m)
180	2000	304.5

	3000	293
	4000	325.5
360	2000	51.9
	3000	55.2
	4000	96.5
540	2000	26.4
	3000	20.2
	4000	33
720	2000	19.7
	3000	16.8
	4000	16.8

Now at any time instant during simulation, if the forward velocity and rudder angle is known, the corresponding optimal hydrodynamic coefficients can be calculated by two dimensional linear interpolations of the data. Hence, the 3 DOF motion equations can now be solved in the entire operational domain of the craft to obtain the global X, Y coordinates and the heading angle. As we can see, turning diameter results from sea trials are the only requirements for using this math model. Conducting sea trials to obtain turning diameter data is far less time consuming and significantly less expensive than conducting captive model tests. Hence this model provides the required flexibility to the user.

As far as the other 3 DOF motions (roll, pitch and heave) are concerned, a simple method proposed by Katayama was used. These motions were not obtained by solving the motion equations but by conducting two dimensional linear interpolations on the running attitude data obtained from experiments. Running attitude data published by Katayama can be initially used to create this database for any FRC and tuning of data can be done at a later stage with the help of sea trial results and by visual inspection of an FRC pilot. Katayama's data (Katayama et al., 2005b; Katayama et al., 2006) were used to create the running attitude database. These data are given in Table 3.

Now at any time instant during simulation, if the forward velocity and drift angle

($\beta = -\sin^{-1}\dfrac{v}{U}$) is known, the corresponding roll angle, pitch angle and heave can be calculated by two dimensional linear interpolations of the data given in Table 3. Hence, all 6 DOF motions can now be accounted for.

After the input databases were prepared, turning circle maneuvers were simulated. Table 4 shows a comparison between experimental and simulated (using the new program) turning diameters of the craft.

Table 3: Running Attitude of a 7.5m Rigid Hull Inflatable Boat

	Heave (mm)	Pitch (degree)	Roll (degree)
u (knots) / β (degree)	0.0		
0	0	0	0
10	0	0	0
20	0	0	0
30	0	0	0
u (knots) / β (degree)	5.81		
0	-31.7257	0.37	0
10	-39.0453	0.37	0
20	-70.771	0.418	0
30	-70.771	0.418	0
u (knots) / β (degree)	7.9		
0	-33.3547	2.2	0
10	-47.8926	2.2	0
20	-114.703	3.019	0
30	-114.703	3.019	0
u (knots) / β (degree)	10.56		
0	16.2104	3.1	0
10	0	3.2	3.28
20	49.4782	6.686	17.81
30	49.4782	6.686	17.81
u (knots) / β (degree)	14.79		
0	83.8609	3.4	0
10	129.3426	4.3	11.72
20	227.9369	4.802	22.5
30	227.9369	4.802	22.5
u (knots) / β (degree)	19.56		
0	185.6988	4.2	0
10	224.5196	3.8	14.53
20	261.1251	1.722	19.69
30	261.1251	1.722	19.69
u (knots) / β (degree)	24.3		
0	229.3994	3.9	0
10	258.6852	2.7	15.94
20	270.8918	1.16	17.81
30	270.8918	1.16	17.81
u (knots) / β (degree)	29.59		
0	258.6852	3.5	0
10	270.8918	1.9	15.47
20	380.7082	0.427	23.44
30	380.7082	0.427	23.44
u (knots) / β (degree)	35.62		
0	258.6852	3.5	0
10	270.8918	1.9	15.47
20	380.7082	0.427	23.44
30	380.7082	0.427	23.44

Table 4: Comparison between Turning Diameters

Steering Wheel Rotation/Outboard Motor Rotation (deg)	RPM/Max Forward Velocity/(knots)	Experimental Turning Diameter (m)	Turning Diameter Simulation (m)
180/9	2000/8	304.5	303
	3000/16.5	293	292
	4000/26.6	325.5	321
360/19	2000/8	51.9	51
	3000/16.5	55.2	53
	4000/26.6	96.5	98
540/29	2000/8	26.4	26
	3000/16.5	20.2	20
	4000/26.6	33	31
720/40	2000/8	19.7	18
	3000/16.5	19.8	16
	4000/26.6	16.8	17

As expected, there is very good agreement between the experimental results and current method. To check the visuals, a 90 second arbitrary maneuver was simulated as a test case using the new program and results were visualized in a MATLAB numerical simulation with 3D image generation from an FRC full mission simulator. The test case was defined as follows:

- At T = 0, Simulation begins with the craft at rest
- At T = 10 sec, both propeller's rpm commanded to 4000 (corresponding speed = 27 knots), Thrust angle = 0
- At T = 30 sec, Thrust angle = 30 deg
- At T = 38 sec, Thrust angle = 0 deg
- At T = 60 sec, Thrust angle = -10 deg
- At T = 66 sec, Thrust angle = -30 deg
- At T = 78 sec, Thrust angle = 0 deg
- At T = 82 sec, Propeller rpm commanded to 0
- At T = 90 sec, End of simulation

Fig.4: Simulaiton at time 6.5 seconds

Fig.5: Simulation at time 19 seconds

Fig.6: Simulation at time 36 seconds

The visual results were very satisfactory and the roll, pitch and trim motions during maneuvers were displayed clearly. Some of the screenshots are given in Figure 4, Figure 5 and Figure 6.

6. Conclusions

In this study, a mathematical model was developed to simplify planing hull maneuvering simulation. The most favorable aspect of the model is that turning diameter results from sea trials are the only requirements for using this simulation model. Conducting sea trials to obtain turning diameter data is far less time consuming and expensive than conducting captive model tests. This model was tested for a twin outboard 7.5m rigid hull inflatable boat and the simulation results were satisfactory. The developed program can be plugged into a commercial FRC simulator for training purpose.

7. Acknowledgements

This research was financially supported by the NSERC CREATE research program for Offshore Technology Research, MITACS Accelerate Fund and ACOA Atlantic Innovation Fund. The authors would like to express their thanks to Virtual Marine Technology Inc. for providing trials data and for making their FRC simulator available to evaluate the model.

References

Ishiguro, T.; Uchida, K.; Manabe, T.; Michida, R. (1993), *A study on the maneuverability of the Super Slender Twin Hull*, Proceedings of FAST'93, Yokohama.

Katayama, T.; Kimoto, R.; Ikeda, Y. (2005), *Effects of Running Attitudes on Maneuvering Hydrodynamic Forces for Planing Hulls*, Proceedings of the 8th International Conference on Fast Sea Transportation (FAST'2005), St. Petersburg, Russia.

Katayama, T.; Iida, T.; Ikeda, Y. (2006), *Effects of Change in Running Attitude on Turning Diameter of Planing Craft*, Proceedings of 2nd Pan Asian Association of Maritime Engineering Societies (PAAMES) and Advanced Maritime Engineering Conference (AMEC2006), pp. 177-183, Jeju Island, KOREA.

Katayama, T.; Taniguchi, T.; Fujii, H.; Ikeda, Y. (2009), *Development of Maneuvering Simulation Method for High Speed Craft Using Hydrodynamic Forces Obtained from Model Tests*, 10th International conference on Fast Sea Transportation, FAST 2009, Greece.

Motora, S. (1960) *On the Measurement of Added Mass and Added Moment of Inertia fro Ship Motions: Part 2. Added Mass Abstract for the Longitudinal Motion*, Journal of the Society of Naval Architects of Japan, 106:59-62.

Plante, M.; Toxopeus, S.L.; Blok, J.; Keuning, A. (1998), *Hydrodynamic manoeuvring aspects of planing craft*, Proceedings of International Symposium and Workshop on Forces acting on a manoeuvring vessel, Val de Rueil.

Power, J.; Simões Re, A. (2007), *Assessment of the performance of 1:7 scale model liferafts under tow by a carriage and fast rescue craft*, Institute Report TR-2007-23, Institute of Ocean Technology, Canada.

Tajima, S.; Ikeda, Y.; Katayama, T.; Okumura H. (1999), *Measurements of Hydrodynamic Forces Acting on Planing Hull at High-Speed by Planar Motion Mechanism Test*, Journal of the Kansai Society of Naval Architects, Japan, 232:71-76.

Toxopeus, S. (1996), *A Time Domain Simulation Program for Manoeuvring of Planing Ships*; Report No. 1065-S, Delft University of Technology.

The Proposal of the Optimal Framework to Perform Multidisciplinary Design Optimization of the Power Yachts Hull Design

Dong-Hyun Ahn, Department of Naval Architecture and Industrial Engineering, Seoul National University, Seoul, Korea, dong8@snu.ac.kr
Philippe Lee, Xinnos Co., Ltd., Seoul, Korea, philippe_lee@xinnos.com
Jong-Gye Shin, Department of Naval Architecture and Ocean Engineering, Seoul National University, Seoul, Korea, jgshin@snu.ac.kr

Abstract

This paper presents a new integrated software tool for basic modeling of power yachts. This tool includes modules for modeling hull and outfitting, and a module for checking scantling rules. The modules developed in the tool are optimized for power yachts, so that it reflects characteristics of power yachts, for example, dimensions, materials, etc., which are different from other commercial vessels. The software tool is designed based on 3D CAD and is implemented in UG NX.

1. Introduction

The conventional hull design has been made through the following process in general. It mostly starts from the mother ship and is modified to have the characteristic value meeting the requirements. Then, the various performance estimations possible in a given design environment are performed by this modified hull. Analyzing estimated performance of the hull and modifying the hull design are carried out repeatedly. Most of the hull design follows a similar process as described above based on the information of mother ship.

The hull design process presented in this paper is to design a hull using only the requirements and the main dimensions that are determined when a concept design of a power yacht is completed. It produces a basic hull shape for the one-chined mono-hull power yacht from several characteristic values and the main dimensions of the hull given by the requirements of ship. Multidisciplinary design optimization (MDO) can be applied to this procedure. This paper proposes a framework for power yacht design optimization using MDO.

2. Multidisciplinary Design Optimization

MDO is an analysis to perform the optimization in consideration of a various engineering fields with different nature at the same time. Engineering design of modern products does not just mean a modeling to draw pictures simply according to the figures. One must consider meeting all the requirements and performances of various sectors when designing products. However, the existing engineering analysis is conducted in a manner to obtain the result range to meet the requirements by applying the methodology for one purpose. The results obtained as so might get the design criteria to satisfy one purpose but may not be able to meet the necessary conditions in the other criteria. It is often difficult to reach the best design unanimously in the modern design organization that is comprised of various experts with different disciplines. MDO aims to obtain the design criteria given the different purposes simultaneously and also the algorithm to find the optimal value by connecting a variety of design parameter. The examples of helicopter design cases (Kim Sanghum & Lee Dong-Ho,

2005) or analysis of car crash cases (Liao Xingtao, Li Qing, Yang Xujing, Zhang Weigang, Li Wei, 2008) which obtained satisfactory results by applying this methodology demonstrated the effects. This study applys MDO to the hull design of power yachts, examples of which is relatively difficult to find, and proposes a framework to perform MDO of power yacht hull design.

3. The hull design process of power yachts

3.1. The features of hull design

The general flowchart of a hull design is summarized as follows through the conventional hull design practices and research results.

Fig.1: Basic Flow of Ship Basic Hull Design

There may be repetitive processes which are not presented in the figure, in fact, because the hull may go through the steps of redesign and optimization depending on the results of the basic ship calculation, stability performance calculation and fluid dynamics analysis after a hull form derived as a result of the input values in the hull design.

Also, it can be seen in Fig.2 what kind of relations the hull design has in the entire ship design process. It is assumed for the hull design to be included in the basic design in this figure. The hull design can be redesigned by the various succeeding design steps, analyses and verifications.

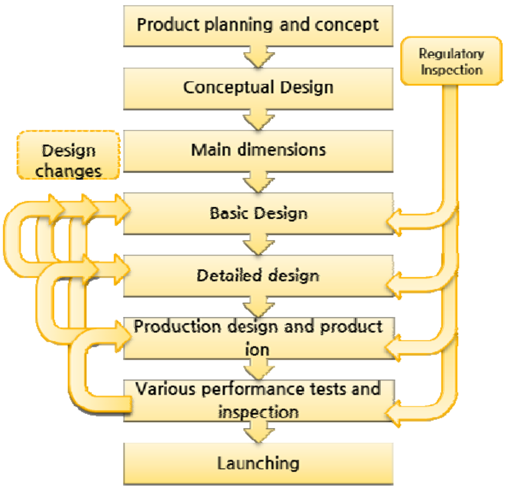

Fig.2: Yacht ship design process flowchart

The hull design in the basic design step is carried out by taking the main dimensions and major points as input values and the design may change due to a variety of causes during the entire design process. The more detailed features are as follows.

First, in the basic design step, main dimensions and major points are taken as input values. Whether the hull is designed from a mother ship or a hull design of the same type, or from a design of a stylist, this procedure is applied consistently. If there is a mother ship or a same type ship, design parameters including major dimensions are taken from this referred hull and entered as input values.

Second, redesign is required due to various causes in the whole design process and therefore the hull design needs to be modified frequently. The various reasons that cause redesign include change of requirements from the ship owner, changes for the performance improvement as a result of the performance estimation and analysis, changes to comply with regulations for inspection, etc.

3.2. The design change in the hull design

Hull design may need to be redesigned due to the result of a variety of tasks.

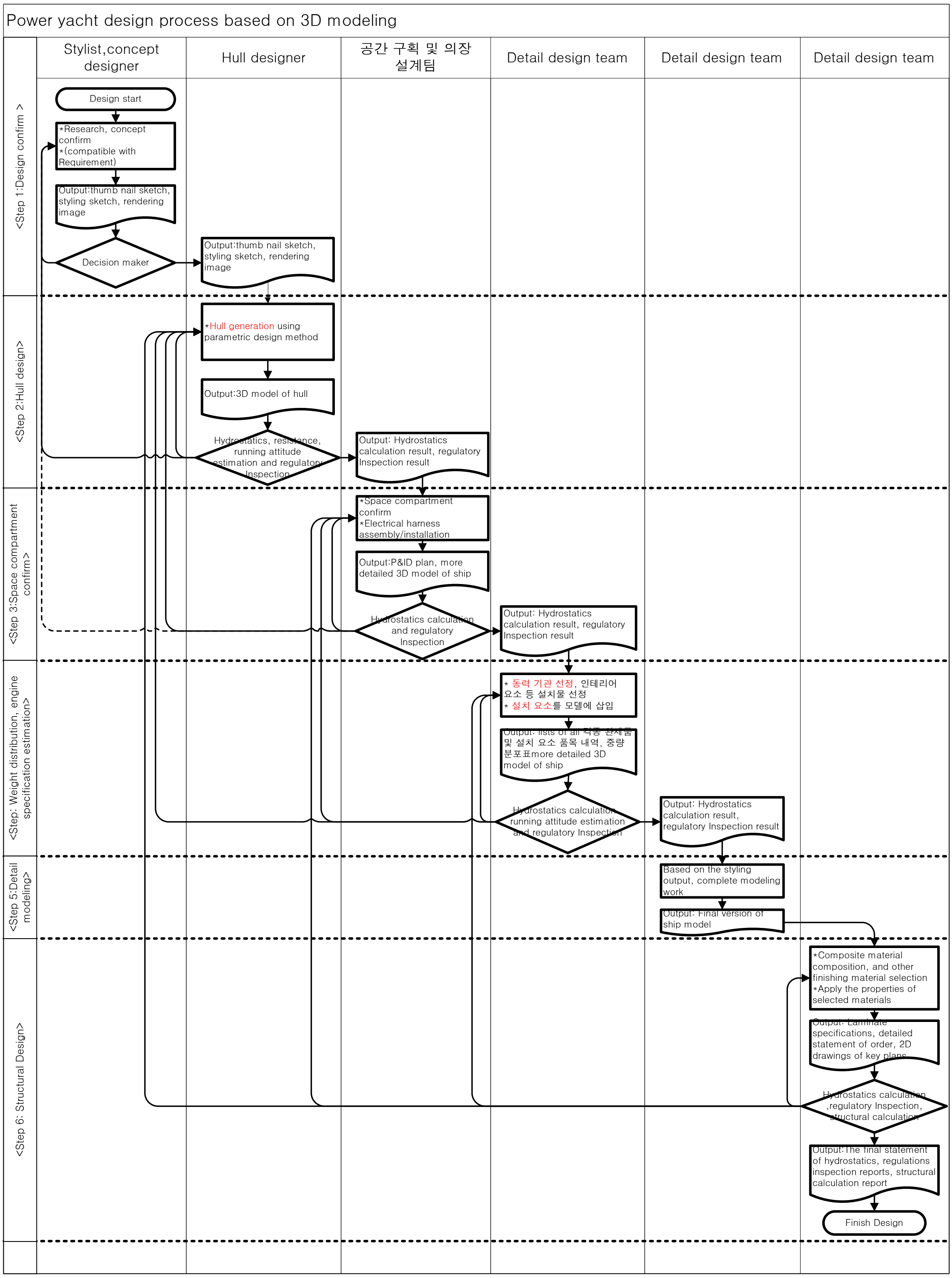

Fig.3: Power Yacht Design Process Based on a Single Model

In recent design environment, there have been technical demands for optimization technique that can improve the results of multiple design criteria in addition to the efficient redesign.

3.3. The power yachts hull form optimization framework

The optimal framework this paper proposes is based on response surface methodology (RSM) and is shown below.

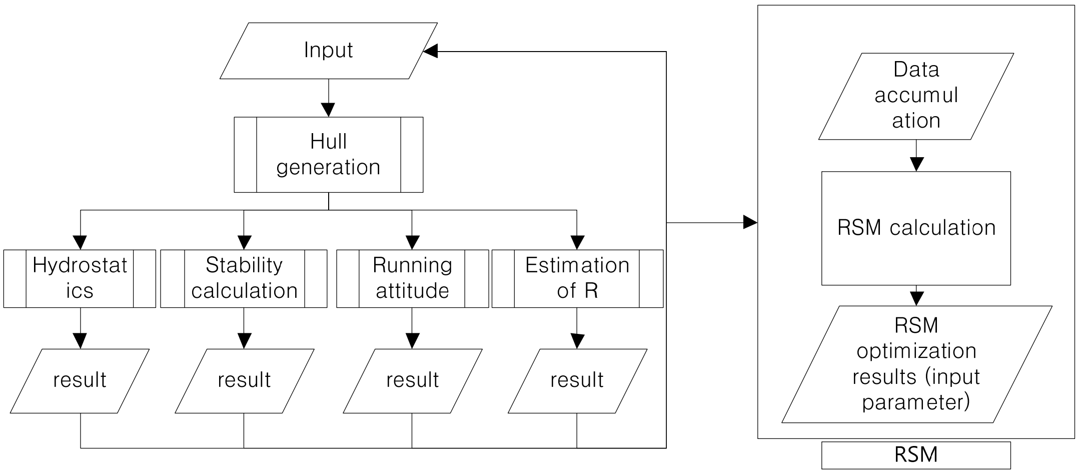

Fig.4: Power Yacht Hull Design Optimization Framework Based on RSM

For each design process work unit, the optimal solution can be obtained by performing RSM using the input values and results of the corresponding work unit. Also by using the results of each design process as a constraint of optimization for other processes, the optimized input values that can improve the results of multiple calculation areas can be obtained. These input values are the parameters that generate the hull form.

The following describes the flowchart in Fig.4 starting from "the input values." Once the input values are set based on the requirements or design constraints, the parametric hull generation applications are implemented in 3D CAD to generate hull model. The generated hull model becomes an input for each individual design process, such as hydrostatics, decision of running attitude, estimation of resistance, etc. The results of individual design processes are accumulated as data which is required to perform RSM calculation with input values in an integrated environment. More reliable calculation of RSM can be performed based on the results of performance of many baseline design model. The calculated results of RSM are used again as input values to determine the hull model.

It is also possible to optimize multiple design processes in addition to a single design process when enough data are accumulated.

4. The design of power yachts hull optimization application

4.1. The structure of hull design application

The power yacht hull modeling application is based on the parametric design and implemented by developing add-in modules based on UG NX, which is a general-purpose mechanical design CAD. Typically, Korean power yacht industry uses AutoCAD for the outfitting design and Rhino2D or Maxsurf for the hull design. However, the application developed in this study is based on a general-purpose CAD which can be used even from the conceptual design stage because the goal of this study is to unify the design stages composed of separate applications.

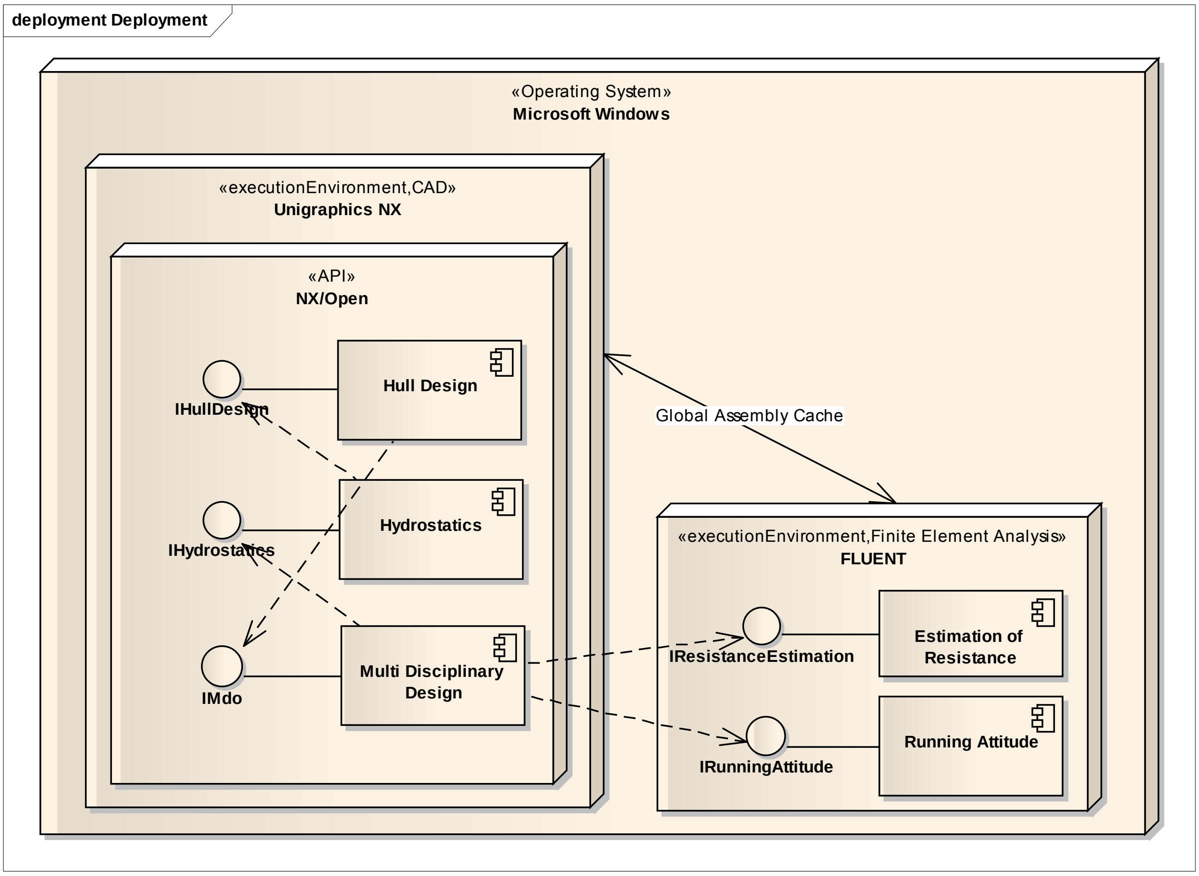

Fig.5: OOCBD Deployment Diagram

The figure above shows software architecture of physical deployment level of the hull design application developed in this study in UML (Unified Modeling Language). User interface part is integrated with NX because a commercial CAD is used as a base. The actual implementation is also done with OpenNX, which is an API UG NX is providing.

It is designed with MVC (Model – View – Controller) pattern considering scalability and maintenance of applications, and user interface part corresponds to View. The following shows the software architecture of the hull design application in a logical form. MVC architecture is clearly revealed because the software consists of logical layers. Scantling and outfitting parts are not covered in this study because they are not included in the hull design, and components corresponding to the hull design are the target to be implemented.

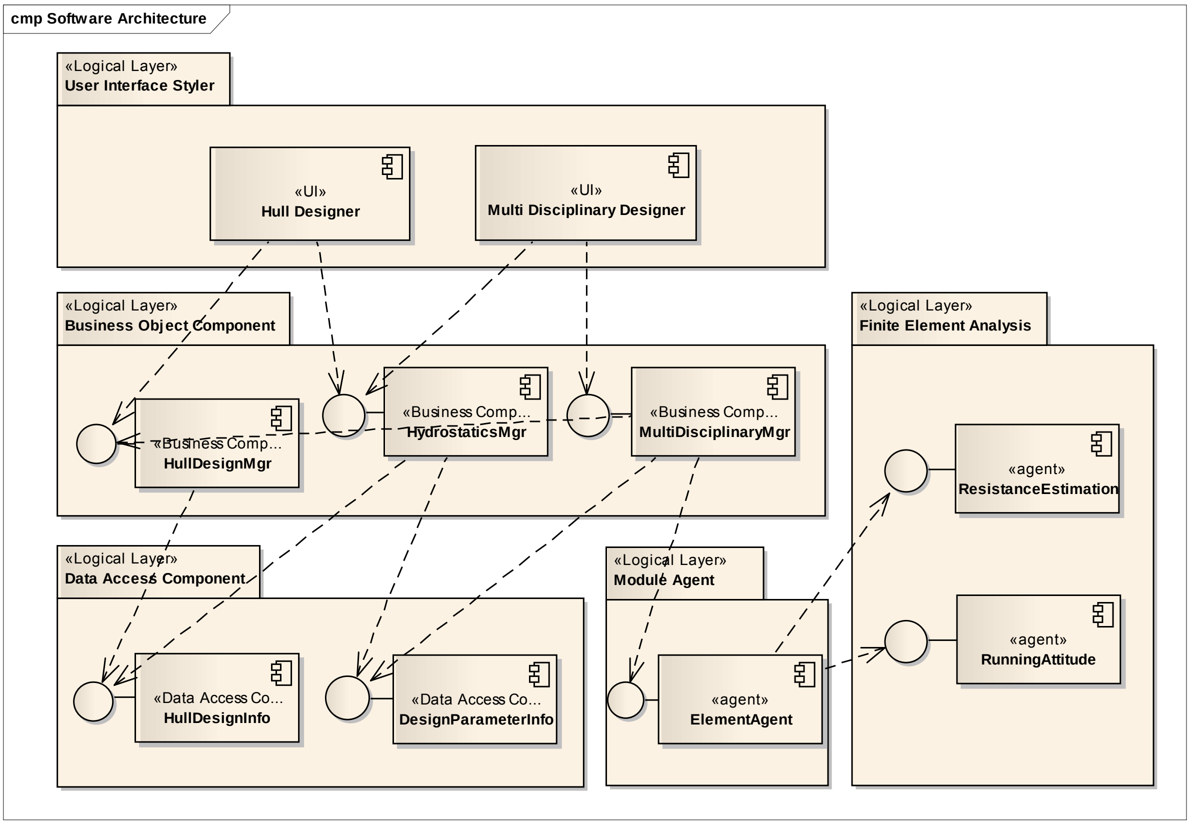

Fig.6: OOCBD Logical Structure Diagram

4.2. The interface of hull optimization application

The hull design application designs the hull form after receiving 12 input parameters from the user interface as summarized in Section 3.1. The generated hull is stored inside the application as a model of UG NX to support parametric design and the form changes as input parameters change. Therefore the above input parameters are the dominant values which are the base of MDO because the hull form will change if input parameters change.

Find: x_{hull}

Where x_{hull}^T = { K_Loa, K_Height, K_CL_Height, K_R, MS_C_Height, TS_C_Height, CL_M_Beam, CL_T_Beam, DL_M_Beam, DL_T_Beam, K_T_Height, CL_Length, K_BmaxStation, K_Transomrake_Angle, K_Keelline_Angle, K_Bowrake_Angle, MS_F_Angle, MS_C_Angle, TS_F_Angle, TS_C_Angle, TS_D_Angle, CS_T_Angle, CL_Entry_Angle_1, CL_T_Angle, DL_Entry_Angle, DL_T_Angle, MS_D_Angle, CS_K_Angle, CL_Entry_Angle_2}

Minimiza or maximaze: $Z_i(x_{hull}^T)$

Satisfy: $Const_1 < 0$, $Const_2 < 0$, $Const_3 < 0$

The hull design application generates a hull form depending on the 12 input parameters. Thus, if an external module is allowed to access the input parameters, then it is an MDO-ready interface for the application. As described earlier, the hull design application is developed on the basis of UG NX and each component is developed using .Net Framework. It is sufficient to keep .Net Framework of the same kind for the interface exposure because this study does not assume the interface between different kinds. The hull design input parameters, to send and to be sent in the interface, are designed as a separate class according to the object oriented concept. The following two figures are a UML diagram corresponding to the interface added to the software architecture and a class diagram of input parameters dealt in section 4.1.

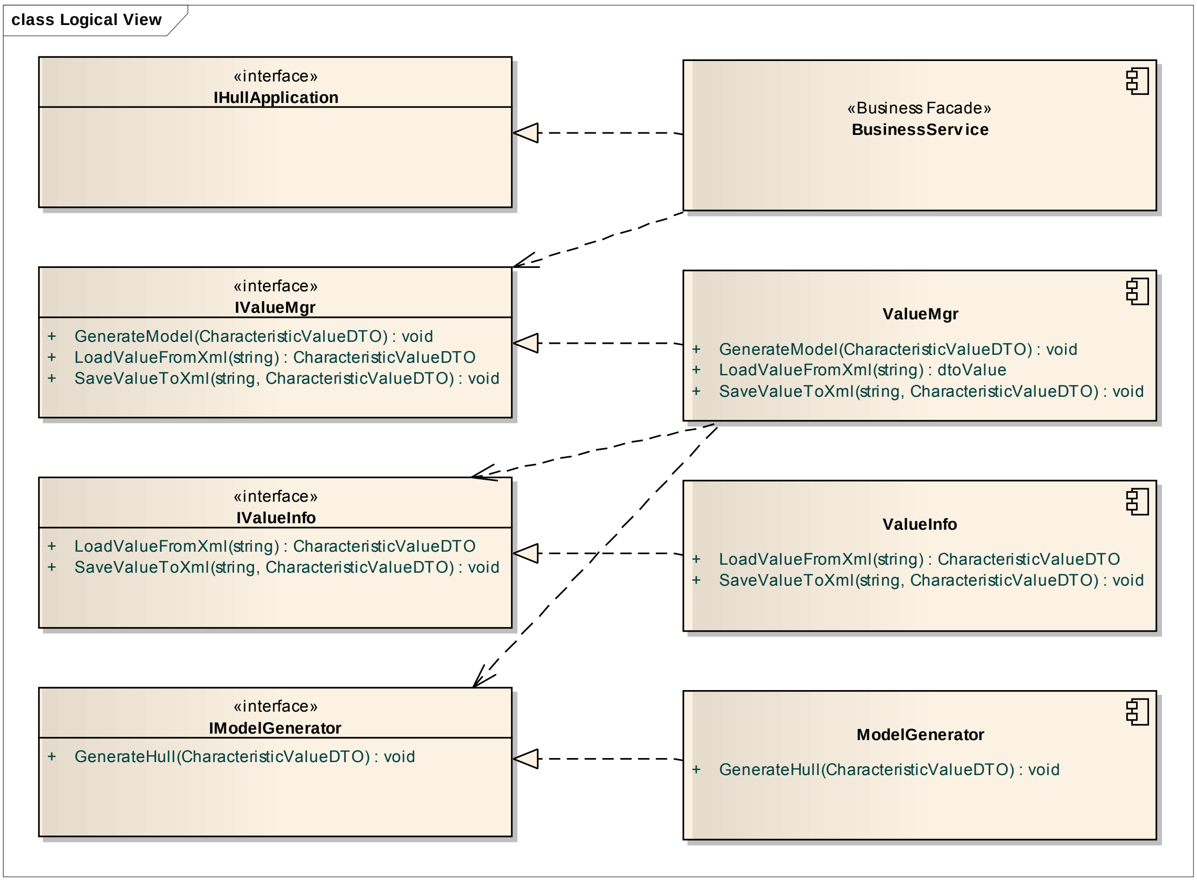

Fig.7: Hull Generation Application Component Diagram

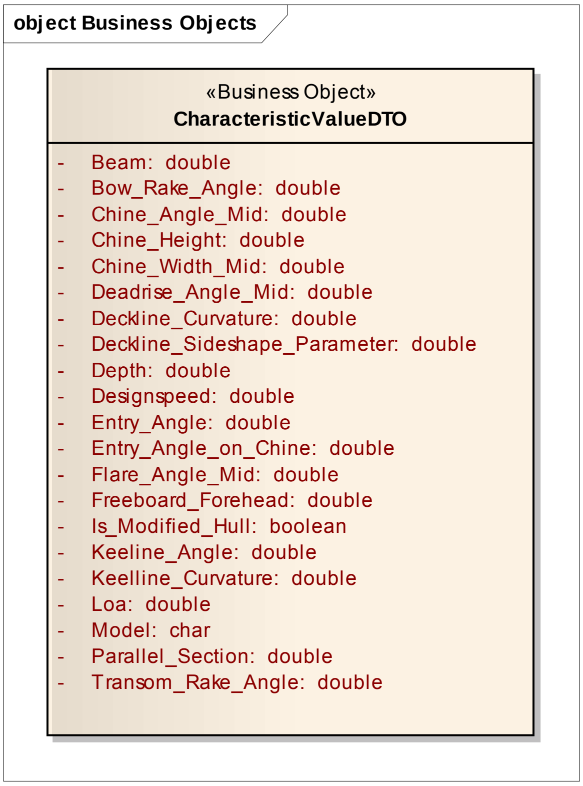

Fig.8: Hull Generation Input Value Class Diagram

4.3 The data flow components of the hull optimization application

The hull design input parameters exposed through the interface are used as the dominant values of the hull optimization in MDO iteration. Therefore, the optimal values are to be obtained with iteration of processes as defined in section 3.3 and the optimal solution is to be determined by applying RSM method.

Each information starts from the initial values which are used to design the first hull form. After some required analyses are carried out, the information is updated based on the result of MDO iteration. Then, the updated information is again fed as input parameters in the next iteration.

The change process of data is as follows when expressed in State Machine Diagram of UML.

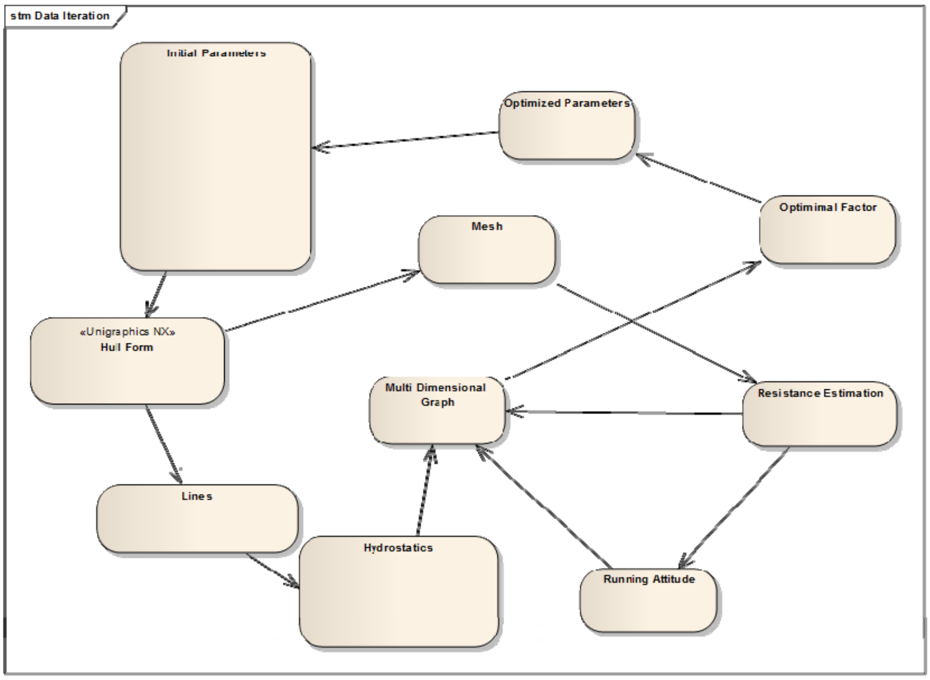

Fig.9: State Machine Diagram of Data Transfer

5. Power yacht hull optimization framework cases

In this section, the power yacht hull optimization framework based on RSM, proposed in this paper, is applied to an example of actual hull design case.

5.1. Hull optimization framework cases

Hydrostatics, resistance estimations and prediction for running attitude are selected as our target processes of the hull optimization framework configured in this paper. It is considered to be sufficient to choose the above three processes because the process selection doesn't make a big difference in the configuration of the framework and adding a process for optimization does not affect the overall framework when constructing an actual integration environment based on a single 3D CAD in the future. It is also determined that there is no insufficiency because it contains all of the most important processes to affect the hull design and performance in terms of research.

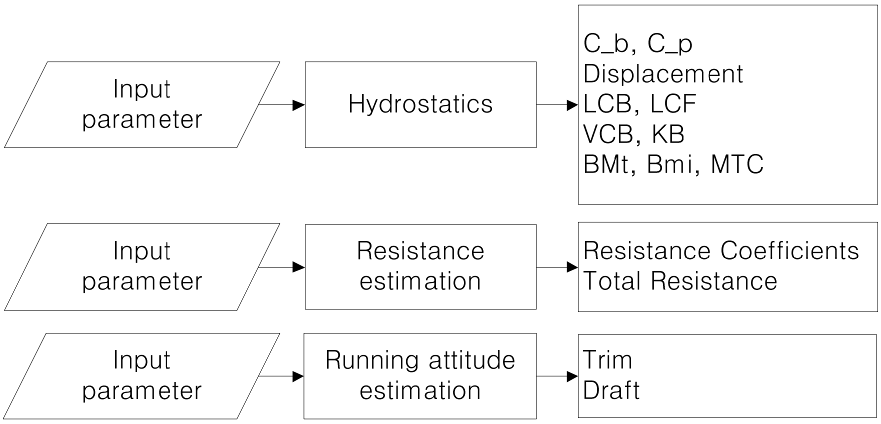

Fig.10: Result value list of target for optimization

Each design process gives outputs as shown in the figure. For an optimization using RSM, two or more variables are to be extracted as design variables, from the result values list for state variables and from the input values. The variable selected as a design variable is to be diversified through CCD (Central Composite Design) method. The list of design variable provides "analysis result" for "response surface creation" which is the next step to RSM. The optimum value is calculated with RS (response surface) from approximation of "the analysis result."

Optimization can be achieved either for the performance or the features depending on the priority or preferences. The hull model of the optimization application is generated by parametric design methodology for efficient RSM and automates the calculation of this one cycle.

The configuration of State Machine Diagram at the implementation level is shown as follows by adding state transition analyzed in section 4.3 to a functional component.

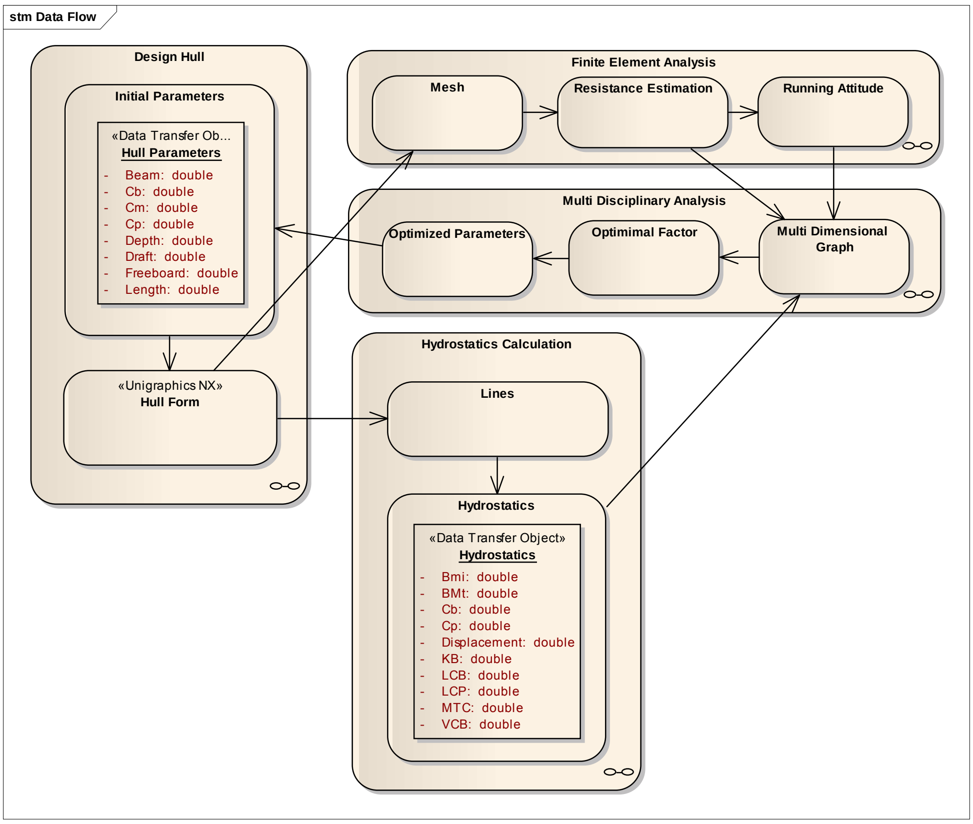

Fig.11: State machine diagram on implementation level

5.2. Perform hull optimization

The optimization of hull can be performed by applying CO (Collaborative Optimization) method. CO method categorizes the optimization problem under two levels; System Level and Subspace Level. Through the segmentalization, it finds the optimum point of system level by performing independent optimization of subspace level and adjusting this optimum point. The advantages of performing optimization of subspace level, which is segmentalized through CO method, are it can perform only with the relevant design variable, and can reduce the time consumption as it could parallelize the optimized system process. This study chose RSM as a methodology to find the optimum point of each level, system level and subspace level, and a methodology of CO method is used to find the optimum point among the each level.

6. Conclusion

It always has been an important issue to make more efficient design work environment in manufacturing industry. In addition, the hull design is ahead of other processes of a power yachts design and is the most frequent process of redesign or optimization affected by the results of other design processes. Therefore, in this study, we make the hull optimization design framework possible for the actual performance by making the hull model using a parametric hull generation technique and inserting the model to the optimization environment to perform MDO. We also prove its effectiveness by building the optimization practices with scenario to redesign the hull of the actual design ship.

We also obtain the potential for applying methodology to perform the optimization by giving appropriate weights to the multiple results in the future, by automating the creation of the hull model through the parametric design methodology. This is in the direction for the future research and can be the foundation for the development of single optimization application which can include the overall hull design process.

7. Acknowledgement

This research was supported in part by the ‘Development of 20feet/60feet power yacht with CAE total design and new production system’ program of the Korean Ministry of Knowledge and Economy, Republic of Korea.

References

Batill, S.M.; Stelmack, M.A.; Yu, X.Q. (1999), *Multidisciplinary design optimization of an electric-powered unmanned air vehicle*, Aircraft Design 2, pp.1-18.

Harries, S. (1998), *Parametric Design and Hydrodynamic Optimization of Ship Hull Forms*, PhD Thesis, Technische Universität Berlin.

Kuahai, Y.; Yanbin, X.; Yanbin, Z.; Zhufeng, Y. (2011), *Mathematical Programming Models and Algorithms for Multidisciplinary Design Optimization*, Energy Procedia 13, pp.5272-5280.

Park, C.K.; Yang, Y.S. (2008), *Development of Web-based MDO Framework for Design and Analysis Integration*, Journal of the Society of Naval Architects of Korea, Vol.45, No.3, pp.322-328.

Roshanian, K. (2006), *Effect of Variable Selection on Multidisciplinary Design Optimization-a Flight Vehicle Example*, Chinese Journal of Aeronautics 20, pp.96-96.

Shin, P.S.; Chung, H.K.; Woo, S.H. (2009), *A Magnet Pole Shape Optimization of a Large Scale BLDC Motor Using a RSM With Design Sensitivity Analysis*, Trans. KIEE. Vol.58, No.4, pp.735-741

Automatic surface capturing of CFK propellers

Olaf Grewe, Fraunhofer AGP, Rostock/Germany, olaf.grewe@hro.ipa.fraunhofer.de

Martin-Christoph Wanner, Fraunhofer AGP, Rostock/Germany, martin-christoph.wanner@hro.ipa.fraunhofer.de

Abstract

The Fraunhofer AGP was part of the network research project "CFK-Prop-6m" ,KRÖGER et. al (2011). In this project technologies had to be developed to enable the production of CFK propellers of up to 6m diameter. Therefore new methods for the design, construction, production and quality control of such propellers had to be developed.

As part of the project the Fraunhofer AGP worked on techniques to control and optimize the geometric quality of propellers. To achieve this, for two main subjects efficient solutions had to be developed:

- *surface based 3d measurement for composite propeller structures*
- *computing of the propeller parameters from surface data*

1. Motivation

The geometric parameters have a great influence on the propeller performance like efficiency, noise, vibration and cavitation. Therefore the geometric parameters and the design of a propeller have to be optimized for each individual ship. To achieve the designed performance parameters the difference between the designed and the actual geometry should be a minimum. For the following two reasons this is challenging for composite propellers:

1) In difference to casted propellers we have three manufacturing (positive model, negative model, final product) and one assembly step. The casted propeller gets its final geometry through milling and sanding. Therefore the final surface can be optimized. While the composite propeller is formed directly in the mould. It´s geometry can´t be adjusted and must be in tolerance for every propeller blade.
2) Composite propeller blades can bend quiet easily in comparison to casted propeller blades. The parameters for stiffness can be optimized for great performance over a wide range of operation modes.

2. State of the technology

The propeller geometry and the basic geometric parameters are described in the ISO 3715. Based on the ISO 484 the tolerances for the individual parameters can be determined using the following classifications:

- Diameter (484/1 >2500 mm; 484/2 800 - 2500 mm)
- Quality class (s, 1, 2, 3)

Examples of the used tolerances are shown in figure 1.

D = 0,8 - 2,5m (484/2)				lokale Steigung		Steigung pro Schnitt pro Blatt		Steigung pro Blatt		Steigung je Propeller	
Genauigkeitsklasse				± %	Minimum [mm]	± %	Minimum [mm]	± %	Min [mm]	± %	Min [mm]
	S	S	Sehr Hoch	1,5	10	1	7,5	0,75	5	0,5	4
	1	I	Hoch	2	15	1,5	10	1	7,5	0,75	5
	2	II	Medium	3	20	2	15	1,5	10	1	7,5
	3	III	Breit			5	25	4	20	3	15

Fig.10: Tolerances for pitch

2.1. Tactile measurement

Propeller manufactures use tactile measurements as state of the art. An example of such a measurement device is shown in figure 2. These kinds of devices are based on an centralized measurement arm which is mounted to the propeller axis. The measurement arm defines the actual probing cylinder. The probe is then pointed downwards onto the propeller surface. The height values are recorded in defined angular steps.

The number of cylindrical intersections depends on the quality class. Up to eight intersections have to be measured. On each intersection about twelve measurement points are recorded. This measurement method requires smooth surface without any dents or buckles.

The following geometric parameters of the propeller are then calculated via the measurement points, ALLEN et. al (1995/2005):

- Pitch
- Rake
- Skew
- Profile height

These parameters determine the performance parameters, like impulse, noise, vibration and cavitation. In the ISO 484 the quality control of the edges is described as a manual method based on templates.

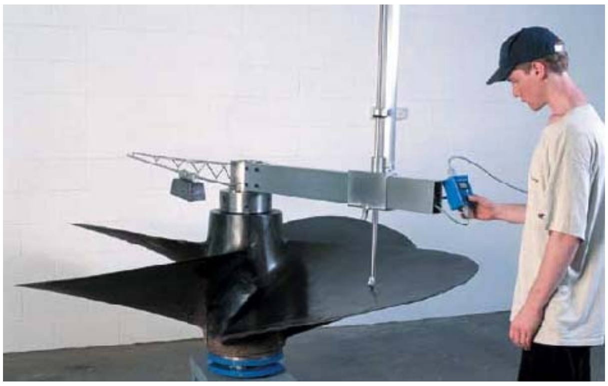

Fig.11: Manual quality control of a smaller propeller, PROPELLER DYNAMICS (2009)

2.2. 3d measurement devices

Surface based 3d measurements are not state of the art for the quality control of marine propellers. These techniques acquire the surface of technical or natural objects with very high accuracy in short time. The measurement distance for technical applications reaches up to 200 meters with current devices.

A lot of different scanner types are available on the market. These scanners differentiate in the measurement technology and the reachable accuracy. For larger measurement volumes the accuracy gets smaller. 3d scanners with high accuracy can only reach small measurement distances. Surface based, optical 3d measurement devices reach about $\frac{1}{10.000}$ of the measurement volume as achievable accuracy.

Objects have to be scanned from several stations, to acquire the complete surface. These scans have to be related to each other and transformed into one coordinate system. This process can be done automatically with the sensor itself or with the help of an superior reference system. Such reference system should be acquired using a measurement system with higher accuracy.

The result of a surface based measurement is a 3d point cloud. For every 3d measurement point the x, y, z coordinate is stored in this file. The analysis of such point clouds is mostly a manual job. The operation of analysis software for the 3d measurement data is currently done by highly educated engineers.

For the analysis of propeller data software for the tactile measurements is available, COLBY (2001). For surface based measurement data from scanners such software must be developed.

Tests with laser scanners showed great potential for:

- Increased measurement speed
- Improvement in quality and quantity of the measurement data
- Reduction of errors

3. Development areas

Two operators need at least one working day for the tactile quality control of an propeller. This time should be decreased dramatically. The experience of the operator has great influence on the quality of the results. The likeliness of errors or the human factor should be reduced also. Edges and by conducted blades blocked surface parts can´t be controlled using the tactile method. These parts of the propeller are currently reviewed subjectively.

For the development of a new system to control the quality of propellers two development areas were defined:

- Measurement methods:
  First step is the determination of an appropriate measurement method for the surface based testing of CFK propellers and components. This method of measurement must meet the accuracy requirements of the ISO Standards and allow for inspection during production of carbon fiber propellers.

- Software development:
  Development of processing algorithms and functional software modules, which allow a semi automated evaluation of the recorded data.

4. Measurement methods

4.1. Measurement device

To determine a suitable measuring method initially a specification with the necessary requirements was developed. This specification was an active document, in which the project partners added requirements and goals, if necessary, over the time of the project. For the application of marine propellers seven different measurement devices can accomplish the accuracy requirements. These systems are compared in figure 3.

Criteria for the comparison have been established and weighted, to determine the optimal measurement device. The weighting was determined by a hierarchical evaluation. For the assessment a rating system from one to five which scales between "very good" and "insufficient" was used. The assessment is based on the technical specifications of the systems.

Taking the required investment into account the comparison and the evaluation showed that the structured light projector (for example the GOM ATOS) is best suited for the surface recording. To evaluate the suitability of the different measuring volumes for the use case measurement accuracy and the required measurement time were used.

The evaluation of measurement uncertainty was based on three criteria:

- propeller pitch
- shape of the edges
- chord length

	Messsystem													
	Wert	Note	Wert	Note	Wert	Note	Wert	Note	Wert	Note	Wert	Note	Wert	Note
	Streifenlichtprojektion		Messarm		Leica T-Scan + Tracker		Leica T-Scan + Optotrak		Pro-SPOT		Konica Minolta Range7		Laserradar	
Messvolumen	≤ 2 x2 x2 m	2	≤ 0,2 x 0,15 m | F = 3,6 m	1	0,09 x 0,08 m | R = 18 m	1	0,09 x 0,08 m | 4 x 3 x 6 m	1	6 x 6 m	1	0,3 x 0,3 x 0,2 m	4	R = 24 m	1
Messgeschw.	> 8s / 4m²	2	manuell	5	manuell	5	manuell	5	< 1s / 36 m²	1	> 2s / 0,1 m²	5	2 pts/sec	4
Messgenauigk.	85 µm	3	37 + 100 µm	4	20 + 60 µm	3	20 + 100	4	60 µm	3	40 µm	2	53 µm	2
Mobilität	Gut	2	Sehr gut	1	Ausreichend	4	Gut	2	Gut	2	Sehr gut	1	Ausreichend	4
Robustheit	Gut	2	Gut	2	Ausreichend	4	Gut	2	Gut	2	Sehr gut	1	Befriedigend	3
Nebenzeiten	Befriedigend	3	Gut	2	Gut	2	Sehr Gut	1	Befriedigend	3	Befriedigend	3	Gut	2
Bedienung	Gut	2	Befriedigend	3	Befriedigend	3	Gut	2	Gut	2	Sehr gut	1	Ausreichend	4
Investition	75 t€	3	80 t€	3	> 200 t€	5	> 100 t€	4	> 450 t€	5	40 t€	2	> 250 t€	5
Betriebskosten	Gut	2	Sehr gut	1	Gut	2	Gut	2	Befriedigend	3	Sehr gut	1	Gut	2
Verknüpfung	Passmarken, Kulisse	3	Passmarken, Adapter	4	Lasertracker	1	Optotrak	1	Passmarken, Kulisse	2	Passmarken, Kulisse	5	Passadapter, Spiegel	2
Gesamtnote		2,4		3,0		3,0		2,7		2,2		3,0		2,9
Abbildung	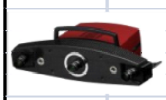						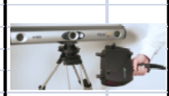		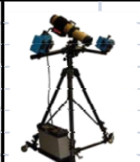					
Hersteller (Bsp.)	GOM LINK		ROMER LINK		Leica LINK		Steinbichler LINK		Geodetic LINK		Konica Minolta LINK		Nikon (Metris) LINK	

Fig.12: Comparison matrix for the measurement devices (parameters taken from the technical specification of the manufactures)

Based on these three criteria a calculation of the measurement uncertainty was done for various propeller and measurement volumes. It was determined that the measurement volume 1500 x 1500 mm (MV1500) is ideal for testing the entire geometry of the propellers, blades and moulds. Only for the inspection of the edge and propellers up to a radius of 750 mm the measuring volume 500 x 500 mm (MV500) should be used. With the MV1500 measurement accuracy (depending on the measurement configuration) of 0.15 to 0.45 mm can be achieved. With the smaller MV500 up to 0.05 mm can be achieved.

The adaption of the structured light scanner for a single blade is shown in figure 4.

Measurement	Surface comparison	Analysis of the intersections
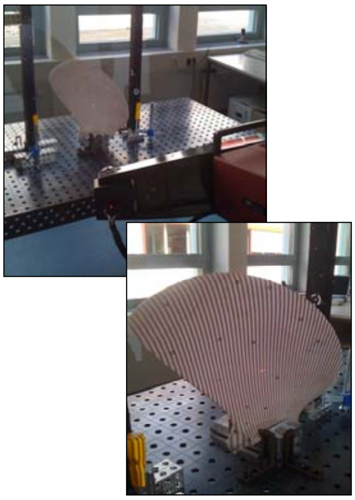	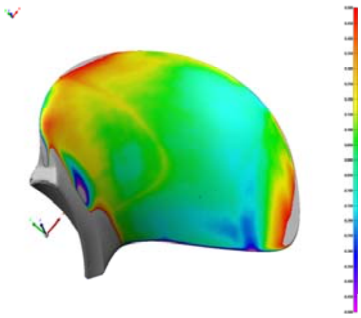	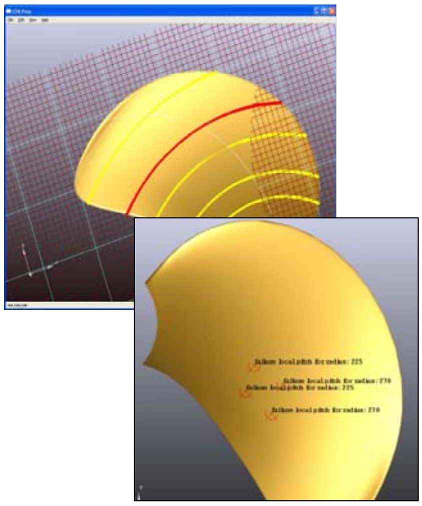

Fig.13: Evaluation of a propeller blade with a structured light scanner

4.2. Quality concept

Based on the defined measurement tasks and the choice of instrument a flow chart was developed (see figure 5). This concept contains the steps that are performed during production and the quality gates in which an evaluation of the geometric properties is required.

For the use case "repair" in which an used propeller needs to be inspected has been covered separately.

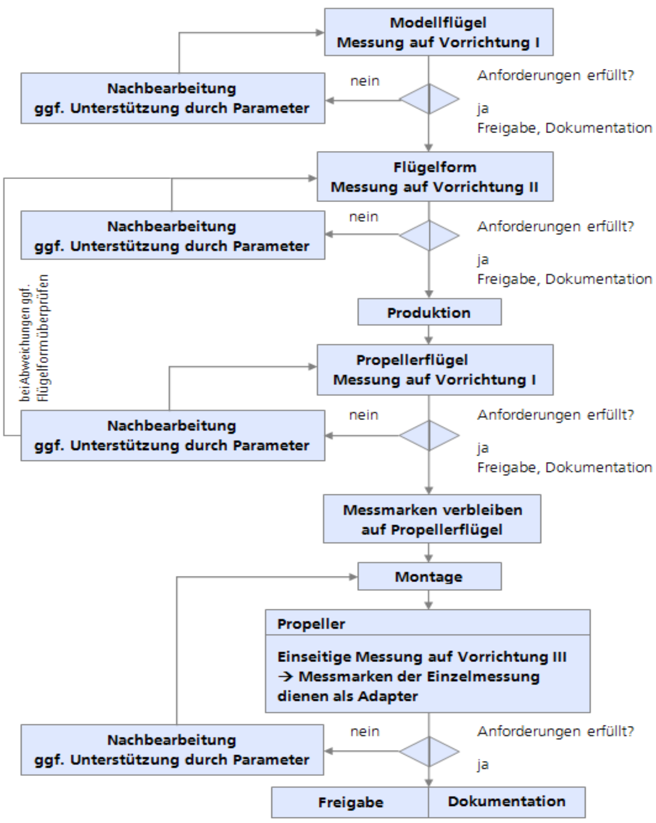

Fig.14: Quality concept

4.3. Measurement configuration

Multiple stations are required for the scan of an entire propeller with a structured light scanner. To speed up this process and make sure that the required accuracy is reached a concept for semi automatic orientation of each scan was developed and tested. Therefore the propeller should be mounted on a turntable or a rotary axis with centric clamping. The system for the scan orientation is based on calibrated bars. These bars have a known reference point configuration which is determined with an photogrammetric system. They are used to reference the suction and pressure side into an superior system. This reference system can be created with an accuracy of about 0.02 mm, which meets the requirements for the accuracy of the superior system.

Subsequently a test station, as shown in Figure 6, was designed and built.

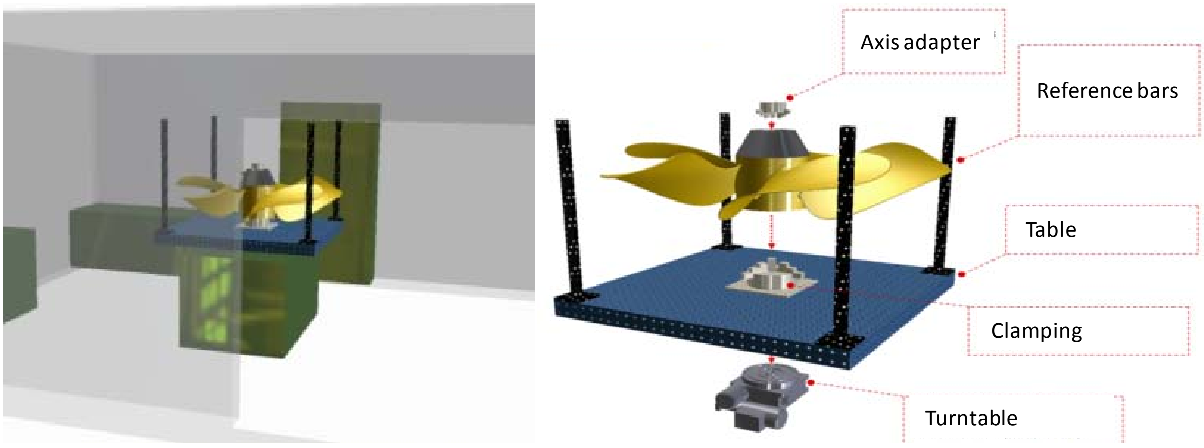

Fig.15: Measurement configuration

For the measurement of propellers, which are already mounted onto ships, the configuration has to be adapted to the situation. For the quality control of very large propellers with lower accuracy requirements (four meters diameter and greater) or if other constrains prevent the use of an structured light scanner a laser scanner may be used as measurement instrument. As part of the testing such an approach, figure 7 shows an exemplary scan of a mounted propeller.

Fig.16: Measurement of a mounted propeller

With the adoption of the measurement concept for the scanning of mounted propellers the following information can be gathered very efficiently:

- Check of the installation position with reference to the propeller shaft and the ships coordinate system
- Proof of the propeller characteristics regarding ISO
- Evaluation of deformation and damage

4.4. Measurement results

When measuring with the structured light scanner four million 3d data points are acquired in about two seconds. This creates a surface model which can be compared with the reference CAD model. This makes it possible to perform surface evaluations, which are based on quantifiable parameters. An example is shown in figure 8.

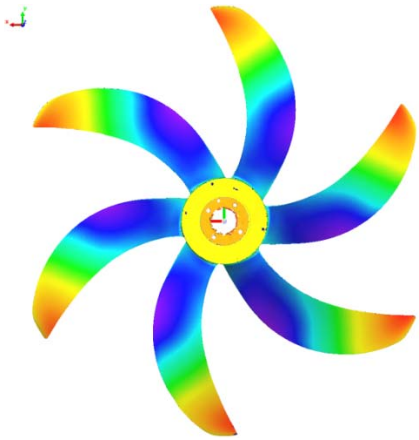

Fig.17: Color coded deviation between actual and designed surface

With such 3d measurement data the edges and the geometric parameters, which are defined by the ISO 484, can be evaluated. The analysis of such an intersection is shown in figure 9.

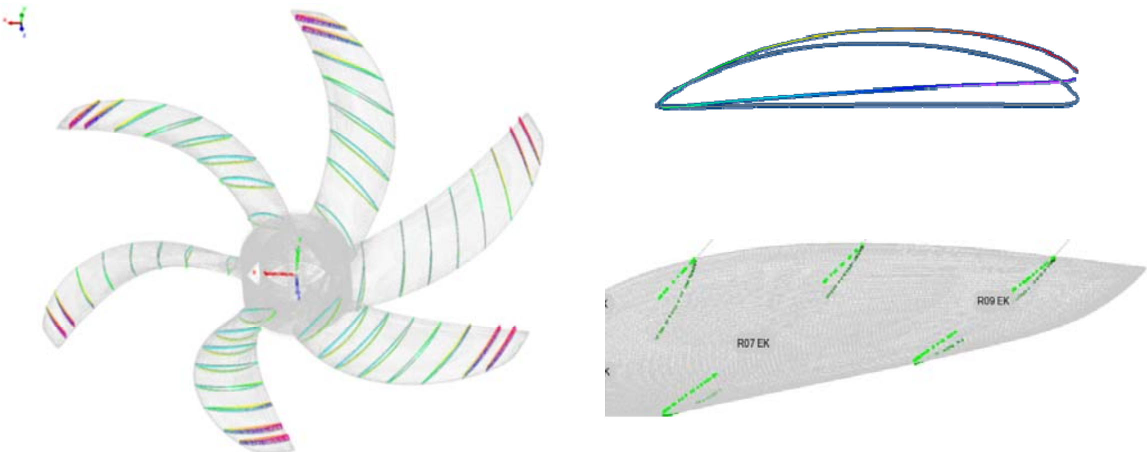

Fig.18: Evaluation of the geometric propeller parameters

5. Software development

5.1. Concept and structure

The following functionality has been determined as required:

- Import and 3d representation of the collected data and CAD models
- Creation of algorithms for processing the point or surface data
- Mathematical extraction of the geometric parameters of the blades and the propeller
- Evaluation of the parameters in reference to the tolerances of the ISO
- Reporting and presentation of the evaluation results

To accomplish these requirements, the following main software modules were developed:

1) **Geometry and CAD module:**
   Import of geometry data and possibilities to perform geometric operations
2) **Test module:**
   Global or selective implementation of the test method, display and log the results
3) **Calculation module:**
   Evaluation of the geometric criteria

   Software implementation of testing procedures according to the individual criteria

5.2. Realization

For the geometry and CAD module the CAD library Opencascade from the company OPEN CASCADE SAS was used. It is an open source software development platform, which is designed for applications like CAD or CAE.

The test module was implemented based on existing test development structures. These are based on the so called unit tests that have been developed for certain software processes. This makes it possible to start entire branches or single tests in a tree structure very efficient.

The development of test algorithms was implemented in C.

After a software run the performed tests and the results are displayed (see figure 10). The contents of the output can be adapted, copied or exported. The parameters for the tolerance test are stored in text format and can be adjusted quickly. The determined propeller characteristics are exported to a text file.